The role of mammalian TRC40 in membrane-protein targeting and chaperoning

Dissertation

for the award of the degree
"Doctor of Philosophy"
Division of Mathematics and Natural Sciences
of the Georg-August-Universität Göttingen
within the Göttingen Graduate School for Neurosciences, Biophysics and Molecular Biosciences (GGNB),
of the Georg-August-University School of Science (GAUSS)

Submitted by
Francisco Javier Coy Vergara
from Tobarra, Spain

Göttingen, April 2018

Members of the Thesis Committee and Examination Board:

Supervisor:	**Prof. Dr. Blanche Schwappach-Pignataro** Department of Molecular Biology University Medical Center Göttingen Max Planck Institute for Biophysical Chemistry
Thesis committee:	**Prof. Dr. Michael Kessel** Department of Molecular Cell Biology Max Planck Institute for Biophysical Chemistry
Thesis committee:	**Dr. Nuno Raimundo** Institute for Cellular Biology University Medical Center Göttingen
Examiner:	**Prof. Dr. Michael Meinecke** Department of Cellular Biochemistry University Medical Center Göttingen
Examiner:	**Dr. Hans Dieter Schmitt** Department of Neurobiology Max Planck Institute for Biophysical Chemistry
Examiner:	**Prof. Dr. Ralph Kehlenbach** Department of Molecular Biology University Medical Center Göttingen

Date of oral examination: 4th June 2018

Affidavit

I, Francisco Javier Coy Vergara, hereby declare that I prepared the PhD thesis “The role of mammalian TRC40 in membrane-protein targeting and chaperoning” on my own and with no other sources and aids than quoted.

Göttingen, April 5th 2018 Francisco Javier Coy Vergara

To Ángel and Juana,

the ones who taught me the most valuable and unforgettable lessons.

Las tierras, las tierras, las tierras de España,
las grandes, las solas, desiertas llanuras.
Galopa, caballo cuatralbo,
jinete del pueblo,
al sol y a la luna.

¡A galopar,
a galopar,
hasta enterrarlos en el mar!

A corazón suenan, resuenan, resuenan
las tierras de España, en las herraduras.
Galopa, jinete del pueblo,
caballo cuatralbo,
caballo de espuma.

¡A galopar,
a galopar,
hasta enterrarlos en el mar!

Nadie, nadie, nadie, que enfrente no hay nadie;
que es nadie la muerte si va en tu montura.
Galopa, caballo cuatralbo,
jinete del pueblo,
que la tierra es tuya.

¡A galopar,
a galopar,
hasta enterrarlos en el mar!

Capital de la Gloria - Rafael Alberti

The lands, the lands, the lands of Spain
the great, lonely, deserted plains.
Gallop, white horse,
people's jockey,
to the sun and to the moon.

Let's gallop,
let's gallop,
until they're buried in the sea!

The lands of Spain sound and resound like
hearts on the horseshoes.
Gallop, people's jockey,
white horse,
foam horse.

Let's gallop,
let's gallop,
until they're buried in the sea!

No one, no one, no one, there's no one to face; 'cause death is no one if she goes on your saddle.
Gallop, white horse,
people's jockey,
'cause the land is yours.

Let's gallop,
let's gallop,
until they're buried in the sea!

Capital of Glory - Rafael Alberti

Ever tried. Ever failed. No matter. Try again.
Fail again. Fail better.

Worstward Ho – Samuel Beckett

Acknowledgments

When I was a child I was quite lucky, I found myself among six parents. Ángel and Juana, you have been my role models, my constant motivation and my most beautiful story. This thesis is a late gift for you. Another two, Juan and Paqui, managed to be babysitters, cooks, teachers, advisers, psychologists, maids, funders, drivers, etc. and on top of that you had your own job. Your days did not have 24 hours but many more. Thanks to your efforts and your multiple sacrifices you put me in the position of being able to fight for dreams like this one. The last two, Juanma and Quique, when I was growing you were the mirror I looked myself into. I used to follow you everywhere. I wanted to learn all from you. I always tried for fill your shoes even if they were too big for me and following your steps I found myself in this path. Nothing of these would have been possible without the six of you. My success is the success of all of those who struggled and fought for me to be here. Thanks to you I just had the easiest part of this story. My success is your success. Thanks for making me the person I am right now.

Thanks to Blanche Schwappach for giving me the chance to do what I love: Science. It has been a dream come true that, after this years, I am still enjoying. She took me in her big family, gave me constant advice and carved this raw material in the making. She is inspirational. Thanks, Blanche.

Life taught me that family is not necessarily the one you share blood with but the one whose links root deep in you. Thanks to Jhon, Tobias and Laura for standing in my path, you have been a constant source of learning and growing. Nothing that you can read in the following pages would have been possible without the endless help and discussion from Jhon and Eric. It has been a pleasure growing next to you both, thanks! Thanks to Kirsten whose efficient and diligent work enables us to do our everyday science. She is outstanding and always shining by her willingness and readiness to help. Thanks to Fabio and Will who got me started in the lab and provided me with feedback. Thanks to Markus and Julia, who made my days shorter, for your friendship.

Thanks to Evelina who had to read this story in a record time. Thanks to the rest of the Schwappach lab and to the department of Molecular Biology.

So far, the way to get up to this point has been an amazing ride. Thanks to Ana and Toñi who saw something where there was nothing, with you I started crawling. Thanks to Paulina and Luismi who taught me so much in and outside a lab, you blindly trusted on me, made me a better person and my first baby steps happened next to you. For Jesús Salvador who kindly offered me a room full of toys where I played to be a scientist and María Salvador who patiently taught me how to use those toys, with you I started to walk. Thanks to those who fed my endless curiosity: Pilar Rozalén, Margarita Fernández, María Jesús Oset, Mercedes Grande, Carmen de Juan, Carmen Arce, etc. To those who challenged me to keep growing and exploring my limits. To those whose stories inspired me. A piece of this thesis belongs to you because I am nothing but the result of the experiences and stories you all shared with me.

Table of contents

Abstract

Tail-anchored (TA) proteins are distinguished from other membrane proteins due to their particular topology. The best-characterized pathway for the targeting of TA-proteins is the GET pathway in yeast or the TRC pathway in mammals. Recently, several studies have reported that more than one post-translational pathway operate during targeting of TA-proteins to the ER-membrane such as the EMC pathway, Hsp40/Hsc70, the SND pathway and the PEX pathway.

TRC40 is the cytoplasmic effector of the TRC pathway. This study aims to investigate the reliance of TA-proteins on the TRC pathway at the steady-state *in vivo* in mammalian cells. Moreover, the role of several functional domains of TRC40 during TA-proteins targeting to ER-membrane and chaperoning *in vivo* is addressed in this study. Furthermore, this study wants to explore the potential alternative role of TRC40 as redox-regulated chaperone.

A panel of cmyc-tagged TRC40 mutants was created and screened by immunofluorescence. The screen identified $TRC40_{D74E}$, an ATPase-impaired mutant, as a trapping mutant that leads to an accumulation of TA-protein in the cytoplasm. This makes $TRC40_{D74E}$ a good tool for the study of TA-protein biogenesis and for determining the interactome of TRC40 *in vivo*.

Eleven TA-proteins showed *in vivo* TRC-dependence by knocking-down TRC-pathway components such as WRB and TRC40. In contrast, another six TA-proteins did not show any evidence of *in vivo* TRC-dependence in this study, neither affected by down-regulation of TRC components nor by the presence of $TRC40_{D74E}$. Many of the TA-proteins (e.g. USE1, UBE2J1, Vti1a) tested in this study were not reported to be TRC-dependent in literature. TMD hydrophobicity may be a major contributor in the TRC-dependence of the TA-proteins. However, the cytoplasmic domain may also contribute. The loss BAG6, essential for the TA-targeting according to the proposed model in literature, strikingly showed no effect on the level of the TA-proteins in membranes at the steady-state; suggesting that BAG6 might not be essential for TA-protein targeting *in vivo*.

Finally, the TRC pathway is kept in balance by a mechanism that tightly regulates the steady-state levels of its components. Upon the loss of some of the components others get severely reduced in their steady-state levels. This TRC-pathway balance is not symmetrical and shows a hierarchical organization within the pathway.

1. Introduction

1.1. Integral membrane proteins

Membrane proteins constitute around 20-30% of the proteins encoded by the genome (Wallin and von Heijne 1998; Stevens and Arkin 2000; Krogh et al. 2001; Almén et al. 2009; Bill et al. 2011). These proteins are involved in many processes such as active transport, communication between contact sites, anchorage, cell marker recognition and signaling. Membrane proteins can be classified as peripheral membrane proteins or integral membrane proteins (IMPs). Peripheral membrane proteins do not fully penetrate the membrane but associate externally with the membrane. This membrane association is mediated by different physicochemical mechanisms for instance by non-specific hydrophobic associations, covalently-bound lipid anchors, such as palmitoylation, glycosylphosphatidylinositol (GPI), myristoylation, etc. (Silvius 2002). IMPs have at least one hydrophobic transmembrane segment. The transmembrane domain (TMD) of the IMPs enables the protein to be anchored in the membrane. Membrane proteins are further classified based on their topology (**Fig. 1**).

1.2. Tail-anchored proteins

Tail-anchored (TA) proteins are distinguished from other membrane proteins due to their particular topology (Borgese, Colombo, and Pedrazzini 2003; Kutay, Hartmann, and Rapoport 1993). This topology consists of a single transmembrane segment that lies at the very C-terminus of the protein with the N-terminus oriented to the cytoplasm. The TMD is found in the region of the last 50 amino acids and there is a short C-terminal tail oriented to the lumen no longer than 40 amino acids. TA-proteins lack of signal sequence and they are post-translationally inserted (Borgese, Colombo, and Pedrazzini 2003; Kutay, Hartmann, and Rapoport 1993) (**Fig. 2**). Single-pass type

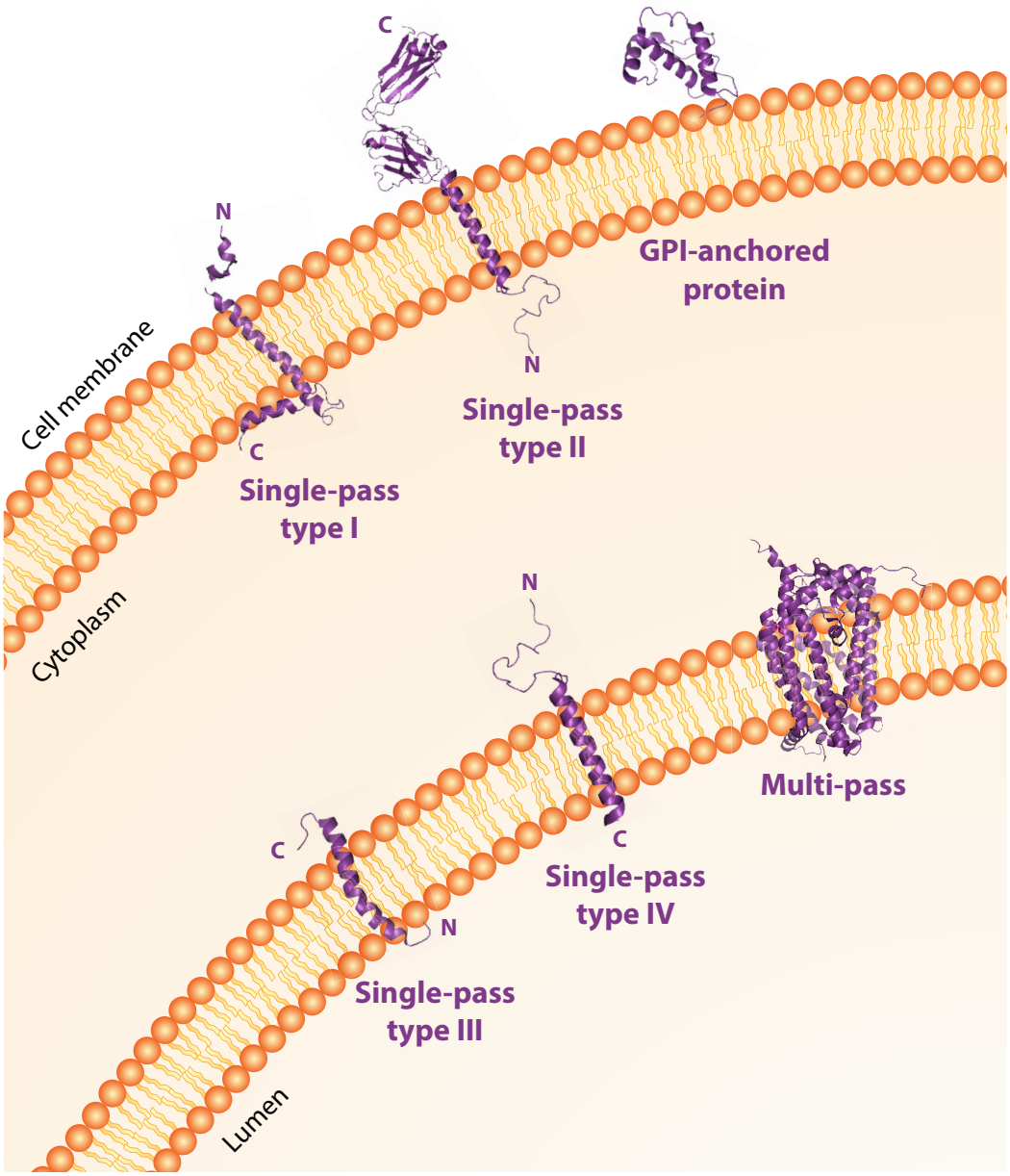

Figure 1. Membrane proteins. Scheme depicting the different membrane proteins according to UniProt (The UniProt Consortium 2017). Single-pass type I (PDB ID: 2JO1) are those spanning the membrane just once whose N-terminus is on the extracellular side of the membrane and gets its signal sequence removed. Single-pass type II (PDB ID: 4CMH) are those single-span membrane proteins N-terminus is on the cytoplasmic side of the membrane. The transmembrane domain is close to the N-terminus serving as an anchor. Single-pass type III (PDB ID: 2LAT) are membrane proteins that span once the membrane and the N-terminus is on the extracellular side of the membrane but lack of signal sequence (in contrast to type I). Single-pass type IV (PDB ID: 2LPF) are those single-span membrane proteins N-terminal is on the cytoplasmic side of the membrane. The transmembrane domain is close to the C-terminus serving as an anchor (in contrast to type II). They are the so-called tail-anchored proteins (TA-proteins). Multi-pass membrane protein (PDB ID: 5SYT) are those proteins that span the membrane more than once. GPI-anchored protein (PDB ID: 1LG4) are those whose C-terminus is bound to the membrane through a GPI-anchor (glycosylphosphatidylinositol-anchor).

IV membrane proteins are TA-proteins (**Fig. 1**). TA-proteins account for around 3-5% of the proteome (Beilharz et al. 2003; Kalbfleisch, Cambon, and Wattenberg 2007; Kriechbaumer et al. 2009). TA-proteins mediate several cell functions that include apoptosis (i.e. Bcl-2, Bcl-XL), vesicular transport (most SNAREs are TA-proteins, i.e. Stx5 and Stx6), protein translocation (i.e. Sec61β and Sec61γ), lipid homeostasis (i.e. VAPA and VAPB) and protein quality control (i.e. UBE2J1 and UBE2J2) among others.

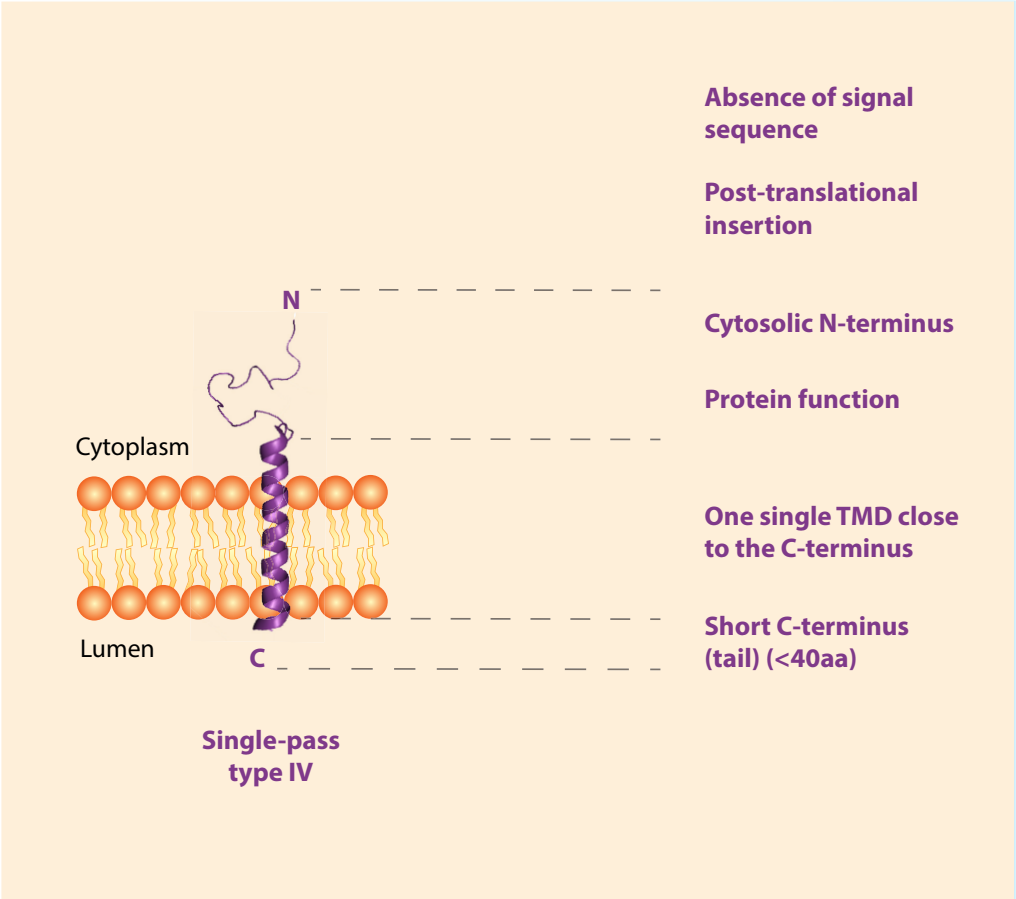

Figure 2. Tail-anchored proteins characteristics. Scheme illustrating the TA-protein features. They are single-pass type IV membrane proteins. They are transmembrane polypeptides with a particular topology: one single transmembrane domain (TMD) at the very C-terminus, N-terminus oriented to the cytoplasm and a short tail after the TMD that is oriented towards the organelle lumen.

The transmembrane segment of the TA-proteins contains a targeting signal for membrane insertion and the proper delivery of the TA-protein to its final organelle destination (endoplasmic reticulum, mitochondrial outer membrane, plasma membrane and peroxisomes) (Borgese, Brambillasca, and Colombo 2007; Rabu et

al. 2009; Borgese and Fasana 2011; Hegde and Keenan 2011). Additionally, it has also been a long-standing assumption that a TA-protein of the secretory pathway, that includes plasma membrane and Golgi, are inserted into the endoplasmic reticulum (ER) membrane (Borgese et al. 2001; Bulbarelli et al. 2002; Borgese, Colombo, and Pedrazzini 2003; Borgese, Brambillasca, and Colombo 2007). The secretory pathway sorts cargo via transport vesicles to the Golgi apparatus and from Golgi they can be transported to other organelles or can be secreted (reviewed in C. K. Barlowe and Miller 2013; C. Barlowe and Helenius 2016; Kim and Gadila 2016; Arakel and Schwappach 2018).

1.3. Protein biogenesis. Targeting and insertion of ER-membrane proteins

Newly synthesized membrane proteins present a variable number of hydrophobic domains compared to cytoplasmic proteins that are synthesized in a hydrophilic cytosol. Many pathways have evolved to prevent the aggregation of the nascent membrane proteins in the cytoplasm and ensure the correct targeting and membrane insertion of the protein. The nascent integral membrane protein has to be recognized once exiting the ribosome. Next, it has to be targeted to the right organelle and inserted with the right topological orientation of the protein (Cross et al. 2009; Akopian et al. 2013). The most well-characterized pathway that targets IMPs involves the signal recognition particle (SRP) pathway (Blobel and Dobberstein 1975a; Blobel and Dobberstein 1975b).

1.3.1. SRP pathway

The SRP pathway mediates the translocation of single- or multi-spanning proteins into the ER membrane (**Fig. 3**). It can also translocate soluble polypeptides from the cytoplasm. SRP recognizes a hydrophobic N-terminal sequence from the nascent protein while translation is taking place on the ribosome. This N-terminal

sequence is cleavable and is known as a signal sequence (SS) (Rapoport 2007; Grudnik, Bange, and Sinning 2009) (**Fig. 3, step 1**). The interaction between the SRP and the ribosome nascent chain complex (RNC) slows down elongation and stalls translation (Halic et al. 2004). After binding the RNC, the SRP targets it to the SRP receptor that resides in the ER-membrane. The SRP receptor is formed by two subunits: SRα and SRβ (Gilmore, Blobel, and Walter 1982; Gilmore, Walter, and Blobel 1982). Once recruited by the SRP receptor, the RNC interacts with the Sec61 translocon channel in the membrane and the SRP-SRP receptor dissociates. This process is GTP-mediated due to the GTPase activity of the SRP receptor subunits (Connolly and Gilmore 1986). The RNC aligns with the Sec61 translocon channel, then translation is resumed and the elongating polypeptide is subsequently targeted into the channel (**Fig. 3, step 2**). This process is known as co-translational protein targeting, given that it occurs while translation is taking place (Rapoport 2007; Grudnik, Bange, and Sinning 2009). The SRP pathway is conserved in all three domains of life (Pool 2005). Recently, it has been reported that SRP is important for targeting membrane proteins independent of the relative position of the transmembrane segment(s), except TA-proteins (Costa et al. 2018). Nevertheless, many proteins that contained a N-terminal SS were co-translationally targeted regardless of the absence of SRP (Costa et al. 2018).

Many IMPs are targeted to the ER membrane by the SRP pathway. However, the absence of a SS in TA-proteins precludes co-translational, SRP-dependent targeting. TA-proteins remain in the ribosome until translation ends making it impossible for the SRP to bind the TMD at the very C-terminus. Therefore, it was proposed that TA-proteins are inserted post-translationally (Kutay, Hartmann, and Rapoport 1993; Kutay et al. 1995). The best-characterized pathway for the targeting of TA-proteins is the GET pathway in yeast or the TRC pathway in mammals (Stefanovic and Hegde 2007; Favaloro et al. 2008; Schuldiner et al. 2008). Recently, several studies have reported that more than one post-translational pathway targets TA-proteins to the ER membrane such as the EMC pathway (Guna et al. 2018), Hsp40/Hsc70 (Rabu et al. 2008; Rabu et al. 2009), the SND pathway (Aviram et al. 2016; Haßdenteufel et al. 2017) or the PEX pathway (Jones, Morrell, and Gould 2004; Fujiki et al. 2014; Buentzel et al. 2015).

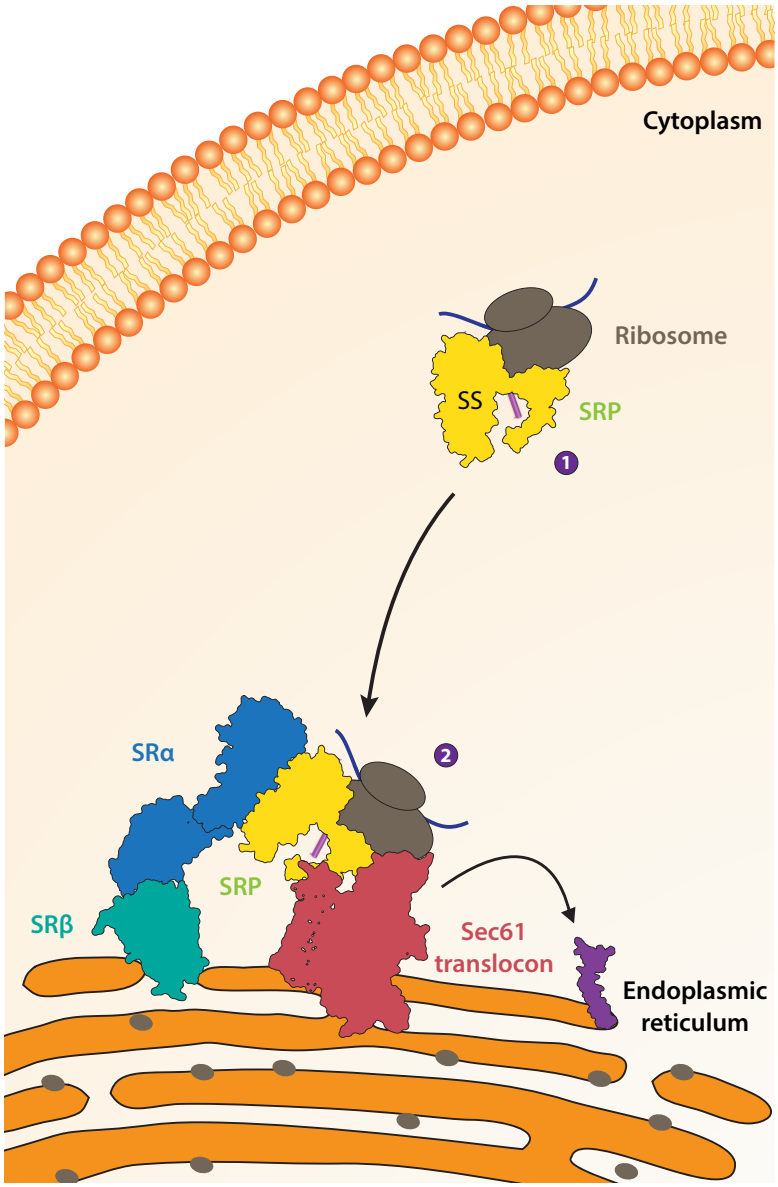

Figure 3. SRP pathway. (1) SRP (PDB ID: 5GAF) recognizes the signal sequence (SS) from the nascent protein on the ribosome. The interaction slows down the translation and stalls it. **(2)** SRP is recruited by the heterodimer SRP-receptor (SR) via SRα (PDB ID: 2FH5, 5L3Q). The ribosome nascent chain complex interacts with the Sec61 translocon channel (PDB ID: 3J7Q). The RNC aligns with the Sec61 translocon and then the translation is resumed. The elongating polypeptide is then funneled into the Sec61 translocon channel.

1.3.2. Yeast GET pathway

Get3 is a homodimeric P-loop ATPase that is localized in the cytoplasm (Shen et al. 2003; Leipe et al. 2002; Bange and Sinning 2013). Get3 was shown to be genetically linked to Get1 and Get2 in yeast (Schuldiner et al. 2005). Get1 and Get2

were revealed to be the receptor for Get3. These proteins were reported to be involved in TA-protein insertion into ER-membranes in yeast (Schuldiner et al. 2008). Sgt2 is a cochaperone that can interact with heat-shock proteins (Hsps) (F. H. Liu et al. 1999; Scheufler et al. 2000; Liou, Cheng, and Wang 2007). It has been reported to identify and capture the TA-protein while exiting from the ribosome (Chang et al. 2010; Leznicki et al. 2010; Simpson et al. 2010; F. Wang et al. 2010; Rao et al. 2016) (**Fig. 4, step 1**). Sgt2 interacts with Get5 and Get4 to form the so-called pre-targeting complex (Jonikas et al. 2009; Battle et al. 2010; Chang et al. 2010; Simpson et al. 2010) (**Fig. 4, step 2**). The pre-targeting complex interacts with Get3 via Get4 (Jonikas et al. 2009; Gristick et al. 2014; Gristick et al. 2015) facilitating the handover of the TA-protein from Sgt2 to Get3 (F. Wang et al. 2010) (**Fig. 4, step 3**). The Get1/2 receptor assembles into an ER-membrane resident complex (Schuldiner et al. 2008; Mariappan et al. 2011; F. Wang et al. 2014). Get3 delivers the TA-protein to the Get1/2 receptor in a process dependent on ATP-hydrolysis (Mariappan et al. 2011; Stefer et al. 2011; F. Wang et al. 2011; F. Wang et al. 2014) (**Fig. 4, step 4**). The Get1/2 receptor acts as an insertase inserting the TA-protein into the ER-membrane (F. Wang et al. 2011; F. Wang et al. 2014) (**Fig. 4, steps 5 and 6**). As noted before, the proteins of the secretory pathway will be sorted to their final destination (Borgese et al. 2001; Bulbarelli et al. 2002; Borgese, Colombo, and Pedrazzini 2003; Borgese, Brambillasca, and Colombo 2007). The impairment of the GET pathway can cause mislocalization of TA-proteins to mitochondria (Schuldiner et al. 2008). The AAA+ ATPase Msp1 was reported to be part of the quality control mechanism of the mitochondrial outer membrane (MOM). Msp1 was found to function in the clearance of mislocalized TA-proteins in the MOM in yeast (Okreglak and Walter 2014; Weir et al. 2017; Wohlever et al. 2017). ATAD1 is the mammalian homolog of Msp1 and in a similar fashion it was found to be required in mammals for the clearance of mislocalized TA-proteins into MOM (Y.-C. Chen et al. 2014).

TA-protein targeting of the GET pathway is driven by the ATPase cycle of Get3 along with its many conformational changes within this ATPase cycle (Hegde and Keenan 2011; Wereszczynski and McCammon 2012; Chio et al. 2017).

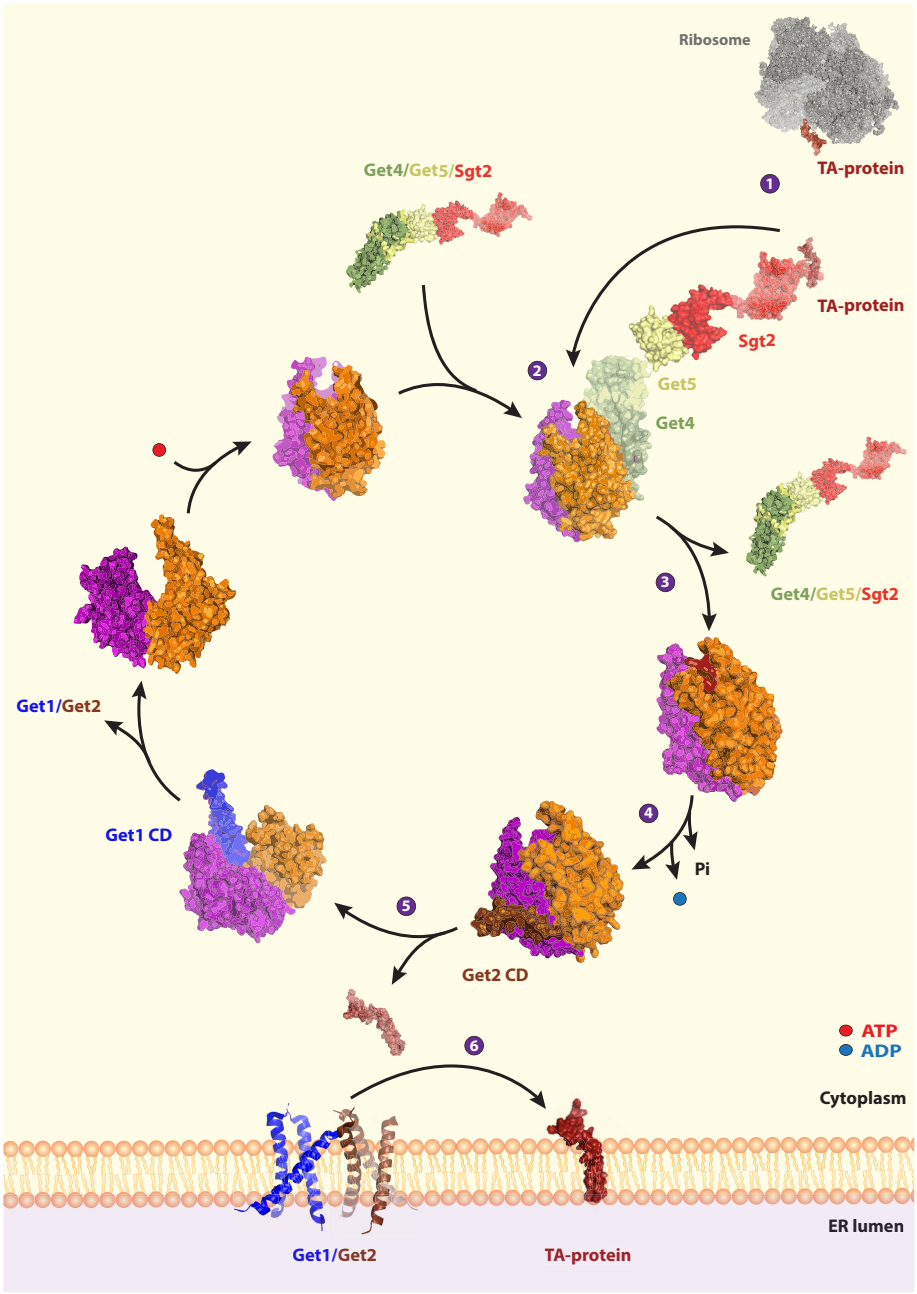

Figure 4. Yeast GET pathway. (1) Sgt2 (PDB ID: 3ZDM, 5LYP) captures the newly synthesized TA-protein (PDB ID: 2LPF) from the ribosome (PDB ID: 6EK0). Sgt2 can interact with Get4/Get5 (PDB ID: 4PWX) via Get5. **(2)** The pre-targeting complex, through Get4, has preferentially a higher affinity for Get3 in a close state conformation (PDB ID: 4PWX). The binding of Get4/Get5 inhibits the ATPase activity of Get3. **(3)** The TA-protein is subsequently loaded into Get3 (PDB ID: 4XTR) from Sgt2. This interaction makes Get3 lose its affinity for Get4/Get5 and they dissociate. Get3 is loaded with the TA-protein and ATP in this state. **(4)** Get3, after its dissociation from Get4/Get5, hydrolyzes ATP and interacts with the cytoplasmic domain of Get2 (PDB ID: 3ZS9). Get2 tethers Get3 loaded with the TA-protein to the ER membrane. **(5)** Get3 then interacts with the cytoplasmic coiled-coil domain of Get1 (PDB ID: 3SJB) which provokes more conformational changes in Get3 and makes the TA-protein to be loose. **(6)** The TA-protein is handed off to the receptor that has insertase activity and inserts it into the membrane. Get3 subunits are depicted in orange and deep purple. CD stands for cytoplasmic domain.

1.3.2.1. Get3 ATPase cycle

Once dissociated from Get1/2, Get3 is believed to be in an *apo*-Get3 conformation. This refers to an open Get3 conformation with no nucleotides bound (Hu et al. 2009). However, it remains unclear whether this conformation exists *in vivo* (Chio, Cho, and Shan 2017). The binding of ATP to the Walker A or P-loop of Get3 triggers a conformational change towards a so-called close state (Bozkurt et al. 2009; Mateja et al. 2009; Suloway et al. 2009; Mateja et al. 2015) (**Fig. 5, step 1**). The pre-targeting complex, via Get4, has preference for Get3 in a close state (Chartron et al. 2010; Rome et al. 2013; Rome et al. 2014; Gristick et al. 2014) and the binding of Get4/Get5 inhibits the ATPase activity of Get3 (Rome et al. 2013) (**Fig. 5, step 2**). Next, Sgt2 hands off the TA-protein to Get3 (F. Wang et al. 2010; Rome et al. 2013; Rao et al. 2016). This interaction weakens the affinity between Get3 and Get4/Get5 and allow them to dissociate (Rome et al. 2014). At that point of the cycle, Get3 is loaded with the TA-protein and ATP (**Fig. 5, step 3**). After dissociation of Get4/Get5, Get3 subsequently hydrolyzes ATP. Get2 has a high affinity for Get3 loaded with the TA-protein and ADP and tethers it to the ER membrane (Mariappan et al. 2011; Stefer et al. 2011; Zalisko et al. 2017). The interaction with Get2 destabilizes the ADP within Get3 and ADP is released (**Fig. 5, step 4**). Additional conformational changes in Get3 upon the release of Get2 allows for an interaction with Get1. which provokes more conformational changes in Get3 and renders the TA-protein free to dissociate from Get3 (Mariappan et al. 2011; F. Wang et al. 2011). The TA-protein is handed off to the receptor that has insertase activity and inserts it into the ER-membrane (F. Wang et al. 2011; F. Wang et al. 2014) (**Fig. 5, step 5**). Get1 loses its affinity for Get3 after the handover of the TA-protein. Get3 is believed to be released from the ER membrane in a nucleotide-free state (Mariappan et al. 2011; Stefer et al. 2011; Kubota et al. 2012; Rome et al. 2014; Zalisko et al. 2017) (**Fig. 5, step 6**).

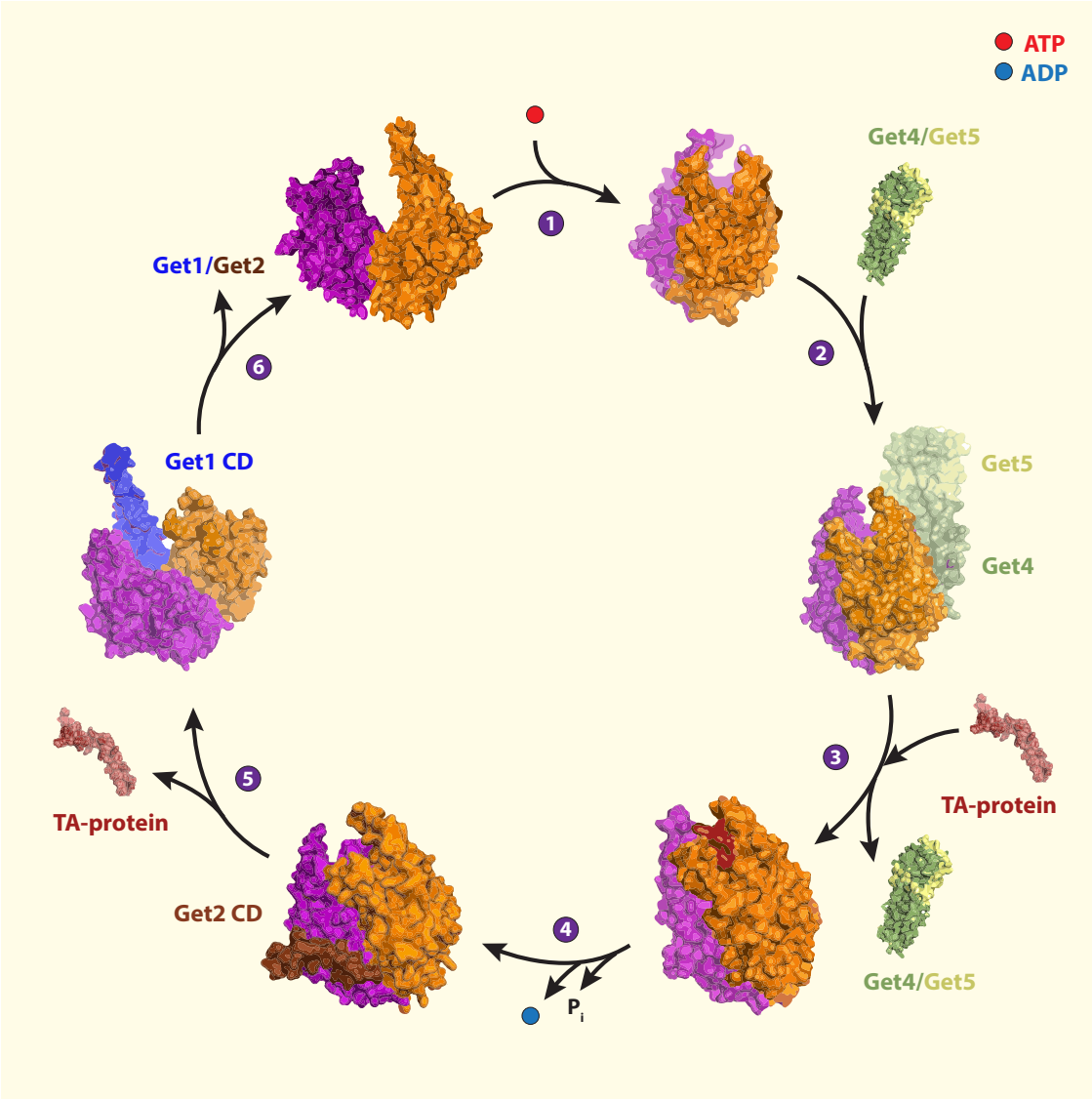

Figure 5. The Get3 ATPase cycle model. (1) Get3 is in an *apo*-Get3 conformation (PDB ID: 3H84). This is an open Get3 conformation with no nucleotides bound. The binding of ATP triggers a conformational change towards a so called close state (PDB ID: 2WOJ). **(2)** The pre-targeting complex, through Get4, has a higher affinity for this close state preferentially (PDB ID: 4PWX). The binding of Get4/Get5 (additionally Sgt2, not shown in the figure) inhibits the ATPase activity of Get3. **(3)** The TA-protein (PDB ID: 2LPF) is thus loaded into Get3 (PDB ID: 4XTR) from Sgt2. This interaction makes Get3 lose its affinity for Get4/Get5 and they dissociate. Get3 is loaded with the TA-protein and ATP. **(4)** Get3, after dissociation of Get4/Get5, hydrolyzes ATP. Get2 has affinity for Get3 loaded with the TA-protein and ADP and tethers it to the ER membrane (PDB ID: 3ZS9). This ADP is released after the interaction with Get2. **(5)** Additional conformational changes in Get3 upon the release of Get2 allow the interaction with Get1 (PDB ID: 3SJB) which provokes more conformational changes in Get3 and makes the TA-protein to be loose. The TA-protein is handed off to the receptor that has insertase activity and inserts it into the membrane. **(6)** Get1 loses affinity for Get3 after handing off the TA-protein. Get3 subunits are depicted in orange and deep purple. CD stands for cytoplasmic domain.

1.3.2.2. Get3 functional domains

Get3 is a homolog of the archaeal ATPase ArsA (C. M. Chen et al. 1986; T Zhou and Rosen 1997; Shen et al. 2003). Get3 is a cytoplasmic P-loop ATPase that belongs to the signal recognition particle (SRP), MinD, and BioD (SIMIBI) ATPase class (Leipe et al. 2002; Bange and Sinning 2013; Shan 2016). Get3 has three very well conserved domains from ArsA and all of them are involved in the ATPase activity of the protein: (i) a Walker A or P-loop motif where the nucleotide binds (Walker et al. 1982; Saraste, Sibbald, and Wittinghofer 1990), (ii) an ATPase switch I domain and (iii) a DTAP switch II domain (Mateja et al. 2009; Stefer et al. 2011) (**Fig. 6**). These regions are named after the Switch I and Switch II domains of ArsA (Tongqing Zhou et al. 2001) that due to similarity were named after the correspondent GTPase domains (Sprang 1997; Tongqing Zhou et al. 2001). Get3 is a homodimer that is stabilized by a zinc ion coordinated by two CXXC motifs (C_{285} and C_{288}), one per monomer (Bozkurt et al. 2009; Mateja et al. 2009; Suloway et al. 2009; Hu et al. 2009; Yamagata et al. 2010). Mutations involving those cysteines were unable to rescue a *get3* deletion strain under different stress conditions (Metz et al. 2006).

As previously mentioned, Get3 undergoes many conformational changes during its ATPase cycle (Hegde and Keenan 2011; Wereszczynski and McCammon 2012; Chio et al. 2017). These conformational changes make regions of Get3 accessible, enabling the interaction with different partners. The N-terminal domain of Get4 interacts with Get3, preferentially in an ATP-bound state (Gristick et al. 2014). There are additional interactions in the interface of Get4-Get3 that inhibit the ATPase activity of Get3 (Gristick et al. 2014). The region of Get3 where Get4 interacts overlaps with the interaction surface of Get1 and Get2 (Mariappan et al. 2011; Stefer et al. 2011; F. Wang et al. 2011) (**Fig. 6A**). Get3 binding with Get1 and Get2 is mediated by electrostatic interactions involving acidic residues in the helix 11 of Get3, the so called DELYED motif (Mariappan et al. 2011; Stefer et al. 2011) (**Fig. 6A**). There is a second interaction interface between Get1 and Get3. Get1 is believed, through this second interface, to reconfigure Switch I and Switch II into a conformation similar to the open state (Stefer et al. 2011) (**Fig. 6A**). Binding of ATP promotes a close conformation of that brings together helical domains with hydrophobic residues that will form a

hydrophobic groove (Mateja et al. 2015). This is the so-called TA-protein binding groove where the TA-proteins bind to Get3 (Mateja et al. 2009; Mateja et al. 2015) (**Fig. 6A**).

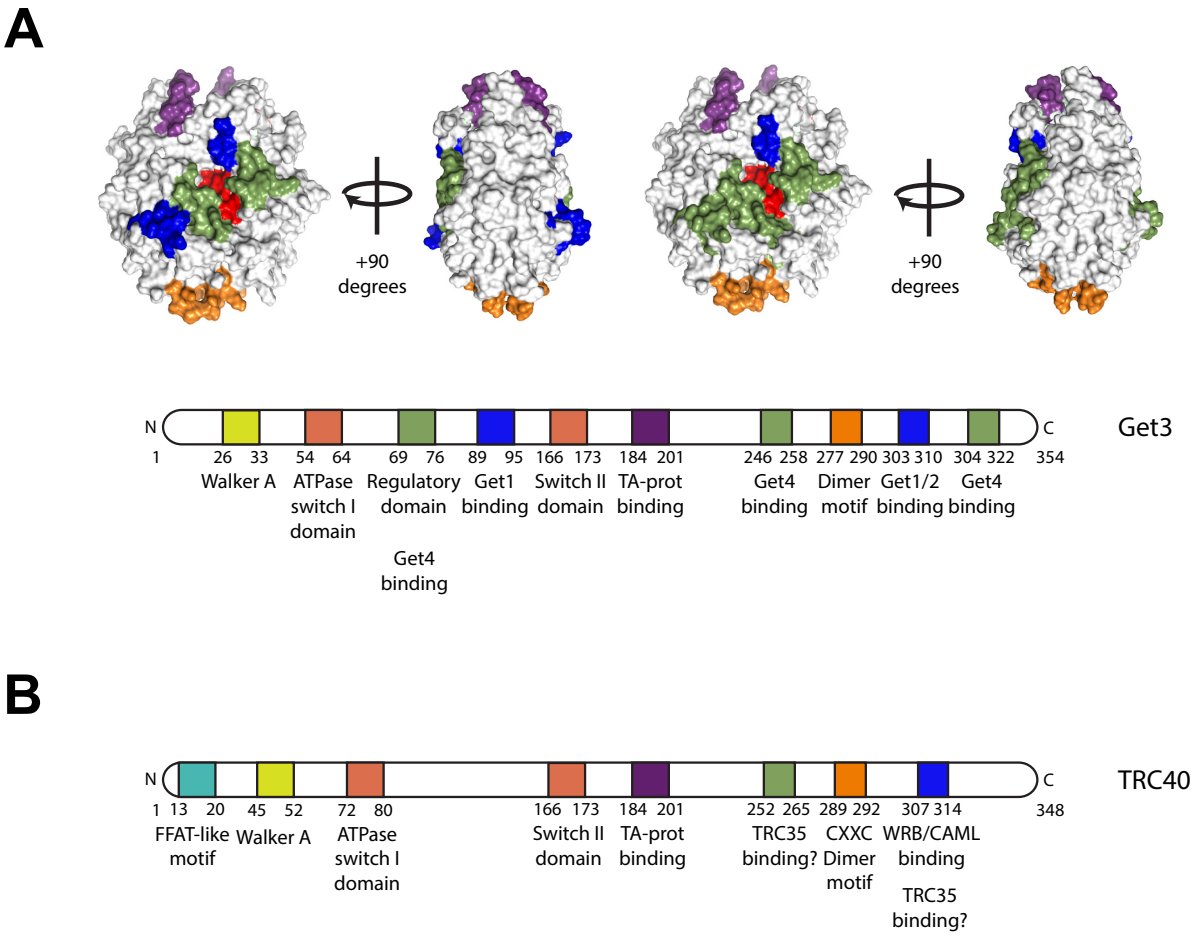

Figure 6. Get3 functional domains. (A) Scheme illustrating the functional domains described for Get3. Get3 structure highlighting these functional domains. Binding sites for Get1/2 and Get4 close to the C-terminal are overlapping. Due to this overlapping, the binding site of Get1/2 (blue) is shown on the left and Get4 binding site (light green) on the right. **(B)** TRC40 scheme depicting the functional domains based on the conserved residues after alignment of Get3 and TRC40.

1.3.2.3. Alternative roles of Get3

Apart from TA-protein targeting, other roles have been described for Get3. Yeast cells have been shown to survive in the absence of Get3 (Shen et al. 2003; Metz et al. 2006). However, Δ*get3* yeast cells present different phenotypes such as heat

sensitivity, copper sensitivity or hygromycin sensitivity (Shen et al. 2003; Metz et al. 2006; Schuldiner et al. 2008; Kohl et al. 2011; Kiktev et al. 2012; Voth et al. 2014). Connected to heat sensitivity, Get3 was predicted to have a heat shock transcription element in its native promoter (Yunkai Liu, Ye, and Erkine 2009).

Get3 has also been reported to be potentially involved in the targeting of GPI-anchored proteins, along with other chaperones, in an SRP-independent way (Ast, Cohen, and Schuldiner 2013). In addition, it has been reported to be a guanine-nucleotide exchange factor (GEF) for the Gα subunit Gpa1p (Lee and Dohlman 2008).

Get3 was found in foci in glucose-depleted cells colocalizing with unfolding proteins and chaperones such as Hsp104, Hsp42, Ssa1 or Sis1 (Powis et al. 2013). Furthermore, Get3 foci were found in *Δget1/Δget2* cells in normal glucose conditions (Powis et al. 2013). Recently, Get3 was reported to be a redox-regulated chaperone under oxidative stress conditions (Voth et al. 2014). Hsp33, a bacterial redox-regulated chaperone, shares some features with Get3 (Jakob et al. 1999; Kumsta and Jakob 2009), such as a CXC-X_n-CXXC motif that is the key of the redox switch of Hsp33 (Jakob et al. 1999; Voth et al. 2014). Upon oxidation *in vitro*, Get3 undergoes drastic structural rearrangements that result in the release the Zn^{2+} ion coordinated by the dimer interface, bury the TA-protein binding hydrophobic groove and turn Get3 into an ATP-independent holdase (Voth et al. 2014) (**Fig. 7**). This conformational rearrangement is reversible upon restoration of reducing conditions and Zn^{2+} is present in the medium. Interestingly, Get3 can form tetramers and high-order oligomers under oxidative conditions. Moreover, Get3 ATPase activity is severely reduced upon oxidation stress conditions (**Fig. 7**) (Voth et al. 2014).

1.3.3. Mammalian TRC pathway

Most of the proteins of the yeast GET pathway are conserved in mammals (except Get2 that has a functional ortholog in CAML). Therefore, the pathway is conserved and is known as the TRC pathway. Interestingly, the TRC pathway includes

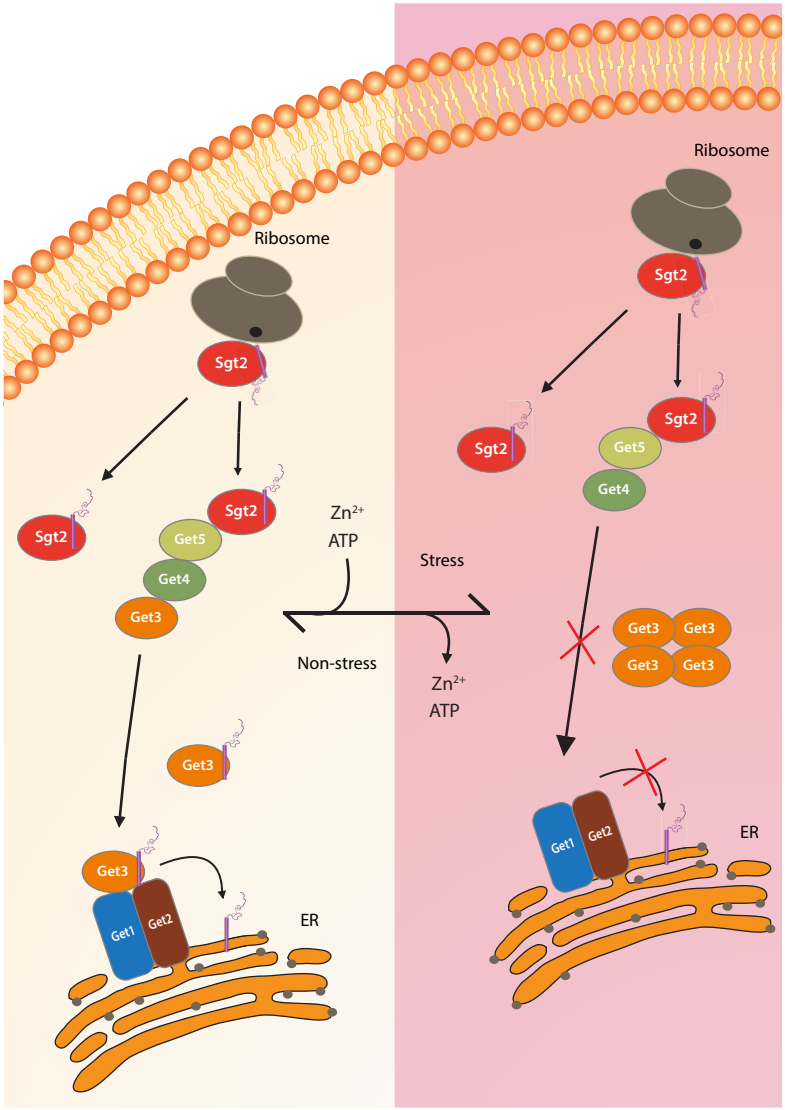

Figure 7. Get3 can act as a redox-regulated chaperone. Get3 has been reported to be a redox-regulated chaperone *in vitro* (Voth et al. 2014). Upon stress like oxidation or ATP depletion, Get3 releases the Zn^{2+} ion coordinated by the dimer and the loaded ATP and undergoes conformational changes. This structural reorganization involves the burying of the ATPase pocket and the TA-binding groove. Get3 forms higher oligomer species, being tetramers the most abundant ones. This switch is reversible, upon non-oxidative conditions and in presence of Zn^{2+} and ATP Get3 recovers its ATPase activity and its conformation. According to the model, under stress conditions Get3 chaperone could not target TA-proteins to the Get1/2 receptor due to the inaccessibility of the TA-binding groove.

BAG6, that is a protein not present in yeast (Leznicki et al. 2010; Mariappan et al. 2010) but later in evolution (Mock et al. 2017). Homologs or functional orthologs between the yeast GET pathway and the mammalian TRC pathway are enlisted in the following **Table 1**.

Table 1. Components of the GET/TRC pathways.

	Yeast	Mammals
Pre-targeting complex	-	BAG6
	Sgt2	SGTA
	Get5	UBL4A
	Get4	TRC35
Cytoplasmic ATPase effector	Get3	TRC40
Receptor	Get2	CAML
	Get1	WRB

The pathway is conserved as little difference exist between the GET pathway and the TRC pathway. First, BAG6 is thought to interact with the ribosome, along with TRC35 and UBL4A, and bind nascent substrates after their release from the ribosome (Mariappan et al. 2010). Second, TRC35 and UBL4A do not directly interact, in contrast to yeast where Get4 and Get5 directly interact (Mock et al. 2015). This is due to the fact that the Get4 β-loop that was involved in the Get4-Get5 interaction interface is missing in TRC35 (Chartron et al. 2010). The Get4 β-loop is only present in yeast but not in other Opisthokonta (Mock et al. 2017). Additionally, the N-terminal domain of Get5 is not present in UBL4A, so the interaction between Get4 and Get5 cannot happen in either way (Chartron et al. 2010; Mock et al. 2015). Instead, UBL4A and TRC35 bind to BAG6, which serves as a scaffolding protein. TRC35 interacts with the region of BAG6 containing the nuclear localization sequence (NLS) masking it and UBL4A docks on the BAG domain of BAG6 (Mock et al. 2015; Kuwabara et al. 2015; Mock et al. 2017) (**Fig. 8A**). Subsequently, SGTA is recruited, via the UBL domain, to either BAG6 or UBL4A (preferentially this last one) (Xu et al. 2012; Leznicki et al. 2013; Darby et al. 2014) (**Fig. 8A**). Therefore, BAG6 is the pre-targeting-complex cornerstone protein. In fact, a truncated version of BAG6 containing just the C-terminal domain (comprising the BAG6 and NLS domains) is sufficient for the *in vitro* handover of a TA-protein to TRC40 (Mock et al. 2015; Shao et al. 2017). A more detailed description of the components of the TRC pathway is described in the following lines.

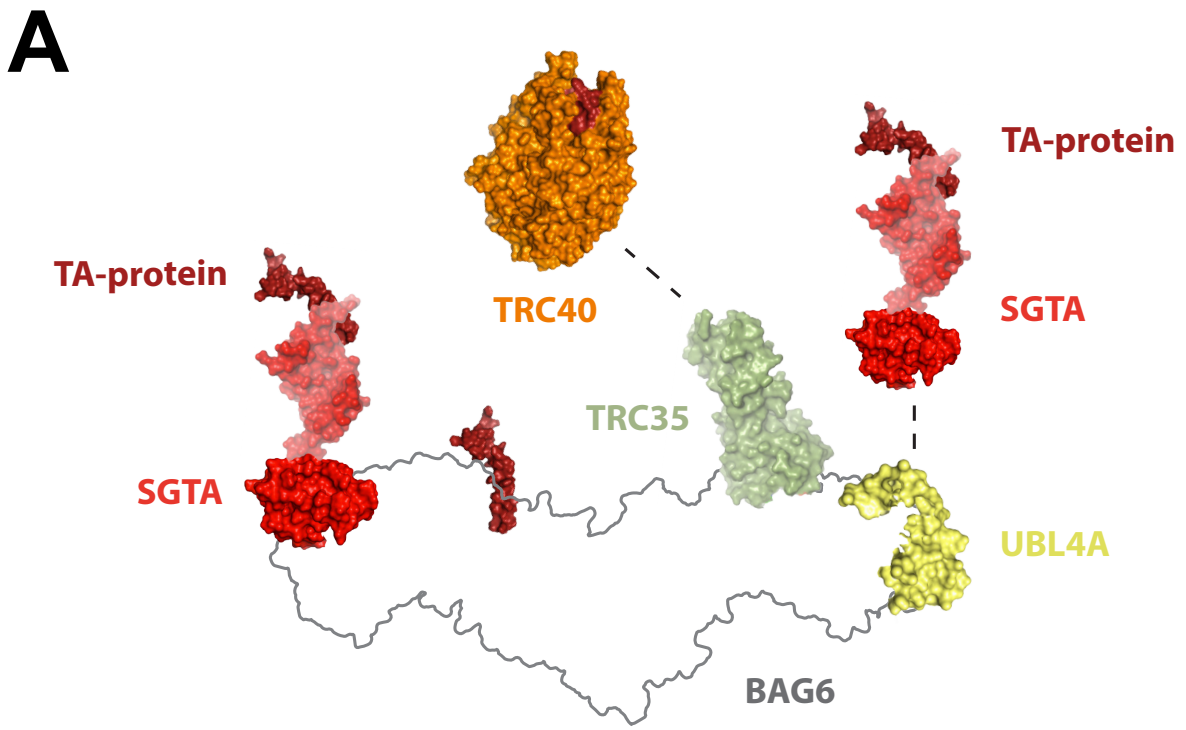

Figure 8. Pre-targeting complex of the TRC pathway. (A) Scheme illustrating the BAG6 heterotrimeric complex and its interactions with SGTA and TRC40. The PDB IDs are the following: Get3 (4XTR), TA-protein (2LPF), SGTA (4CPG, 5LYP), TRC35 (6AU8), UBL4A (4X86). TRC40 is represented with the Get3 protein structure and BAG6 is depicted as a silhouette due to the lack of reported structure for both.

1.3.3.1. TRC40

TRC40 is the human homolog of yeast Get3 and is also known as ASNA1. TRC40 shares 46% identity to Get3 (Bhattacharjee, Ho, and Rosen 2001; Shen et al. 2003). TRC40 heterozygous mice (Asna1$^{+/-}$) presented a similar phenotype as the wild-type (wt) whereas the TRC40 homozygous mice (Asna1$^{-/-}$) showed early embryonic lethality between E3.5 and E8.5 (E stands for embryonic day) (Mukhopadhyay et al. 2006). In contrast, two TRC40-knockout pancreatic β-cells and pancreatic epithelial cells showed impaired retrograde transport (plasma membrane-to-*trans*-Golgi network and Golgi-to-ER), hypoinsulinemia, impaired insulin secretion and pancreatic agenesis due to perturbation of pancreatic progenitor differentiation (Norlin et al. 2016; Norlin, Parekh, and Edlund 2018). Likewise, it was reported that TRC40 favorably regulated

insulin secretion in *Caenorhabditis elegans* and mammalian cells (Kao et al. 2007). The knockdown of TRC40 increases the sensitivity to arsenite and chemotherapy platinating agents (such as cisplatin, carboplatin or oxaliplatin) in *C.elegans*, ovarian cancer and melanoma cells (Hemmingsson, Zhang, et al. 2009; Hemmingsson, Nöjd, et al. 2009; Hemmingsson et al. 2010).

TRC40 was found to be the cytoplasmic factor involved in TA-protein targeting in mammalian cells (Stefanovic and Hegde 2007; Favaloro et al. 2008). Additionally, TRC40 was also found to be involved in the delivery of short secretory proteins, such as apelin and statherin, to the Sec61 translocon (Johnson et al. 2012). Interestingly, the knockdown of either BAG6 or TRC40 lead to an accumulation of ubiquitinated proteins (Q. Wang et al. 2011; Akahane et al. 2013) and to defects in the core proteasome assembly (Akahane et al. 2013; Sahara et al. 2014). Interestingly, TRC40 has been found necessary for the efficient release of herpes simplex virus 1 virions (Ott et al. 2016).

1.3.3.2. WRB

WRB was identified while mapping the chromosome region connected to congenital heart disease of Down syndrome patients (Egeo et al. 1998). The down-regulation of WRB has been reported to cause severe heart disorder and eye and heart abnormalities in medaka fish (Murata et al. 2009). Likewise, WRB has been found to associate to CASZ1, a transcription factor, during cardiac morphogenesis and they are essential to maintain tissue integrity (Sojka et al. 2014). WRB was reported to be the ER-membrane receptor for the TRC pathway (Vilardi, Lorenz, and Dobberstein 2011). It has been suggested that WRB and Get1 belong to the Oxa1 superfamily. This superfamily would contain the evolutionary conserved members Oxa1/Alb3/YidC that mediate membrane protein biogenesis in different organelles (Anghel et al. 2017). WRB and CAML are suggested to act as an insertase for inserting TA-proteins into ER-membrane (F. Wang et al. 2011; Y. Yamamoto and Sakisaka 2012; reviewed in Y. Yamamoto and Sakisaka 2015). The first two Get1/WRB helices form a coiled-coil, localized in the cytoplasmic domain of Get1/WRB (Stefer et al. 2011). This coiled-coil

domain of WRB is the one interacting with the DELYED motif on Get3/TRC40 (Mariappan et al. 2011; Stefer et al. 2011; F. Wang et al. 2011). Several WRB-knockout animals were generated and caused synaptic hearing impairment, demonstrating how WRB is essential in inner-ear hair cells in zebrafish (Lin et al. 2016; Vogl et al. 2016) and in mice (Vogl et al. 2016). Furthermore, WRB loss caused impairment of the synaptic transmission in photoreceptors in zebrafish (Daniele et al. 2016; Lin et al. 2016). TA-protein biogenesis was affected in a cardiomyocyte-specific and a hepatocyte-specific WRB-knockouts (Rivera-Monroy et al. 2016).

1.3.3.3. CAML

CAML was firstly identified as a cyclophilin B interactor in calcium signaling after a yeast two-hybrid screen (Bram and Crabtree 1994). WRB and CAML were reported to act as an insertase for inserting TA-proteins into ER-membrane (F. Wang et al. 2011; Y. Yamamoto and Sakisaka 2012) and to be sufficient to mediate the insertion of TA-proteins (Vilardi et al. 2014). A RERR motif present in the first helix of the cytoplasmic domain of Get2 is responsible of the interaction with the DELYED motif of Get3 (Mariappan et al. 2011; Stefer et al. 2011; F. Wang et al. 2011). The RERR motif is not present in CAML, instead a RRRK motif at the N-terminus is responsible for binding TRC40 (Y. Yamamoto and Sakisaka 2012; Y. Yamamoto and Sakisaka 2015). CAML was shown to be involved in epidermal growth factor (EGFR) and p56 Lck signaling and has been reported to be necessary for the survival of specialized immune cells (Tran et al. 2005; Zane et al. 2012; Chan et al. 2015). CAML-knockout mouse embryonic fibroblasts present chromosome instability and anaphase failure (Yu Liu et al. 2009). In contrast, CAML-knockout mouse presented early embryonic lethality (Tran et al. 2003). Interestingly, an inner-ear hair cells specific CAML-knockout resulted in deafness in mice (Bryda et al. 2012) in a similar line as reported for WRB-knockout animals (Lin et al. 2016; Vogl et al. 2016).

1.3.3.4. BAG6

BAG6, also known as BAT3 or Scythe, is a nucleo-cytoplasmic protein that was mapped in chromosome 6 (Spies et al. 1989). It belongs to the BAG-family of antiapoptotic proteins that share a BAG domain (reviewed in Behl 2016). BAG6 contains a UBL domain at the N-terminus (Banerji et al. 1990). This UBL domain can interact with other proteins such as SGTA (Leznicki et al. 2013; Darby et al. 2014), gp78 (Q. Wang et al. 2011), RNF126 (Rodrigo-Brenni, Gutierrez, and Hegde 2014), etc. Also in the N-terminus of BAG6, is the BUILD domain where short hydrophobic segments can be recognized (H. Tanaka et al. 2016). BAG6 has a DEQD canonical cleavage site that can be cleaved by caspase-3 and subsequently triggering apoptosis (Y.-H. Wu, Shih, and Lin 2004; Preta and Fadeel 2012). BAG6 carries a NLS that enables it to translocate into the nucleus (Manchen and Hubberstey 2001). TRC35 interacts with this NLS region (Mock et al. 2015; Mock et al. 2017). Finally, the BAG domain that characterizes the BAG-family can be found at the C-terminus (Thress et al. 2001). The BAG domain has been reported to modulate the activity of molecular chaperones Hsp70 (reviewed in Kabbage and Dickman 2008). However, unlike the other members of the BAG-family, the BAG domain of BAG6 cannot interact with the nucleotide binding domain of Hsp70 (Mock et al. 2015). UBL4A interacts with the BAG domain of BAG6 (Mock et al. 2015; Kuwabara et al. 2015). The UBL domain is conserved from invertebrates whereas the BAG domain is only present in vertebrates but not in invertebrates (Kawahara, Minami, and Yokota 2013).

Different than TA-protein targeting, BAG6 has been reported to have a relevant role in protein quality control of mislocalized secretory and membrane proteins (MLPs) (Minami et al. 2010; Hessa et al. 2011; Leznicki and High 2012; Leznicki et al. 2013; Wunderley et al. 2014; Rodrigo-Brenni, Gutierrez, and Hegde 2014). BAG6 has been extensively linked to the ubiquitin-proteasome system. SGTA-BAG6 interplay with hydrophobic substrates to determine the fate of these substrates. BAG6 has been shown to recruit RNF126, a cytoplasmic E3 ubiquitin ligase, that can ubiquitylate MLP substrates (Zhi et al. 2013; Rodrigo-Brenni, Gutierrez, and Hegde 2014; Krysztofinska et al. 2016). Thus, BAG6 is thought to promote protein degradation (Leznicki and High 2012). BAG6 downregulation leads to accumulation of ubiquitinated proteins (Q. Wang et al. 2011; Akahane et al. 2013) and to defects in the assembly of the proteasome (Akahane et al. 2013; Sahara et al. 2014). It has been reported that BAG6 can interact

with the proteasome receptor subunit PSMD4 or Rpn10 (Kikukawa et al. 2005; Minami et al. 2010; Hessa et al. 2011).

Nevertheless, BAG6 is connected to more protein quality control processes. It was reported that BAG6 can also play a role in regulating the degradation of polytopic ERAD substrates (Payapilly and High 2014). BAG6 was found to chaperone translocated ERAD-substrates (Q. Wang et al. 2011). Likewise, BAG6 was reported to collaborate in the dislocation of misfolded glycopeptides (Claessen and Ploegh 2011). Furthermore, Ubiquilin-4 (UBQLN4) and BAG6 interact and cooperate in the recognition of defective newly synthesized polypeptides (Suzuki and Kawahara 2016). Additionally, BAG6 has been reported to mediate substrate-degradation in preemptive quality control (pQC) required for the maintenance of ER homeostasis (Kadowaki et al. 2015).

BAG6 heterotrimeric complex was found to translocate into the nucleus upon DNA damage. It is believed to be part of the DNA damage response (DDR) pathway (Krenciute et al. 2013). Constitutive BAG6 knockout in mice is embryonically lethal and causes developmental defects in several organs (Desmots et al. 2005; Sebti et al. 2014). BAG6 can interact and form a complex with the acetyl-transferase p300 (Sasaki et al. 2007). The interaction between BAG6-p300 enhances the acetylation of p53 and thus p53 transcriptional activity (Sasaki et al. 2007). BAG6 modulates the nucleo-cytoplasmic localization of p300 (Sebti et al. 2014) and regulates autophagy via p300-mediated acetylation of p53 upon starvation. In contrast, BAG6 inhibits the p300-mediated acetylation of ATG7 (Sebti et al. 2014).

1.3.3.5. SGTA

SGTA is a tetratricopeptide repeat (TPR)-containing protein which contains three TPRs (Lamb, Tugendreich, and Hieter 1995; Kordes et al. 1998; Blatch and Lässle 1999). TRP-containing proteins have been shown to interact with the EEVD motif of molecular chaperones like Hsp70 and Hsp90 (S. Chen et al. 1998; Scheufler et al. 2000). Additional to TA-protein targeting, SGTA has been described to have an

important role in protein quality control of MLPs (Hessa et al. 2011; Leznicki et al. 2013; Rodrigo-Brenni, Gutierrez, and Hegde 2014; Wunderley et al. 2014). Opposite to BAG6, SGTA was reported to promote deubiquitylation (Leznicki and High 2012; Wunderley et al. 2014). In fact, SGTA interacts with the proteasomal ubiquitin receptor Rpn13 modulating quality control (Leznicki et al. 2015; Thapaliya et al. 2016). Rpn13 has been reported to bind the deubiquitinase UCH37 (UCHL5) and it has been speculated that this could revert the fate of ubiquitylated-proteins chaperoned by SGTA (Sahtoe et al. 2015; Vander Linden et al. 2015). SGTA was reported to help BAG6 chaperoning ERAD-translocated substrates (Xu et al. 2012). Additionally, SGTA was found to interact with Hsp70 and DNAJC5 in neurons and to have a role in synaptic transmission. Over-expression of SGTA in hippocampal neurons results in impaired synaptic transmission (Tobaben et al. 2001) and SGTA-knockout mouse showed reduced body size and decrease the offspring viability (Philp et al. 2016).

1.3.3.6. TRC35

TRC35, also known as GET4, CEE or C7orf20, was identified as a conserved gene during evolution (Fernandes et al. 2008). TRC35, apart from TA-protein targeting, was reported to shuttle as a part of a complex with UBL4A and BAG6 into the nucleus upon DNA damage where they are believed to be part of the DDR pathway (Krenciute et al. 2013). TRC35 has been reported to regulate the nuclear-cytoplasmic distribution of BAG6 (Q. Wang et al. 2011; Mock et al. 2017) by binding the NLS of BAG6 and therefore masking it (Mock et al. 2015; Mock et al. 2017). BAG6 prevents the RNF126-mediated ubiquitylation and subsequent degradation of TRC35 (Mock et al. 2017).

1.3.3.7. UBL4A

UBL4A, also known as GdX, was identified in the 1980s (Toniolo, Persico, and Alcalay 1988; Yang, Skaletsky, and Wang 2007). Apart from TA-protein targeting, UBL4A has been reported to be involved in Akt signaling by promoting Arp2/3-dependent actin branching (Yu Zhao et al. 2015). Moreover, UBL4A was also involved

with STAT3 signaling (Y. Wang et al. 2014). UBL4A was found to translocate into the nucleus, along with TRC35 and BAG6, upon DNA damage and are also believed to be part of the DDR pathway (Krenciute et al. 2013). UBL4A-knockout mice were generated (Y. Wang et al. 2012; Y. Wang et al. 2014; Yu Zhao et al. 2015; Liang et al. 2018) and show that UBL4A null mice presented (i) increased neonatal mortality and defects in the liver synthesis of glycogen (Yu Zhao et al. 2015); (ii) perturbed genes related to osteogenesis and chondrogenesis leading to dysregulation of these processes (Liang et al. 2018).

1.3.4. Redundancy in the insertion pathways

Several studies have suggested the existence of other post-translational pathways operating in the ER-targeting of TA-proteins (**Fig. 9, Fig. 10**). Some of these pathways overlap in their substrate spectra and may compensate in the targeting of certain TA-proteins. The following pathways are described in the literature:

1.3.4.1. EMC pathway

In a recent study, calmodulin (CaM) was identified to interact with the TA-protein squalene synthase (SQS) (Guna et al. 2018). SQS is a TA-protein that presents a TMD with moderate hydrophobicity. CaM was found to shield TA-proteins with low-hydrophobic TMDs (Guna et al. 2018) (**Fig. 10E**). Likewise, CaM was reported to interact with TA-proteins in another study (Haßdenteufel et al. 2011). In addition, CaM was also shown to bind hydrophobic regions (Shao and Hegde 2011). CaM was proposed to deliver the TA-protein to the ER membrane protein complex (EMC). Interestingly, EMC was found to be an ER-insertase for moderately hydrophobic TMDs (Guna et al. 2018) (**Fig. 10E**). In contrast, CaM was shown to inhibit the ER-insertion of certain TA-proteins in an insertion assay using rabbit reticulocyte lysate (RRL) and rough microsomes (RMs) (Haßdenteufel et al. 2011). Some TA-proteins were shown to have partial dependence on the EMC pathway and in the TRC pathway (Guna et al.

2018). Based on those results, the authors proposed an approximate point where both pathways might overlap around the Sec61β TMD hydrophobicity (Guna et al. 2018).

1.3.4.2. PEX pathway

This pathway is responsible of peroxisomal membrane proteins (PMPs) targeting to the ER-membrane or to preexisting peroxisomes (Jones, Morrell, and Gould 2004; reviewed in Mayerhofer 2016). Peroxin-19 (PEX19) is the cytoplasmic factor that recognizes a peroxisomal targeting sequence (PTS) (Gould et al. 1989; Swinkels et al. 1991) in the PMPs and targets them to the receptor PEX3 (Muntau et al. 2003; Fang et al. 2004; Jones, Morrell, and Gould 2004; Yuqiong Liu, Yagita, and Fujiki 2016) (**Fig. 9A, Fig. 10D**). PEX3 is a membrane protein localized in the ER and peroxisomes (Toro et al. 2007; Aranovich et al. 2014; Mayerhofer et al. 2016; Schrul and Kopito 2016). The pathway is conserved in yeast and mammals. There are seven PMPs that are TA-proteins (**Table 17**). The PMPs TA-proteins are targeted to peroxisomes using this pathway. However, Pex15p is targeted using the GET pathway in yeast (van der Zand, Braakman, and Tabak 2010). In contrast, the insertion of the functional homolog of Pex15p in mammals, PEX26, is TRC-independent (Halbach et al. 2006; Yagita, Hiromasa, and Fujiki 2013; Buentzel et al. 2015). The presence of PTS and basic residues following the TMD are responsible for the PEX19-targeting of the PMP TA-proteins (Yagita, Hiromasa, and Fujiki 2013).

1.3.4.3. SND pathway

The SRP-independent targeting (SND) pathway was recently described in yeast (Aviram et al. 2016). SND components described were the cytoplasmic Snd1 and the ER-resident proteins Snd2 and Snd3 (**Fig. 9B**). Snd1 was predicted to bind the RNC (Fleischer et al. 2006) whereas Snd2 and Snd3 are found in a complex with the translocon (Aviram et al. 2016). The SND pathway predominantly targets membrane proteins whose transmembrane segments are in the middle of the protein. The SND pathway has been shown to compensate for the loss of the SRP pathway and the GET

pathway (Aviram et al. 2016), acting as a rescue pathway. In mammals, Snd2 (also known as TMEM208), homolog of the homonym yeast protein, is the only conserved protein from the yeast SND pathway. So far, there are no reported pathway-partners for Snd2 (**Fig. 10F**) (Yuanbo Zhao et al. 2013; Haßdenteufel et al. 2017).

1.3.4.4. Ubiquilins

Ubiquilins (UBQLN1-4) were reported to be able to chaperone mitochondrial membrane proteins in cytoplasm (Itakura et al. 2016). Mitochondrial TA-proteins are suitable to be UBQLN-substrates (**Fig. 10A**). In addition, they can also triage these membrane proteins and target them for degradation (Itakura et al. 2016).

1.3.4.5. Hsp40/Hsc70

In a reconstituted system, Hsp40/Hsc70 are able to promote the membrane-insertion of TA-proteins (B. M. Abell et al. 2007; Rabu et al. 2008). However, when tested in HeLa cells in the presence of selective inhibitors of Hsp40/Hsc70 only a small subset of TA-proteins, characterized by low hydrophobicity in their TMDs, was affected (Rabu et al. 2008) (**Fig. 9D, Fig. 10B**).

1.3.4.6. SRP pathway

VAMP2 and Sec61β *in vitro* insertion was reported to be SRP-dependent in a post-translational manner (Benjamin M. Abell et al. 2004; B. M. Abell et al. 2007). Likewise, SRα-downregulated HeLa M cells showed a decrease of SERP1 and Sec61β steady-state levels (Casson et al. 2017). This would suggest that some TA-protein might require the SRP pathway to be targeted to the ER (Casson et al. 2017) (**Fig. 10G**). Interestingly, Get4-Get5 have been shown to compete for co-translationally-inserted substrates with SRP in a Sgt2-independent way (Zhang et al. 2016).

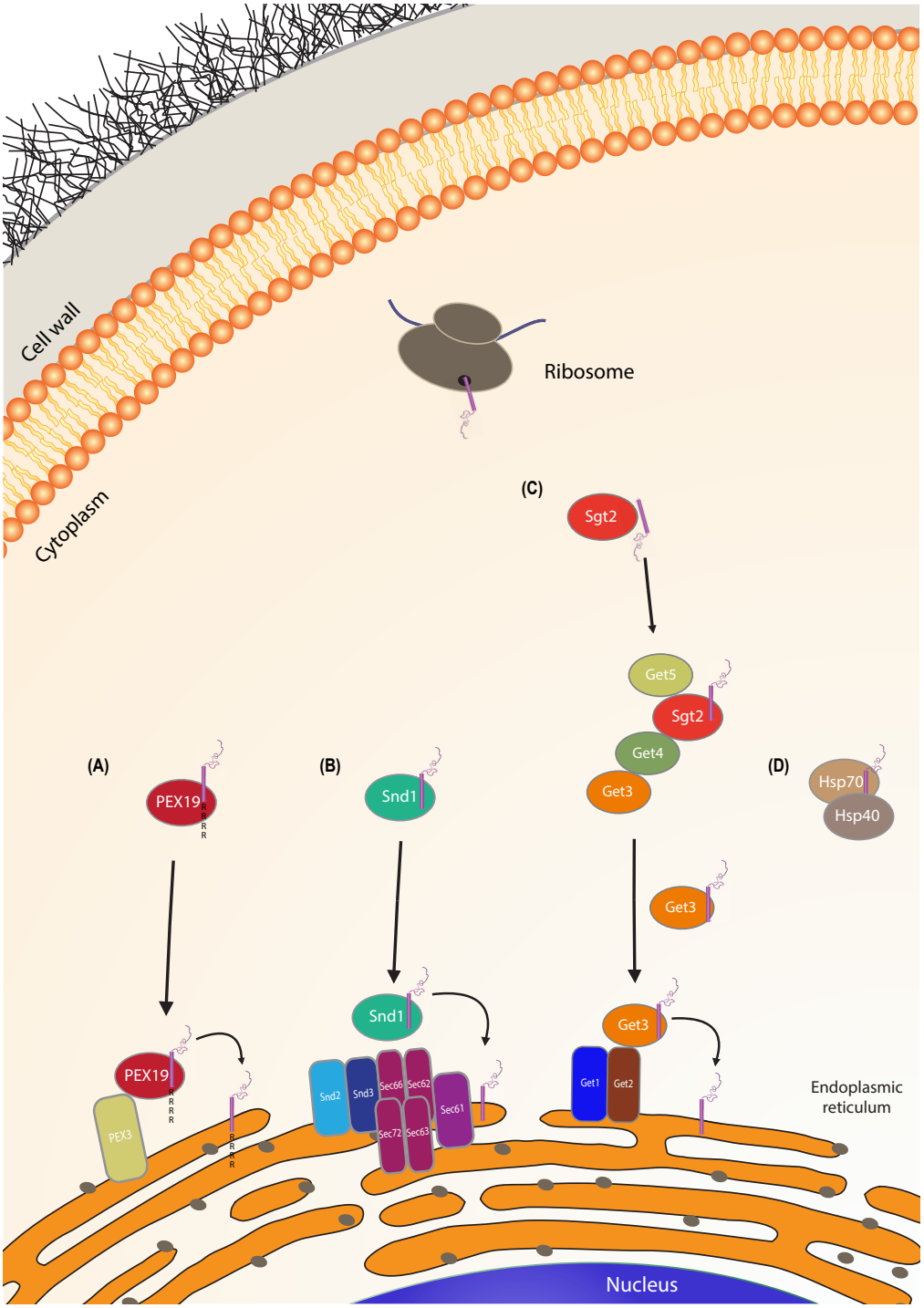

Figure 9. Tail-anchored protein insertion pathways in yeast. (A) Pex19 targets PMPs that are TA-proteins with basic residues in its C-terminal tail to its receptor Pex3. Pex3 can be localized in ER or peroxisomes. **(B)** In the SND pathway, Snd1 can take TA-proteins to its receptor Snd2/Snd3 that forms a complex Sec66, Sec62, Sec72, Sec63 and Sec61. **(C)** The GET pathway begins when Sgt2 grabs the TA once exits the ribosome, it binds the pre-targeting complex composed of Get4 and Get5 and it hands the TA off to Get3. Get3 is the cytoplasmic factor that carries the protein to the Get1/Get2 ER-receptor and it releases it in an ATP-dependent manner. The receptor is an insertase that inserts the protein into the ER. **(D)** Hsp70/Hsp40 have been proposed as alternative cytoplasmic factors that can hold TA-proteins. TA-protein model is PLN (PDB ID: 2LPF).

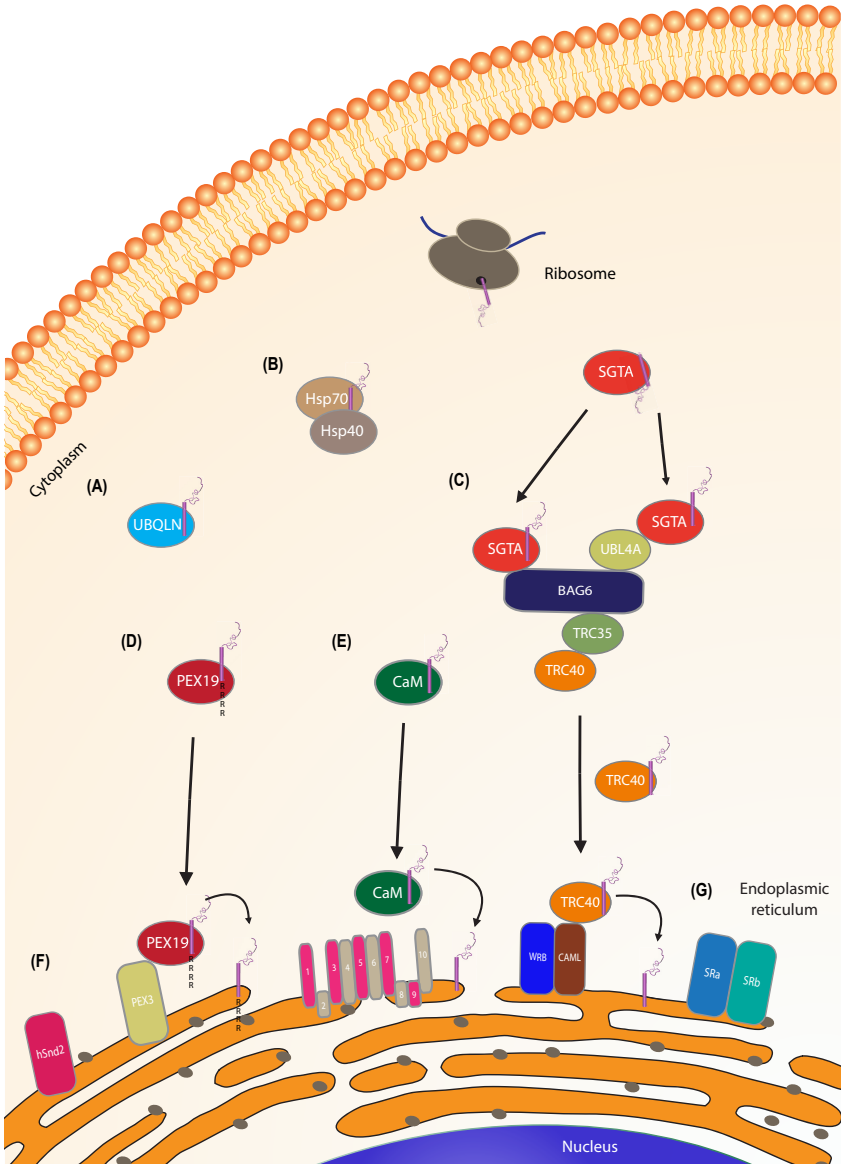

Figure 10. Tail-anchored protein insertion pathways in mammals. (A) Ubiquilins are believed to target mitochondrial TA-proteins. **(B)** Hsp70/Hsp40, in a similar fashion to yeast, have hypothetically been proposed as alternative cytoplasmic factors that can hold TA-proteins. **(C)** The TRC pathway is analog to the Get pathway in yeast but with the addition of the mammalian protein BAG6. SGTA grabs the TA once exits the ribosome, it binds the pre-targeting complex composed of BAG6, UBL4A and TRC35 and it hands the TA off to TRC40. TRC40 is the cytoplasmic factor that carries the protein to the WRB/CAML ER-receptor and it releases it in an ATP-dependent manner. The receptor is an insertase that inserts the protein into the ER. **(D)** The PEX19 pathway is analog to the one in yeast. PEX19 targets PMPs that are TA-proteins with basic residues in its C-terminal tail to its receptor PEX3 such as PEX26. PEX3 can be localized in ER or peroxisomes. **(E)** Calmodulin can target TA-proteins that contain a TMD with low hydrophobicity to the ER membrane protein complex (EMC) that is formed by 10 subunits. **(F)** Snd2, homolog of the homonym yeast protein, is the only conserved protein in mammals of the yeast SND pathway. There are no reported pathway-partners for Snd2. **(G)** Some TA-protein might require the SRP pathway to be post-translationally targeted to the ER. TA-protein model is PLN (PDB ID: 2LPF).

1.3.4.7. Unassisted insertion of TA-proteins

Cytochrome b5 (Cytb5) is a TA-protein that is localized at the ER-membrane. It was the first TA-protein studied (Anderson, Mostov, and Blobel 1983). Cytb5 has a low-hydrophobicity TMD. It has been reported that can be inserted into protein-free liposomes in an unassisted-manner (Yabal et al. 2003; Brambillasca et al. 2005; Brambillasca et al. 2006; Sara F. Colombo, Longhi, and Borgese 2009). In addition, it might require Hsp40/Hsc70 chaperoning (Rabu et al. 2008). In a similar line, Cytb5 has been reported not to require the TRC pathway for ER-targeting (Stefanovic and Hegde 2007; Favaloro et al. 2008). Cytb5 localized in MOM in cytosol-free semipermeabilized cells (Figueiredo Costa et al. 2018). Therefore, it was proposed that MOM might be the default destination of TA-proteins able to be inserted in an unassisted-manner (Figueiredo Costa et al. 2018).

1.4. Glucocorticoid receptor signaling

Glucocorticoids are a class of steroid hormones that are produced by the adrenal cortex under a strong regulation of the hypothalamic-pituitary-adrenal gland axis (reviewed in Vandevyver, Dejager, and Libert 2014). They are involved in a broad variety of processes such as inflammatory and immune responses, development, reproduction, metabolic homeostasis, etc. Glucocorticoids interact with their intracellular receptor called glucocorticoid receptor (GR) (**Fig. 11**). GR belongs to the steroid-hormone receptor (SR) family (reviewed in Whitfield et al. 1999). GR predominantly localizes in cytoplasm in the absence of ligand but it is continuously shuttling between the cytoplasm and the nucleus (Madan and DeFranco 1993; Guiochon-Mantel et al. 1994). In the cytoplasm, the GR is part of a multimeric complex composed of heat-shock proteins (e.g. Hsp40, Hsp70 and Hsp90) and TPR-containing proteins (e.g. Hop, SGTA, Chip, FKBP52, FKBP51, Hip among others) (S. Chen et al. 1998; S. Chen and Smith 1998; Hernández, Chadli, and Toft 2002; Paul et al. 2014; reviewed in Cheung and Smith 2000; reviewed in Smith 2004). The stimulation of the GR with a glucocorticoid receptor agonist results in a conformational rearrangement that exposes two nuclear localization signals (NLS) (Picard and Yamamoto 1987). This

conformational change remodels the chaperone complex and leads to the association of FKBP52 that interacts with dynein to drive the GR along microtubules to the nucleus (Davies, Ning, and Sánchez 2002; Harrell et al. 2004). GR is translocated to the nucleus after interaction with importins (Guiochon-Mantel et al. 1991; Haché et al. 1999; M. Tanaka et al. 2003; Freedman and Yamamoto 2004). GR homodimerizes and binds to specific DNA regions called glucocorticoid response elements (GREs). These GREs are located in the promoter region of glucocorticoid-regulated genes (Beato 1989; Del Monaco et al. 1997; Meijsing et al. 2009; Surjit et al. 2011). Then, GR can interact with other coactivators/corepressors and regulate the expression of glucocorticoid-responsive genes (Phuc Le et al. 2005; Surjit et al. 2011).

GR presents different domains in its structure. At the N-terminus sits the N-terminal domain (NTD). The NTD contains AF1 that is required for maximal transcription activation (Dieken and Miesfeld 1992). In the central portion of the protein is located the so-called DNA-binding domain (DBD). The DBD contains two zinc fingers that recognize the GREs and also contains the homodimerization motif (Härd et al. 1990; Luisi et al. 1991; Watson et al. 2013). Glucocorticoids interact with the ligand-binding domain (LBD) that is located towards the C-terminus of the protein (reviewed in Vandevyver, Dejager, and Libert 2014). A hinge region links the DBD with the LBD. Hsp90 was reported to bind the LBD due to its elevated hydrophobicity (Bresnick et al. 1989; Picard et al. 1990; Ricketson et al. 2007).

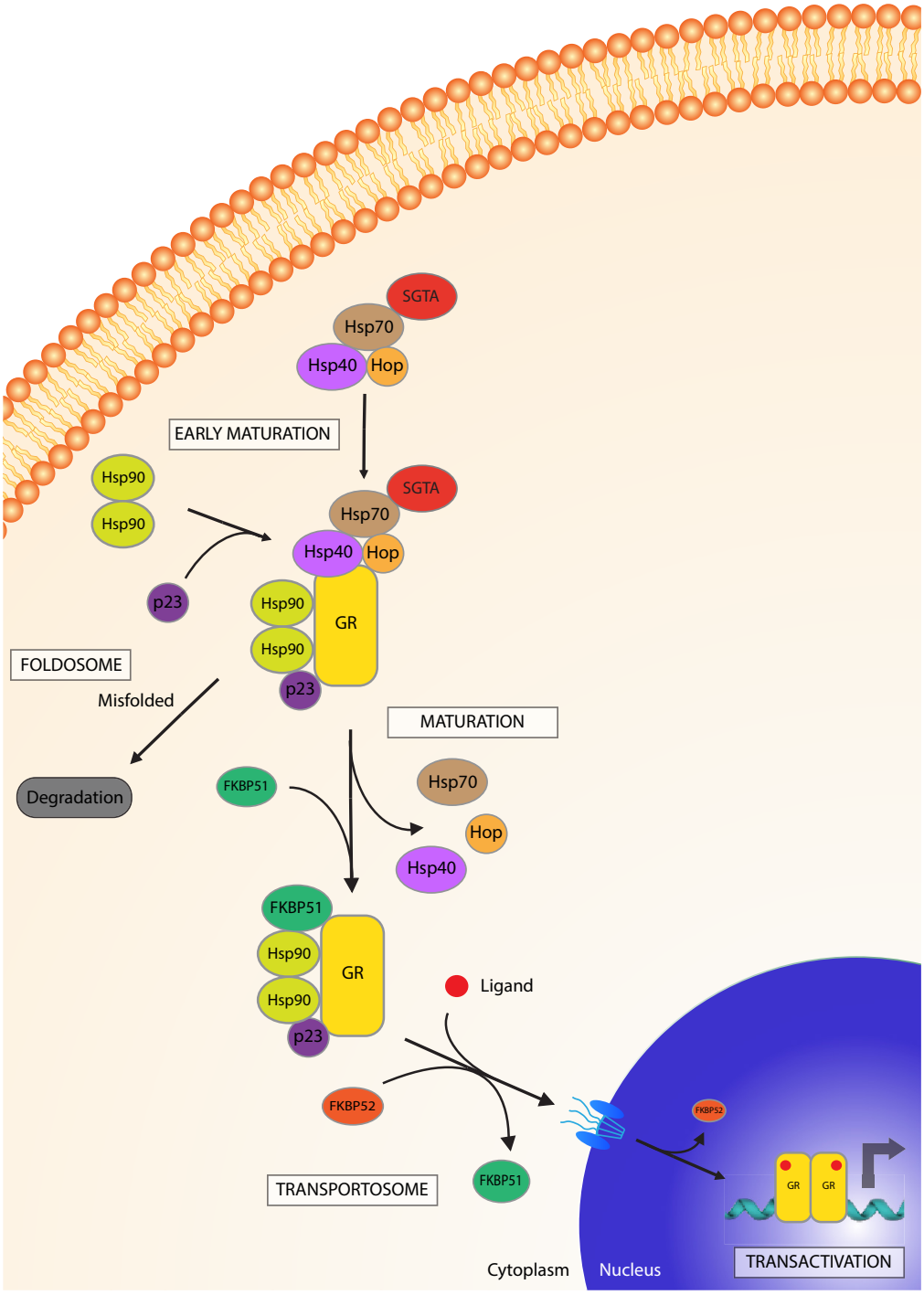

Figure 11. Glucocorticoid receptor signaling pathway. The GR is kept soluble in cytoplasm by a chaperone machinery composed by several proteins from the heat shock proteins (Hsps) as Hsp40, Hsp70, Hsp90 and TPR-containing proteins like p23, SGTA and Hop. Once the protein is mature it gets rid of Hsp70, Hsp40 and Hop and FKBP51 binds, this form is ready to bind the ligand and get activated. The ligands can diffuse through the plasma membrane and get into the cytoplasm. In the presence of the ligand, FKBP52 interacts with the GR and FKBP51 exits the complex. Once bound to FKBP52, the GR can shuttle into the nucleus, it dimerizes and binds to the glucocorticoid response elements (GREs) in the DNA through which the GR mediates the transactivation or transrepression of several genes. Adapted from (Cato et al. 2014).

1.5. Aims

- The first aim of this study is to explore the role of several functional domains of TRC40 in targeting TA-proteins targeting to ER-membrane and chaperoning *in vivo* in mammalian cells.

- The second aim of this study is to investigate the dependence of TA-proteins on the TRC pathway at the steady-state *in vivo* in mammalian cells. Recently, several post-translational pathways for TA-protein targeting have been described, but little is known about TRC-dependence in mammalian cells *in vivo*.

- Yeast Get3, TRC40 homolog, was characterized by Voth *et al*. to have an alternative role as a redox-regulated chaperone. Almost nothing is known about the redox behavior of TRC40, which shares homology with yeast Get3. My aim was to investigate the redox behavior of TRC40 *in vitro* to elucidate whether it can act as a redox-regulated chaperone as well as to explore the behavior of TRC40 under oxidative conditions *in vivo* in human cell lines. This study is interested in the identification of putative substrates of this potential TRC40 chaperone.

2. Material and Methods

2.1. Material

2.1.1. Bacterial strains

Table 2. Bacterial strains used in this study.

Strain	Genotype	Reference
Escherichia coli BL21 (DE3)	F- *ompT gal dcm lon hsdSB(rB- mB-) λ(DE3 [lacI lacUV5- 7 gene 1 ind1 sam7 nin5]*	Novagen. Catalog #: 69450
E. coli ElectroTen blue	Δ(*mcr*A)183 Δ(*mcr*CB*hsd*SMR*mrr*)173 *end*A1 *supE*44 *thi*1 *r ec*A1 *gyr*A96 *rel*A1 *lac* Kan^r [F' *pro*AB *lacI*^{q}ZΔ*M 15* Tn*10* (Tet^r)]	Agilent. Catalog #: 200159

2.1.2. Yeast (*S. cerevisiae*) strains

Table 3. Yeast strains used in this study.

Strain	Genotype	Background	Reference
BY4741	MATa *his3Δ1 leu2Δ0 met15Δ0 ura3Δ0*	S288C	(Brachmann et al. 1998)
BY4741 Δ*get3*	MATa *his3Δ1 leu2Δ0 met15Δ0 ura3Δ0 ydl100c*::KanR	BY4741	(Schuldiner et al. 2008; Jonikas et al. 2009)

BY4741 Δ*get1/2*	MATa *his3Δ1 leu2Δ0 met15Δ0 ura3Δ0 get1*::KanR *get2*::NatR	BY4741	(Schuldiner et al. 2008)
BY4741 Δ*sgt2*	MATa *his3Δ1 leu2Δ0 met15Δ0 ura3Δ0 yor007c*::KanR	BY4741	This study
BY4742	MATα *his3Δ1 leu2Δ0 met15Δ0 ura3Δ0*	S288C	(Brachmann et al. 1998)
BY4742 Δ*get3*	MATα *his3Δ1 leu2Δ0 met15Δ0 ura3Δ0 ydl100c*::KanR	BY4742	This study
K700α	MATα *ade2-1 trp1-1 can1-100 leu2-3,112 his3-11,15 ura3 GAL*$^+$ *psi*$^+$ *ssd1-d2*	W303	Nasmyth, K.
K700α Δ*get3*	MATα *ade2-1 trp1-1 can1-100 leu2-3,112 his3-11,15 ura3 GAL*$^+$ *psi*$^+$ *ssd1-d2 ydl100c*::KanR	K700α	This study

2.1.3. Cell lines

Table 4. Cell lines used in this study.

Strain	Organism	Derived from	Reference
HeLa P4	Human	Epithelial cells from cervix	(Scherer, Syverton, and Gey 1953; Charneau et al. 1994)
Flp-In T-REx 293 Stx5-opsin	Human	Embryonic kidney cells	Invitrogen. Catalog#: R78007

2.1.4. Mouse lines

All the procedures involving animals were reviewed and approved by the Institutional Animal Care and Use Committee of the University Medical Center Göttingen, in compliance with the human care and use of laboratory animals.

Wrb$^{fl/fl}$ line was previously described (Vogl et al. 2016). This mouse line was bred with a Myh6-MerCreMer (B6.FVB(129)-A1cf$^{Tg(Myh6\text{-}cre/Esr1*)1JmK}$/J) that was acquired from the Jackson Laboratory (Stock# 005657). The MerCreMer is an engineered Cre recombinase version composed by the fusion of this protein with two mutant estrogen-receptor (Mer) ligand binding domains (LBD). This engineered Cre recombinase is able to recombine regions flanked with recombinase recognition sequences (loxP sites or fl). The MerCreMer expression is under the control of the α-myosin heavy chain promoter (Myh6), what confines its expression to cardiac tissue (Sohal et al. 2001). *Wrb*$^{fl/fl}$ presents exons two and four flanked by loxP sites (Vogl et al. 2016; Rivera-Monroy et al. 2016). The fusion of the Cre recombinase to the Mer makes Cre a tightly-controlled cytoplasmic protein that only can translocate into the nucleus upon the addition of tamoxifen, that is an agonist/antagonist of the estrogen receptor (Metzger et al. 1995; Schwenk et al. 1998; Sohal et al. 2001). Upon the MerCreMer translocation to the nucleus, Wrb exons 2 to 4 will be excised leaving a truncated non-functional version of Wrb. Hence, the result was a cardio-specific WRB conditional knockout where the WRB is controlled spatial-temporally.

MerCreMer-dependent recombination was induced in six-week old animals by injection of 40 mg/kg of tamoxifen (diluted in ethanol-soybean oil) as previously described (Lexow et al. 2013).

2.1.5. Plasmids

Table 5. Plasmids used in this study.

Internal database ID	Short name	Description	Bacterial marker	Yeast marker	Reference
Z1257	Get3	pQE80-10xHis-2xZZ-TEV-Get3	Amp	-	(Metz et al. 2006)
	His-MBP-TRC40	pQE80-10xHis-MBP-TRC40	Amp	-	Vilardi, F.
AI1730	3GRE-LacZ	pUCΔSS-26X-3GRE-LacZ	Amp	URA3	(Schena and Yamamoto 1988)
AI1729	ratGR	pDS-063-ratGR	Amp	LEU2	(Schena and Yamamoto 1988; Picard et al. 1990)
X1153	p413	p413RS	Amp	HIS3	(Sikorski and Hieter 1989)
AM1926	p413_Get3	pRS413Met25_Get3	Amp	HIS3	
AM1927	p413_Get3_D57E	pRS413Met25_Get3_D57E	Amp	HIS3	
AM1928	p413_Get3_CCCC240,242,285,288TTTT	pRS413Met25_Get3_CCCC240,242,285,288TTTT	Amp	HIS3	
AM1929	p413_Get3_C317T	pRS413Met25_Get3_ C317T	Amp	HIS3	

AM1930	p413_Get3_ CCC36,85,317TTT	pRS413Met25_Get3_ CCC36,85,317TTT	Amp	HIS3	
AM1931	p413_Get3_ CCCCC36,85,285,288,317TTTTT	pRS413Met25_Get3_ CCCCC36,85,285,288,317TTTTT	Amp	HIS3	
AM1932	p413_Get3_ CCCC36,85,240,242TTTT	pRS413Met25_Get3_ CCCC36,85,240,242TTTT	Amp	HIS3	
AM1933	p413_Get3_ CCCCC36,85,240,242,317TTTTT	pRS413Met25_Get3_ CCCCC36,85,240,242,317TTTTT	Amp	HIS3	
AM1934	p413_Get3_I193D	pRS413Met25_Get3_ I193D	Amp	HIS3	
AP2064	mVenus	pVenus-C1	Kan	-	
AP2065	mVenus-TRC40	pVenus-TRC40	Kan	-	Vilardi, F.
AP2089	mVenus-ratGR	pVenus-ratGR	Kan	-	
AJ1798	MBP-TEV-TRC40/ZZ-EMD-op	pQE80_MBP-TEV-TRC40_10xHis-ZZ-EMD-opsin	Amp	-	(Favaloro et al. 2010; Pfaff et al. 2016)
AO2049	pcDNA3.1(-)	pcDNA3.1(-)	Amp	-	Invitrogen
AO2050	pcDNA3.1_cmyc-TRC40	pcDNA3.1(-)_cmyc-siTRC40ins wt	Amp	-	
AP2052	pcDNA3.1_cmyc-TRC40_G46R	pcDNA3.1(-)_cmyc-siTRC40ins_G46R	Amp	-	
AP2054	pcDNA3.1_cmyc-TRC40_D74E	pcDNA3.1(-)_cmyc-siTRC40ins_D74E	Amp	-	

AP2056	pcDNA3.1_cmyc-TRC40_I193D	pcDNA3.1(-)_cmyc-siTRC40ins_I193D	Amp	-	
AP2058	pcDNA3.1_cmyc-TRC40_CC246,248SS	pcDNA3.1(-)_cmyc-siTRC40ins_CC246,248SS	Amp	-	
AP2051	pcDNA3.1_cmyc-TRC40_F15A	pcDNA3.1(-)_cmyc-siTRC40ins_F15A	Amp	-	
AP2057	pcDNA3.1_cmyc-TRC40_Y256F	pcDNA3.1(-)_cmyc-siTRC40ins_Y256F	Amp	-	
AP2061	pcDNA3.1_cmyc-TRC40_L303V	pcDNA3.1(-)_cmyc-siTRC40ins_L303V	Amp	-	
AP2060	pcDNA3.1_cmyc-TRC40_CCCC246,248,289,292SSSS	pcDNA3.1(-)_cmyc-siTRC40ins_CCCC246,248,289,292SSSS	Amp	-	
AP2062	pcDNA3.1_cmyc-TRC40_Y310C	pcDNA3.1(-)_cmyc-siTRC40ins_Y310C	Amp	-	
AQ2106	pcDNA3.1_cmyc-TRC40_E259R	pcDNA3.1(-)_cmyc-siTRC40ins_E259R	Amp	-	
AP2063	pcDNA3.1_cmyc-TRC40_P344S	pcDNA3.1(-)_cmyc-siTRC40ins_P344S	Amp	-	
AQ2108	pcDNA3.1_cmyc-TRC40_P75R	pcDNA3.1(-)_cmyc-siTRC40ins_P75R	Amp	-	
AQ2110	pcDNA3.1_cmyc-TRC40_R189W	pcDNA3.1(-)_cmyc-siTRC40ins_R189W	Amp	-	
AQ2107	pcDNA3.1_cmyc-TRC40_E307R/D308R	pcDNA3.1(-)_cmyc-siTRC40ins_E307R/D308R	Amp	-	
AP2053	pcDNA3.1_cmyc-TRC40_CC53,55SS	pcDNA3.1(-)_cmyc-siTRC40ins_CC53,55SS	Amp	-	

AS2236	pcDNA3.1_cmyc-TRC40_D74E/I193D	pcDNA3.1(-)_cmyc-siTRC40ins_ D74E/I193D	Amp	-	
AS2239	pcDNA3.1_cmyc-TRC40_ D74E/L190D/I193D	pcDNA3.1(-)_cmyc-siTRC40ins_ D74E/L190D/I193D	Amp	-	
AL1886	pOG44	pOG44	Amp	-	Invitrogen Catalog#: V600520
	pcDNA5_Stx5-opsin	pcDNA5/FRT/TO_Stx5-opsin	Amp	-	Rivera-Monroy, J.
AG1603	p413_mCherry-Sbh2	pRS413Met25_mCherry-Sbh2	Amp	HIS3	Vilardi, F.

2.1.6. Primers

The DNA oligos were ordered from Sigma with desalted purification and in dry format. The oligos were HPLC-purified in case they were bigger than 50 bp.

Table 6. DNA oligos used in this study.

Internal database ID	Name	Sequence (5'-3')
JavPR98	XhoI-ratGR-For	ATACTACTCGAGGAATGGACTCCAAA GAATCCTTAGC
JavPR99	ratGR-BamHI-Rev	ATACTAGGATCCTCATTTTTGATGAAA CAGAAGCTTTTTG
JhonPR59	EcoRI-TRC40-For	ATACTAGAATTCATGGCGGCAGGGGT GGCCGG
JhonPR60	TRC40-BamHI-Rev	ATACTAGGATCCCTACTGGGCACTGG GGGGCT
JhonPR61	siTRC40ins-For	TCCCCCTTTATTTCCCAAATGTGCAAC ATGCTGGGCCTGG
JhonPR62	siTRC40ins-Rev	TTGGGAAATAAAGGGGGAGATCTGGT TCTTGATCTGCAT
JhonPR63	XhoI-cMyc-TRC40-For	ATACTACTCGAGATGGAGCAGAAACT CATCTCTGAAGAGGATCTGATGGCGG CAGGGGTGGCC
JavPR70	TRC40_D74E-For	GTGTTCTGATCATCTCCACAGAGCCA GCACACAACATCTCAG
JavPR71	TRC40_D74E-Rev	CTGAGATGTTGTGTGCTGGCTCTGTG GAGATGATCAGAACAC
JavPR72	TRC40_G46R-For	GGATCTTCGTCGGGGGCAAGCGGGG TGTGGGCAAGACCACC
JavPR73	TRC40_G46R-Rev	GGTGGTCTTGCCCACACCCCGCTTGC CCCCGACGAAGATCC

JavPR74	siTRC40ins_I193D-For	CCTGGGCCGGCTTATGCAGGACAAGAACCAGATCTCC
JavPR75	siTRC40ins_I193D-Rev	GGAGATCTGGTTCTTGTCCTGCATAAGCCGGCCCAGG
JavPR86	TRC40_CC246,248SS-For	GCAGACAACTTTCATCAGCGTAAGCATTGCTGAGTTCCTGTCC
JavPR87	TRC40_CC246,248SS-Rev	GGACAGGAACTCAGCAATGCTTACGCTGATGAAAGTTGTCTGC
JavPR138	TRC40_L190D/I193D-For	GGAGCGGGGCCTGGGCCGGGACATGCAGGACAAGAACCAG
JavPR139	TRC40_L190D/I193D-Rev	CTGGTTCTTGTCCTGCATGTCCCGGCCCAGGCCCCGCTCC
JavPR76	TRC40_F15A-For	GGTTGAGGCAGAGGAGGCCGAAGATGCTCCTGATGTGG
JavPR77	TRC40_F15A-Rev	CCACATCAGGAGCATCTTCGGCCTCCTCTGCCTCAACC
JavPR78	TRC40_P75R-For	GTTCTGATCATCTCCACAGACCGAGCACACAACATCTCAGATGC
JavPR79	TRC40_P75R-Rev	GCATCTGAGATGTTGTGTGCTCGGTCTGTGGAGATGATCAGAAC
JavPR80	TRC40_Y256F-For	GCATTGCTGAGTTCCTGTCCCTGTTTGAGACAGAGAGGCTGATCC
JavPR81	TRC40_Y256F-Rev	GGATCAGCCTCTCTGTCTCAAACAGGGACAGGAACTCAGCAATGC
JavPR82	TRC40_Y310C-For	GGACCAGATGGAGGACCTGTGTGAAGACTTCCACATCG
JavPR83	TRC40_Y310C-Rev	CGATGTGGAAGTCTTCACACAGGTCCTCCATCTGGTCC
JavPR84	TRC40_P344S-For	CCTCCTGGAGCCCTACAAGTCCCCCAGTGCCCAGTAGG
JavPR85	TRC40_P344S-Rev	CCTACTGGGCACTGGGGGACTTGTAGGGCTCCAGGAGG

JavPR88	TRC40_CC289,292SS -For	CGACCCCGAGAAGCCCAGCAAGATGT CTGAGGCCCGTCAC
JavPR89	TRC40_ CC289,292SS -Rev	GTGACGGGCCTCAGACATCTTGCTGG GCTTCTCGGGGTCG
JavPR96	TRC40_L303V-For	CAAGATCCAGGCCAAGTATGTGGACC AGATGGAGGACCTG
JavPR97	TRC40_L303V-Rev	CAGGTCCTCCATCTGGTCCACATACT TGGCCTGGATCTTG
JavPR103	TRC40_CC53,55SS-For	GGCAAGACCACCAGCAGCAGCAGCC TGGCAGTCCAGCTCTC
JavPR104	TRC40_ CC53,55SS -Rev	GAGAGCTGGACTGCCAGGCTGCTGC TGCTGGTGGTCTTGCC
JavPR109	TRC40_R189W-For	CGTGGAGCGGGGCCTGGGCTGGCTT ATGCAGATCAAGAACC
JavPR110	TRC40_R189W-Rev	GGTTCTTGATCTGCATAAGCCAGCCC AGGCCCCGCTCCACG
JavPR134	TRC40_E259R-For	CCTGTCCCTGTATGAGACAAGGAGGC TGATCCAGGAGCTGG
JavPR135	TRC40_E259R-Rev	CCAGCTCCTGGATCAGCCTCCTTGTC TCATACAGGGACAGG
JavPR136	TRC40_E307R/D308R -For	CCAAGTATCTGGACCAGATGAGGAGG CTGTATGAAGACTTCCACATCG
JavPR137	TRC40_ E307R/D308R -Rev	CGATGTGGAAGTCTTCATACAGCCTC CTCATCTGGTCCAGATACTTGG

2.1.7. Small interfering RNA

Table 7. Small interfering RNA (siRNA) used in this study.

Internal database ID	Target	Sense (5'-3')	Antisense (5'-3')	Overhang	Provider	Source
si2	BAG6 #1	UUUCUCCAAGAGCAGUUUA	UAAACUGCUCUUGGAGAAA	[dT][dT]	Sigma	(Minami et al. 2010)
si3	BAG6 #2	AUGAUGCACAUGAACAUUC	GAAUGUUCAUGUGCAUCAU	[dT][dT]	Sigma	(Minami et al. 2010)
si4	Luciferase	CGUACGCGGAAUACUUCGA	UCGAAGUAUUCCGCGUACG	[dT][dT]	Sigma	Dharmacon. Catalog#: D-001100-01
si5	TRC40	GCCCUUUCAUCUCACAGAU	AUCUGUGAGAUGAAAGGGC	[dT][dT]	Sigma	Ambion. Catalog': s1675. (Pfaff et al. 2016; Rivera-Monroy et al. 2016)
si7	WRB	AAAUCCAACAGGUAAUUCCAACACC	GGUGUUGGAAUUACCUGUUGGAUUU	[dT][dT]	Sigma	(Y. Yamamoto and Sakisaka 2012; Rivera-Monroy et al. 2016)
si15	NT				Ambion. Catalog#: AM4635	

2.1.8. Antibodies

2.1.8.1. Primary antibodies

The antibodies used for different techniques such as Western-blot (WB), indirect immunofluorescence (IF) or immunoprecipitation (IP) are listed in the following tables (**Tables 8-10**). They contain the information about the commercial antibodies and the working dilution used in this study.

Table 8. Primary antibodies used in this study.

Unique ID	Name	Raised in	Company	Catalog no.	Lot #	Dilution (WB)	Dilution (IF)
Ab0021	β-Actin	mouse	Santa Cruz	sc-47778	A2315	1:10000	
Ab0076	BAG6	mouse	Abnova	H00007917-B01P	FC071	1:2000	
Ab0072	BAG6 #5 AP	rabbit	Custom made				1:300
Ab0073	BAG6 #5 Ser	rabbit	Custom made			1:2000	
Ab0071	BAG6 #7	rabbit	Custom made			1:2000	
Ab0074	BAG6 CT	rabbit	Custom made			1:2000	1:300
Ab0436	Calnexin	mouse	BD Transduction Laboratories	610524			1:200
Ab0069	CAML	guinea pig	Synaptic Systems	359004	359004/1	1:1000	
Ab0144	EEA1	mouse	BD Transduction Laboratories	610456	03689		1:200
Ab0133	Emerin	rabbit	Santa Cruz	sc-15378	H1115	1:1000	1:150

Ab0442	FDFT1	mouse	Santa Cruz	sc-271602		1:1000	
Ab0159	GAPDH	mouse	NeoBiotech	NB-29-00852	16/06-G4-C5	1:40000	
Ab0163	Get3 #1	guinea pig	Custom made			1:2000	
Ab0172	GFP	rabbit	Torrey Pines biolabs	TP401	081211	1:5000	
Ab0188	GM130	mouse	BD Transduction Laboratories	610823	24277	1:1000	1:300
Ab0660	GOSR2	rabbit	Synaptic Systems	170003	170003/4	1:1000	1:200
Ab0192	GR	rabbit	Santa Cruz	sc-8992	G1614	1:1000	1:250
Ab0193	GR	mouse	Santa Cruz	sc-393232	C1115	1:1000	
Ab0679	HIF-1α	mouse	BD Transduction Laboratories	610959		1:1000	
Ab0203	Hsc70	mouse	StressMarq Biosciences	SMC-151	0904		1:200
Ab0204	Hsc70	rat	Enzo Life Sciences	ADI-SPA-815-F	12051444	1:1000	
Ab0205	Hsp40	rabbit	abcam	ab69402	6R195077-8	1:1000	
Ab0206	Hsp90α/β	mouse	Santa Cruz	sc-13119	B2316	1:1000	1:200
Ab0214	JNK1	mouse	Cell Signaling	3708	1	1:1000	
Ab0280	**P**-JNK (Thr183/Tyr185)	rabbit	Cell Signaling	4668	12	1:1000	
Ab0642	Lamin-A/C	mouse	abcam	ab40567			1:200
Ab0236	myc	mouse	Santa Cruz	sc-40	B0116	1:1000	1:200
Ab0615	myc	chicken	abcam	ab172	GR221409-9		1:150
Ab0239	Na+/K+-ATPase α1	mouse	Santa Cruz	sc-21712	B1516	1:1000	
Ab0555	Opsin	mouse	From Bernhard Dobberstein			1:1000	
Ab0270	PGK1	mouse	Thermo Fisher Scientific	459250	459250/K8914	1:3000	
Ab0630	PTP1B	rabbit	Sigma-Aldrich	HPA012542		1:1000	1:100

Ab0657	Sec22b	rabbit	Synaptic Systems	186003	186003/1-8	1:1000	1:200
Ab0346	Sec61β	rabbit	From Bernhard Dobberstein			1:1000	1:300
Ab0350	SGTA #5143	chicken	From Steve High			1:2000	
Ab0353	Syntaxin 1	mouse	Synaptic Systems	110011	110011/13	1:1000	
Ab0354	Syntaxin 5	rabbit	Synaptic Systems	110053	110053/16	1:2000	1:250
Ab0355	Syntaxin 6	rabbit	Synaptic Systems	110062	110062/9	1:1000	1:300
Ab0358	Syntaxin 8	rabbit	Synaptic Systems	110083	110083/1-11	1:1000	1:300
Ab0452	Syntaxin 18	rabbit	Synaptic Systems	110183			1:1000
Ab0400	TRC40	mouse	Sigma-Aldrich	WH0000439M3	D3011-2H3	1:1000	1:100
Ab0401	TRC40	rabbit	Proteintech	15450-1-AP	00021130	1:1000	
Ab0405	TRC40 #4	rabbit	From Bernhard Dobberstein			1:1000	
Ab0676	UBE2J1	mouse	Santa Cruz	sc-377002	H2917	1:1000	
Ab0391	Ubiquitin	mouse	Enzo Life Sciences	BML-PW8810	5021240	1:1000	
Ab0668	USE1	rabbit	Proteintech	25218-1-AP	00022214	1:1000	
Ab0650	VAPA	rabbit	Proteintech	15275-1-AP		1:1000	
Ab0629	VAPB	rabbit	Proteintech	14477-1-AP		1:1000	1:200
Ab0407	Vti1a	mouse	BD Transduction Laboratories	611220	0000073424-K	1:1000	
Ab0408	Vti1b	mouse	BD Transduction Laboratories	611404	0000073424-L	1:1000	
Ab0659	Vti1b	rabbit	Synaptic Systems	164002	164002/7		1:200
Ab0417	WRB serum 7676	rabbit	Synaptic Systems	324002	324002/1-2	1:1000	
Ab0210	IgG (normal mouse)	mouse	Santa Cruz	sc-2025	E3117		
Ab0655	IgG (normal rabbit)	rabbit	Cell Signaling	2729	8		

The opsin monoclonal antibody (R2-15) comes from the laboratory of Bernhard Dobberstein from the University of Heidelberg and it was a kind gift from Paul A. Hargrave from the University of Florida that was described long time ago (Adamus et al. 1991).

The mouse anti-GR, rabbit anti-TRC40 #4 and rabbit anti-Stx5 were also used for immunoprecipitation. 5µg of these antibodies were used for each IP. As a control 5µg of IgG (normal mouse) or IgG (normal rabbit) were used respectively.

2.1.8.2. Secondary antibodies

Table 9. WB secondary antibodies used in this study.

Short Name	Raised in	Against	Conjugated to	Company	Catalog no.	Lot #	Dilution
α-mouse HRP		mouse IgGκ	HRP	Santa Cruz	sc-516102	F2017	1:10000
α-rabbit 800	donkey	rabbit	IRDye 800CW	LI-COR	926-32213		1:5000
α-rabbit 680	donkey	rabbit	IRDye 680LT	LI-COR	926-68023		1:5000
α-mouse 800	donkey	mouse	IRDye 800CW	LI-COR	926-32212		1:5000
α-mouse 680	goat	mouse IgG1	IRDye 680LT	LI-COR	926-68050		1:5000
α-guinea pig 680	donkey	guinea pig	IRDye 680LT	LI-COR	926-32421		1:5000
α-rat 800	donkey	rat	IRDye 800CW	LI-COR	926-32219		1:5000
α-chicken 800	donkey	chicken	IRDye 800CW	LI-COR	926-32218		1:5000

Table 10. IF secondary antibodies used in this study.

Short Name	Raised in	Against	Conjugated to	Company	Catalog no.	Lot #	Dilution
α-rabbit 488	goat	rabbit	Alexa Fluor 488	Invitrogen	A11034	1616933	1:1000
α-rabbit 488	goat	rabbit	Alexa Fluor Plus 488	Invitrogen	A32731	SE250296	1:1000
α-mouse 546	goat	mouse	Alexa Fluor 546	Invitrogen	A11030	1829584	1:1000
α-mouse 647	goat	mouse	Alexa Fluor 647	Invitrogen	A21235	1511346	1:1000
α-mouse 647	goat	mouse	Alexa Fluor Plus 647	Invitrogen	A32728	SE250294	1:1000
α-chicken 647	goat	chicken	Alexa Fluor 647	Invitrogen	A21449	1806124	1:1000

2.1.9. Media and buffers

Table 11. List of media and buffer used in this study and their composition.

Name	Composition
ATP buffer	4 mM ATP
ATPase activity assay buffer	100 mM HEPES 10 mM $MgCl_2$ 20% Glycerol 5 U/µL Pyruvate kinase in 3,2M $NH_4(SO_4)_2$ pH 6 75 U/µL Lactate dehydrogenase in 3,2M $NH_4(SO_4)_2$ pH 7 100 mM ATP 100 mM Phosphoenol pyruvate 50 mM NADH
Ampicillin stock solution (1000x)	100 mg/mL
Coomassie destaining solution	20% (v/v) Ethanol 10% (v/v) Acetic acid
Coomassie staining solution	45% (v/v) Ethanol 10% (v/v) Acetic acid 0,1% (w/v) Coomassie brilliant blue G250
DMEM++ medium	500 mL Dulbecco's Modified Eagle Medium 10% (v/v) Fetal bovine serum 2 mM L-Glutamine
DNA loading buffer (6x)	30% (v/v) Ficoll 400 0,04% Orange G
Elution buffer (maltose)	50 mM HEPES-HCl pH 7 150 mM KOAc 10 mM MgAc 20 mM Maltose
Elution buffer (imidazole)	50 mM HEPES-HCl pH 7 150 mM KOAc 10 mM MgAc

	20 mM Imidazole
Extraction buffer	50 mM HEPES-HCl pH 7 150 mM KOAc 10 mM MgAc
High-salt buffer	500 mM KOAc
Homogenization buffer	320 mM Sucrose 20 mM HEPES pH 7,4 2 mM EDTA 50 mM NaCl 1x Protease inhibitors (cOmplete, Roche)
Kanamycin stock solution (1000x)	50 mg/mL
Kpi buffer	40 mM KH_2PO_4 pH 7,5
LB medium	10 g/L Tryptone 5 g/L Yeast extract 5 g/L NaCl Adjust to pH 7
Lithium acetate stock (10x)	1 M Lithium acetate dihydrate
Lysis stock buffer	50 mM HEPES-NaOH pH 7,5 150 mM NaCl 1,5 mM $MgCl_2$ 1 mM Na-EGTA 1x Protease inhibitors (cOmplete, Roche)
Lysis buffer for hypoxia	400 mM NaCl 10 mM Tris-HCl pH 8 1 mM EDTA 1% (v/v) Triton X-100 1x Protease inhibitors (cOmplete, Roche)
PBS	137 mM NaCl 2,7 mM KCl 8 mM Na_2HPO_4 1,5 mM KH_2PO_4
PEG stock solution	50% (v/v) Polyethylene glycol

4% PFA in PBS pH 7,4	4% (w/v) Paraformaldehyde in PBS pH 7,4
SDS loading buffer	250 mM Tris-HCl pH 6,8 50% (v/v) Glycerol 10% (v/v) SDS 0,5% (w/v) Bromophenol blue
SDS running buffer	25 mM Tris-HCl pH 8,3 250 mM Glycine 0,1% (v/v) SDS
SOC medium	20 g/L Trypton 5 g/L Yeast extract 10 mM NaCl 2,5 mM KCl 10 mM $MgCl_2$ 20 mM Glucose Adjust pH to 7,4
Solubilization buffer based on (Kline et al. 2009)	1,5% (v/v) Triton X-100 0,1% (v/v) SDS 50 mM Tris pH 7,4 10 mM NaCl 5 mM EDTA 2,5 mM Na-EGTA 0,75% (w/v) Sodium deoxycholate 1x Protease inhibitors (cOmplete, Roche)
T4 ligase buffer (10x)	50 mM Tris-HCl pH 7,4 10 mM $MgCl_2$ 1 mM DTT 1 mM ATP 50 g/L Polyethylene glycol
TAE buffer	40 mM Tris-acetate 20 mM Glacial acetic acid 1 mM EDTA Adjust pH to 8
TE buffer stock (10x)	100 mM Tris-HCl pH=7,5

	10 mM EDTA pH=8
Tetracycline stock solution (1000x)	10 mg/mL
TEV cleavage buffer	50 mM HEPES-HCl pH=7 150 mM KOAc 10 mM MgAc 0,5 mM DTT 0,5 mM EDTA
Transfer buffer	192 mM Glycine 250 mM Tris pH=8,3
Transport buffer	20 mM HEPES 110 mM KOAc 2 mM $Mg(OAc)_2$ 1 mM EGTA, pH 7,3 2 mM DTT 0,1 mM PMSF 1 µg/mL Leupeptin 1 µg/mL Pepstatin 1 µg/mL Aprotinin
Yeast synthetic complete (SC) medium/selective medium	6,7 g Yeast nitrogen base X g Dropout mix (according to manufacturer's instructions) 20 g/L Glucose According to what is needed: 40 mg/L Adenine 20 mg/L L-Histidine 100 mg/L L-Leucine 20 mg/L Uracil 20 mg/L L-Methionine 50 mg/L L-Tryptophan
Yeast agar	15 g/L Bactoagar for yeast
Yeast agar plates	50% (v/v) Yeast agar 50% (v/v) Yeast medium

2.1.10. Kits and other reagents

Table 12. Kits and other reagents used in this study.

Name	Company	Catalog No.	Lot No.
Agar	Invitrogen	30391-023	
Amylose agarose	New England Biolabs	E8021L	0161403
ATP	Roth	K054.4	101.288
b-AP15	Millipore	662140	2881385
Coomassie Plus Protein Assay Reagent	Thermo-Fisher Scientific	1856210	SA245727
cOmplete EDTA-free inhibitor cocktail	Roche	04693132001	
CSM dropout mix (-Ade, -His, -Leu, -Met, -Trp, -Ura)	MP Biomedicals	4560-222	47264
CSM dropout mix (-Ade, -His, -Leu, -Trp)	Formedium	DCS1229	FM1A215/006441
Deoxycorticosterone or 21-Hydroxyprogesterone (DOC)	Sigma	D6875	SLBG9391V
Dexamethasone (DEX)	Sigma	D4902	
4′,6-Diamidino-2-phenylindole dihydrochloride (DAPI)	Sigma	D9542	096M4014V
Digitonin	Fluka	37008	7D011626
5-5’-Dithiobis(2-nitrobenzoic acid) (DTNB)	Sigma	D8130	SHBF2531V
DMEM (Dulbecco's Modified Eagle Medium)	Gibco	41966-029	

DMSO	Thermo-Fisher Scientific	F515	
Expand High Fidelity PCR System	Roche	11759167001	
Fast alkaline phosphatase	Thermo-Fisher Scientific	EF0654	
FBS Superior	Biochrom	S0615	
Fluorescein di-β-D-galactopyranoside (FDG)	Life Technologies	F1179	1445261
GFP-trap M	ChromoTek GmbH	gtm-20	
L-Glutamine	Gibco	25030-024	
Guanidine hydrochloride (GdnCl)	PanReac AppliChem	144229.1211	6L010646
High Pure PCR Product Purification Kit	Roche	11732676001	
Immobilon Western Chemiluminescent HRP Substrate	Millipore	WBKLS0500	16066902
Nitrocellulose Amersham Protran Premium 0,45	GE Healthcare	10600003	A10074169
Lactate dehydrogenase (LDH) from rabbit muscle	Roche	10127230001	14908627
Laminin 1mg mouse	Corning	354232	
Lipofectamine 2000 transfection reagent	Thermo-Fisher Scientific	11668-019	
Lipofectamine RNAiMAX transfection reagent	Thermo-Fisher Scientific	13778-150	
Methanol	Roth	4627.5	

β-Nicotinamide adenine dinucleotide, reduced disodium salt hydrate (NADH)	Sigma	N8129	SLBJ2605V
Ni-NTA agarose	Qiagen	30230	127147847
dNTP Set	Thermo-Fisher Scientific	R0181	
NucleoBond Xtra Midi	Macherey-Nagel	740410	
NucleoSpin Plasmid EasyPure	Macherey-Nagel	740727	
Opti-MEM Reduced serum medium	Gibco	31985-070	
PageRuler Prestained Protein Ladder	Thermo-Fisher Scientific	26616	
Paraformaldehyde BioChemica	PanReac AppliChem	A3813,0250	
Phosphoenol pyruvate (PEP)	Sigma	P7002	088K3783
Phos-STOP	Roche	04906837001	
Phusion polymerase	Homemade		
PMSF BioChemica	PanReac AppliChem	A0999	
PNGase F	New England Biolabs	P0704	
Protein A Sepharose 4 Fast flow	GE Healthcare	17-5280-01	10241063
Protein G Sepharose 4 Fast flow	GE Healthcare	17-0618-01	10244349
Pyruvate kinase (PK)	Sigma	P1506-5KU	SLBH1134
SafeView	NBS-Biologicals	NBS-SV1	
T4 DNA ligase	Thermo-Fisher Scientific	EL0011	00546681

0,25% Trypsin-EDTA	Gibco	25200-056	
Tween-20	Millipore	822184	
Yeast nitrogen base w/o amino acids	Melford	Y2004	

2.2. Methods

2.2.1. Plasmid construction

For pRS413met25_Get3 and the different mutants they were obtained by digesting previous p416met25 vectors containing these mutants with XbaI and XhoI and ligating them into pRS413me25.

For mVenus-C1-ratGR it was obtained after subcloning it from pDS-063-ratGR. ratGR was amplified by PCR with primers JavPR98 and JavPR99. These amplified DNA fragments were digested with XhoI and BamHI, along with an empty vector mVenus-C1, and ligated them later.

For pcDNA3.1(-)_cmyc-siTRC40ins it was obtained after subcloning it from MBP-TEV-TRC40/ZZ-EMD-op into a pcDNA3.1(-) using overlap extension PCR. Primers for mutagenesis of the TRC40 for making it insensitive to the siRNA were included. On the one hand, one PCR using a forward primer containing an N-terminal cmyc-tag for TRC40 and a restriction site for XhoI (JhonPR63) and the reverse primer (JhonPR62) was containing the sequence to be mutagenized. On the other hand, a second PCR using a forward primer (JhonPR61) overlapping the sequence on JhonPR62 and a reverse primer targeting the C-terminus of TRC40 and containing a restriction site for BamHI (JhonPR60). A third PCR using as template 2 µL of the PCR products coming from the two previous PCRs was performed. The primers used for this PCR were JhonPR63 and JhonPR60. The DNA fragments obtained and an empty pcDNA3.1(-) vector were digested with XhoI and BamHI first, incubated the backbone for 10 min at 37°C with 1 U of fast alkaline phosphatase and later ligated.

For the pcDNA3.1(-)_cmyc-siTRC40ins mutants they were obtained by using site-directed mutagenesis with two primers, forward and reverse, with overlapping sequences containing the mutation in the middle of the primer. The primers used can be found in **Table 6**. The PCR products were later digested with DpnI.

All sequences were submitted for Sanger sequencing (GATC Biotech, Konstanz, Germany) and the obtained sequences were carefully aligned and checked with the expected one.

2.2.2. Polymerase chain reaction (PCR)

Polymerase chain reaction (PCR) (Saiki et al. 1985) was employed for the amplification of DNA fragments. 50 ng of DNA template were mixed with 16 µM of a mixture of deoxynucleotides (dNTPs) (Thermo-Fisher Scientific), 250 nM of the correspondent oligonucleotide primers, 5% DMSO, 2 U of a thermo-stable proofreading DNA polymerase (homemade Phusion polymerase) and 1-fold expand high-fidelity buffer (Roche, Basel, Switzerland). The reaction mixture was then subjected to multiple cycles in a thermocycler as it follows:

	○ Initial denaturation step	95°C	2 min
10x	○ DNA-melting step	95°C	1 min
	○ Annealing step	50°C*	45 sec
	○ Extension step	72°C	X min = (1 min per Kb of DNA) + 30 sec
20x	○ DNA-melting step	95°C	1 min
	○ Annealing step	52°C*	45 sec
	○ Extension step	72°C	X min = (1 min per Kb of DNA) + 30 sec
	○ Final extension step	72°C	1,5X min

*Adjust the annealing temperature according to the lowest melting temperature of the oligonucleotide primers.

Primers were designed with a length of 18-30 annealing bp for regular PCR and 44-60 bp for site-directed mutagenesis. All primers used can be found in **Table 6**.

PCR products were loaded and run in agarose gels. Next, the correspondent bands were excised from the gel and purified using a DNA purification kit (High Pure PCR Product Purification; Roche) according to manufacturer's instructions.

2.2.3. Site-directed mutagenesis

PCR was performed for site-directed mutagenesis. The PCR mix was as described before. The reaction mixture was then subjected to multiple cycles in a thermocycler as it follows:

	○ Initial denaturation step	95°C	2 min
18x	○ DNA-melting step	95°C	30 sec
	○ Annealing step	52°C	1 min
	○ Extension step	72°C	X min = (1 min per Kb of DNA) + 30 sec
	○ Final extension step	72°C	1,5X min

PCR products were loaded and run in agarose gels. Next, the correspondent bands were cut off from the gel and purified using a DNA purification kit (Roche) according to manufacturer's instructions. The PCR products were then subjected to DpnI (Fermentas, Waltham, USA) digestion with 1 U of DpnI for 4 h at 37°C. Later, the digested PCR products were transformed into electro-competent ElectroTen blue cells.

2.2.4. Agarose gel electrophoresis

Agarose gels were used for the separation of the DNA fragments based on their size for later excision and purification. The DNA samples were mixed with 6x DNA loading buffer and loaded into the correspondent agarose gel. SafeView (NBS-Biological, Huntingdon, UK) was used as a nucleic acid stain for casting the agarose gels. The gels were subjected to electrophoresis at 180 V (constant V). A DNA ladder (Fermentas) was also loaded and run with the DNA samples. The gel was analyzed

under ultra violet (UV) light at 365 nm and the correspondent bands containing the DNA fragments were excised from the gel for later DNA purification.

2.2.5. DNA ligation

Linearized vector and DNA fragments suitable for insertion were mixed with 1 U of T4 DNA-ligase (Thermo-Fisher Scientific) and 1-fold of T4 DNA-ligase buffer. They were incubated for 2 h or O/N at 18°C. Then, T4 DNA-ligase was heat-inactivated at 70°C for 10 min.

2.2.6. DNA-transformation in bacterial-cells by electroporation

2 µL of the heat-inactivated ligation products or 1,5 µL of the DpnI digested product were transformed into electro-competent ElectroTen blue cells. They were mixed with 50 µL of bacterial cells and later transferred into pre-cooled electroporation-cuvettes. The electroporation unit (Gene Pulse; BioRad, Hercules, USA) was set to 25 µF and 2,5 kV. The pulse controller was set to 400 Ω. They were resuspended in 1 mL of SOC medium and incubated for 30 min at 37°C with medium shaking. Cells were spinned-down and resuspended in 50 µL that were plated in to LB plates with the correspondent selective antibiotic.

2.2.7. Yeast culture

Yeast strains used for this study are listed above (**Table 3**). Yeast cultures were grown O/N in yeast SC or selective media at 30°C incubator at 150 rpm shaking. For having the yeast culture in mid-log phase, yeast cultures were spinned-down and washed with sterile water and diluted 1:10 and incubate it at 30°C in a new tube for 4 h.

2.2.8. Yeast transformations

Yeast plasmids used for this study are listed above (**Table 5**). For yeast transformations a modified version of the lithium acetate-PEG method was used (Ito et al. 1983). Yeast were grown O/N in SC or selective media as described before. Cells were pelleted and washed twice with sterile water. Then cells were resuspended in 1,4 mL of a solution of lithium acetate/PEG in TE buffer. Next 0,5 µg of the plasmid along

with 18 µg of carrier DNA were added. The mixture was vortexed intensely until full homogenization and incubated for 1 h at 37°C and later 20 min at 42°C. Cells were centrifuged at 10.000 rpm for 5 min and the supernatant was discarded. Cells were resuspended in water and plated in SC selective agar plates. The selectivity was given by the absence of the amino acid for the selection of the transformed cells. The plates were grown for 48 h in the yeast incubator at 30°C until colonies were grown enough.

2.2.9. Yeast β-galactosidase assay

Yeast strains were grown in the correspondent selective media O/N at 30°C and 150 rpm shaking. The OD_{600} of the cultures were measured and cultures were diluted to OD_{600}=0,2 and grown for four more hours at 30°C for reaching mid-log phase. Cell were pelleted and washed with water and resuspended them in selective media. Each strain was split into two tubes: to one of the tubes I added deoxycorticosterone (DOC) to a final concentration of 100 nM and to the second one I added the same volume of absolute ethanol (DOC solvent). Incubate them for 2 h at 30°C shaking at 150 rpm. I prepared a FDG solution *in situ* containing: 500 µM of FDG, 0,25% Triton X-100 in 125 mM PIPES. In a 96-well plate, I added 100 µL of each strain the cell cultures by triplicate followed by 20 µL of the FDG solution per well. The plates were shaken gently and briefly the plates. I covered them in aluminum foil and incubated them at 37°C for 90 min. Once the incubation was over, I added 20 µL of 1 M Na_2CO_3 per well to stop the enzymatic reaction. The plates were shaken gently and briefly the plates. The plates were read with a plate reader (Synergy HT; BioTek, Winooski, USA) using an excitation wavelength of 485 nm and an emission wavelength of 530 nm. Read it by triplicate. Besides, read the absorbance, OD_{600}, for normalize the fluorescence readings to the cell density. Read it by duplicate. For the analysis of the experiment the following step for calculations were made: first, the fluorescence readings were averaged and divided by the averaged OD_{600} for normalizing them to the cell density. Second, average the normalized fluorescence was averaged among the three technical replicates added into the 96-well plates. Third, the averaged autofluorescence coming from cells not transformed with the GR construct was subtracted from the fluorescence calculated in step two obtaining the absolute fluorescence signal. The GR activity was calculated by dividing the fluorescence

intensities (coming from the previous step) from stimulated cells by the non-stimulated ones.

2.2.10. Yeast NaOH lysis for protein extraction

I used 1 mL from the correspondent yeast cultures, pelleted by centrifuging at 2000 rpm for 5min and discarded the supernatant. The cells were resuspended in a freshly prepared solution of 250 mM of NaOH + 12 µL/mL β-mercapethanol. Cells were briefly vortexed and incubated 10 min on ice. The OD_{600} was measured in a spectrophotometer for later adjusting the amount of SDS loading buffer added. OD_{600} * 4= volume of loading buffer to add (in mL). TCA precipitation was performed with each sample after the incubation with NaOH was over.

2.2.11. TRC40 protein purification

BL21 (DE3) cells expressing a 10xHis-MBP-TEV-TRC40 construct. O/N cell cultures were diluted 1:100 in regular LB media. Cells were grown at 37°C until reaching OD_{600}= 0,6. Next, the cells were induced with 0,4 mM IPTG for 4 h at 30°C shaking at 160 rpm. After induction, cells were centrifuged at 6000 *g* for 20 min at 4°C. The supernatant was discarded and the pellet was resuspended in 40 mL of cold extraction buffer. Cells were centrifuged at 5300 *g* for 10 min at 4°C. The supernatant was discarded. The pellet was resuspended in 30 mL of cold extraction buffer supplemented with 1 mM phenylmethanesulfonyl fluoride (PMSF), half a tablet of protease inhibitors (Roche), 3 mM DTT and a tip of DNase I. Cells were lysed with an Emulsiflex-C3 high-pressure homogenizer (Avestin, Ottawa, Canada). The crude-cellular lysates were cleared by centrifuging at 25.000 rpm for 30 min at 4°C. In parallel, 5,5 mL of dry amylose resin (New England Biolabs, Ipswich, USA) were used and they were pre-equilibrated with cold extraction buffer. The lysate supernatant was subsequently put in contact with the pre-equilibrated amylose resin and incubated during 90 min slightly shaking at 4°C. The lysates-resin were loaded into purification columns and washed six times following the next scheme:

- 2 times with 2 volumes of ATP buffer.
- 2 times with 2 volumes of high-salt buffer.
- 2 times with 2 volumes of extraction buffer.

The protein was eluted from the resin with maltose elution buffer and the flow-through was collected in fractions tubes. TRC40-containing fractions were pooled together. The purified protein was cleaved with a 1:100 6xHis-tagged TEV protease and dialyzed for 24 h at 4°C against TEV cleavage buffer. The content of the dialysis tube was transferred into a new tube and centrifuged at 5.000 *g* for 15 min at 4°C for removing aggregates. In parallel, 3 mL of Ni-NTA resin (Qiagen, Hilden, Germany) were pre-equilibrated with extraction buffer. The pre-washed Ni-NTA was loaded into a purification column. The pre-cleared dialyzed protein was run into the Ni-NTA columns for subsequently remove the uncleaved TRC40 and the 6xHis-TEV protease. The flow-through was collected in fractions tubes. Cleaved TRC40-containing fractions were pooled together and the protein was concentrated with concentrator tubes (Spin-X UF 20, #431489; Corning, Corning, USA) up to 100 µM. The Ni-NTA was eluted with imidazole elution buffer. The recombinant protein was stored at -80°C with 2 mM DTT. The efficiency of purification and cleavage were monitored by SDS-PAGE.

2.2.12. TRC40 reduction and oxidation

The recombinant TRC40 was diluted in 40 mM HEPES-KOH (pH 7,5). For the reduction of TRC40, I used 5 µM of the freshly purified protein and added 5 mM of DTT, 5 µM $ZnCl_2$ and 0,5 mM of ATP. I incubated the mixture at 30°C at 450 rpm for 5 h. I used desalting columns (Thermo Fisher Scientific, #89890), equilibrated with 40 mM HEPES-KOH (pH 7,5) for getting rid of the reductants. For the oxidation of TRC40, I used freshly reduced TRC40 and I added 2 mM H_2O_2 and 50 µM $CuCl_2$ at 37°C at 450 rpm for 10 min. For removing the oxidants H_2O_2 and $CuCl_2$ I used again desalting columns as described before. I measured the protein concentration by Bradford using a BSA standard curve.

2.2.13. ATPase activity assay

To monitor the ATP hydrolysis I performed a NADH-coupled ATPase assay (Kiianitsa, Solinger, and Heyer 2003) in a 96-well plate. The assay is based on an ATP regeneration system that turns out into the oxidation of NADH upon ATP hydrolysis by the ATPase protein. This regeneration system is formed by phosphoenol pyruvate (PEP), pyruvate kinase (PK), L-lactate dehydrogenase (LDH) and β-Nicotinamide adenine dinucleotide, reduced (NADH) that are part of the ATPase activity assay buffer

described above. The system works as it follows: PEP is converted to pyruvate by the PK upon the regeneration of ATP back from ADP. The pyruvate is subsequently processed by the LDH into lactate upon the oxidation of NADH into NAD^+ (Nørby 1988). The oxidation of NADH can be monitored by the decrease of absorbance at 340 nm that is coupled to the steady-state rate of ATP hydrolysis. The assay was performed with recombinant TRC40 protein oxidized and reduced as described before in a 96-well plate and measured in a plate reader (Synergy HT, BioTek) using an absorbance wavelength of 340 nm over time.

2.2.14. Ellman's assay

To explore the redox state of TRC40, I performed an Ellman's assay (Ellman 1958; Riddles, Blakeley, and Zerner 1983) that enables to monitor the free thiols present in the protein. The Ellman's reagent or 5-5'-Dithiobis(2-nitrobenzoic acid) (DTNB) (Ellman 1958), via the aromatic disulfide, interacts with free thiols releasing a mole of 2-nitro-5-benzoate per mole of thiol group in the protein. This 2-nitro-thiobenzoate (TNB) in a mild alkaline media (pH around 7-8) results in 2-nitro-5-thiobenzoate anion (TNB^{2-}) that is a yellow compound that can be monitored in a spectrophotometer at 412 nm. I used 1 µM of recombinant TRC40 protein oxidized and reduced, obtained as described before, in Kpi buffer plus 165 µg/mL DTNB and 6 M GndCl. The GndCl at high concentrations denatures proteins, in this case it served for exposing all the residues to the DTNB. Kpi buffer plus DTNB and GndCl without TRC40 was used as a blank. The mixtures were incubated in the darkness at RT for 15 min. The assay was performed in a 96-well plate and measured in a plate reader (Synergy HT, BioTek) using an absorbance wavelength of 412 nm. The following equation was applied in order to calculate the free thiols:

$$\text{Free thiols} = \frac{A_{412}\ \text{sample} - A_{412}\ \text{blank}}{\varepsilon_{TNB} * M_{TRC40} * d}$$

$\varepsilon_{TNB} = 13800\ M^{-1}\ cm^{-1}$

$M_{TRC40} = 0{,}000001\ M$

$d = 0{,}6\ cm$

M stands for the molarity of TRC40, d for the optical pathlength in cm^2 and ε for the molar extinction coefficient of TNB^{2-} that is 13800 $M^{-1}\ cm^{-1}$ in 6M GndCl.

2.2.15. Human cell lines culture

HeLa P4 cells (Charneau et al. 1994) were obtained from the NIH AIDS Reagent Program and T-REx 293 Stx5-opsin cells were grown both in DMEM supplemented with 10% (v/v) FBS and 2 mM L-glutamine (DMEM++) under 5% CO_2 at 37°C. No antibiotics were added. They were tested for contamination by mycoplasma on a regular basis.

2.2.16. Cell passaging

Cells were passaged when around 80% of confluence was reached. The DMEM++ medium was removed and they were washed with sterile PBS. One fifth of the original volume was added of a medium containing 0,25% Trypsin-EDTA, distributed over the plate and removed. The plate was kept on a hotplate at 37°C for 5 min. The cells were suspended in 10 mL of DMEM++ medium and the correspondent dilution was done in a new plate. The cell dilution was always higher than 2%.

2.2.17. T-REx 293 Stx5-opsin cell line generation

Flp-In T-REx 293 cells were obtained (Invitrogen, Carlsbad, USA). They were cultured with DMEM++ plus 10 µg/mL blasticidin. This cell line stably expresses the blasticidin gene for cell line selection. The following plasmids were co-transfected: pOG44 and pcDNA5/FRT/TO_Stx5-opsin. The Flp-In T-REx 293 has integrated a Flp Recombination Target (FRT) site. pOG44 plasmid expresses a Flp recombinase under the control of a CMV promoter. The construct of pcDNA5/FRT/TO_Stx5-opsin carries Stx5-opsin under the control of a CMV promoter, two tetracycline operators (TetO2) sites adjacent to the promoter, a FRT site and a hygromycin resistance gene. The expression of the Flp recombinase mediates the insertion of the pcDNA5/FRT/TO_Stx5-opsin construct integrated into FRT site in the genome (O'Gorman, Fox, and Wahl 1991). The TetO2 sites repress the expression of the gene under their control in absence of tetracycline in the medium, upon the presence of tetracycline the gene expression is induced. 48 h after transfection, cells were incubated with DMEM++ supplemented with 200 µg/mL hygromycin B and 15 µg/mL blasticidin for two weeks. Cells were split every 5 days renewing the selective media. Control cells transfected with only the pOG44 construct (thus hygromycin-sensitive)

were subjected to the same protocol to determine the sensitivity to hygromycin of Stx5-opsin non-transfected cells. The expression of Stx5-opsin from the stable transfectants selected with hygromycin and blasticidin was tested by Western blot. They were tested for contamination by mycoplasma before preparing freezing stocks and on a regular basis.

2.2.18. Stx5-opsin induction in T-REx 293 Stx5-opsin cell line

Tetracycline was added into DMEM++ medium up to a concentration of 10 µg/mL. The cell medium was removed and washed once with PBS. The DMEM+tetracycline was added and the cells were incubated at 37°C into the cell incubator for 6 h.

2.2.19. Plasmid transient transfection in human cell lines

HeLa P4 or T-REx 293 cells were seeded to be 60-80% the day of transfection. Lipofectamine 2000 (Invitrogen) was used for transfections. The lipofectamine transfection solution was prepared under the cell culture hood in two different tubes. Depending on the plate volume, the preparation of the solutions was as it follows:

Table 13. Recipe of the transfection solutions used in this study according to plate size.

	Tube 1			Tube 2		
Plate	**Plate volume (mL)**	**OptiMEM volume (µL)**	**Lipofectamine 2000 volume (µL)**	**Plate volume (mL)**	**OptiMEM volume (µL)**	**Amount of plasmid (µg)**
10 cm	10	1000	30	10	1000	14
6-well	2	200	6	2	200	2,8
12-well	0,85	85	2,55	0,85	85	1,2
24-well	0,5	50	1,5	0,5	50,0	0,7

Tube 1 and Tube 2 were incubated separately for 5 min at RT. Next, it was the content of both tubes by pipetting and incubated the mix for 15 min at RT under the hood. The cells were washed with PBS and added the correspondent volume of OptiMEM. Finally, it was added the Lipofectamine+plasmid solution and incubated for 6 h at 37°C

within the cell incubator. Once the Lipofectamine incubation was over, the cells were washed with PBS and split the cells to a new plate in a 1:5 dilution. Cell were harvested 48 h after Lipofectamine 2000 transfection.

2.2.20. siRNA-mediated gene silencing in human cell lines

HeLa P4 or T-REx 293 cells were seeded to be 60-80% the day of siRNA transfection. Lipofectamine RNAiMAX (Invitrogen) was used for transfections. The RNAiMAX transfection solution was prepared under the cell culture hood in two different tubes. Depending on the plate volume, the preparation of the solutions was as it follows:

Table 14. Recipe of the silencing solutions used in this study according to plate size.

	Tube 1			Tube 2		
Plate	**Plate volume (mL)**	**OptiMEM volume (µL)**	**Lipofectamine RNAiMAX volume (µL)**	**Plate volume (mL)**	**OptiMEM volume (µL)**	**Amount of 10µM siRNA (µL)**
10 cm	10	500	30	10	500	40
6-well	2	100	6	2	100	8
12-well	0,85	42,5	2,55	0,85	43	6,8
24-well	0,5	25	1,5	0,5	25	4

Tube 1 and Tube 2 were incubated separately for 5 min at RT. Next, it was the content of both tubes by pipetting and incubated the mix for 15 min at RT under the hood. The cells were washed with PBS and added the correspondent volume of DMEM++. Finally, it was added the Lipofectamine RNAiMAX+siRNA solution and incubated for 24 h at 37°C within the cell incubator. The next day once the Lipofectamine RNAiMAX incubation was over, the cells were washed with PBS and split the cells into a new plate in a 1:3 dilution.

A second round of silencing was done (necessary for down-regulating TRC40, not necessary for WRB or BAG6) exactly as described. Cells were split into a new plate in a 1:5 dilution. Cell were harvested 48 h after this last round of Lipofectamine RNAiMAX silencing.

2.2.21. siRNA-mediated gene silencing plus plasmid transient transfection in human cell lines

HeLa P4 or T-REx 293 cells were seeded to be 60-80% the day of siRNA transfection. Lipofectamine RNAiMAX (Invitrogen) was used for transfections. The RNAiMAX transfection solution was prepared under the cell culture hood in two different tubes. Depending on the plate volume, the preparation of the solutions was as it follows:

Table 15. Recipe of the co-transfection (silencing + transfection) solutions used in this study according to plate size. Round 1.

	Tube 1			Tube 2		
Plate	**Plate volume (mL)**	**OptiMEM volume (µL)**	**Lipofectamine RNAiMAX volume (µL)**	**Plate volume (mL)**	**OptiMEM volume (µL)**	**Amount of 10µM siRNA (µL)**
10 cm	10	500	30	10	500	40
6-well	2	100	6	2	100	8
12-well	0,85	42,5	2,55	0,85	43	6,8
24-well	0,5	25	1,5	0,5	25	4

Tube 1 and Tube 2 were incubated separately for 5 min at RT. Next, it was the content of both tubes by pipetting and incubated the mix for 15 min at RT under the hood. The cells were washed with PBS and added the correspondent volume of DMEM++. Finally, it was added the Lipofectamine RNAiMAX+siRNA solution and incubated for 24 h at 37°C within the cell incubator. The next day once the Lipofectamine RNAiMAX incubation was over, the cells were washed with PBS and split the cells into a new plate in a 1:3 dilution.

The second round of silencing was a co-transfection of siRNA and plasmid into the cell lines. In contrast with the first round, Lipofectamine 2000 (Invitrogen) was used for transfections. The Lipofectamine 2000 transfection solution was prepared under the cell culture hood in two different tubes. Depending on the plate volume, the preparation of the solutions was as it follows:

Table 16. Recipe of the co-transfection (silencing + transfection) solutions used in this study according to plate size. Round 2.

	Tube 1			Tube 2			
Plate	**Plate volume (mL)**	**OptiMEM volume (µL)**	**Lipofectamine 2000 volume (µL)**	**Plate volume (mL)**	**OptiMEM volume (µL)**	**Amount of plasmid (µg)**	**Amount of 10µM siRNA (µL)**
10 cm	10	1000	30	10	1000	14	40
6-well	2	200	6	2	200	2,8	8
12-well	0,85	85	2,55	0,85	85	1,2	6,8
24-well	0,5	50	1,5	0,5	50,0	0,7	4

Tube 1 and Tube 2 were incubated separately for 5 min at RT. Next, it was the content of both tubes by pipetting and incubated the mix for 15 min at RT under the hood. The cells were washed with PBS and added the correspondent volume of OptiMEM. Finally, it was added the Lipofectamine 2000+siRNA+plasmid solution and incubated for 6 h at 37°C within the cell incubator. Once the Lipofectamine 2000 incubation was over, the cells were washed with PBS and split the cells into a new plate in a 1:5 dilution. Cell were harvested 48 h after Lipofectamine 2000 transfection.

2.2.22. Hypoxic incubation

HeLa P4 cells were cultured in an *in vivo* hypoxia workstation (Ruskinn Technologies, Bridgend, South Wales, UK) in defined hypoxic conditions (94% N_2, 5% CO_2, 1% O_2) for 6 h or 24 h. The sample processing was done within the hypoxia workstation using a lysis buffer for hypoxia detailed previously (**Table 11**) for 1h and following with TCA-precipitation.

2.2.23. Glucocorticoid receptor stimulation in HeLa cells

For the glucocorticoid receptor stimulation, HeLa P4 cells were treated with the corresponding volume of solvent (absolute ethanol) or a stock resulting in a final concentration of 100 nM of dexamethasone in DMEM for 60 min at 37°C within the cell incubator.

2.2.24. Deubiquitinases (DUBs) inhibition in HeLa cells

For the inhibition of DUBs, HeLa P4 cells were treated with the corresponding volume of solvent (DMSO) or a stock resulting in a final concentration of 1 µM of b-AP15 in DMEM for 6 h at 37°C within the cell incubator.

2.2.25. Cardiomyocyte primary cells isolation

The primary cell isolation protocol was performed as described (Rivera-Monroy et al. 2016).

2.2.26. Homogenization and protein extraction of mammalian tissue

After organ extraction, keep the tissue on ice or snap-freeze with liquid nitrogen. For processing, 1 mL of pre-cold homogenization buffer was added to a flat-bottom eppendorf tube containing the organ. The sample was processed with a homogenizer (MICCRA D-1; MICCRA GmbH, Müllheim, Germany) and followed by 15-20 strokes with a dounce homogenizer. Homogenate samples were centrifuged at 4°C at 100.000 *g* for 30 min. 300 µL of solubilization buffer were added and it was incubated for 30 min on ice, agitating smoothly with no air bubbles. The solubilized samples were again centrifuged for 30 min at 100.000 *g* at 4°C and the supernatant was transferred into a new tube. Protein concentration of the samples was determined after this step and the samples were subjected to TCA precipitation.

2.2.27. Protein extraction from cell lines

DMEM++ medium was removed and the cells were washed once with PBS. 600 µL of solubilization buffer were added to the plates and they were incubated for 1 h in the cold room at 4°C light shaking. The solubilized samples were collected into ultracentrifugation tubes and centrifuged for 35 min at 100.000 *g* at 4°C and the supernatant was transferred into a new tube. Protein concentration of the samples was determined after this step and the samples were subjected to TCA precipitation.

2.2.28. Protein extraction from isolated cardiomyocytes

Cells were resuspended in 300 µL of solubilization buffer and incubated for 1 h on ice. The solubilized samples were collected into ultracentrifugation tubes and centrifuged for 35 min at 100.000 *g* at 4°C and the supernatant was transferred into a new tube. Protein concentration of the samples was determined after this step and the samples were subjected to TCA precipitation.

2.2.29. Cell fractionation

Cell medium was removed, washed once with PBS and they were harvested with 750µL of PBS. Next, they were centrifuged at 200 *g* for 5 min. PBS was removed and the cells were resuspended in 700 µL of cold lysis stock buffer (for more details check **Table 11**, section 2.1.9). Cells were lysed with a dounce homogenizer and the lysate was centrifuged at 180.000 *g* for 1 h at 4°C in order to sediment the membranes. The supernatant, cytosol, was kept for later TCA-precipitation. The pellet, membranes, was resuspended with 700µL of cold lysis stock buffer and then centrifuged at 180.000 *g* for 20 min at 4°C for washing the membranes. After centrifugation the supernatant was removed and the pellet underwent to protein extraction with solubilization buffer (for more details check **Table 11**, section 2.1.9) for 30 min at 4°C. Cells were centrifuged at 15.000 rpm for 20 min and the supernatant was kept and the pellet was discarded. Protein from cytosol and membranes was measured by a Bradford assay. Finally, both fractions underwent TCA-precipitation.

2.2.30. TCA precipitation

TCA was added to the samples to a final concentration of 12,5% (w/v) (from a stock solution of 50% (w/v) TCA), gently vortexed the tubes and incubated on ice for 30 min. Then, the samples were centrifuged at 10.500 rpm for 7 min at 4°C and the supernatant was discarded. The pellet was then resuspended and washed with -20°C cold acetone. Samples were centrifuged at 10.500 rpm for 7 min at 4°C and the supernatant was discarded. The pellet was washed a second time with cold acetone and centrifuged. The supernatant was discarded and the pellet was dried at 37°C for 15 min until complete evaporation of acetone. SDS loading buffer was added according to protein concentration calculations and the samples in loading buffer were incubated at 1.200

rpm for 20 min at 30°C. Finally, samples were ready for loading them into SDS-PAGE gels.

2.2.31. Bradford assay for protein quantification

Protein in solution was measured using Coomassie Plus Protein Assay Reagent Thermo Scientific). 1 mL of the reagent was added into a plastic cuvette plus 2 µL of the sample to be measured. Samples were vortexed and incubated for 5 min with the reagent. Correspondent blank samples were incubated with 2µL of the correspondent buffers. Known protein concentration solutions of BSA were prepared in order to obtain a standard curve for absorbances. Absorbance at 595 nm was determined in a spectrophotometer for the samples. The protein quantification was calculated based on the OD_{595} obtained for the BSA standard curve.

2.2.32. SDS-PAGE

To separate proteins by SDS-PAGE (Laemmli 1970) gels were casted following these recipes (Sambrook and Russell 2006). Higher acrylamide percentage gels were casted when interested in low MW proteins and lower acrylamide percentage gels were casted when interested in big proteins. They were casted in gel casters (Hoefer, Hollister, USA) and the height of the stacking was around 1/3 of upper part of the gel whereas the resolving was 2/3 of the lower part of the gel. Gels were electrophoresed at 20 mA (constant amperage) per gel during 90 min in SDS running buffer in electrophoresis units (SE250 Mighty small II, Hoefer).

2.2.33. Western blotting

Proteins separated by SDS-PAGE were subsequently blotted into nitrocellulose membranes (GE Healthcare) using a wet blotting tank (TE22 Mighty small transfer tank, Hoefer) filled with transfer buffer. The gel was placed onto the nitrocellulose membrane and they were sandwiched by two blotting papers pre-equilibrated with transfer buffer. The membrane sandwich was then placed into a blotting cassette that was inserted into the blotting tank with the membrane directed towards the anode. They were electroblotted at 60 V (constant voltage) and the current limited at 0,5 A for 70 min. Once blotted, the membranes were blocked in a solution of 5% Milk in PBS plus 0,1% Tween-20 (Millipore) and shaking for 1 h. Primary antibodies were prepared

in the same blocking solution consistent of 5% Milk in PBS plus 0,1% Tween-20 (Millipore) and the incubation took place O/N at 4°C while shaking. The list of primary antibodies and the WB dilutions used can be found in **Table 8**. Membranes were washed thrice with enough volume of PBS plus 0,1% Tween-20 for 5 min each washing step. 1:5000-diluted fluorescent secondary antibodies (LI-COR Biosciences, Lincoln, USA) (**Table 9**) were added to the membranes in blocking solution and they were incubated for 90 min. Membranes were washed thrice with enough volume of PBS plus 0,1% Tween-20 for 5 min each washing step. The detection of the fluorescent antibodies was carried out with an Odyssey Sa Imaging System (LI-COR) and the acquired images were analyzed and quantified with ImageStudio Lite 5.2.5 software (LI-COR).

2.2.34. Coomassie staining

In order to visualize the proteins in polyacrylamide gels, Coomassie staining is a method commonly used. For that the gel was soaked in fixation buffer (30% v/v, 15% v/v acetic acid) for around 15 min at RT while shaking. Next, the gels were stained by soaking the gel in Coomassie staining buffer (30% v/v ethanol, 10% v/v acetic acid and 0,2% w/v Coomassie brilliant blue). This solution was quickly boiled in the microwave for 15-20 sec and incubated for 20 min at RT while shaking. For removing gel-unspecific Coomassie staining, the gel was left O/N in destaining solution at RT while shaking.

2.2.35. GFP-trap pulldown

HeLa P4 cells were transfected with the correspondent plasmids for EV, Venus and Venus-TRC40$_{wt}$ or Venus-GR. Cells were washed with PBS and harvested. Cells were resuspended in 700 µL of IP binding buffer (150 mM KCl, 5 mM $MgCl_2$, 20 mM Tris pH 7,4). Cells were lysed with a dounce homogenizer and the lysate was centrifuged at 100.000 *g* for 35 min at 4°C in order to pellet the membranes. I kept the supernatant and discarded the pellet. I took 10% of the supernatant volume was subjected to TCA precipitation and served as the input control of the pulldown. The rest of the supernatants were incubated with pre-washed GFP-trap M magnetic beads (ChromoTek, Martinsreid, Germany), using 20 µL per reaction, for 60 min at 4°C in a rotation wheel. Briefly, the beads were washed with IP binding buffer incubating them

in a rotation wheel at 4°C for 20 min and doing four more washes in the magnetic rack, the two first of which contained 0,1% Triton X-100 and the two latest with no detergent. After the incubation with the beads was over, I placed the tubes into the magnetic rack and discarded the supernatant and washed four times with IP binding buffer with no detergent. The beads were eluted with 50 µL of SDS loading buffer and incubated them for 10 min at 30°C 1000 rpm shaking, then samples were ready for Western blot.

2.2.36. Co-immunoprecipitation of Stx5 and TRC40

T-REx 293 Stx5-opsin stable cell line was transfected with the correspondent plasmids for EV, $TRC40_{wt}$, $TRC40_{D74E}$. Cells were treated for 6 h with tetracycline for the induction of the expression of Stx5-opsin. Cells were washed with PBS and harvested. Cells were subjected to cell fractionation as described above. I was just interested in the cytosolic fraction, I discarded the pellets. Protein concentration of the samples was quantified by Bradford. I took 10% of the volume of the cytosolic fractions and I performed TCA precipitation, they served as the input controls. The Protein G beads (GE Healthcare, Chicago, USA) were incubated with the correspondent antibody: IgG normal rabbit as IP control, anti-Stx5 or anti-TRC40 at 4°C for 1 h in a rotation wheel followed by four washes with lysis stock buffer. After the washes, the pre-loaded beads were incubated with a solution containing 3% of BSA for 20 min at 4°C in the rotation wheel. The cytosolic fractions were then incubated with Protein G beads pre-loaded with the correspondent antibody for 150 min at 4°C in a rotation wheel. Once the incubation was over, the supernatant was discarded and the beads were washed four times with lysis stock buffer. No detergents were added in any step. The beads were incubated for 15 min at RT with SDS loading buffer and then eluted. Samples were ready for Western blot.

2.2.37. Co-immunoprecipitation of the GR and TRC40

HeLa P4 cells were cultured up to 70% confluency. They were washed with PBS and harvested. Cells were subjected to cell fractionation as described above. I was just interested in the cytosolic fraction, I discarded the pellets. Protein concentration of the samples was quantified by Bradford. I took 10% of the volume of the cytosolic fractions and I performed TCA precipitation, they served as the input controls. The Protein A beads (GE Healthcare) were incubated with the mouse anti-GR antibody (serving IgG

normal mouse as control) at 4°C for 1 h in a rotation wheel followed by four washes with lysis stock buffer. The Protein G beads (GE Healthcare) were incubated with the rabbit anti-TRC40 antibody (serving IgG normal rabbit as control) at 4°C for 1 h in a rotation wheel followed by four washes with lysis stock buffer. After the washes, the pre-loaded beads were incubated with a solution containing 3% of BSA for 20 min at 4°C in the rotation wheel. The cytosolic fractions were then incubated with the beads pre-loaded with the correspondent antibody for 150 min at 4°C in a rotation wheel. Once the incubation was over, the supernatant was discarded and the beads were washed four times with lysis stock buffer. No detergents were added in any step. The beads were incubated for 15 min at RT with SDS loading buffer and then eluted. Samples were ready for Western blot.

2.2.38. PNGase F treatment

T-REx 293 Stx5-opsin stable cell line was transfected with the correspondent plasmids for EV, $TRC40_{wt}$, $TRC40_{D74E}$. Cells were treated for 6 h with tetracycline for the induction of the expression of Stx5-opsin. Cells were washed with PBS and harvested. Cells were subjected to cell fractionation as described above with some modifications. Membranes were solubilized with solubilization buffer for 30 min on ice and centrifuged at 180.000 *g* for 30 min at 4°C, pellet was discarded afterwards. Protein concentration was quantified by Bradford. TCA precipitation to both membranes and cytosol fractions was carried out. TCA pellets were washed twice with cold acetone and dried 10 min at 37°C. PNGase F buffer (consistent of 1-fold glycoprotein denaturing buffer, 1-fold G7 buffer, 2,5% NP-40 in ddH_2O) was added to the TCA precipitates and incubated at 37°C for 30 min at 1400 rpm. Per 300 µg of total protein, 50 µL of PNGase F buffer was added. Once the incubation for denaturing glycoproteins was over, 1 µL of PNGase F (10 U/µL in the final volume) (New England Biolabs) was added and the samples were incubated at 37°C for 30 min. Samples were supplemented afterwards with 5x SDS loading buffer and DTT for Western blot analysis.

2.2.39. Digitonin semipermeabilization

Coverslips with HeLa P4 cells were transferred into a 12-well plate. They were washed once with PBS and placed the 12-well plate on ice. A cold solution of 0,007% of digitonin in transport buffer (for more details check **Table 11**, section 2.1.9) was added

and incubated for exactly 5 min. The digitonin solution was quickly removed and the coverslips were washed twice with cold transport buffer. The coverslips were then suitable for starting an indirect fluorescence protocol.

2.2.40. Indirect immunofluorescence (IF)

UV-sterilized 10 mm coverslips were added to the plates and HeLa P4 cells seeded on top. When it was due the harvesting, cells were washed twice with PBS and later they were fixed with 4% (w/v) PFA in PBS for 15 min. Secondly, they were permeabilized with 0,3% Triton X-100/0,05% SDS in PBS for 10 min at room temperature. Samples were blocked with 10% FBS in PBS for 30 min and incubated with primary antibodies diluted in blocking buffer overnight at 4°C. Incubation with Alexa Fluor secondary antibodies (Invitrogen) (**Table 10**) was performed for 60 min at room temperature. The samples were mounted with Mowiol-DAPI for the confocal microscope. 2x PBS washes were performed in between the different steps.

In the case of digitonin-semipermeabilized cells, the PFA fixation was done right after and the Triton X-100/SDS permeabilization step was skipped.

2.2.41. Imaging with a LSM 510-META confocal microscope

Cells were analyzed using an Axiovert 200M fluorescence microscope with a 63× Plan-Neofluar 1.3 NA water-corrected objective and appropriate filter settings. Images were taken using a LSM 510-META confocal laser scanning microscope (Zeiss, Jena, Germany). For confocal imaging a UV laser (405 nm) at 25 mW, a tunable Argon laser (488 nm) at 30 mW, HeNe laser line (543 nm) at 1 mW, HeNe laser lines (633 nm) at 3 mW were used for excitation. Emission filters: 450/60 nm, 518/25 nm, 588/56 nm, long-pass (LP) 650 nm respectively.

2.2.42. Imaging with an Imaging Machine 03-dual widefield screening microscope

HeLa P4 cells were seeded in laminin-coated (Corning #354232) 384-well glass-bottom plates (Matriplate, Brooks Life Science Systems #MGB101-1-2-LG-L; Manchester, United Kingdom) and there the immunostaining was performed as

described above. The plates were automatically imaged on an Imaging Machine 03-dual widefield high-content screening microscope (Acquifer; Karlsruhe, Germany) equipped with a white light-emitting diode array for brightfield imaging, a light-emitting diode fluorescence excitation light source, a sCMOS (2,048 × 2,048 pixel) camera, and a stationary plate holder in combination with movable optics. Images were acquired with 405-nm, 470-nm and 625-nm filter cubes (excitation 390/40 nm, emission 452/45 nm, and dichroic 405 nm; excitation 469/35 nm, emission 525/39 nm, and dichroic 497 nm; and excitation 628/40 nm, emission 692/40 nm, and dichroic 660 nm; respectively) with a 40× CFI Super Plan Fluor ELWD NA 0.60 (Nikon; Tokyo, Japan). Integration times were fixed at 50ms for the 405-nm channel and 100 ms for the other two fluorescence channels. The focal plane was detected in the 405-nm channel using an autofocus algorithm.

2.2.43. Indirect immunofluorescence image quantification

The images acquired were loaded into the open-source image-analysis software CellProfiler (Version 2.1.1 (rev 6c2d896)) (Carpenter et al. 2006) that was used to analyze and measure intensities. ImageJ was used to convert the lsm format files generated by the confocal software into TIFF files recognized by CellProfiler. GR- or BAG6-background discrimination was done on Otsu threshold to the GR or BAG6-channel images. A cell mask was created based on the area covered by the GR- or BAG6-channel image differentiated from the background. The nucleus discrimination relied on the DAPI-channel images, based as well on Otsu threshold. A nucleus mask was created based on the area covered by the DAPI staining, from the previous step, on the GR or BAG6-channel images. A cytosolic mask was creating by subtracting the nucleus mask to the cell mask. GR or BAG6 mean intensities within the nucleus mask and the cytosol mask were measured. The GR/BAG6 nucleus-mask intensities were divided by the cytosol-mask intensities giving the nucleo-cytoplasmic ratio. In the case of the BAG6 nucleo-cytoplasmic ratio in the presence of TRC40 variants, there was an extra mask. This mask was made from the cmyc-channel images for filtering and measure only those transfected cells. This mask was placed and applied before the others. All the measurements and calculations were automatically exported into a csv file. Further details from the algorithm can be found in the 7.5.1 and 7.5.2 in the Appendix section.

2.2.44. Statistics and software

Statistical analyses were calculated with Graph Prism 6.0 for MacOS (GraphPad Software Inc., San Diego, USA) using a two-tail unpaired t test with equal SD. The dot-plots and scatter-plots were also done in Graph Prism 6.0 for MacOS.

Indirect immunofluorescence images analyses were performed with ImageJ 1.51w software (US National Institutes of Health, Bethesda, USA) (Schneider, Rasband, and Eliceiri 2012). Quantification of the images was done using CellProfiler (Version 2.1.1 (rev 6c2d896)) (Carpenter et al. 2006). CellProfiler pipelines used for quantification can be found in sections 7.5.1 and 7.5.2 in Appendix.

Blot quantification were done in ImageStudio Lite 5.2.5 software (LI-COR). For the blot figures scanned images were exported from ImageStudio, rotated and cropped in Adobe Photoshop CS6 (Adobe, San José, USA) and the composition was done in Adobe Illustrator CS6 (Adobe, San José, USA).

Structure figures were generated using PyMOL (The PyMOL Molecular Graphics System, Version 2.0 Schrödinger, LLC.) and the Protein Data Bank files were obtained from RCSB PDB (www.rcsb.org) (Berman et al. 2000). The PDB IDs were provided in the correspondent figure legends.

For plasmid edition, sequencing alignment and primer design were done using SnapGene 4.1.6 software (GSL Biotech, Chicago, USA).
mRNA expression levels from human tissue was coming from the human Genotype-Tissue Expression database v6, GTEx (GTEx Consortium 2015; Melé et al. 2015; Rivas et al. 2015). Data available here: https://www.gtexportal.org/home/.

Protein sequences alignments were performed with Clustal Omega (https://www.ebi.ac.uk/Tools/msa/clustalo/) (Li et al. 2015). The FASTA sequences provided for the alignments and the UniProt accession numbers were obtained from UniProt (http://www.uniprot.org) (The UniProt Consortium 2017). NCBI protein accession numbers were obtained from NCBI Protein (https://www.ncbi.nlm.nih.gov/protein).

The transmembrane segment of the TA-proteins was predicted using the TMHMM algorithm (Krogh et al. 2001; Möller, Croning, and Apweiler 2001) using the website TMHMM Server 2.0 (http://www.cbs.dtu.dk/services/TMHMM/).

The helical wheel analysis was performed using the application wheel.pl v1.4 (Zidovetzki et al. 2003). Available here: http://rzlab.ucr.edu/scripts/wheel/wheel.cgi

The sequence logo was generated using the web-based generator Seq2Logo 2.0 (Thomsen and Nielsen 2012). Available here: http://www.cbs.dtu.dk/biotools/Seq2Logo/. Parameters used in the analysis are available in section 7.5.3 in Appendix.

The phylogenetic tree was generated using the web tool Interactive Tree of Life (iTOL) v4.2 (Letunic and Bork 2016). Available here: http://itol.embl.de

3. Results

3.1. $TRC40_{D74E}$, a mutant for the study of TA-protein biogenesis *in vivo*

Since the role of Get3 in the GET pathway was published (Schuldiner et al. 2008), its structure and domains have been described in multiple papers (Mateja et al. 2009; Suloway et al. 2009; Bozkurt et al. 2009; Hu et al. 2009; Yamagata et al. 2010; Stefer et al. 2011; Mariappan et al. 2011; Kubota et al. 2012; Gristick et al. 2014; Mateja et al. 2015; Gristick et al. 2015). The relevance of mutations within those domains, in particular mutations affecting the ATPase domain or the TA-binding groove of Get3, has been characterized. Nevertheless, little is known about TRC40 structure and domains apart from the assumption that similar, or conserved, domains execute the same functions.

A well characterized mutant of Get3 is $Get3_{I193D}$, which substitutes a side chain facing the TA-protein binding groove. This mutant, whose interaction with TA-proteins was shown to be impaired *in vitro* (Mateja et al. 2009), has also been proposed to represent a fully chaperone-active form (Voth et al. 2014). Another widely-used mutant is the $Get3_{D57E}$, which targets the conserved Switch I ATPase domain. As expected, this mutation, or another exchange at the same position, i.e. $Get3_{D57N}$, affects the ATPase-activity of Get3 (Mateja et al. 2009; Powis et al. 2013; F. Wang et al. 2011; Stefer et al. 2011; Chio et al. 2017). There is also insight into the effects of changing D45 in the Switch I domain of the bacterial homolog ArsA (Tongqing Zhou and Rosen 1999). A third mutant, $Get3_{G30R}$ which targets the P-loop or Walker A motif, has been used as an ATPase-dead mutant of Get3 in several papers (Shen et al. 2003; Schuldiner et al. 2005; Suloway et al. 2009; F. Wang et al. 2011; Johnson, Powis, and High 2013). This mutant has been shown to be deficient in nucleotide-binding (Saraste, Sibbald, and Wittinghofer 1990).

3.Results

For the purpose of dissecting the chaperone function of TRC40 *in vivo* and its relation to the TRC-pathway components and substrates I created a panel of cmyc-tagged TRC40 mutants (**Fig. 12B**). This set is very useful for screening changes in subcellular localization of potential substrates by indirect immunofluorescence. These mutants were resistant (siTRC40ins) to the siRNAs established for TRC40 knock-down (Pfaff et al. 2016), thus one can down-regulate the endogenous TRC40 and monitor the transfected cmyc-tagged TRC40.

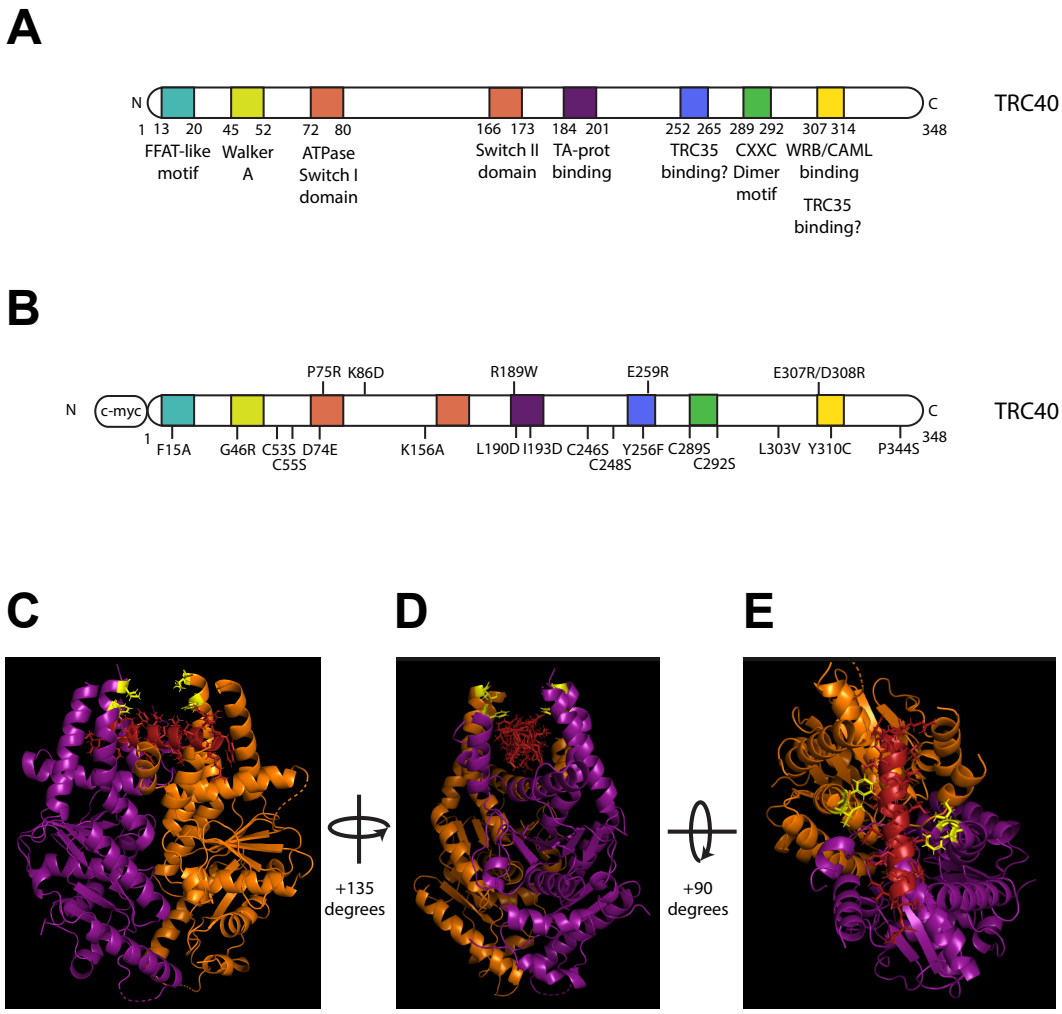

Figure 12. Investigated TRC40 mutants in the context of TRC40 domains. (A) TRC40 scheme illustrating functional domains based on the residues between Get3 and TRC40. **(B)** Mutations generated for the different functional domains of TRC40. **(C)** The mutations generated in the TA-protein binding groove of TRC40 are highlighted (in yellow) in the conserved residues of Get3 crystal structure. Side view. **(D)** A 135º plane rotation. Frontal view. **(E)** A 90º plane rotation. Top view. Get3 subunits are depicted in orange and deep purple whereas TA-protein is depicted in red. PDB ID: 4XTR.

The SNARE protein syntaxin 5 (Stx5) is the best characterized TRC40 substrate (Rivera-Monroy et al. 2016; Norlin et al. 2016; Casson et al. 2017; Norlin, Parekh, and Edlund 2018). Similarly, yeast syntaxin 5 (Sed5) requires Get3 for proper targeting and localization (Schuldiner et al. 2008; Jonikas et al. 2009; Powis et al. 2013; Voth et al. 2014). Therefore, I used Stx5 subcellular localization by IF as a reliable readout of the impairment of TRC40-dependent TA-targeting in the analysis of TRC40 mutants. First, I silenced the endogenous TRC40 and then transfected HeLa cells with the set of TRC40 mutants. I performed IF co-staining for Stx5 and cmyc-TRC40. Among the mutants analyzed there was one with a striking effect: upon transfection with the $TRC40_{D74E}$ mutant, Stx5 changed its subcellular localization showing an apparently cytoplasmic staining instead of the Golgi-staining reflecting proper targeting and sorting of Stx5 (**Appendix Fig. 1A**).

3.1.1. In the presence of $TRC40_{D74E}$, certain TA-proteins accumulate in cytoplasm

I set out to dissect the effects of the $TRC40_{D74E}$ mutant on Stx5. First, I tested whether the $TRC40_{D74E}$ mutant had its striking effect only in the absence of endogenously expressed TRC40 and transfected the constructs without prior siRNA-mediated silencing of TRC40. Indeed, it turned out that the effect on Stx5 distribution was indistinguishable from the previous result obtained after knockdown of endogenous TRC40 (data not shown). To test the contribution of the TA-protein binding groove on the effects of $TRC40_{D74E}$ expression, I generated a couple of D74E mutants that additionally carried mutations in the region encoding the TA-protein binding groove (**Fig. 12C**) such as $TRC40_{D74E/I193D}$ and $TRC40_{D74E/L190D/I193D}$ (Mateja et al. 2009; F. Wang et al. 2010; Shao et al. 2017). I transfected HeLa cells with these TRC40 constructs and performed an indirect immunofluorescence staining for the TRC40 variants, for Stx5, and for Emerin (EMD), a second TA-protein, which has been shown to be a substrate of the TRC pathway (Pfaff et al. 2016; Rivera-Monroy et al. 2016).

3.Results

In the presence of the $TRC40_{D74E}$, both Stx5 and EMD showed cytoplasmic staining (**Fig. 13A**, **Fig. 14A**). Moreover, no Golgi staining was observed for Stx5 in $TRC40_{D74E}$-transfected cells. Whereas for Stx5 the over-expression of $TRC40_{wt}$ did show partial cytoplasmic staining, for EMD there were no major effects compared to transfection with the empty vector. Quantification of the results is shown in **Fig. 19A, Fig. 19B**. Regarding the D74E TA-protein binding mutants, the phenotype of both, Stx5 and EMD, was maintained in the presence of the mutant carrying one single mutation, compared to $TRC40_{D74E}$, but the phenotype was milder and reduced in the presence of the mutant with two mutations changing side chains within the TA-protein binding groove. Interestingly, Stx5 subcellular localization in the presence of $TRC40_{D74E/L190D/I193D}$ was intermediate between the one observed in the case of the $TRC40_{D74E}$ transfection and the one observed after transfection of the empty vector. This indicates that the mutations investigated might not be sufficient to completely disrupt the interaction of Stx5 with the TA-protein binding groove or that the binding of Stx5 to TRC40 also involves a different region of TRC40.

Stx5 plays an important role in the maintenance of Golgi apparatus structure (Suga et al. 2005; Amessou et al. 2007) and an impairment of the TRC pathway results in reduced steady-state levels of Stx5 and a fragmented Golgi structure (Rivera-Monroy et al. 2016; Norlin, Parekh, and Edlund 2018). In those cells transfected with the $TRC40_{D74E}$, the protein GM130, which is a component of the *cis*-Golgi stack that helps to maintain the Golgi structure (Barr and Short 2003; Gillingham and Munro 2016), and hence serves as a marker for the Golgi apparatus, revealed a fragmented Golgi (**Fig. 13A**). In conclusion, reduced targeting of Stx5 to the Golgi may result in an altered structure of this organelle. In contrast, mistargeting of EMD did not affect its target compartment, the inner nuclear membrane (INM). In fact, lamin A/C, a marker protein for the INM, was unaffected in the presence of $TRC40_{D74E}$ over-expression (**Fig. 21A**) indicating that the INM is not altered in these cells.

Based on these results, which suggest that $TRC40_{D74E}$ can be used as a tool to uncover the interaction of TRC40 with substrates. I expanded the panel of TA-proteins tested with the $TRC40_{D74E}$ mutant. Upon the over-expression of this mutant, later experiments revealed that Stx8 also showed cytoplasmic staining in $TRC40_{D74E}$-transfected HeLa cells (**Fig. 15A**). Stx8 is a t-SNARE localized to endosomes. Similar

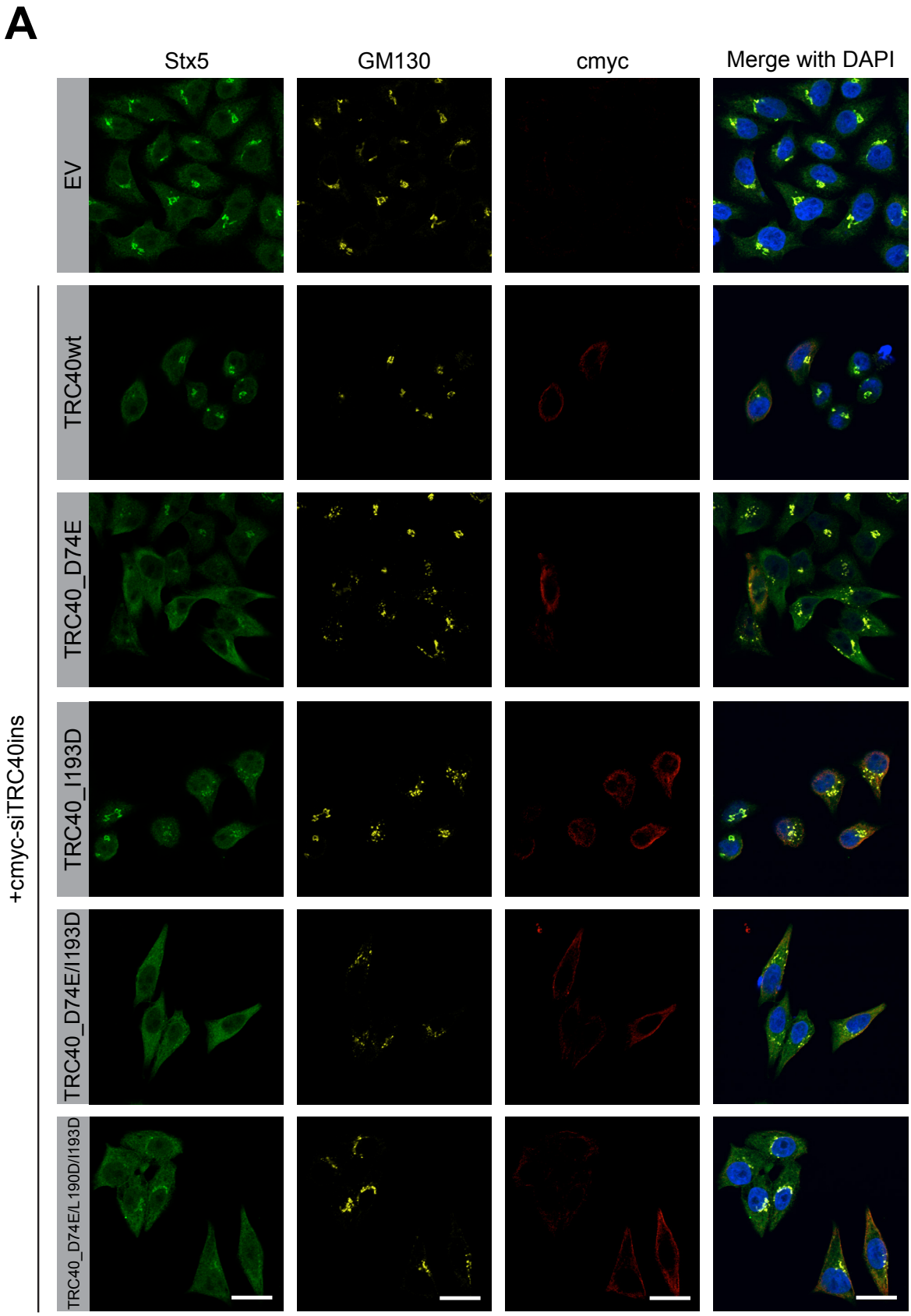

Figure 13. TRC40$_{D74E}$ alters the subcellular localization of the v-SNARE Stx5. (A) Immunofluorescence of Stx5 upon over-expression of different TRC40 variants in HeLa cells. Images of Stx5, the *cis*-Golgi marker GM130, and cmyc-TRC40 stained by indirect immunofluorescence are shown. Three to seven biological replicates were analyzed. Scale bars: 20 µm.

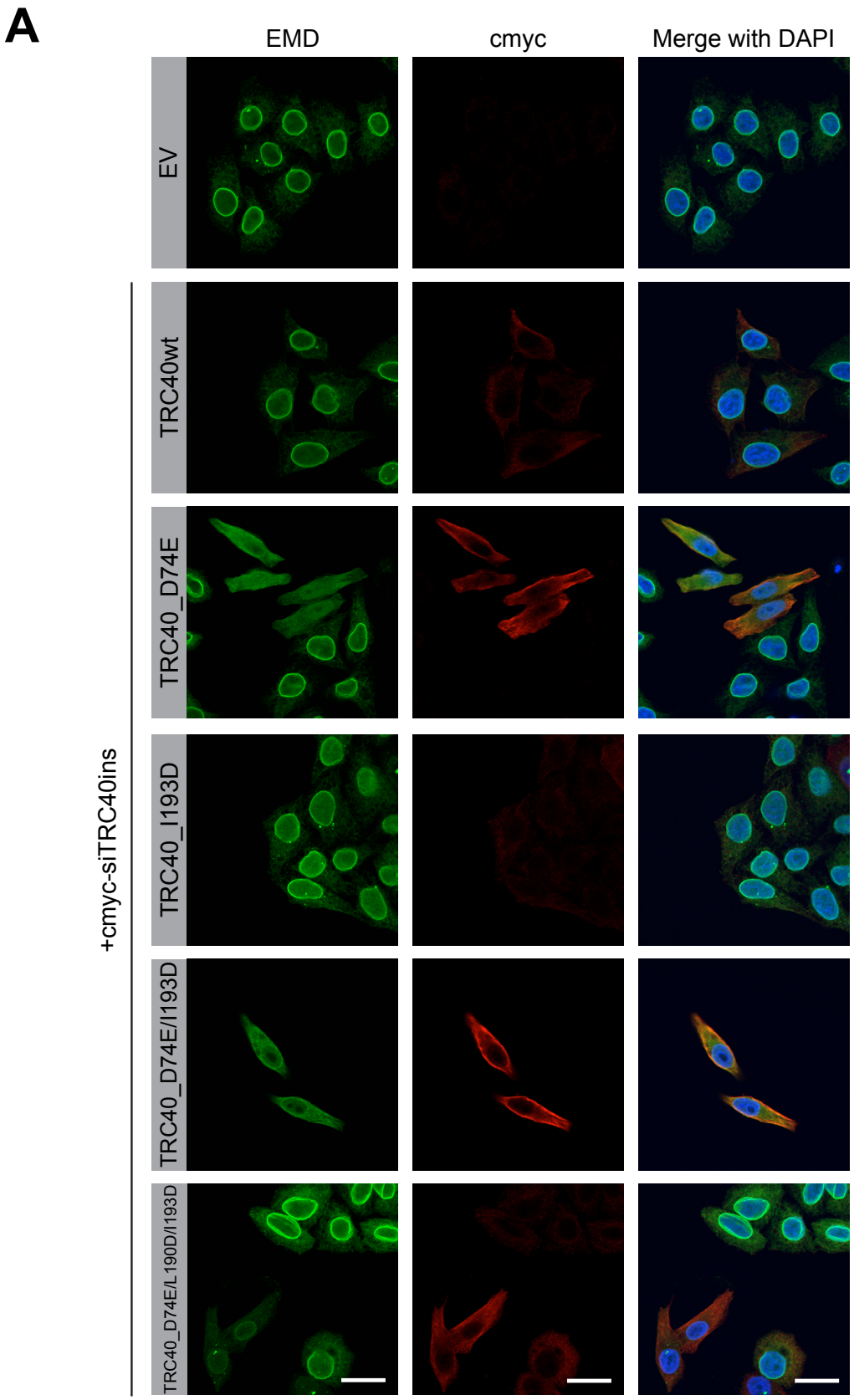

Figure 14. TRC40$_{D74E}$ alters the subcellular localization of the inner nuclear membrane protein EMD. (A) Immunofluorescence of EMD upon over-expression of different TRC40 variants in HeLa cells. Images of EMD and cmyc-TRC40 stained by indirect immunofluorescence are shown. Four to six biological replicates were analyzed. Scale bars: 20 µm.

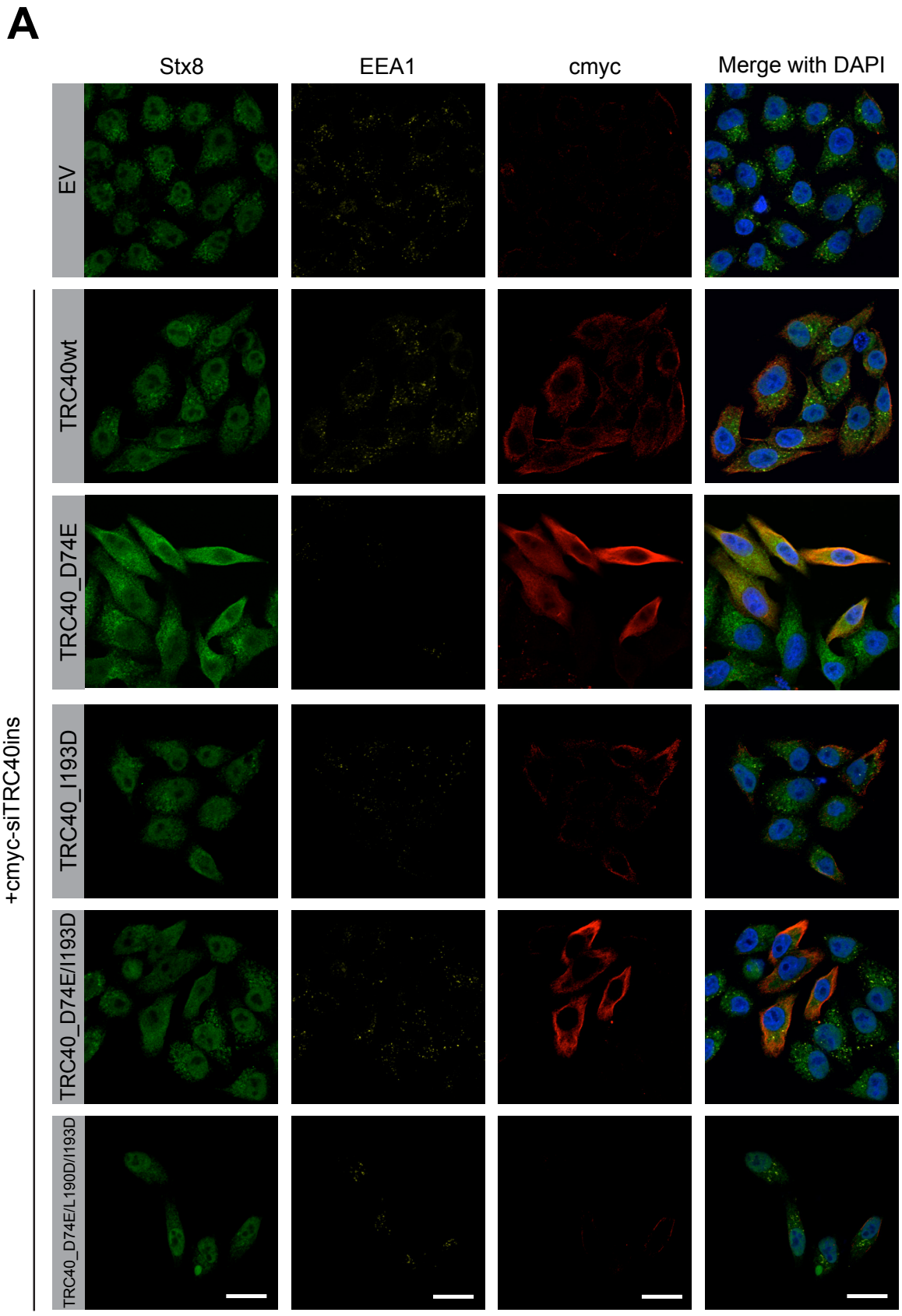

Figure 15. TRC40$_{D74E}$ does alter the subcellular localization of the endosomal t-SNARE protein Stx8. (A) Immunofluorescence of Stx8 upon transfection of different TRC40 variants in HeLa cells. Images of Stx8, the early endosomal marker EEA1, and cmyc-TRC40 stained by indirect immunofluorescence are shown. Three biological replicates were analyzed. Scale bars: 20 µm.

to the staining of EMD, Stx8 was not altered in the $TRC40_{wt}$-over-expressing cells or the double TA-groove mutant but the phenotype of the D74E/I193D mutant still presented a cytoplasmic staining. Quantification of the results is shown in **Fig. 19A** and **Appendix Fig. 6**.

In contrast, other TA-proteins like Sec61β, an ER-protein that forms part of the Sec61 translocon and has been extensively used to probe TRC40-dependence in *in vitro*-experiments (Stefanovic and Hegde 2007) remained unaffected regardless of the TRC40 variant over-expressed (**Fig. 16A**). No cytoplasmic population was observed, instead colocalization with the ER marker protein calnexin was complete. Sec61β phenotype was quantified in **Fig. 19A**. Like Sec61β, PTP1B and VAPB are both ER-resident TA-proteins. They were unaffected by the presence of the $TRC40_{wt}$ or the mutants (**Fig. 17A, Fig. 18A**). D74E effect was quantified in **Fig. 19A**.

The $TRC40_{D74E}$ mutant affects some TA-proteins altering their native subcellular localization to a cytoplasmic one but it has no effect on other TA-proteins. For two proteins affected by this mutant, Stx8 and EMD, one additional mutation in the TA-protein binding groove, I193D, is not sufficient to revert the phenotype. Whereas the combination of the D74E, exchanged with two mutations in the TA-protein binding groove, L190D and I193D, is enough to abolish the sequestration in the cytoplasm. Surprisingly, the triple mutant still affected the subcellular localization of Stx5, albeit to a lesser degree. This suggests a potential additional binding region relevant to the interaction of TRC40 with Stx5.

3.1.2. Stx5 and EMD cytoplasmic accumulation upon $TRC40_{D74E}$ is sensitive to semipermeabilization with digitonin

In order to discriminate whether the cytoplasmic staining pattern seen for Stx5 and EMD in $TRC40_{D74E}$-transfected cells indeed reflects localization to the cytoplasm, I performed a semipermeabilization with digitonin before the IF. Digitonin, at low concentrations and short incubation times on ice, is able to permeabilize preferentially the plasma membrane leaving the rest of the cell membranes, including the nuclear

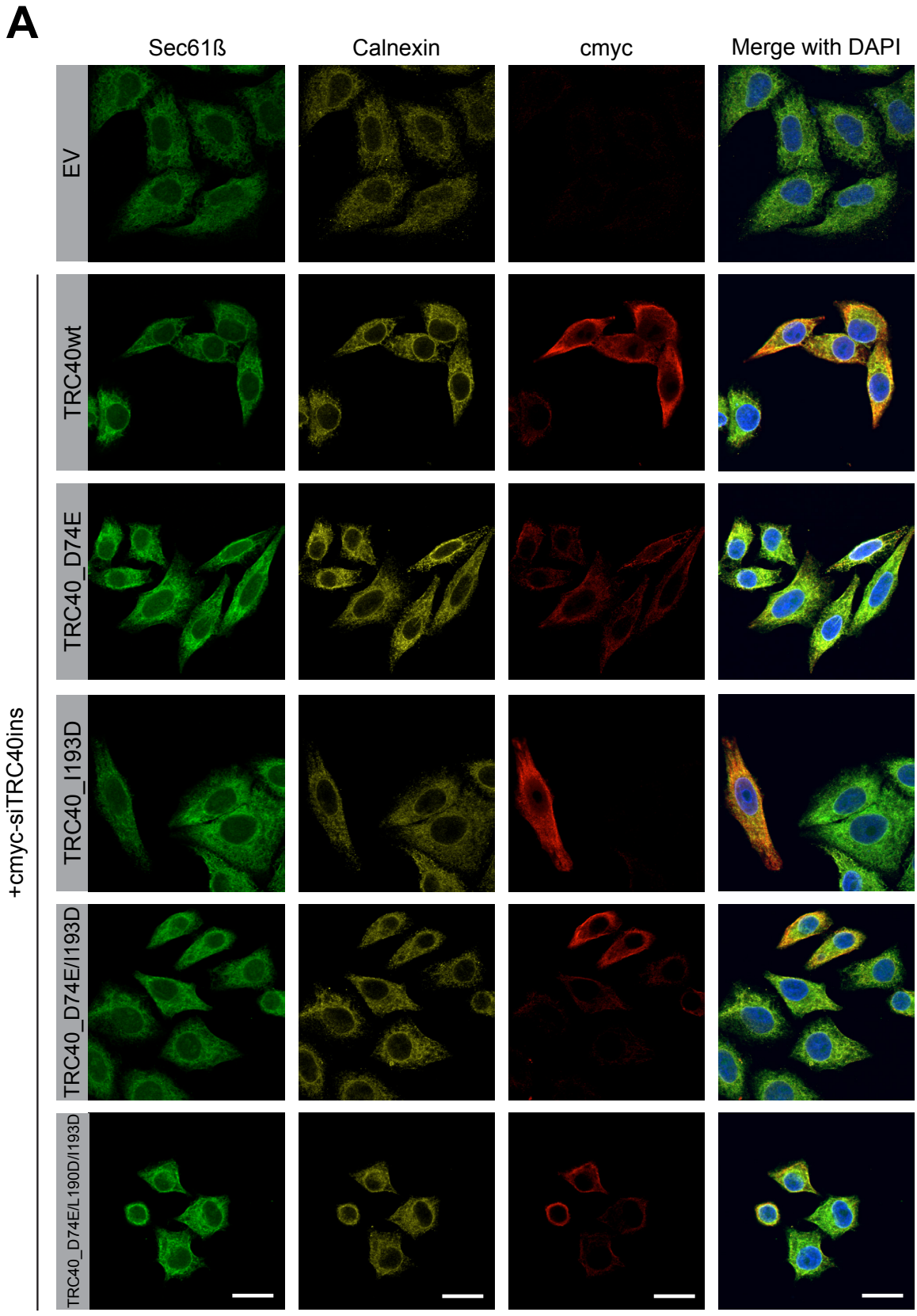

Figure 16. TRC40$_{D74E}$ does not alter the subcellular localization of the ER protein Sec61ß. (A) Immunofluorescence of Sec61ß upon over-expression of different TRC40 variants in HeLa cells. Images of Sec61ß, the ER marker calnexin, and cmyc-TRC40 stained by indirect immunofluorescence are shown. Three to four biological replicates were analyzed. Scale bars: 20 µm.

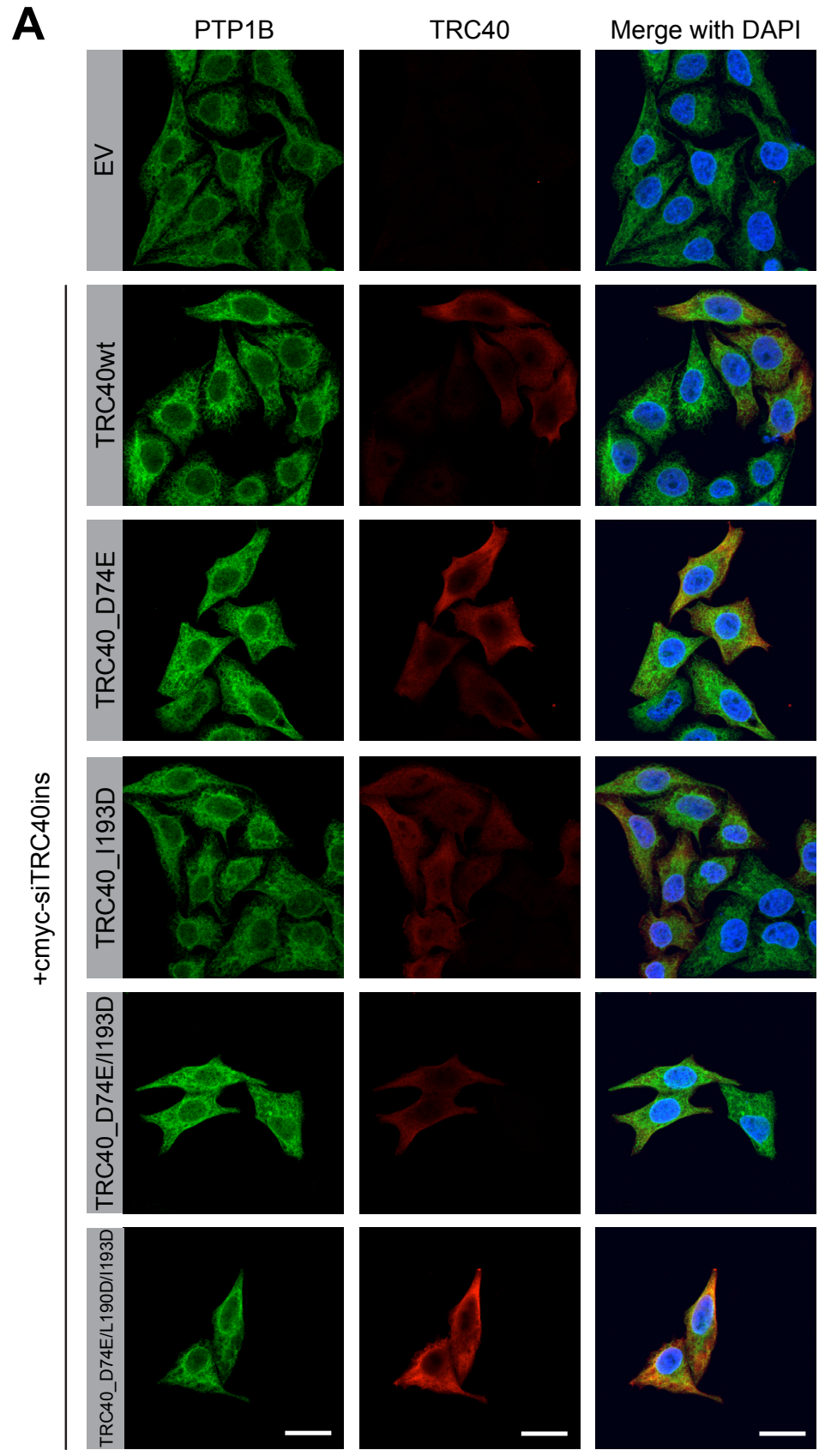

Figure 17. TRC40$_{D74E}$ does not alter the subcellular localization of the ER protein PTP1B. (A) Immunofluorescence of PTP1B upon over-expression of different TRC40 variants in HeLa cells. Images of PTP1B and TRC40 stained by indirect immunofluorescence are shown. Three biological replicates were analyzed. Scale bars: 20 µm.

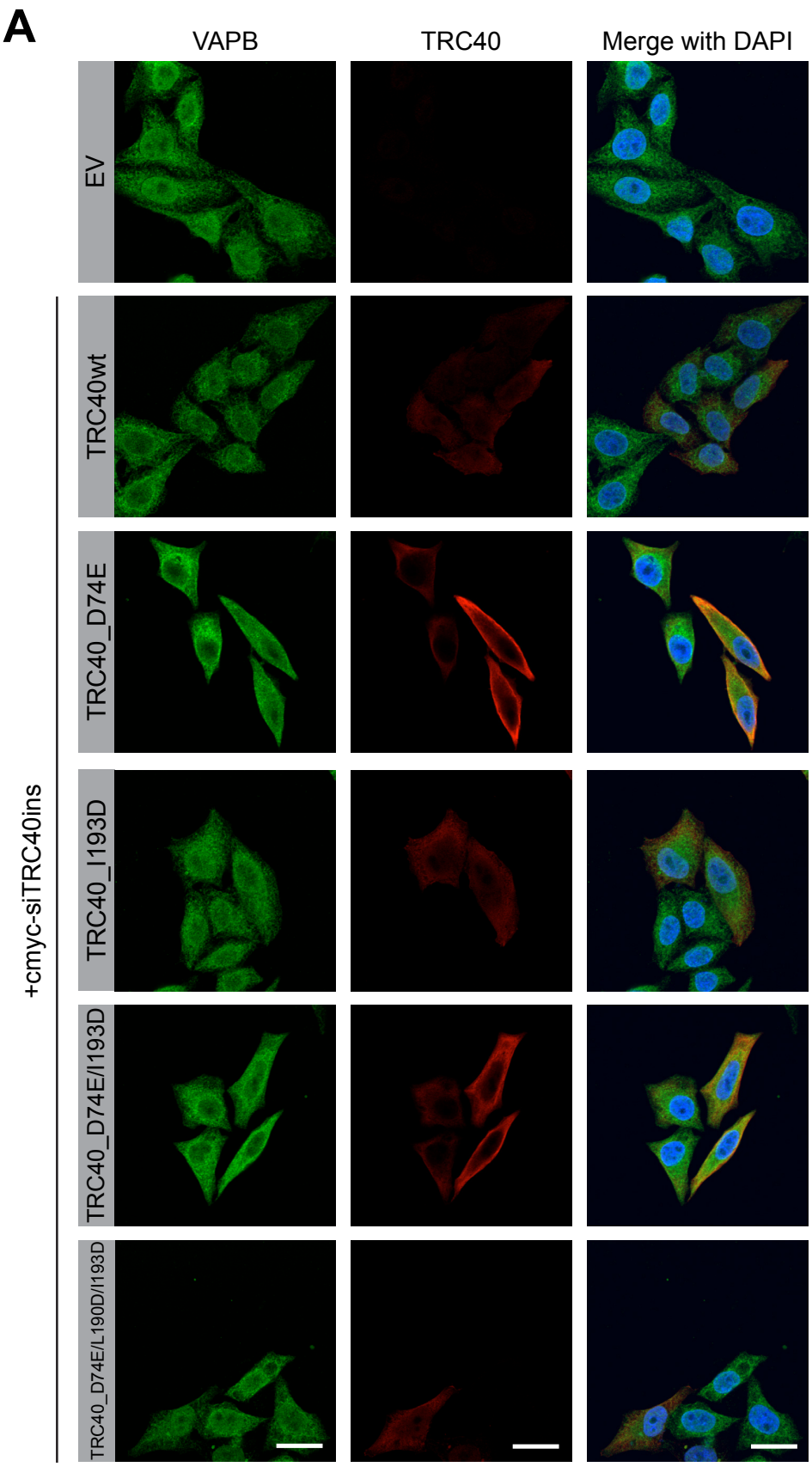

Figure 18. TRC40$_{D74E}$ does alter the subcellular localization of the ER protein VAPB. (A) Immunofluorescence of VAPB upon over-expression of different TRC40 variants in HeLa cells. Images of VAPB and TRC40 stained by indirect immunofluorescence are shown. Three biological replicates were analyzed. Scale bars: 20 µm.

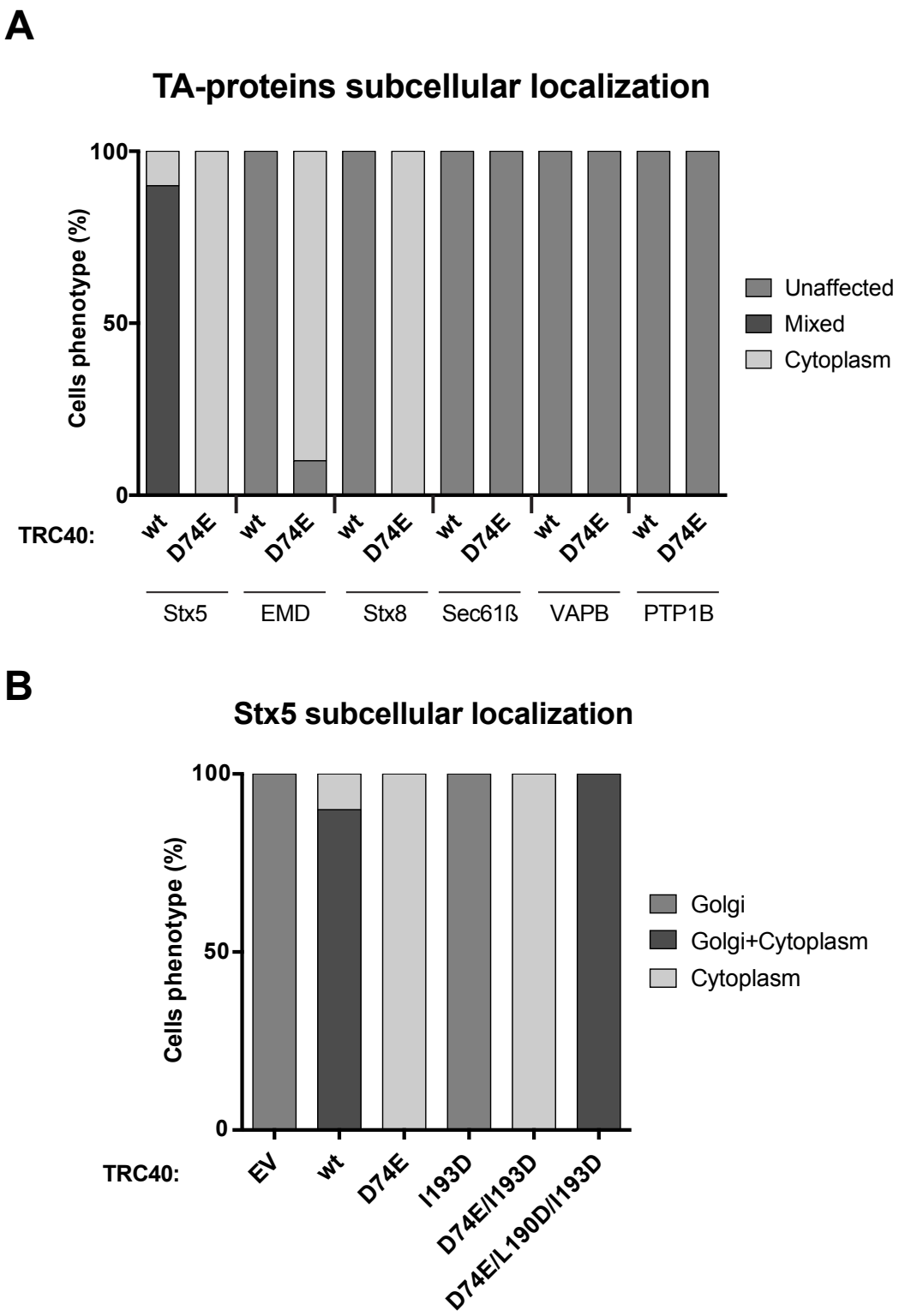

Figure 19. Quantification of the subcellular localization phenotype of the TA-proteins in the presence of different TRC40 mutants. (A) $TRC40_{D74E}$ effect over the subcellular localization of the TA-proteins tested in **Fig. 13-18** using $TRC40_{wt}$ as control. The mixed phenotype represents a Golgi-localized Stx5 that also shows in cytoplasm. From each protein 27 to 151 cells are represented. Two to seven biological replicates. **(B)** Quantification of the subcellular localization phenotype of Stx5 in the presence of TRC40 mutants tested in Fig. 13. n= 60-311 cells are represented. Three to seven biological replicates. Extended quantification panel for EMD and Stx8 can be found in **Appendix Fig. 6**.

envelope, intact (Plutner et al. 1992; Wilson et al. 1995). To ensure that only the plasma membrane had been permeabilized, I assessed the integrity of the nuclear compartment. Lamin A/C, a INM protein marker, served as a control for the intact nuclear membrane, and demonstrated successful semi-permeabilization.

Interestingly, Stx5 was washed out from the D74E-semipermeabilized cells compared to the control (where the cells were fixed in the first place and then permeabilized with Triton X-100). In contrast, semipermeabilization of the cells transfected with the empty vector revealed that Stx5 remains in the Golgi membrane (**Fig. 20B**). Taken together, this confirms that Stx5 was cytoplasmic, as suggested by indirect immunofluorescence staining. $TRC40_{D74E}$ therefore has the capacity to trap Stx5 in the cytoplasm.

In the case of EMD, the putative cytoplasmic population present in the D74E-transfected and semipermeabilized cells could be washed out. However, a fraction of the protein was still observed in the ER and at the nuclear rim (**Fig. 21B**). Hence, I was able to detect a cytoplasmic EMD population upon D74E transfection that was cytoplasmic, but unlike Stx5 EMD was also present in the membranes.

3.1.3. Stx5 is not affected by the inhibition of deubiquitinases in $TRC40_{D74E}$-transfected cells

The lack of some components of the GET pathway in yeast provokes the accumulation of Sed5 in punctate foci (Schuldiner et al. 2008; Battle et al. 2010; Kohl et al. 2011; Vilardi et al. 2014; Voth et al. 2014; Powis et al. 2013). Get3 colocalizes with Sed5 in those puncta. Furthermore, Get3 accumulates in foci upon glucose deprivation (Powis et al. 2013). The addition of deubiquitinase (DUB) inhibitors, such as b-AP15, to glucose-starved yeast prevented the recruitment of Get3 into those foci (Powis 2012). Unlike Get3 in yeast, $TRC40_{D74E}$ does not appear in punctate structures but does colocalize with Stx5, and other substrates in the cytoplasm. DUBs have been implicated to play key roles in Endoplasmic reticulum-associated degradation (ERAD) (Q. Wang, Li, and Ye 2006; Ernst et al. 2009; Yanfen Liu et al. 2014). Moreover, SGTA interacts with the proteasomal ubiquitin receptor Rpn13 modulating quality control

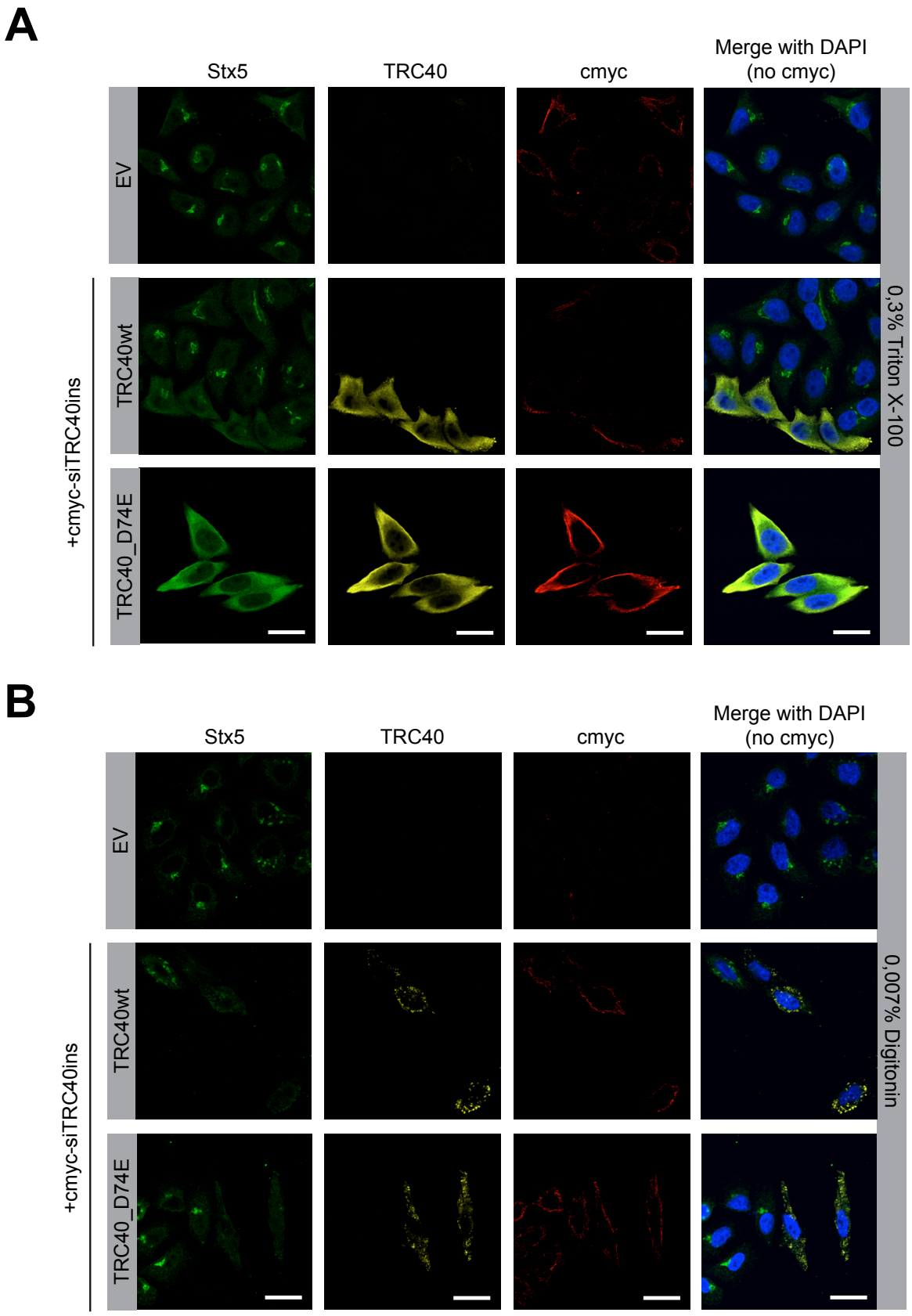

Figure 20. Stx5 is washed out from TRC40 semi-permeabilized, D74E-transfected cells. (A) Immunofluorescence of Stx5 upon over-expression of different TRC40 variants in HeLa cells. Cells were semi-permeabilized with a solution containing 0,007 % digitonin in **(B)**. One biological replicate was analyzed. Scale bars: 20 µm.

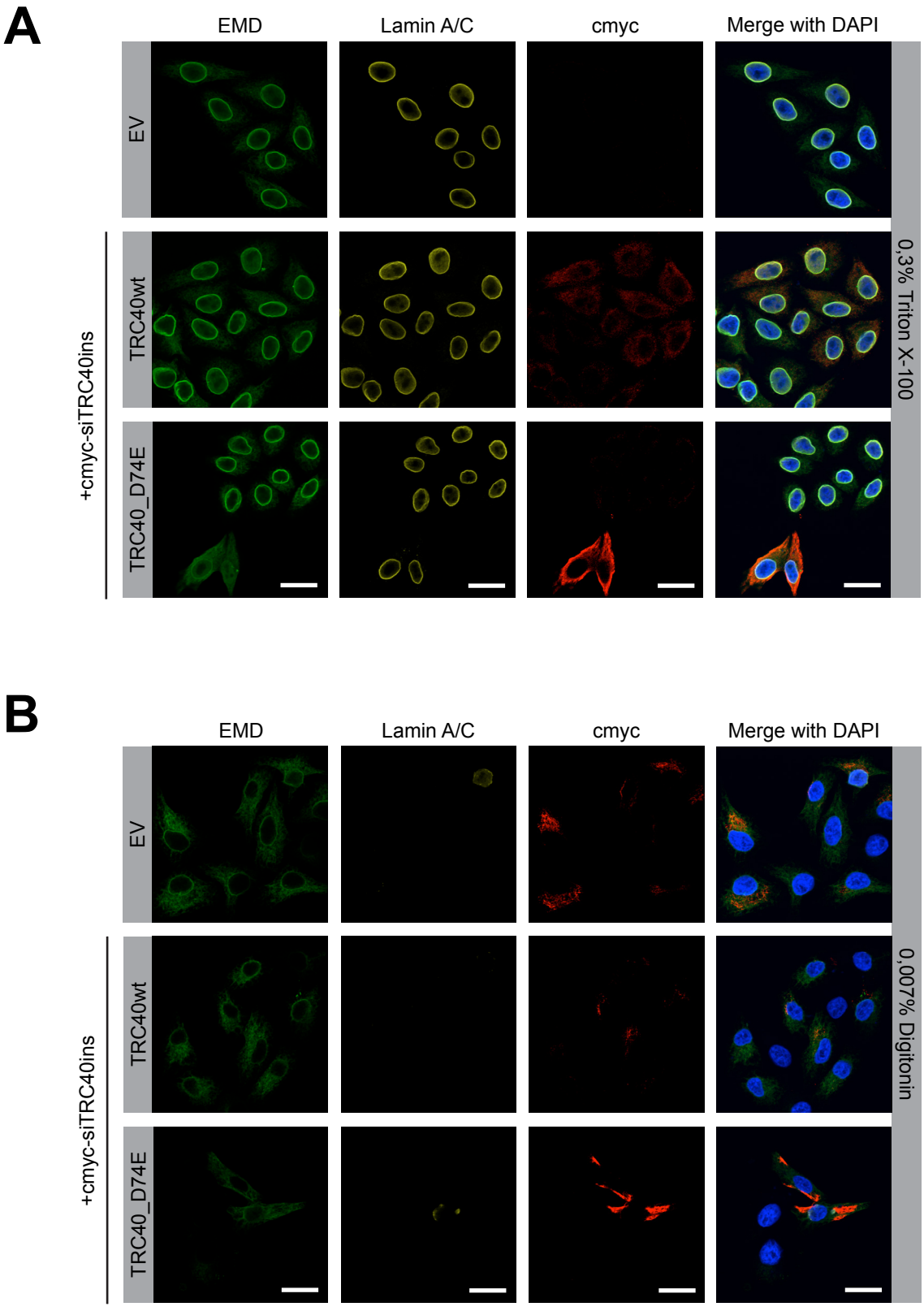

Figure 21. EMD is washed out from semi-permeabilized, TRC40$_{D74E}$-transfected cells. (A) Immunofluorescence of EMD upon over-expression of different TRC40 variants in HeLa cells. Cells were semi-permeabilized with a solution containing 0,007% digitonin in **(B)**. The lamin A/C staining serves as a control demonstrating nuclear permeabilization in the presence of 0,3 % Triton-X 100 but not 0,007% digitonin. Three biological replicates were analyzed. Scale bars: 20 µm.

(Leznicki et al. 2015; Thapaliya et al. 2016). Rpn13 has been reported to bind the deubiquitinase UCH37 (UCHL5) and it has been speculated that this can revert the fate of ubiquitinated-proteins carried by SGTA (Sahtoe et al. 2015; Vander Linden et al. 2015). The DUB inhibitor b-AP15 is specific for the following DUBs: USP14 and UCHL5 (D'Arcy et al. 2011). Stx5 interaction with $TRC40_{D74E}$ might occur in the context of ERAD and the DUBs might be relevant to such an interaction. To explore this hypothesis, I tested the role of DUBs in this interaction and whether, as suggested by the experiments performed in yeast, blocking DUBs was able to prevent the interaction. I transfected HeLa cells with $TRC40_{wt}$, $TRC40_{D74E}$ and used transfection with an empty vector as a control. For the purpose of inhibiting DUBs, I relied on the very-well described b-AP15 and performed an IF.

Upon the addition of b-AP15, the staining of Stx5 changed slightly due to what seemed Golgi dispersion. Although its principal localization to the Golgi seemed unaffected. The inhibition of DUBs does not prevent the cytoplasmic localization of Stx5 in the $TRC40_{D74E}$-transfected cells (**Fig. 22A**) pointing out that they are not required for the interaction to take place. There were also no changes in Stx5 steady-state levels (**Fig. 22B**) as observed by Western blotting.

3.1.4. Stx5 is strongly enriched in cytosol whereas the membrane-inserted population is decreased in $TRC40_{D74E}$-transfected cells

The experiments performed by microscopy indicated that Stx5 accumulates in the cytoplasm upon over-expression of $TRC40_{D74E}$. To further study this effect, we developed a stable cell line (Flp-In T-REx-293) with a Stx5 opsin-tagged at the C-terminus under the control of a tetracycline-inducible promoter. The opsin tag is an N-glycosylation tag, a 13-amino acid tag derived from bovine opsin that gets glycosylated on the luminal side once the protein is inserted into the ER. Thereby it monitors the ER-insertion of the protein (Pedrazzini et al. 2000; Borgese et al. 2001; B. M. Abell et al. 2007; Stefanovic and Hegde 2007; Schuldiner et al. 2008; Favaloro et al. 2010; Kutay et al. 1995; Masaki, Yamamoto, and Tashiro 1996; Honsho, Mitoma, and Ito

1998). In Western blots, membrane integration can be followed by the presence of an additional, slower-migrating, and deglycosidase-sensitive band (**Fig. 23A**).

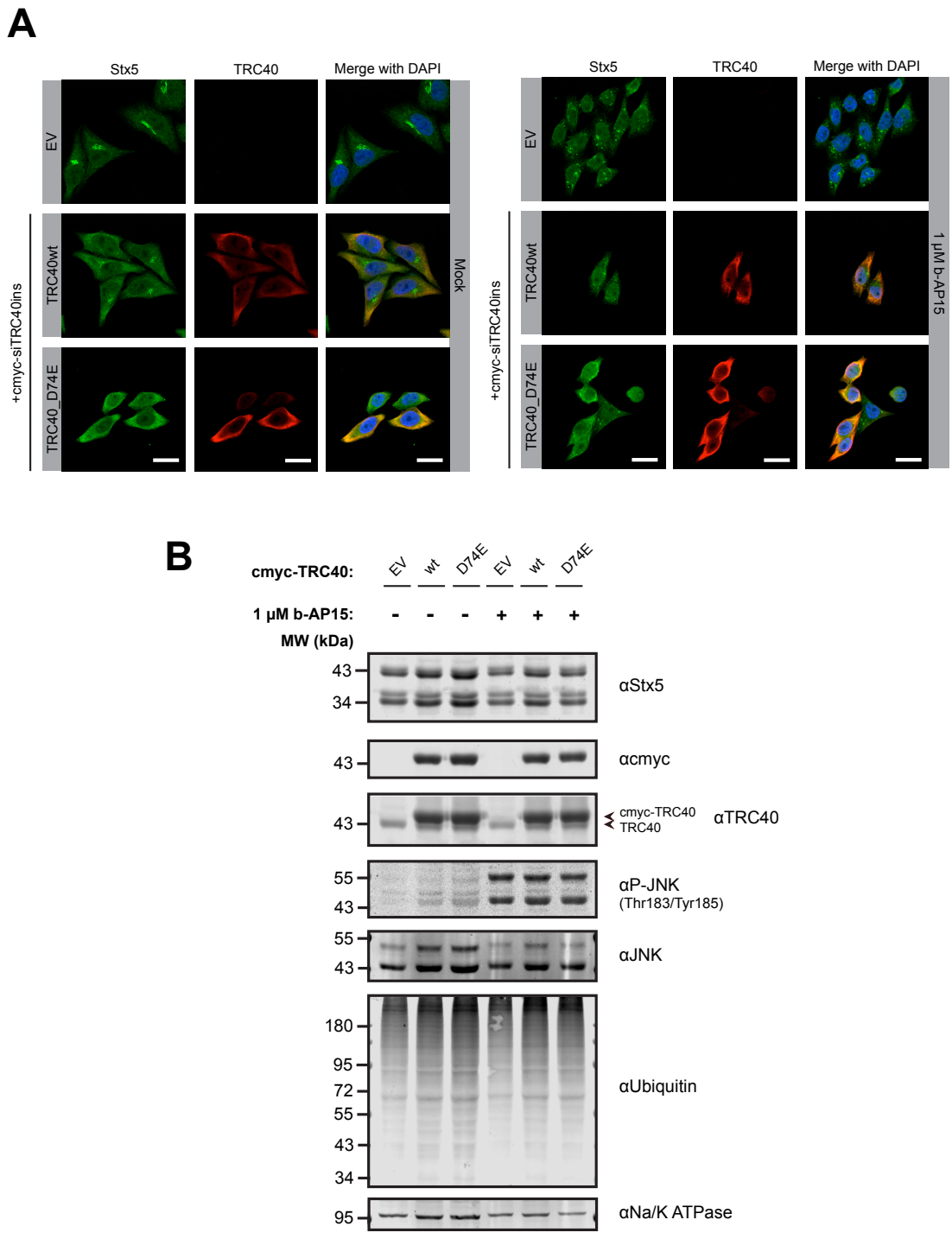

Figure 22. Stx5 is not affected by the inhibition of deubiquitinases in TRC40$_{D74E}$-transfected cells. **(A)** Immunofluorescence of Stx5 upon over-expression of different TRC40 variants in HeLa cells. Cells were treated for 6 h with 1 µM of the deubiquitinating enzyme (DUB) inhibitor b-AP15. Images of Stx5 and TRC40 stained by indirect immunofluorescence are shown. **(B)** Western blot was performed detecting the indicated proteins. phospho-JNK was used as a positive control for DUB inhibition (Brnjic et al. 2014). Two biological replicates were analyzed. Scale bars: 20 µm.

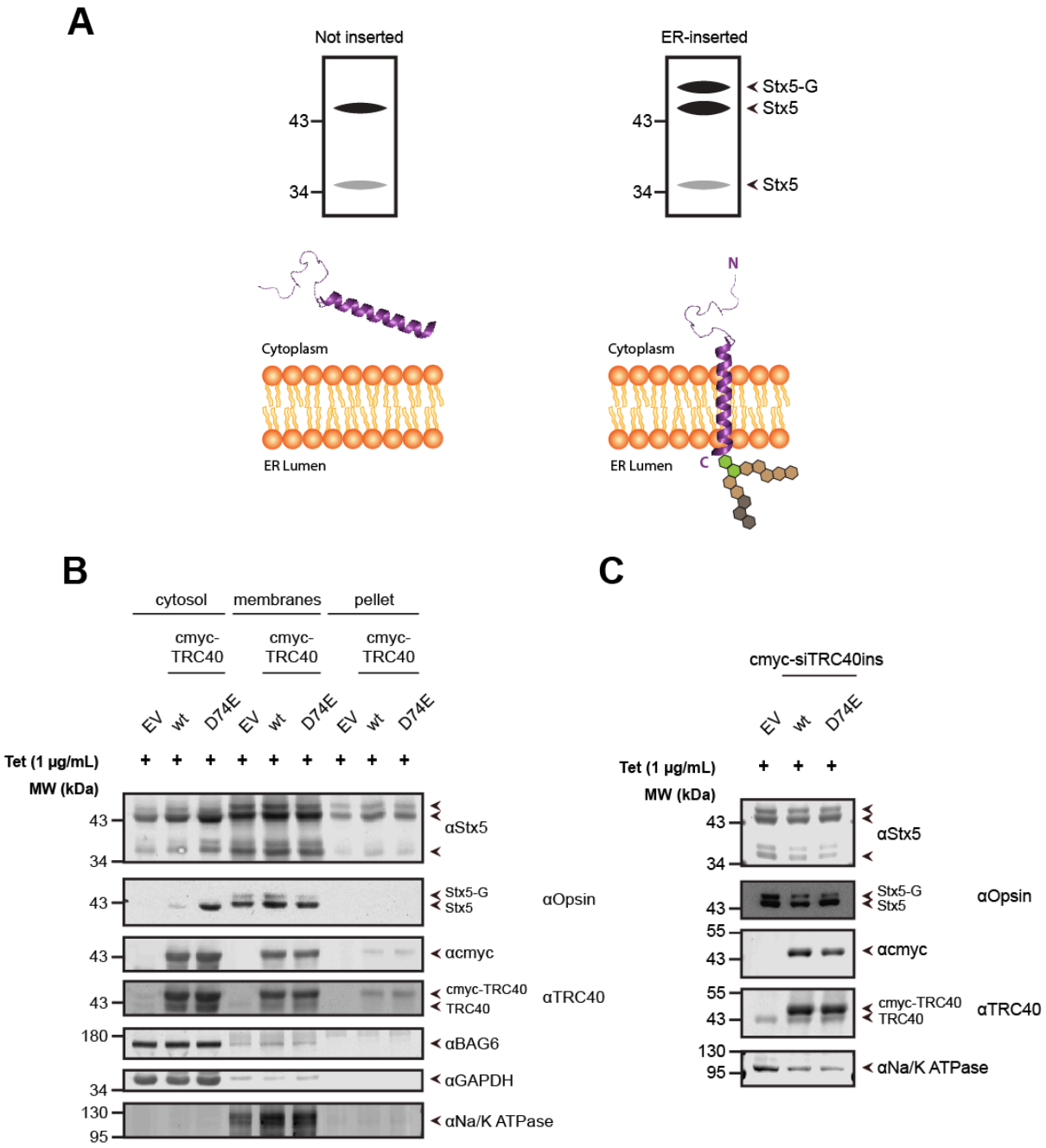

Figure 23. Stx5 is cytosolic and its insertion into the ER membrane is reduced in TRC40$_{D74E}$-transfected cells. (A) Scheme of glycosylation pattern for a TA-protein C-terminally tagged with opsin. **(B)** Cell lysate fractionation from a stable cell line expressing C-terminally opsin-epitope tagged Stx5 (Flp-In T-REx-293 Stx5-opsin) from a tetracycline-inducible promoter. The cells were transfected with either cmyc-TRC40$_{wt}$ or cmyc-TRC40$_{D74E}$. The cells were induced with 1 µg/mL of tetracycline (Tet) for 6 hours. Western blot was performed detecting the indicated proteins. **(C)** Whole-cell lysate from a Flp-In T-REx-293 Stx5-opsin stable cell line. The cells were transfected with either cmyc-TRC40$_{wt}$ or cmyc-TRC40$_{D74E}$. Western blot was performed detecting the indicated proteins. Two biological replicates were analyzed. TA-protein model (PDB ID: 2LPF).

In order to biochemically investigate whether Stx5 is accumulated in the cytosol, as predicted by its apparently cytoplasmic localization observed by IF, I transfected the Stx5-opsin (Stx5-op) stable cell line with $TRC40_{wt}$ and $TRC40_{D74E}$, and an empty vector as a control, performed a subcellular fractionation and analyzed the individual fractions by Western blot. Stx5 steady-state levels are higher in the cytosolic fraction of the $TRC40_{D74E}$-transfected cells than in the ones obtained from cells transfected with the empty vector, confirming the observations obtained by microscopy (**Fig. 13A, Fig. 20B**), and migrated as one band (**Fig. 23B**). At the same time, the fraction of glycosylated-Stx5 (Stx5-G) in membranes was reduced with respect to the total of Stx5 (Stx5+Stx5-G) (**Fig. 23B**). This decrease in glycosylation was also observed in whole cell lysate (**Fig. 23C**), consistent with the interpretation that less Stx5 was inserted into the membrane. Stx5 might be trapped in the cytoplasm by the D74E mutant thereby reducing the amount of Stx5-opsin that can reach the ER-membrane.

3.1.5. Cytosolic Stx5 is minimally glycosylated

Western blot analysis of Stx5-opsin in the fractions obtained by subcellular fractionation revealed a faint band migrating above the Stx5 band, raising the question whether this band reflected glycosylation. To test this hypothesis, I transfected $TRC40_{wt}$ and $TRC40_{D74E}$ in the T-REx-293 stable cell line, I separated cytosol from membranes and treated both fractions with and without PNGase F. This enzyme is an amidase that catalyzes the cleavage of asparagine-linked (N-linked) oligosaccharides from glycoproteins.

Inspection of the membranes fraction revealed that the upper band (Stx5-G) disappeared upon treatment with PNGase and collapsed into the band of Stx5 proving the N-glycosylated nature of Stx5 in membranes (**Fig. 24A**). In the cytosol, the slower migrating form of Stx5 was less abundant but still responsive to PNGase treatment indicating the presence of a small population of glycosylated Stx5 in the control cytosol (**Fig. 24A**). Nevertheless, the proportion of Stx5-G in the cytosol obtained from the D74E-transfected cells is much lower than that observed for the wt or the empty vector. This points to the fact that most of the Stx5 protein present in the cytosol is unglycosylated.

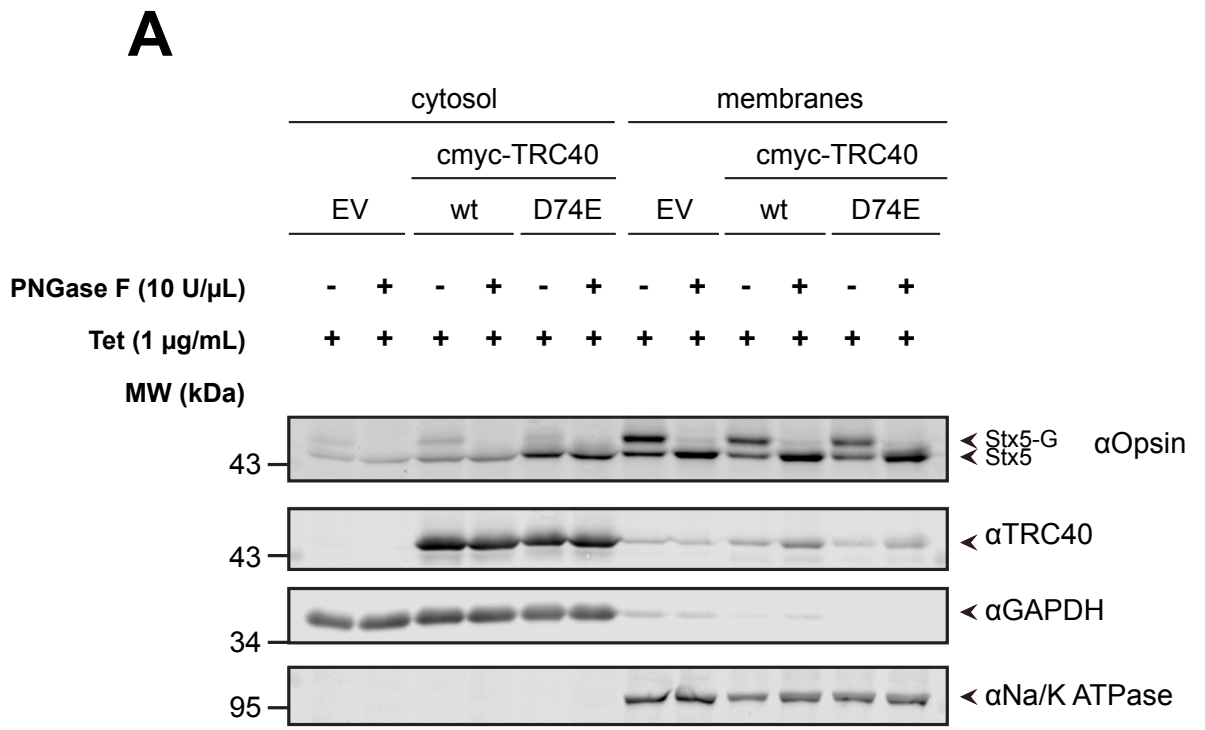

Figure 24. Stx5-op deglycosylation with PNGase F after cellular fractionation. (A) PNGase F treatment (10 U/µL) of cytosol and membrane lysates after cellular fractionation from a stable cell line expressing C-terminally opsin-epitope tagged Stx5 (Flip-In T-REx-293 Stx5-opsin) from a tetracycline-inducible promoter. The cells were transfected with either cmyc-TRC40$_{wt}$ or cmyc-TRC40$_{D74E}$. The cells were induced with 1 µg/mL of tetracycline (Tet) for 6 hours. Western blot was performed and it was blot for the indicated proteins. Two biological replicates were analyzed.

3.1.6. TRC40$_{D74E}$ and Stx5 interact in cytosol

Stx5 was found to be enriched in the cytosol upon over-expression of the D74E mutant (**Fig. 23B**) and at the same time decreased in the membranes (**Fig. 23B**). The glycosylated fraction of Stx5 was reduced under those conditions (**Fig. 24A**). Taken together, these findings might indicate that TRC40$_{D74E}$ interacts with Stx5 in the cytosol and acts as a trap mutant keeping it there instead of allowing its handover to the TRC receptor followed by membrane insertion. Therefore, it was important to determine whether TRC40$_{D74E}$ and Stx5 interact in the cytosol. In order to test this, I transfected an empty vector, TRC40$_{wt}$, TRC40$_{D74E}$ into the Stx5-opsin stable cell line and carried out a co-immunoprecipitation targeting both of the proteins: Stx5 and TRC40. Purified IgG from rabbit was used as a control for the specificity of the antibodies recognizing the target proteins. The experiment yielded the following results:

First, $TRC40_{D74E}$ was co-immunoprecipitated with Stx5 more than four-fold compared to $TRC40_{wt}$ (**Fig. 25A**) as determined by Western blot analysis of the immunoprecipitates. This is consistent and correlates with my previous IF analysis: overexpression of $TRC40_{wt}$ partially affects the subcellular localization of Stx5 (**Fig. 13A**) whereas over-expression of $TRC40_{D74E}$ drastically affects Stx5 which is now observed in a completely cytoplasmic staining pattern (**Fig. 13A**) and can be washed out from semi-permeabilized cells (**Fig. 20B**). TRC40 was not the only protein co-immunoprecipitated with Stx5. BAG6 was also enriched with Stx5, which suggests that is part of a complex formed between Stx5 and $TRC40_{D74E}$ in the cytosol. This would indicate that either the TRC pre-targeting complex or a chaperone scaffold might accumulate with $TRC40_{D74E}$. In contrast, BAG6 was absent from the immunoprecipitate when Stx5 was immunoprecipitated from cells over-expressing $TRC40_{wt}$.

Second, Stx5 was co-immunoprecipitated with TRC40 in the reverse immunoprecipitation (anti-TRC40) (**Fig. 25A**). Western blot analysis using both, anti-Stx5 and anti-Opsin, antibodies demonstrated the presence of Stx5-opsin in the immunoprecipitates. This confirms the presence of a complex containing Stx5 and TRC40 independently of the antibody used for immunoprecipitation. To create a biogenetic pulse of newly synthesized Stx5, cells were first transfected and Stx5-opsin expression was induced 6 h before harvesting the cells at a time point of 48 h after transfection. Thus, Stx5-opsin was induced in the presence of high levels of $TRC40_{wt}$ or $TRC40_{D74E}$. Detection of Stx5-opsin via the anti-opsin antibody enables a comparison between endogenous Stx5 present before the transfection and Stx5-opsin expressed in the presence of high TRC40 levels. More Stx5-opsin was co-immunoprecipitated with $TRC40_{D74E}$ than with $TRC40_{wt}$ (**Fig. 25A**). This finding supports the notion that Stx5 might be trapped by $TRC40_{D74E}$ just after the protein is synthesized. This trapping would then prevent the insertion into the ER-membrane and keep Stx5 soluble in the cytoplasm.

A

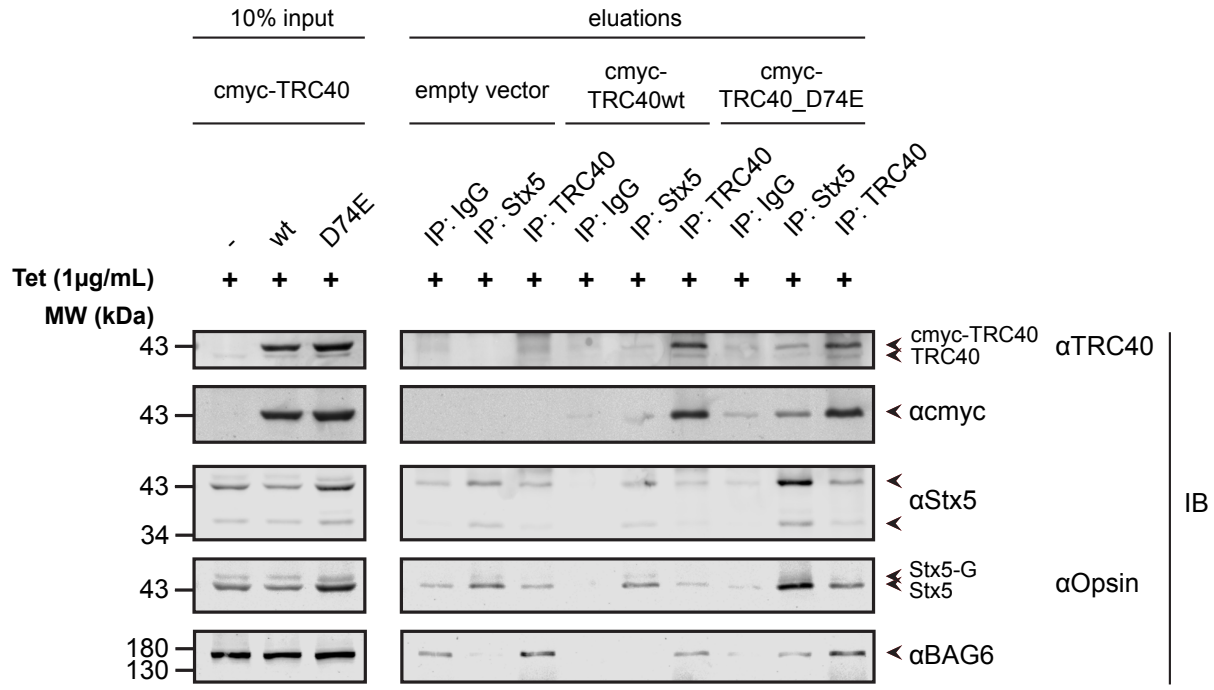

Figure 25. Co-immunoprecipitation shows Stx5, BAG6 and TRC40 in TRC40$_{D74E}$-transfected cells together in cytosol. (A) Immunoprecipitation using a rabbit anti-Stx5 antibody and a rabbit anti-TRC40 antibody from cytosol lysate after cellular fractionation from a stable cell line expressing C-terminally opsin-epitope tagged Stx5 (Flp-In T-REx-293 Stx5-opsin) from a tetracycline-inducible promoter. The cells were transfected with either cmyc-TRC40$_{wt}$ or cmyc-TRC40$_{D74E}$. The cells were induced with 1 µg/mL of tetracycline (Tet) for 6 hours. Western blot was performed and it was blot for the indicated proteins. Two biological replicates were analyzed.

3.2. TA-protein dependence of the TRC pathway *in vivo*

From an early characterization of the general requirements of TA-protein insertion (Kutay, Hartmann, and Rapoport 1993; Kutay et al. 1995; Masaki, Yamamoto, and Tashiro 1996; Honsho, Mitoma, and Ito 1998; Pedrazzini et al. 2000) it took a decade until the components of the GET pathway in yeast (Schuldiner et al. 2008) and the TRC pathway in mammals (Stefanovic and Hegde 2007; Mariappan et al. 2010; Leznicki et al. 2010; Vilardi, Lorenz, and Dobberstein 2011; Y. Yamamoto and Sakisaka 2012) were discovered. It was long assumed that TA-protein biogenesis

depended exclusively on the GET or TRC pathway (Mandon and Gilmore 2007; Mateja et al. 2009; Mariappan et al. 2010) although some studies indicated the possibility of other insertion pathways (Rabu et al. 2008; Rabu et al. 2009; Johnson, Powis, and High 2013). The GET pathway also entered cell biology textbooks (Alberts et al. 2014) as *the* pathway responsible for the insertion of TA-proteins. Recently, the point has been raised that the impairment of the TRC pathway and other insertion pathways, such the SND pathway (Aviram et al. 2016), differentially affects the spectra of TA-proteins *in vivo* (Daniele et al. 2016; Lin et al. 2016; Norlin et al. 2016; Rivera-Monroy et al. 2016; Vogl et al. 2016; Casson et al. 2017; Haßdenteufel et al. 2017; Guna et al. 2018). The same is true for the yeast GET pathway (Rivera-Monroy et al. 2016). Moreover, there are discrepancies between the *in vitro* and *in vivo* TRC-dependence reported results for some TA-proteins. Additionally, certain TA-proteins showed dependence on more than one insertion pathway. For instance Sec61β was shown to depend on the TRC pathway and the EMC pathway (Guna et al. 2018). Moreover, Pex15p, in contrast to the other peroxisomal TA-proteins in yeast, relies on the GET pathway for its insertion into a membrane (van der Zand, Braakman, and Tabak 2010). One differential parameter behind these observations could be the hydrophobicity of the transmembrane segment as pointed out in previous *in vitro* studies (Rao et al. 2016; Guna et al. 2018; F. Wang et al. 2010; Costello, Castro, Camões, et al. 2017).

First, the redundancy of TA-protein insertion pathways; second, the difficulty of correlating the *in vitro* results into *in vivo*; and finally, the fact that little is known about the fate of endogenous TA-proteins when the TRC pathway is impaired motivated me to study what happens to endogenous TA-proteins when knocking-down components of the pathway like TRC40, TRC40 in combination with the receptor or the scaffolding protein of the pre-targeting-complex BAG6. With this strategy I was able to assess the relevance of the TRC pathway in the stability of the TA-proteins integrated in an environment with other insertion and degradation mechanisms present.

3.2.1. TA-proteins show variable degrees of dependence on the TRC pathway impairment

These experiments were performed in HeLa P4 cells and for the purpose of knocking-down the TRC pathway components small interference RNA (siRNA) was used with siRNA targeting luciferase as a control. I performed subcellular fractionations to separate cytosol and membranes. The purpose underlying this fractionation was to assess TA-protein steady-state levels that are actually inserted into the membranes. Small proportions of certain TA-proteins can be found in the cytosol adding noise to the analysis when using whole cell lysate (Larance et al. 2013). I performed a Western blot analysis on the fractions detecting different TA-proteins. This analysis revealed a diverse degree of dependence on the TRC pathway as several of the TA-proteins were affected by the combined knockdown of WRB and TRC40 (**Fig. 26B).** It was also striking that none of the TA-proteins analyzed were reduced upon BAG6 knockdown (**Fig. 26B**). Moreover, the components of the pathway seemed to be affected by the knockdown of other components of the same pathway (**Fig. 26A**). A more detailed analysis of these general conclusions will be presented in the following sections.

3.2.2. WRB and CAML drop upon TRC40 knockdown

The steady-state levels of the heterodimeric receptor of the TRC pathway, WRB and CAML, were decreased upon knockdown of TRC40 (**Fig. 26B**, **Fig. 27B, Fig. 27D**). CAML was severely affected when WRB is down-regulated (**Fig. 26B**, **Fig. 27D**), which has already been described in the literature (Rivera-Monroy et al. 2016; Sara Francesca Colombo et al. 2016; Haßdenteufel et al. 2017).

3.2.3. BAG6 is affected upon WRB/TRC40 knockdown

Unexpectedly, BAG6 steady-state levels in the WRB and TRC40 knockdown-cells were severely decreased (**Fig. 26A**, **Fig. 27C**) while they were unaffected upon the silencing of TRC40.

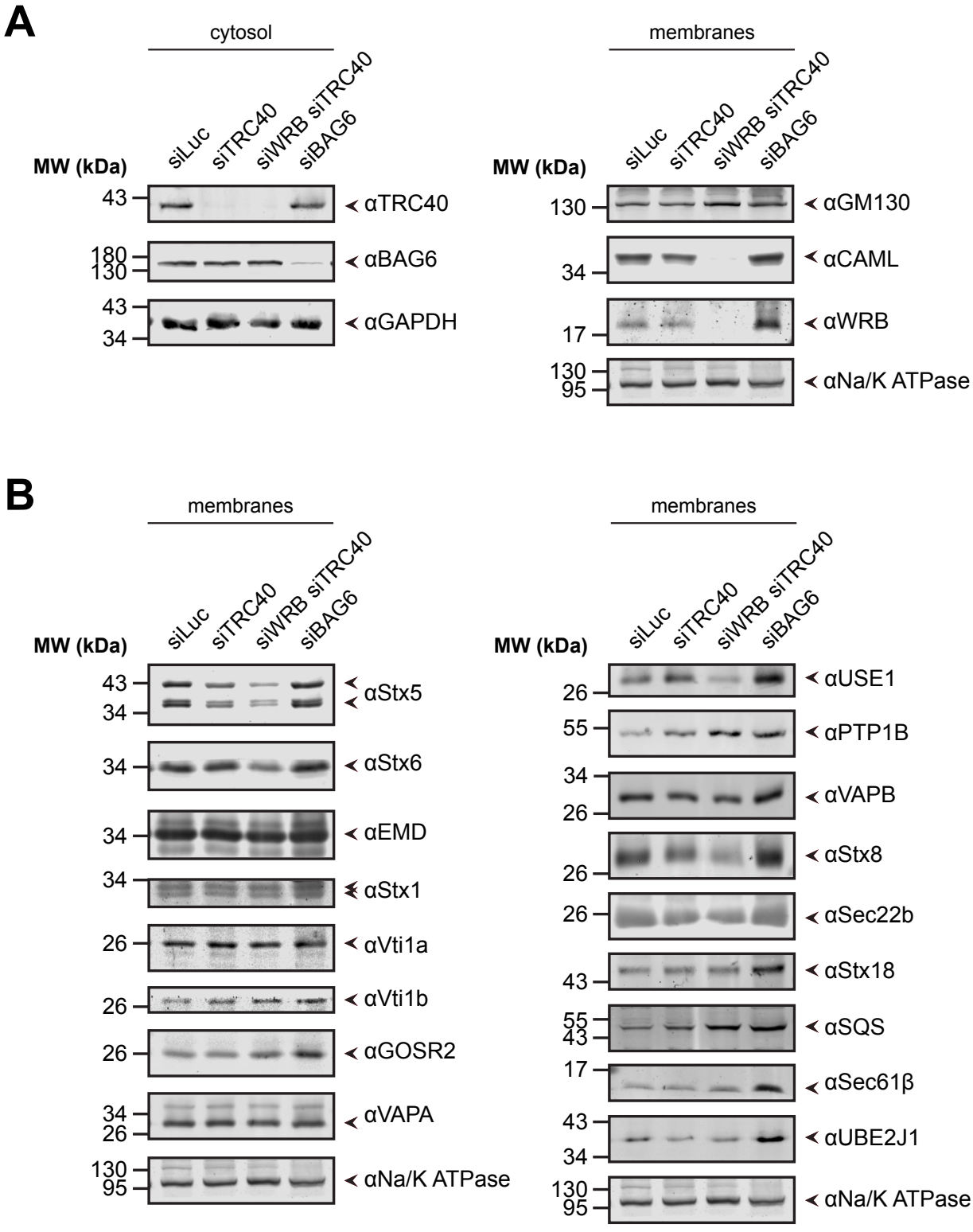

Figure 26. Tail-anchored proteins steady-state levels are altered upon knockdown of TRC40 or the TRC40 receptor. (A) Knock-down of TRC40, WRB/TRC40 or BAG6 performed in HeLa P4 cells. Cytosol and membrane fractions were analyzed for Western blot for the TRC-pathway components and GM130. **(B)** Knock-down of TRC40, WRB/TRC40 or BAG6 performed in HeLa P4 cells. Membrane fraction was analyzed for Western blot for different TA-proteins. Blot are representative of four independent knockdown experiments which are quantified in **Fig. 27-32**.

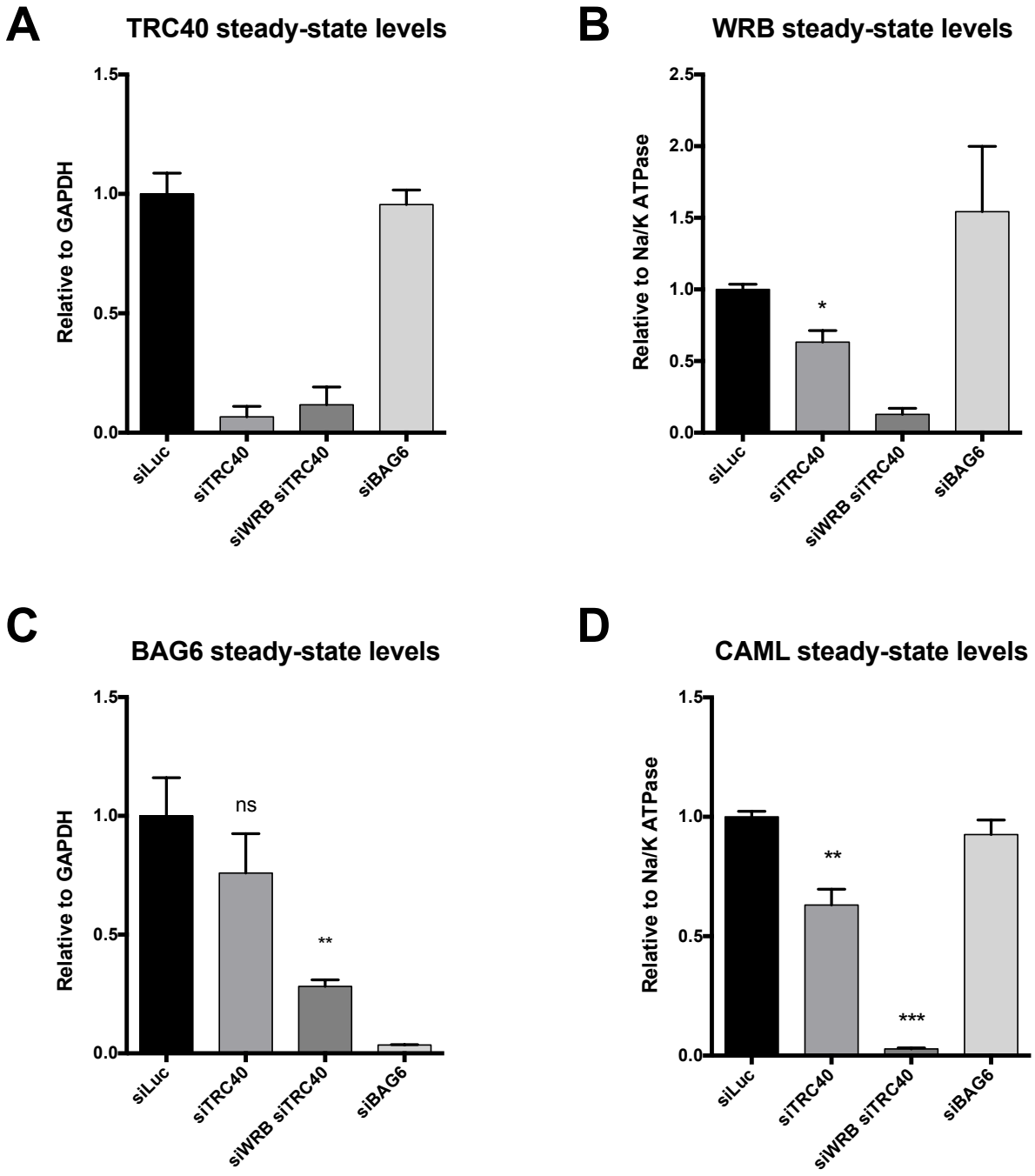

Figure 27. Quantification of the TRC-pathway components upon knockdown of TRC40, the TRC40 receptor or BAG6. (A) Quantification of TRC40 signal intensities from the blots performed in **Fig. 26A**. **(B)** Quantification of WRB signal intensities from the blots performed in **Fig. 26B. (C)** Quantification of BAG6 signal intensities from the blots performed in **Fig. 26A. (D)** Quantification of CAML signal intensities from the blots performed in **Fig. 26B**. Four biological replicates were analyzed. The graphs show the mean and the error bars represent standard error of the mean. * indicates a p-value < 0.05; ** a p-value < 0.05; *** a p-value < 0.001.

3.2.4. Steady-state levels of several TA-proteins decrease drastically upon WRB/TRC40 knockdown

Interestingly, many TA-proteins showed a diverse degree of dependence on the TRC pathway. Several were altered upon the knockdown of WRB and TRC40 (**Fig. 26B).** The simultaneous loss of the receptor (both WRB and CAML are drastically decreased, **Fig. 27B** and **Fig. 27D**) and TRC40 affected the steady-state levels of an overlapping yet distinct set of TA-proteins.

Stx5 was the most affected TA-protein (**Fig. 28A**) along with USE1 (**Fig. 29A**), Stx6 (**Fig. 28B**) and Sec22b (**Fig. 30C**). Stx5's strong dependence on the TRC pathway has been previously described (Rivera-Monroy et al. 2016; Norlin et al. 2016; Casson et al. 2017; Norlin, Parekh, and Edlund 2018). Therefore, it is known to be a *bona fide* substrate of the TRC pathway. Stx5 showed a reduction of 88% at the steady-state level in the membrane fraction (compared to 50% reduction in whole cell lysate, (Rivera-Monroy et al. 2016)) in the combined knockdown of WRB and TRC40. Upon TRC40 knockdown steady-state levels were reduced by 58% with no effects on the steady-state levels when BAG6 was down-regulated (**Fig. 28A**). The vesicle transport protein USE1 is a SNARE protein believed to be involved in the retrograde transport from the Golgi apparatus to the ER (Dilcher et al. 2003). Steady-state levels of USE1 were severely decreased to 18% (**Fig. 29A**). Similarly, Stx6, a Golgi-resident protein involved in vesicular traffic, showed a 75% reduction at the steady-state level (**Fig. 28B**). Sec22b, an ER-resident SNARE protein, reported to be involved in anterograde and retrograde transport (Yiting Liu and Barlowe 2002; Burri et al. 2003), showed a reduction at the steady-state level of around 73% (**Fig. 30C**). The Ubiquitin-conjugating enzyme E2 J1 (UBE2J1), an ER-resident TA-protein involved in ERAD, showed a decrease of 64% in comparison to the control cells (**Fig. 29C**). VAPB is an ER-resident protein involved in linking the ER to other organelles (Costello, Castro, Hacker, et al. 2017; Hua et al. 2017; Gomez-Suaga et al. 2017; Dong et al. 2016) and in lipid trafficking, VAPB was found to be decreased to 59% at the steady-state level (**Fig. 29D**).

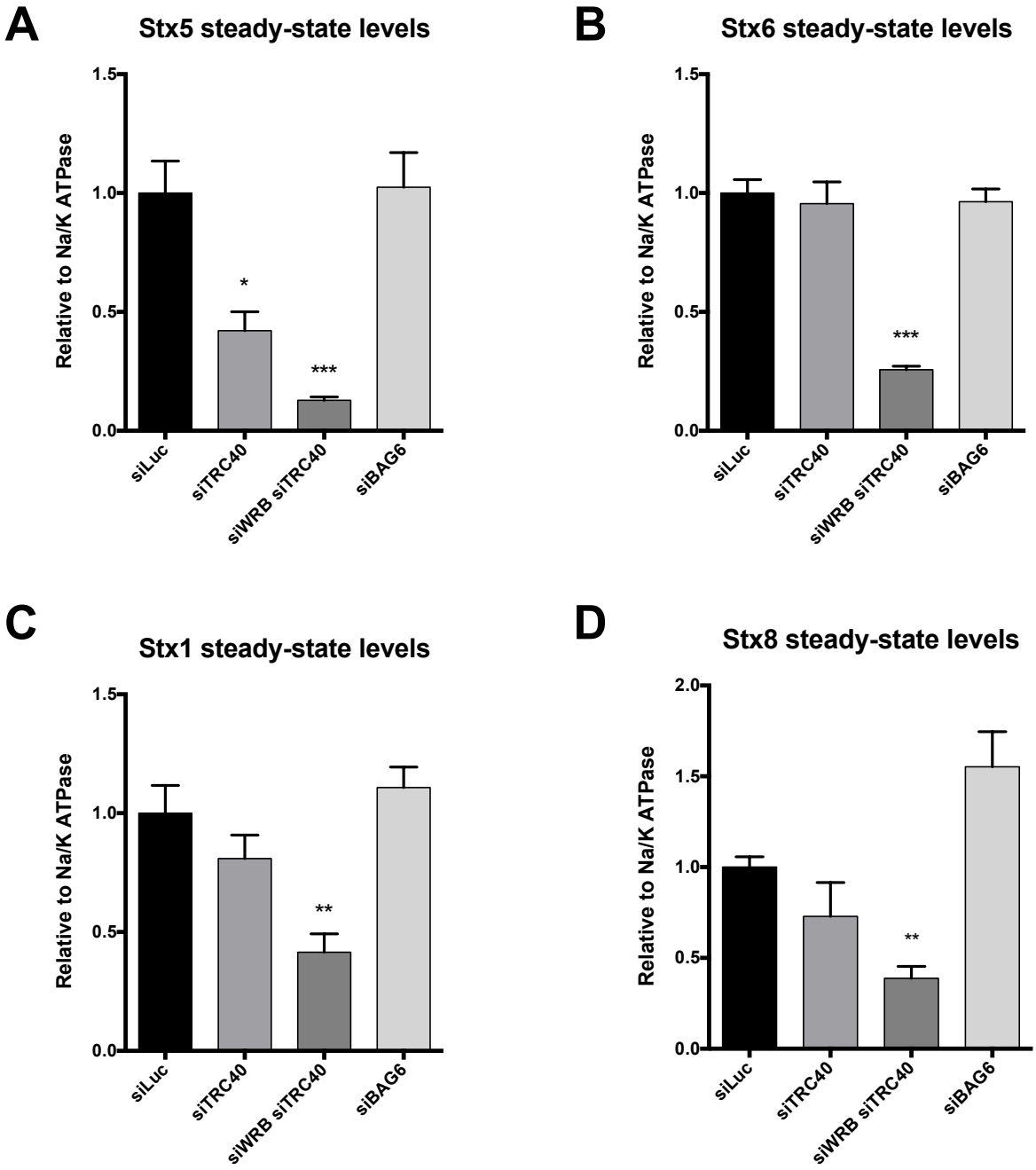

Figure 28. Quantification of a panel of tail-anchored proteins tested upon knockdown of TRC40, the TRC40 receptor or BAG6. (A) Quantification of Stx5 signal intensities from the blots performed in **Fig. 26B. (B)** Quantification of Stx6 signal intensities from the blots performed in **Fig. 26B. (C)** Quantification of Stx1 signal intensities from the blots performed in **Fig. 26B. (D)** Quantification of Stx8 signal intensities from the blots performed in **Fig. 26B**. Four biological replicates were analyzed. The graphs show the mean and the error bars represent standard error of the mean. * indicates a p-value < 0.05; ** a p-value < 0.05; *** a p-value < 0.001.

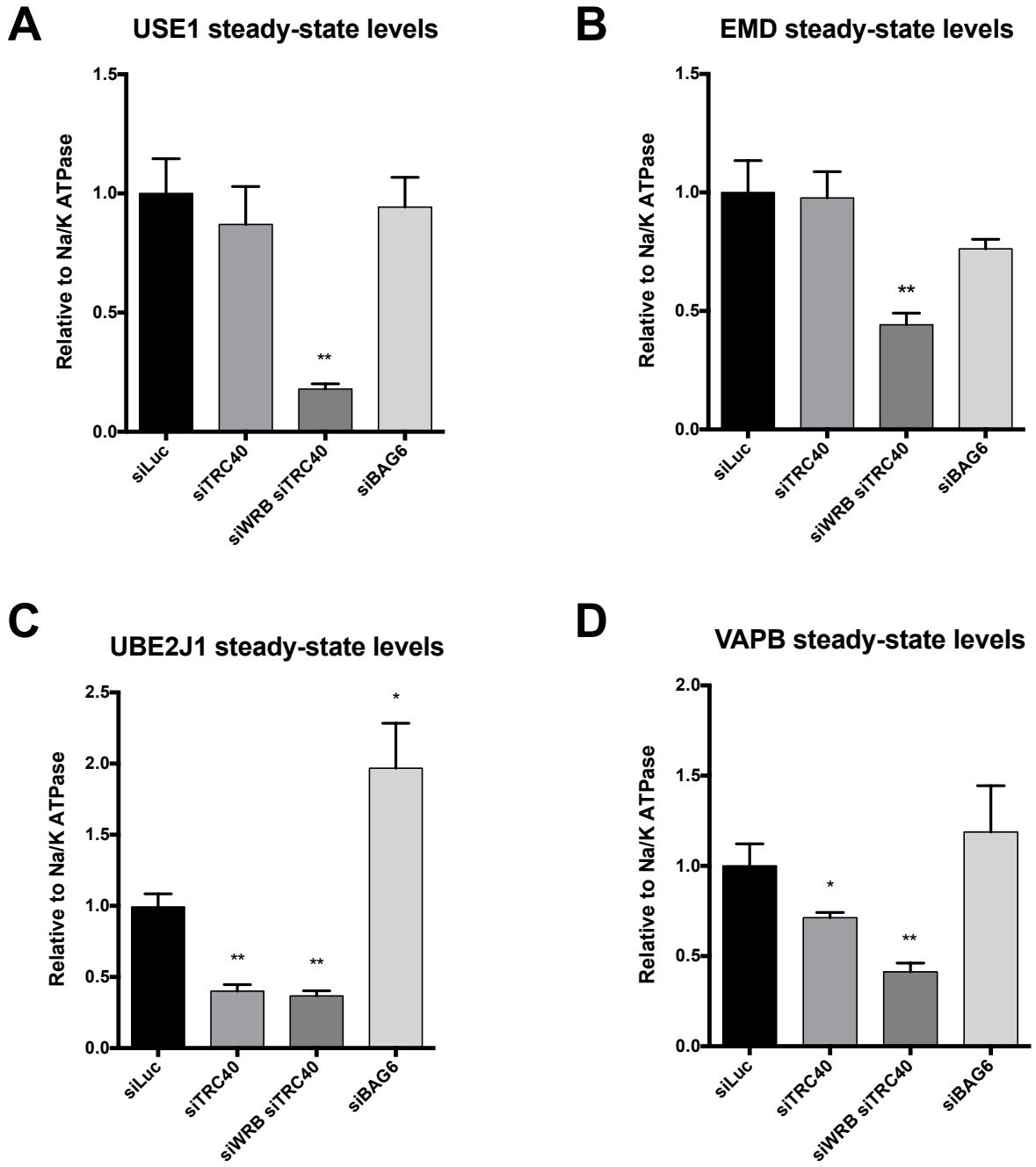

Figure 29. Quantification of the tail-anchored proteins tested upon knockdown of TRC40, the TRC40 receptor or BAG6. (A) Quantification of USE1 signal intensities from the blots performed in **Fig. 26B. (B)** Quantification of EMD signal intensities from the blots performed in **Fig. 26B. (C)** Quantification of UBE2J1 signal intensities from the blots performed in **Fig. 26B. (D)** Quantification of VAPB signal intensities from the blots performed in **Fig. 26B**. Four biological replicates were analyzed. The graphs show the mean and the error bars represent standard error of the mean. * indicates a p-value < 0.05; ** a p-value < 0.05; *** a p-value < 0.001.

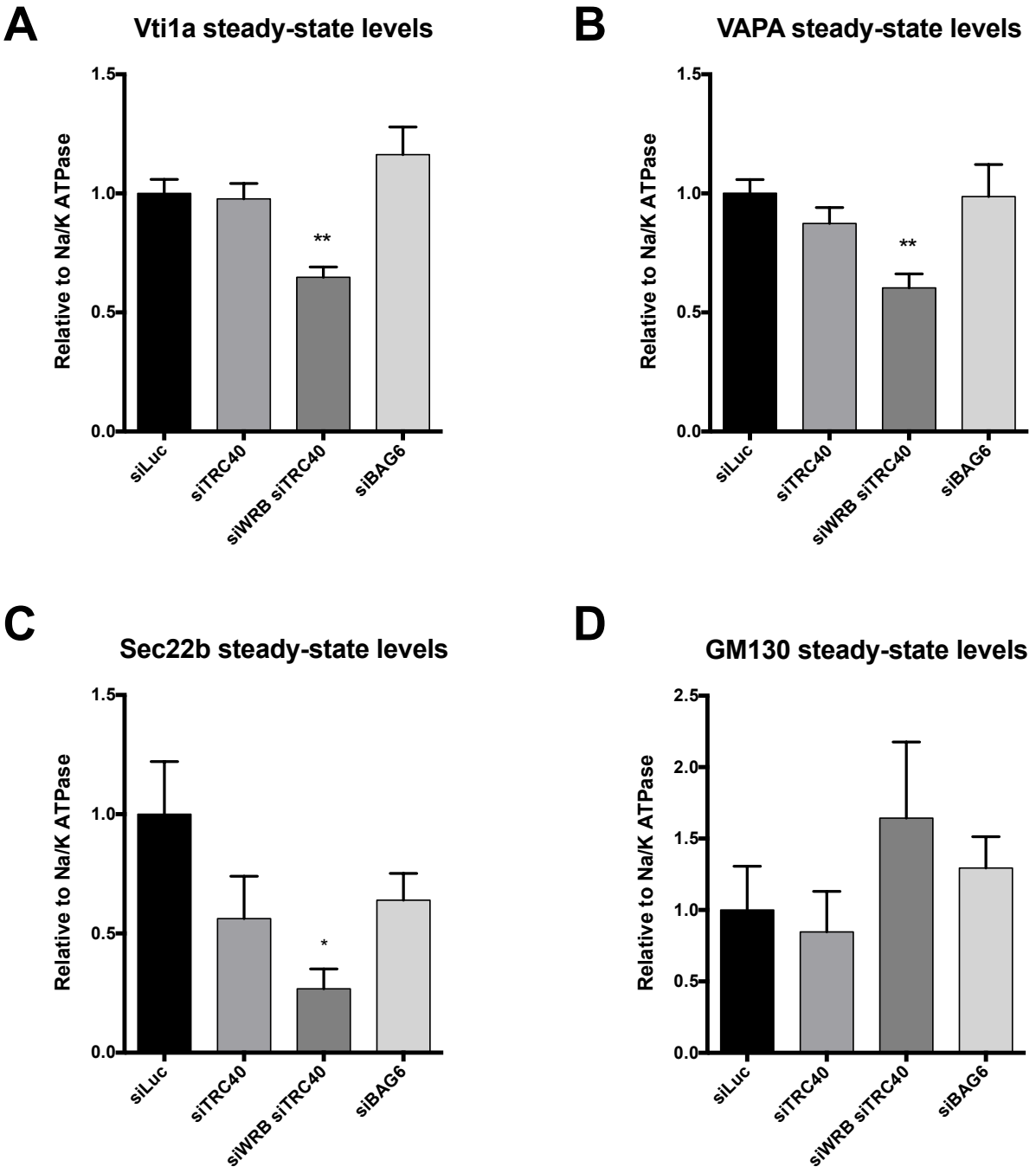

Figure 30. Quantification of a panel of tail-anchored proteins tested upon knockdown of TRC40, the TRC40 receptor or BAG6 plus GM130. (A) Quantification of Vti1a signal intensities from the blots performed in **Fig. 26B. (B)** Quantification of VAPA signal intensities from the blots performed in **Fig. 26B. (C)** Quantification of Sec22b signal intensities from the blots performed in **Fig. 26B. (D)** Quantification of GM130 signal intensities from the blots performed in **Fig. 26A**. Four biological replicates were analyzed. The graphs show the mean and the error bars represent standard error of the mean. * indicates a p-value < 0.05; ** a p-value < 0.05; *** a p-value < 0.001.

EMD is a protein of the inner nuclear membrane and is also localized at the ER (Manilal, Nguyen, and Morris 1998; Pfaff et al. 2016). It showed a decrease of 56% (**Fig. 29B**). EMD was already reported to be a substrate of the TRC pathway (Pfaff et al. 2016) and is known to be affected by the lack of the TRC receptor (Rivera-Monroy et al. 2016). Stx8 is a SNARE protein preferentially located at early endosomes, but also in late endosomes (Prekeris et al. 1999; Subramaniam et al. 2000; Kazuo Kasai et al. 2008). Stx8 steady-state levels were reduced 62% in the combined WRB/TRC40-knockdown cells compared to the siLuc control cells (**Fig. 28D**). Stx1 is a SNARE protein involved in the fusion between vesicles and the plasma membrane (Bennett, Calakos, and Scheller 1992; Söllner et al. 1993). Stx1 showed a reduction by 59% at the steady-state levels upon combined WRB/TRC40 knockdown compared to the control cells (**Fig. 28C**). Two other TA-proteins displayed a milder decrease in the amount of protein at the steady-state: VAPA and Vti1a. VAPA is an ER-resident protein that shares similarity with VAPB and is also involved in ER contact sites and sterol trafficking (Wyles, McMaster, and Ridgway 2002; Dong et al. 2016; Hua et al. 2017). VAPA showed a reduction of around 40% at steady-state level (**Fig. 30B**). Finally, Vti1a is a SNARE protein involved in the traffic between early/late endosomes and *trans*-Golgi network (TGN) (Mallard et al. 2002; Brandhorst et al. 2006; Ganley, Espinosa, and Pfeffer 2008) and upon the knockdown of WRB and TRC40 a 35% reduction at steady-state level was observed (**Fig. 30A**).

The peripheral membrane component of the *cis*-Golgi, GM130, used as a control in the present study, was not altered upon the knockdown of the TRC pathway components tested in this study (**Fig. 30D**).

3.2.5. Stx5, UBE2J1 and VAPB are also affected by TRC40 knockdown

In addition to the previous results, there were some TA-proteins also altered by the single knockdown of TRC40. Stx5 and UBE2J1 had showed a reduction by 60% at the steady-state level (**Fig. 28A**, **Fig. 29C**). Thus, the reduction of UBE2J1 was quite similar to the one observed upon combined WRB/TRC40 knockdown. Yet for Stx5 the

effect on its steady-state levels was less pronounced when comparing the TRC40 single to the WRB/TRC40 double knockdown. VAPB, like Stx5, had a reduction of around 30% that was less than that observed for the WRB/TRC40 down-regulation (**Fig. 29D**). The rest of the analyzed TA-proteins remained unchanged upon the TRC40 knockdown.

Taken together, the majority of the TA-proteins (11 out of 17) tested in this study were affected by the knockdown of TRC40 plus the TRC receptor and a small subset of them (3 out of those 11) were also affected by the knockdown of just TRC40.

3.2.6. Stx18, GOSR2 and UBE2J1 increase upon BAG6 knockdown

Most of the TA-proteins tested in this study did not show any change in their steady-state levels upon BAG6 knockdown. However, three TA-proteins showed a marked increase upon the loss of BAG6. UBE2J1, in contrast to the effect seen for the TRC40 and the WRB/TRC40 knockdown, showed a 2-fold increase upon BAG6 knockdown at the steady-state level (**Fig. 29C**). A similar behavior was found for Stx18 which had an increase higher than 2-fold at the steady-state level (**Fig. 31A**). Stx18 is a SNARE protein involved in Golgi-to-ER retrograde transport (Hatsuzawa et al. 2000; Hirose et al. 2004). GOSR2 was increased by 70% compared to the control cells (**Fig. 31B**). GOSR2 is a SNARE protein involved in ER-to-Golgi anterograde transport (Jesse C. Hay et al. 1997; J C Hay et al. 1998) and in intra-Golgi transport (Lowe et al. 1997).

3.2.7. Several TA-proteins showed no variation at the steady-state level when TRC40 and WRB/TRC40 were impaired

There was a set of TA-proteins that remained unaltered upon the knockdown of TRC40 or TRC40 combined with WRB. Two of them, Stx18 and GOSR2, showed no reaction to these knockdowns but they had an increase at steady-state level upon BAG6 knockdown (**Fig. 31A, Fig. 31B**).

PTP1B is an ER enzyme member of the protein tyrosine phosphatase family and it has been related to ER stress signaling (Gu et al. 2004; Krishnan et al. 2011). Vti1b is a SNARE protein that mediates the vesicle homotypic fusion of late endosomes and it is also involved in the heterotypic fusion of late endosomes with lysosomes (Antonin et al. 2000; Pryor et al. 2004; Itakura, Kishi-Itakura, and Mizushima 2012). Sec61β is a subunit of the ER-resident Sec61 translocon (Meyer, Krause, and Dobberstein 1982; Görlich et al. 1992). SQS is an enzyme localized at the ER that is involved in lanosterol biosynthesis, which is the first step in sterol biosynthesis (Ourisson and Nakatani 1994; Pandit et al. 2000). None of these six TA-proteins are affected upon TRC40 or WRB/TRC40 knockdown (**Fig. 31, Fig. 32**), contrasting to those eleven that were severely affected.

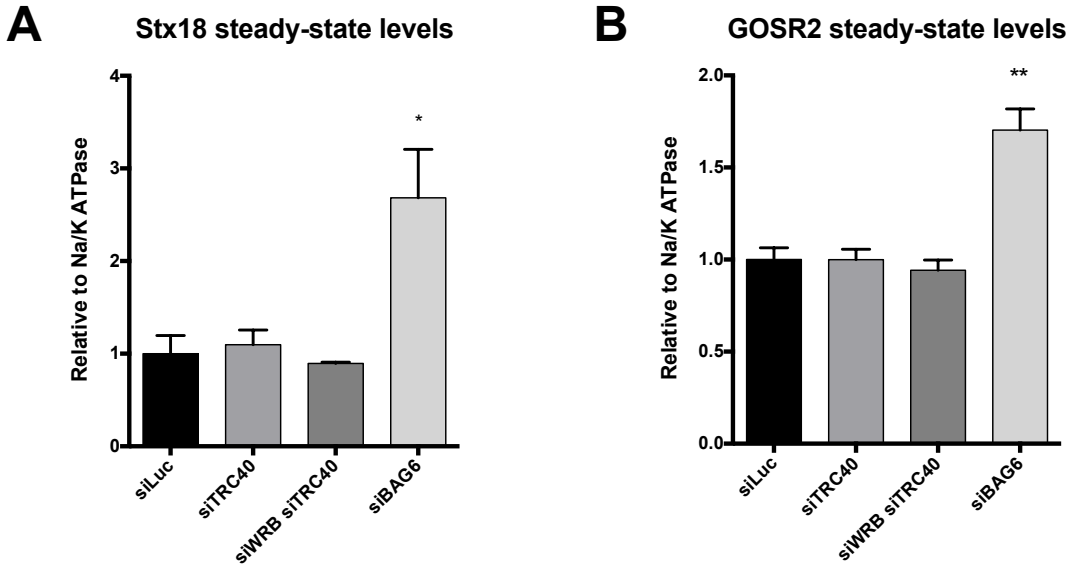

Figure 31. Quantification of the tail-anchored proteins tested upon knockdown of TRC40, the TRC40 receptor or BAG6. (A) Quantification of Stx18 signal intensities from the blots performed in **Fig. 26B. (B)** Quantification of GOSR2 signal intensities from the blots performed in **Fig. 26B**. Four biological replicates were analyzed. The graphs show the mean and the error bars represent standard error of the mean. * indicates a p-value < 0.05; ** a p-value < 0.05; *** a p-value < 0.001.

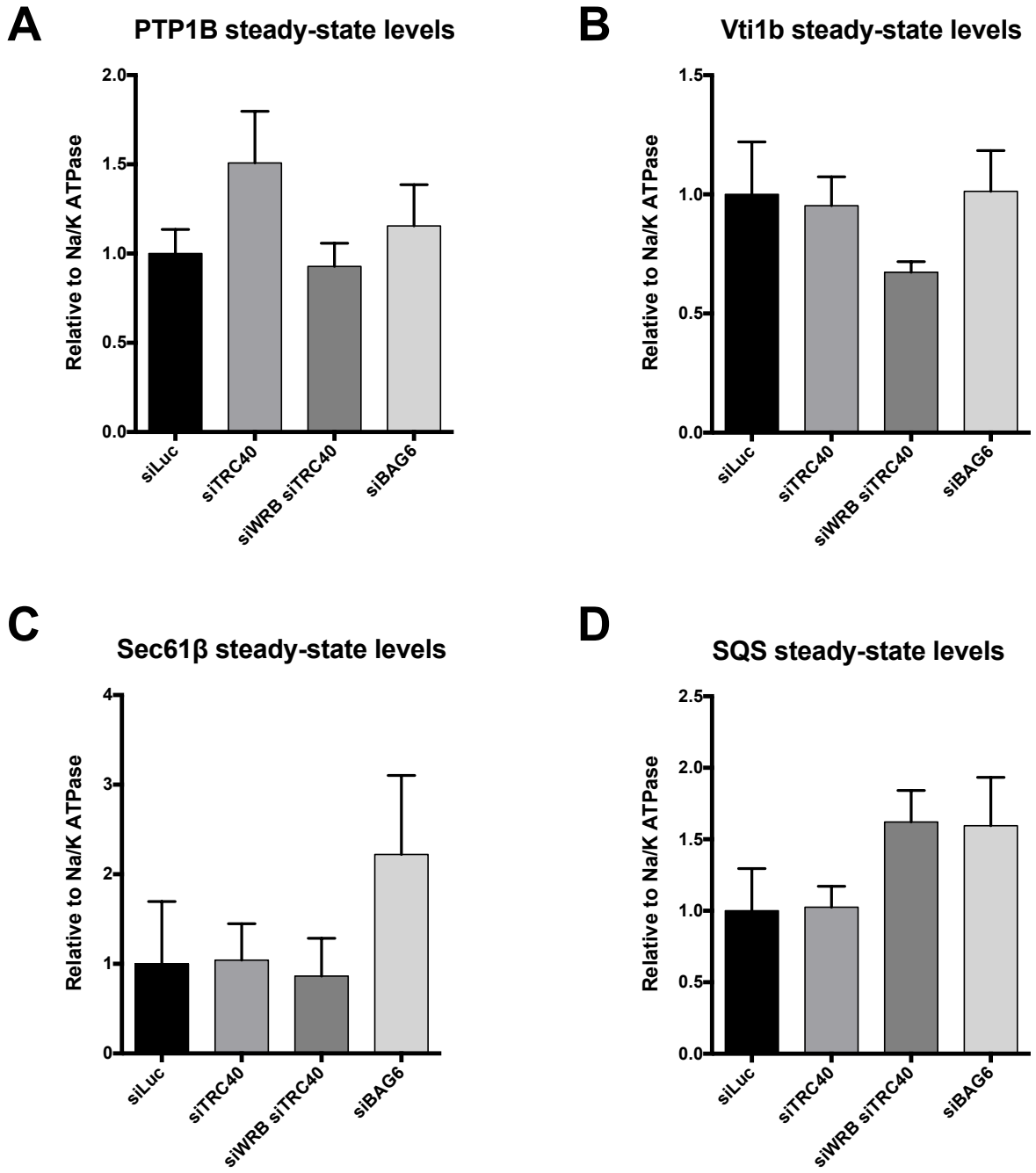

Figure 32. Quantification of a panel of tail-anchored proteins tested upon knockdown of TRC40, the TRC40 receptor or BAG6. (A) Quantification of PTP1B signal intensities from the blots performed in **Fig. 26B. (B)** Quantification of Vti1b signal intensities from the blots performed in **Fig. 26B. (C)** Quantification of Sec61β signal intensities from the blots performed in **Fig. 26B. (D)** Quantification of SQS signal intensities from the blots performed in **Fig. 26B**. Four biological replicates were analyzed. The graphs show the mean and the error bars represent standard error of the mean. * indicates a p-value < 0.05; ** a p-value < 0.05; *** a p-value < 0.001.

3.2.8. TRC pathway-dependence of the TA-proteins and the hydrophobicity of the transmembrane segments

Since the first studies addressing the TA-proteins were conducted, one of the main questions has been how they are targeted to different organelles. There have been many factors taken into consideration: TMD length (Isenmann et al. 1998; Pedrazzini et al. 2000; Bulbarelli et al. 2002; Borgese, Brambillasca, and Colombo 2007), C-terminal tail length and charge (Elgersma et al. 1997; Kuroda et al. 1998; Mullen and Trelease 2000; Horie et al. 2002; Borgese, Brambillasca, and Colombo 2007; Yagita, Hiromasa, and Fujiki 2013; Costello, Castro, Camões, et al. 2017), membrane composition (Borgese, Brambillasca, and Colombo 2007), the cytoplasmic domain (Linstedt et al. 1995; Misumi et al. 2001; Joglekar et al. 2003) and hydrophobicity of the transmembrane segment (Borgese, Colombo, and Pedrazzini 2003; Borgese, Brambillasca, and Colombo 2007). In fact, hydrophobicity has always been considered a key factor for organelle targeting of the TA-proteins. Other *in vitro* and *in vivo* studies have also studied this physicochemical property (Rao et al. 2016; Guna et al. 2018; F. Wang et al. 2010; Costello, Castro, Camões, et al. 2017). In fact, two different bioinformatic approaches were implemented in order to predict yeast and human TA-proteins (Beilharz et al. 2003; Kalbfleisch, Cambon, and Wattenberg 2007). In both analyses, hydrophobicity of the transmembrane segment has been taken into consideration. Multiple hydrophobicity scales have been used in order to establish the relative hydrophobicity of each amino acid residue.

It has long been proposed that the hydrophobicity of mitochondria and the secretory pathway-targeted TA-proteins differ (Borgese et al. 2001; Bulbarelli et al. 2002; Borgese, Colombo, and Pedrazzini 2003; Borgese, Brambillasca, and Colombo 2007). It is also a long-standing assumption that a TA-protein of the secretory pathway, including Golgi and plasma membrane, are inserted into the ER membrane. It is an important hypothesis that Golgi proteins use TMD length as trafficking information (Munro 1995; Sharpe, Stevens, and Munro 2010). From this emerges the idea that secretory pathway TA-proteins will differ in their total hydrophobicity and therefore may need different targeting machinery.

3.Results

In a recent study, mechanistic interpretations of the overlapping targeting activities of the TRC or the EMC pathway have been proposed (Guna et al. 2018). The authors claim that hydrophobicity plays a key role in the pathway-dependence. Sec61β has a moderate hydrophobicity and they suggest that, due to its dependence on both, the TRC and the EMC pathway, it marks the approximate point of substrate overlap between these pathways.

I set out to test how the data obtained for 17 TA-proteins after TRC-pathway knockdown (**Fig. 26-32**) correlated with the most commonly used hydrophobicity scales: transmembrane tendency (G. Zhao and London 2006), Kyte & Doolittle (Kyte and Doolittle 1982), apparent free-energy (ΔG_{app}) (Hessa et al. 2007) and grand average of hydropathicity (GRAVY) (Kyte and Doolittle 1982). I was interested in the hydrophobicity behavior of all the known TA-proteins and how representative the subset of TA-proteins tested was. Based on a good correlation between hydrophobicity and TRC-dependence my results would help to implicate new TRC-pathway substrates. Therefore, I updated and systematically refined a list of predicted human TA-proteins previously published (Kalbfleisch, Cambon, and Wattenberg 2007) (**Table 17**) and calculated the hydrophobicity scores for each TMD according to the different scales. Next, I plotted the result in dot-plots grouping the TA-proteins by subcellular localization and then highlighting the TA-proteins affected by the knockdown of WRB/TRC40. The following table lists the predicted human TA-proteins, predicted TMDs and the calculated hydrophobicity scores (**Table 17**).

First, I plotted the TMD hydrophobicity scores for the transmembrane tendency scale (G. Zhao and London 2006) and clustered the TA-proteins according to the reported subcellular localization (**Fig. 33A**). The TMDs of the mitochondrial TA-proteins presented the lowest overall hydrophobicity scores. In contrast, those of ER, Golgi and nucleus showed a higher score according to this scale. This observation confirms the notion that the biggest divide with respect to transmembrane segment hydrophobicity exists between mitochondrial TA-proteins and those of the secretory pathway. Using this dot-plot as a template, I marked the proteins tested in this study regarding their sensitivity to a combined WRB/TRC40 knockdown (**Fig. 33B**). As a general trend, the TA-proteins sensitive to the knockdown had more hydrophobic TMDs. Moreover, the majority of the TA-proteins insensitive to the loss of WRB/TRC40 presented a

NCBI Accession	UniProt Accession	Symbol	Description	Protein Length	TMD (TMHMM)	TMD (UniProt)	Number of residues	TMD tendency (TMHMM+UniProt)	Kyte & Doolittle (TMHMM+UniProt)	ΔG_{app} (kcal mol^{-1})	GRAVY
NP_001598.1	P09110	**ACAA1**	3-ketoacyl-CoA thiolase, peroxisomal isoform a	424	AYGVVSMCIGTGMGAAAVF	-	19	11,23	29	2,532	1,526
NP_078998.1	Q8NC06-2	**ACBD4**	Acyl-Coenzyme A binding domain containing 4	305	WPLGLPGPALLFFLLWPFVVQW	-	22	16,77	28	0,582	1,273
NP_663736.2	Q5T8D3	**ACBD5**	Acyl-CoA-binding domain-containing protein 5 isoform 1	525	SPGVLTFAIIWPFIAQWLVYLYY	GVLTFAIIWPFIAQWLVYLYY	23	17,78	28,2	0,333	1,226
NP_000373.1	P51648	**ALDH3A2**	Fatty aldehyde dehydrogenase isoform 2	485	LGLLLLTFLGIVAAVLVKA	LGLLLLTFLGIVAAVLV	19	18,05	46,5	-1,222	2,447
NP_940683.1	Q86W74	**ANKRD46**	Ankyrin repeat domain-containing protein 46 isoform 1	228	LGFWRVLLLIFVIALLSLGIAYY	LGFWRVLLLIFVIALLSLGIA	23	25,32	48,1	-4,419	2,091
NP_848029.2	Q8IVJ8-1	**APRG1**	AP20 region protein isoform B	170	-	IALALAGPGAILILELSWFLG	21	16,42	38,3	0,027	1,824
NP_848032.1	Q8IVJ8-3	**APRG1**	AP20 region protein isoform E	119	VNVFGAIINMAASVSGVIG	VNVFGAIINMAASVSGVIG	19	11,4	30,6	4,451	1,611
NP_001003713.1	P56134	**ATP5J2**	ATP synthase subunit f, mitochondrial isoform 2b	88	SISGITMVLACYVLFSYSF	ISGITMVLACYVLFSYSFSY	19	14,29	29,9	0,961	1,574
NP_001179.1	Q16611	**BAK1**	BCL2-antagonist/killer 1	211	LGNGPILNVLVVLGVVLLGQFVV	ILNVLVVLGVVLLGQFVV	23	17,81	45,8	0,779	1,991
NP_620119.2	Q07812	**BAX**	Apoptosis regulator BAX isoform sigma	179	WQTVTIFVAGVLTASLTIW	TVTIFVAGVLTASLTIWKKMG	19	13,92	26,3	0,747	1,384
NP_000624.2	P10415	**BCL2**	B-cell lymphoma protein 2 alpha isoform	239	WLSLKTLLSLALVGACITLGAYL	FSWLSLKTLLSLALVGACITLG	23	15,31	37,1	-1,356	1,613
NP_001182.1	Q07817	**BCL2L1**	Bcl-2-like protein 1 isoform Bcl-X(S)	170	WFLTGMTVAGVVLLGSLFS	FNRWFLTGMTVAGVVLL	19	16,66	32	0,421	1,684
NP_004041.1	Q92843	**BCL2L2**	BCL2-like 2 protein	193	SVRTVLTGAVALGALVTVGAFFA	-	23	13,99	38,4	-0,178	1,670
NP_065129.1	Q9HD36	**BCL2L10**	BCL2-like 10 (apoptosis facilitator)	204	LVQAFLSCLLTTAFIYLWT	LVQAFLSCLLTTAFIYLW	19	15,64	30,8	-0,331	1,621
NP_056182.2	Q9BXK5	**BCL2L13**	BCL2-like 13 (apoptosis facilitator) isoform 2	485	ILLFGGAAAVAILAVAIGVALAL	ILLFGGAAAVAILAVAIGVAL	23	23,84	61,1	-2,398	2,657
NP_005859.1	O15155	**BET1**	BET1 homolog isoform 1	118	LLCYMMLFSLFVFFIIYWI	KLLCYMMLFSLFVFFIIYWII	19	27,05	46,1	-3,098	2,426
NP_001092257.1	Q9NYM9	**BET1L**	BET1-like protein isoform 1	111	LLCGMAVGLIVAFFILSYF	LLCGMAVGLIVAFFILSYFLS	19	21,52	46,1	-1,842	2,426
NP_001188.1	Q13323	**BIK**	BCL2-interacting killer	160	VLLALLLLLALLLPLLSGGLHLL	VLLALLLLLALLLPLLSGGLH	23	25,73	58,4	-2,748	2,539
NP_001196.2	Q12981	**BNIP1**	Vesicle transport protein SEC20 isoform BNIP1	228	LLIFLALALFLATVLYIVK	TDKLLIFLALALFLATVLYIV	19	21,41	49,1	-2,676	2,584
NP_004043.3	Q12983	**BNIP3**	BCL2/adenovirus E1B 19 kDa protein-interacting protein 3	259	FLKVFLPSLLLSHLLAIGLGIYI	VFLPSLLLSHLLAIGLGIYIG	23	18,98	43,1	-0,772	1,874
NP_004322.1	O60238	**BNIP3L**	BCL2/adenovirus E1B 19kD-interacting protein 3-like	219	FLKVFIPSLFLSHVLALGLGIYI	VFIPSLFLSHVLALGLGIYIG	23	18,78	42,5	-0,252	1,848
NP_001103129.1	Q96LL3	**C16orf92**	Uncharacterized protein C16orf92 isoform 1 precursor	110	LFHHILVGLLVVAFFFLLF	PGLFHHILVGLLVVAFFFLLF	19	24,48	48,9	-1,734	2,574
NP_001001701.2	Q8WVX3	**C4orf3**	Hepatitis C virus F protein-transactivated protein 1	66	SYWLDLWLFILFDVVVFLFVYFL	WLDLWLFILFDVVVFLFVYFL	23	25,6	45,9	-2,704	1,996
NP_872333.1	Q86V35	**CABP7**	Calcium binding protein 7	215	SLICAFAIAFIISVMLIAA	LICAFAIAFIISVMLIAANQV	19	20,85	51,7	-1,603	2,721
NP_001017440.1	Q9BXU9	**CALN1**	Calcium-binding protein 8 isoform 2	219	SLICAFAMAFIISVMLIAANQIL	LICAFAMAFIISVMLIAANQI	23	20,61	50,4	-1,354	2,191
NP_073579.4	Q96JN2	**CCDC136**	Coiled-coil domain-containing protein 136 isoform 1	1154	-	IFSLPLVGLVVISALLWCWWA	21	21,76	43,2	-2,371	2,057
NP_653289.3	Q8N6L0	**CCDC155**	Protein KASH5	562	-	LIPAPVLGLLLLLLLSVLLLG	21	23,32	55,5	-2,575	2,643
NP_612502.1	Q9P0B6	**CCDC167**	Coiled-coil domain-containing protein 167	97	MLLSVAIFILLTLVYAYWT	MLLSVAIFILLTLVYAYW	19	21,44	39	-1,988	2,053
A4D256.2	A4D256	**CDC14C**	Dual specificity protein phosphatase CDC14C	554	ILLPSPLAVLTFTLCSVVIWWIV	ILLPSPLAVLTFTLCSVVIWWIV	23	21,39	48,4	-0,703	2,104
NP_060244.2	Q5VV42	**CDKAL1**	Threonylcarbamoyladenosine tRNA methylthiotransferase	579	ALRMSVGLALLGLLFAFFV	CALRMSVGLALLGLLFAFFVKVY	19	18,84	40,8	-1,081	2,147
NP_057648.2	Q8N111	**CEND1**	Cell cycle exit and neuronal differentiation protein 1	149	PLLVAGGVAVAAIALILGVAFLV	LVAGGVAVAAIALILGVAFLV	23	22,59	59,8	-1,845	2,600
NP_057410.1	Q9UBR5-3	**CKLF**	Chemokine-like factor isoform c	67	LVFALVTAVCCLADGALIY	LVFALVTAVCCLADGALIY	19	13,24	41,4	0,654	2,179
NP_922945.1	Q9BXN2-9	**CLEC7A**	C-type lectin domain family 7 member A isoform f	77	LIAVILGILCLVILVIAVVLGTM	LIAVILGILCLVILVIAVVLG	23	29,23	72,8	-4,098	3,165
NP_079010.2	Q96JQ2	**CLMN**	Calmin	1002	MMYFILFLWLLVYCLLLFP	MMYFILFLWLLVYCLLLFPQL	19	25,68	44,9	-2,817	2,363
NP_851800.1	Q8IZ96-7	**CMTM1**	CKLF-like MARVEL transmembrane domain-containing protein 1 isoform 5	61	AAALDLTNSIITAVFLSVVAILA	-	23	15,24	44,9	1,062	1,952
NP_004709.2	O14548	**COX7A2L**	Cytochrome c oxidase subunit VIIa polypeptide 2 like	114	LYRTTMALTVGGTIYCLIALYMA	-	23	13,56	28,1	-0,709	1,222
NP_001904.2	Q13948	**CUX1**	Protein CASP	678	TIGFFYTLFLHCLVFLVLY	IGFFYTLFLHCLVFLVLYKLA	19	20,32	38	-0,605	2,000
NP_683725.1	P00167	**CYB5A**	Cytochrome b-5 isoform 1	134	WWTNWVIPAISAVAVALMYRLYM	WWTNWVIPAISAVAVALMYRLYM	23	15,37	23,8	-0,263	1,035
NP_085056.2	O43169	**CYB5B**	Cytochrome b5 type B	150	CWAYWILPIIGAVLLGFLY	WAYWILPIIGAVLLGFLY	19	19,31	35	-1,336	1,842
NP_115788.1	Q9H1C7	**CYSTM1**	Cysteine-rich and transmembrane domain-containing protein 1	97	-	LGPSTCLTACWTALCCCC	18	2,83	24,2	2,511	1,344
NP_079095.3	Q8WVC6	**DCAKD**	Dephospho-CoA kinase domain containing	231	-	GVLTGLAAIASLLYLLTHYLLPY	23	16,17	32,8	0,337	1,426
NP_001075032.1	Q09013-1	**DMPK**	Myotonin-protein kinase isoform 1	639	-	LLLFAVVLSRAAALGCIGLVA	21	17,37	48,1	0,344	2,290
NP_005519.2	Q9NNZ3	**DNAJC4**	DnaJ homolog subfamily C member 4 isoform 3	241	VLGYCLLLMLAGMGLHYIA	VLGYCLLLMLAGMGLHYIAF	19	16,58	34,4	-0,404	1,811
NP_003485.1	O75923	**DYSF**	Dysferlin	2080	WAIILFIILFILLLFLAIFIYAF	IILFIILFILLLFLAIFIYAF	23	37,77	71,5	-7,177	3,109
NP_000108.1	P50402	**EMD**	Emerin	254	LLLFLVFVIVLFFIYHFMQ	VPLWGQLLLFLVFVIVLFFIY	19	25,93	48,5	-2,678	2,553
Q5RGS3.1	Q5RGS3	**FAM74A1**	Protein FAM74A1	127	LSLLLHLAVFLWIIIAINF	LSLLLHLAVFLWIIIAINFSN	19	22,92	45,8	-1,388	2,411
A6NL05.3	A6NL05	**FAM74A7**	Protein FAM74A7	159	LSLLLHLAVFLWIIIAINF	LSLLLHLAVFLWIIIAINFSN	19	22,92	45,8	-1,388	2,411
NP_775882.2	Q52LJ0-1	**FAM98B**	Protein FAM98B isoform 1	330	LMISYLMFLILVYFSFMS	LMISYLMFLILVYFSFMS	18	22,21	37,5	-0,662	2,083
NP_689613.1	Q8N8J7	**FAM241A**	Uncharacterized protein FAM241A	132	VIVIFFWVMLWFLGLQALGLVAVLCLVIIYV	VIVIFFWVMLWFLGLQALGLV	31	39,97	83	-4,977	2,677
NP_660349.1	Q96D05	**FAM241B**	Uncharacterized protein FAM241B	121	LLLFLLMMLGVRGLLLVGLVYLV	ILLLFLLMMLGVRGLLLVGLV	23	27,99	58,2	-3,185	2,530
NP_149076.1	Q969F0	**FATE1**	Fetal and adult testis expressed transcript protein	183	TLIIAVLVSASIANLWLWM	TLIIAVLVSASIANLWLWM	19	18,71	36,8	-0,220	1,937
NP_000560.6	P08637	**FCGR3A**	Low affinity immunoglobulin gamma Fc region receptor III-A isoform a precursor	254	YQVSFCLVMVLLFAVDTGLYFSV	VSFCLVMVLLFAVDTGLYFSV	23	16,3	38,5	-0,242	1,674
NP_004453.3	P37268	**FDFT1**	Squalene synthase isoform 1	417	-	PIYLSFVMLLAALSWQYLTTL	21	16,02	28,2	0,069	1,343
NP_001034201.2	Q2WGJ9	**FER1L6**	Fer-1-like protein 6	1857	YIIIAFILIILIIFLVLFIYTLP	IIIAFILIILIIFLVLFIYTL	23	33,83	69	-6,425	3,000
NP_057152.2	Q9Y3D6	**FIS1**	Mitochondrial fission 1 protein	152	GLVGMAIVGGMALGVAGLAGLIG	LVGMAIVGGMALGVAGLAGLI	23	18,4	44,6	0,448	1,939
NP_036313.3	Q14318	**FKBP8**	Peptidyl-prolyl cis-trans isomerase FKBP8 isoform 1	413	WLFGATAVALGGVALSVVI	WLFGATAVALGGVALSVVIAA	19	16,88	39,1	0,713	2,058
NP_001002294.1	P31513	**FMO3**	Dimethylaniline monooxygenase [N-oxide-forming] 3	532	CFFFHWLKLFAIPILLIAVFLVL	-	23	25,3	55,2	-2,182	2,400
NP_001452.2	P49326	**FMO5**	Dimethylaniline monooxygenase [N-oxide-forming] 5 isoform 1	533	MTSTMTIGKFMLALAFFAIIIAY	-	23	18,53	38,4	-0,333	1,670
NP_055738.3	Q9Y2H6	**FNDC3A**	Fibronectin type-III domain-containing protein 3A isoform 2	1142	AVILVLFAFFSILIAFIIQYFVI	ILVLFAFFSILIAFIIQYFVI	23	30,82	64,8	-3,177	2,817
NP_073600.3	Q53EP0	**FNDC3B**	Fibronectin type III domain-containing protein 3B	1204	FAAIIVLGFATLSILFAFILQYF	IIVLGFATLSILFAFILQYFL	23	25,65	51,9	-2,290	2,257
NP_001671.2	P54710-1	**FXYD2**	Sodium/potassium-transporting ATPase subunit gamma isoform 1	66	GGLIFAGLAFIVGLLILLS	GGLIFAGLAFIVGLLILL	19	21,72	47,3	-1,332	2,489
NP_061845.2	Q8TB36-1	**GDAP1**	Ganglioside-induced differentiation-associated protein 1 isoform a	358	VLGTTLVVGLLAGVGYFAFMLFR	LGTTLVVGLLAGVGYFAFMLF	23	19,56	40,9	-1,100	1,778

3.Results

NCBI Accession	UniProt Accession	Symbol	Description	Protein Length	TMD (TMHMM)	TMD (UniProt)	Number of residues	TMD tendency (TMHMM+UniProt)	Kyte & Doolittle (TMHMM+UniProt)	ΔG_{app} (kcal mol^{-1})	GRAVY
NP_076939.3	Q96MZ0-1	**GDAP1L1**	Ganglioside-induced differentiation-associated protein 1-like 1	367	SFFGASFLMGSLGGMGYFAYWYL	-	23	17,4	20,8	0,317	0,904
NP_570115.1	Q8WWP7	**GIMAP1**	GTPase, IMAP family member 1	306	WRLGLALLLGGALLFWVLL	SWRLGLALLLGGALLFWVLL	19	20,5	37,3	-2,603	1,963
NP_060854.2	Q96F15	**GIMAP5**	GTPase, IMAP family member 5	307	HYEIFVFLLLCSILFFIIFLFIF	IFVFLLLCSILFFIIFLFIFH	23	29,59	59	-4,426	2,565
NP_005104.3	Q8TBA6	**GOLGA5**	Golgin subfamily A member 5	731	VFVIIYMALLHLWVMIVLLTYTP	VFVIIYMALLHLWVMIVLLTY	23	25	48	-2,261	2,087
NP_004478.3	Q14789-1	**GOLGB1**	Golgin subfamily B member 1 isoform 2	3259	VPLLAAIYFLMIHVLLILCFTGH	VPLLAAIYFLMIHVLLILCFT	23	21,23	47,9	-1,638	2,083
NP_001007025.1	O95249-2	**GOSR1**	Golgi SNAP receptor complex member 1 isoform 3	185	LILGGVIGICTILLLLYAF	SLILGGVIGICTILLLLYAFH	19	21,92	48,9	-2,076	2,574
NP_004278.2	O14653	**GOSR2**	Golgi SNAP receptor complex member 2 isoform A	212	MIGGMLLTCVVMFLVVQYL	YFMIGGMLLTCVVMFLVVQYL	19	18,92	41,2	-0,703	2,168
NP_001012660.1	Q8IUY3	**GRAMD2**	GRAM domain containing 2	354	VFFVLICFLVMSSSYLAFR	LLKVFFVLICFLVMSSSYLAF	19	17,54	37,7	-0,708	1,984
NP_689909.2	Q86Z02-2	**HIPK1**	Homeodomain-interacting protein kinase 1 isoform 2, HIPK1 beta	1075	SAMGYCLLFGPCTVVTFWRTLLL??	-	25	13,3	29,7	-0,563	1,188
NP_002124.1	P09601	**HMOX1**	Heme oxygenase 1	288	APLLRWVLTLSFLVATVAVGLYA	-	23	16,91	38,7	-1,065	1,683
NP_002125.3	P30519-1	**HMOX2**	Heme oxygenase 2 isoform b	316	QFILAAGVALAAGLLAWYY	-	19	15,26	29,7	-0,568	1,563
XP_016862412.1	Q9HDD0	**HRASLS**	Phospholipid-metabolizing enzyme A-C1	168	ISTVEFVTAAVGVFSFLGLFP	ISTVEFVTAAVGVFSFLGLFPKGQ	21	13,71	34,8	1,648	1,657
NP_060348.1	Q9NWW9	**HRASLS2**	HRAS-like suppressor 2	162	GAVTTVGVAAGLLAAASLVGILL	AVTTVGVAAGLLAAASLVGILLA	23	17,26	47,3	-0,067	2,057
NP_003797.1	O00198	**HRK**	Activator of apoptosis harakiri	91	LPTYWPWLCAAAQVAALAAWLLG	WPWLCAAAQVAALAAWLLG	23	12,77	26,5	0,210	1,152
NP_001192209.1	A1L1A6	**IGSF23**	Immunoglobulin superfamily member 23	192	IGLLAAGILGAGALIAGMCFIII	LLAAGILGAGALIAGMCFIII	23	23,13	56,4	-1,316	2,452
NP_001557.1	Q96PE3-4	**INPP4A**	Inositol polyphosphate-4-phosphatase, type 1 isoform beta	954	IPLLALSPNLLIVWLFLSIAYLV	-	23	22,59	48,2	-1,357	2,096
NP_065698.1	Q9HDC5	**JPH1**	Junctophilin 1	661	NSIMIVLVMLLNIGLAILFVHFL	IMIVLVMLLNIGLAILFVHFL	23	24,92	53,2	-1,425	2,313
NP_065166.2	Q9BR39-1	**JPH2**	Junctophilin 2 isoform 1	696	NTILICMVILLNIGLAILFVHLL	ILICMVILLNIGLAILFVHLL	23	23,78	55,2	-2,435	2,400
NP_065706.2	Q8WXH2-1	**JPH3**	Junctophilin 3 isoform 1	748	APILVVMVILLNIGVAILFINFF	LVVMVILLNIGVAILFINFFI	23	26,2	59,4	-1,979	2,583
NP_115828.2	Q96JJ6	**JPH4**	Junctophilin 4	628	-	LVVGAVALLDLSLAFLFSQLLT	22	17,36	44,3	0,297	2,014
NP_005463.1	Q9Y6H6	**KCNE3**	Potassium voltage-gated channel, Isk-related family, member 3	103	SYMYILFVMFLFAVTVGSLILGY	YMYILFVMFLFAVTVGSLILG	23	24,43	43,8	-2,369	1,904
NP_056021.1	Q9UPX6	**KIAA1024**	UPF0258 protein KIAA1024	916	IAALIAAAACTVILVIVVPICTM	IAALIAAAACTVILVIVVPIC	23	20,33	61,6	-1,811	2,678
NP_004853.2	Q99732	**LITAF**	LPS-induced TNF-alpha factor	161	GALTWLSCGSLCLLGCIAGCCFIPFC	-	26	13,91	45,8	-1,610	1,762
NP_055931.1	Q9Y2L9-1	**LRCH1**	Leucine-rich repeats and calponin homology (CH) domain containing 1	728	IGFCLVHILFIVLVYITYHWNAL	-	23	21,08	41,2	-0,734	1,791
NP_006143.2	Q12912-2	**LRMP**	Lymphoid-restricted membrane protein	499	ALWLSIAFIVLFAALMSFL	ALWLSIAFIVLFAALMSFLTG	19	23,83	47,2	-2,536	2,484
NP_060979.2	Q96AG4	**LRRC59**	Leucine-rich repeat-containing protein 59	307	SWAVLKLLLLLLLFGVAGGLVAC	WAVLKLLLLLLLFGVAGGLVA	23	20,55	50,7	-2,463	2,204
NP_071885.1	P21145-4	**MAL**	Myelin and lymphocyte protein isoform d	55	IFEFVFSYIATLLYVVHAVFSLI	-	23	21,15	44,9	1,514	1,952
NP_000231.1	P21397-1	**MAOA**	Amine oxidase [flavin-containing] A isoform 1	527	SVSGLLKIIGFSTSVTALGFVLY	VSGLLKIIGFSTSVTALGFVL	23	13,64	33,2	1,880	1,443
NP_000889.3	P27338-1	**MAOB**	Amine oxidase [flavin-containing] B	520	VPGLLRLIGLTTIFSATALGFLA	PGLLRLIGLTTIFSATALGFLAHKRGL	23	15,35	36,8	0,005	1,600
NP_065797.2	Q7Z434-1	**MAVS**	Mitochondrial antiviral-signaling protein isoform 1	540	PGALWLQVAVTGVLVVTLLVVLY	GALWLQVAVTGVLVVTLLVVL	23	19,62	46,3	-1,304	2,013
NP_068779.1	Q07820	**MCL1**	Induced myeloid leukemia cell differentiation protein Mcl-1 isoform 1	350	VLLAFAGVAGVGAGLAYLI	IRNVLLAFAGVAGVGAGLAYL	19	17,24	41,2	0,040	2,168
NP_001026883.1	Q96AQ8-1	**MCUR1**	Nitochondrial calcium uniporter regulator 1	359	IKYLAGSIFTCLTVALGFYRLW	YLAGSIFTCLTVALGFYRLW	22	12,03	25,2	-0,368	1,145
NP_064579.3	Q9GZY8-1	**MFF**	Mitochondrial fission factor isoform a	342	MVMYSITVAFWLLNSWLWF	VMYSITVAFWLLNSWLWF	19	19,57	25,7	0,482	1,353
NP_689794.1	Q8NHP6-1	**MOSPD2**	Motile sperm domain containing protein 2 isoform 1	518	LSLTMLLLAFVTSFFYLLY	LLLSLTMLLLAFVTSFFYLLY	19	21,2	37,3	-1,518	1,963
NP_004523.3	Q99102-13	**MUC4**	Mucin-4 isoform d precursor	1176	FFGIFFGALGGLLLLGVGTFVVL	FFGIFFGALGGLLLLGVGTFV	23	26,09	52,6	-1,576	2,287
NP_038479.1	Q9NZM1-1	**MYOF**	Myoferlin isoform a	2061	WVIIGLLFLLILLLFVAVLLYSL	WVIIGLLFLLILLLFVAVLLY	23	34,13	68,1	-6,199	2,961
NP_579899.1	Q9NZM1-6	**MYOF**	Myoferlin isoform b	2048	WVIIGLLFLLILLLFVAVLLYSL	WVIIGLLFLLILLLFVAVLLY	23	34,13	68,1	-6,199	2,961
NP_001161803.1	O95168-2	**NDUFB4**	NADH dehydrogenase [ubiquinone] 1 beta subcomplex subunit 4 isoform 2	120	MGALCGFGPLIFIYYII	LMGALCGFGPLIFIYYII	17	15,93	32	1,114	1,882
NP_694540.3	Q6ZNB6	**NFXL1**	NF-X1-type zinc finger protein NFXL1	911	YYLISVCGVVVVVFAWYIT	YYLISVCGVVVVVFAWYI	19	18,54	38,4	-1,388	2,021
NP_071770.1	Q9Y5M6	**OCLM**	Oculomedin	44	ILFYLKILYKSGIIWLSWYSFIL	-	23	18,74	30,8	0,933	1,339
NP_065947.1	Q9H0X9-1	**OSBPL5**	Oxysterol-binding protein-like protein 5 isoform a	879	-	SWFLLCVFLACQLFINHIL	19	16,32	35,5	0,144	1,868
NP_001003712.1	Q9BZF1-3	**OSBPL8**	Oxysterol-binding protein-like protein 8 isoform b	847	DYFIIFLLILLQVIINFMF	YFIIFLLILLQVIINFMF	19	21,67	43,2	-1,184	2,274
NP_733764.1	Q7RTW8-2	**OTOA**	Otoancorin isoform 2	815	AGALQSWGLWLGCPLLVLMAKLL	-	23	13,48	31,6	0,667	1,374
NP_919304.1	Q9HC10-2	**OTOF**	Otoferlin isoform d	1230	LLLLLLLLLLLALFLYSVPGYLV	WLLLKLLLLLLLLLLALFLY	23	29,58	60,8	-4,539	2,643
NP_001274418.1	Q9HC10-5	**OTOF**	Otoferlin isoform e	1997	WLIIKIVLALLGLLMLGLFLYSL	-	23	26,98	54,5	-4,050	2,370
NP_060321.3	Q8N5Y8	**PARP16**	Mono [ADP-ribose] polymerase PARP16	323	FTVMISLYLLLLLIVSVINSSAF	SHWFTVMISLYLLLLLIVSVI	23	23,38	49,5	-1,347	2,152
NP_001006625.1	Q86YL7-6	**PDPN**	Podoplanin isoform c	120	VTLVGIIVGVLLAIGFIGAIIVV	VGIIVGVLLAIGFIGAIIVVV	23	27,7	67,7	-2,251	2,943
NP_003838.1	O75192	**PEX11A**	Peroxisomal membrane protein 11A	247	IIGLGGLVSSIAGMITVAY	GIIGLGGLVSSIAGMITVAY	19	14,95	34,3	2,247	1,805
NP_003837.1	O96011-1	**PEX11B**	Peroxisomal membrane protein 11B isoform 1	259	GIVGLCGLVSSILSILTLIYPWL	GIVGLCGLVSSILSILTLIYPWL	23	19,52	43,6	-0,101	1,896
NP_060399.1	Q7Z412	**PEX26**	Peroxisome assembly protein 26 isoform a	305	-	FFSLPFKKSLLAALILCLLVV	21	14,61	43	0,791	2,048
NP_009000.2	P53816	**PLA2G16**	HRAS-like suppressor 3	162	VIIAASVAGMGLAAMSLIGVMFS	VIIAASVAGMGLAAMSLIGVMFS	23	19,85	47,6	0,812	2,070
NP_067023.1	Q9UF11	**PLEKHB1**	Pleckstrin homology domain containing, family B (evectins) member 1	243	APLAMGMLAGAATGAALGSLMW???	-	25	12,62	27,9	1,429	1,116
NP_060428.2	Q96CS7-3	**PLEKHB2**	Pleckstrin homology domain containing, family B (evectins) member 2 isoform 2	221	LALGMLAGAATGMALGSLFWV	-	21	17,16	34,8	0,251	1,657
NP_002658.1	P26678	**PLN**	Cardiac phospholamban	52	NLFINFCLILICLLLICIIVML	FINFCLILICLLLICIIVMLL	22	27,24	65,8	-4,250	2,991
NP_149992.3	Q6ZSY5-1	**PPP1R3F**	Protein phosphatase 1 regulatory subunit 3F isoform 1	799	VPVALNSGVSLLVLALCLSLAWF	VLAGLVVVPVALNSGVSLLVL	23	18,09	45,3	-0,484	1,970
NP_954652.2	Q7RTY3-2	**PRSS45**	Serine protease 45	228	NGAFSGPCASACLLFLCWLLQ???	-	24	8,49	25,6	1,137	1,067
NP_002818.1	P18031	**PTPN1**	Protein tyrosine phosphatase, non-receptor type 1	435	FLVNMCVATVLTAGAYLCYRFLF	-	23	15,5	36,1	-0,293	1,570
NP_002819.2	P17706	**PTPN2**	Protein tyrosine phosphatase, non-receptor type 2 isoform 1	415	ILTKMGFMSVILVGAFVGWTLFF	-	23	21,21	41,6	-1,502	1,809
NP_004576.2	Q9UL19	**RARRES3**	Retinoic acid receptor responder protein 3	164	VGVATALGILVVAGCSFAI	KVEVGVATALGILVVAGCSFAI	19	15,2	43,2	0,560	2,274
NP_003699.3	O75452	**RDH16**	Retinol dehydrogenase 16	317	LYLPMSYMPTFLVDAIMYWVS	LLYLPMSYMPTFLVDAIMYWV	21	12,38	20,8	2,795	0,990
NP_997274.2	Q6ZS82	**RGS9BP**	Regulator of G-protein signaling 9-binding protein	235	ALAAILFGAVLLAAVALAV	ALAAILFGAVLLAAVALAVCV	19	20,28	52,9	-1,588	2,784
NP_001028738.1	Q8IXI2-7	**RHOT1**	Mitochondrial Rho GTPase 1 isoform 2	659	SFGATVFAVLGFAMYKALL	WLRASFGATVFAVLGFAMYKALL	19	13,04	29,8	0,726	1,568

NCBI Accession	UniProt Accession	Symbol	Description	Protein Length	TMD (TMHMM)	TMD (UniProt)	Number of residues	TMD tendency (TMHMM+UniProt)	Kyte & Doolittle (TMHMM+UniProt)	ΔG_{app} (kcal mol^{-1})	GRAVY
NP_620124.1	Q8IXI1	**RHOT2**	Mitochondrial Rho GTPase 2	618	GLLGVVGAAVAAVLSFSLYRVLV	GLLGVVGAAVAAVLSFSLYRVLV	23	17,65	45,6	-0,462	1,983
NP_055561.2	P50876	**RNF144A**	E3 ubiquitin-protein ligase RNF144A	292	VVGIFAGFGLLLLVASPFLLLAT	VVGIFAGFGLLLLVASPFLLL	23	23,31	53,2	-1,766	2,313
NP_877434.2	Q7Z419	**RNF144B**	E3 ubiquitin-protein ligase RNF144B	303	VVGILVGLGIIALVTSPLLLLAS	VVGILVGLGIIALVTSPLLLL	23	21,86	55,4	-1,168	2,409
NP_775828.1	Q8N8N0	**RNF152**	E3 ubiquitin-protein ligase RNF152	203	TWSGVCTVILVACVLVFLLGIVL	SGVCTVILVACVLVFLLGIVL	23	23,54	58,9	-3,182	2,561
NP_659488.2	Q96D59	**RNF183**	Probable E3 ubiquitin-protein ligase RNF183	192	IFAYLMAVILSVTLLLIFSIFWT	IFAYLMAVILSVTLLLIFSIF	23	28,32	54,1	-3,869	2,352
NP_001140156.1	A6NCQ9	**RNF222**	RING finger protein 222	220	LLLITLIAVVAVVAAILPWVLLV	LITLIAVVAVVAAILPWVLLV	23	28,7	69,3	-4,013	3,013
NP_714919.2	P59025	**RTP1**	Receptor transporting protein 1	263	GWNFCSIPWCLFWATVLLLIIYL	IPWCLFWATVLLLIIYLQFSF	23	21,19	38,1	-1,400	1,657
NP_001004312.2	Q5QGT7	**RTP2**	Receptor transporting protein 2	225	LSLRWCLFWASLCLLVVYLQFSF	LSLRWCLFWASLCLLVVYLQFSF	23	18,93	36,7	-2,182	1,596
NP_113628.1	Q9BQQ7	**RTP3**	Receptor-transporting protein 3	232	NLSIFCCCVILIVIVVIVV	SIFCCCVILIVIVVIVVKTAI	19	21,18	61,3	-1,942	3,226
NP_071430.2	Q96DX8	**RTP4**	Receptor-transporting protein 4	246	LNICVFILLLVFIVVKCFT??	PLNICVFILLLVFIVVKCFTS	21	18,97	50,8	-1,686	2,419
NP_776182.2	Q14D33	**RTP5**	Receptor-transporting protein 5	572	FWIWVSMTVCVFWLMCMCRLNPG	FWIWVSMTVCVFWLMCM	23	15,17	29,3	-0,716	1,274
NP_002957.1	P60903	**S100A10**	Protein S100-A10	97	VGFQSFFSLIAGLTIACNDYFVV	-	23	12,34	31,6	2,577	1,374
NP_004883.3	O75396	**SEC22B**	Vesicle-trafficking protein SEC22b	215	LAAVAVFFIMLIVYVRFWW	KLAAVAVFFIMLIVYVRFWWL	19	22,88	41,5	-2,369	2,184
NP_006799.1	P60468	**SEC61B**	Protein transport protein Sec61 subunit beta	96	VGPVPVLVMSLLFIASVFMLHIW	VPVLVMSLLFIASVFMLHIWG	23	21,62	47,1	0,023	2,048
NP_055117.1	P60059	**SEC61G**	Protein transport protein Sec61 subunit gamma	68	IAMATAIGFAIMGFIGFFV	FQKIAMATAIGFAIMGFIGFFVKLIHIPI	19	20,69	42,5	0,044	2,237
NP_068802.1	O75920	**SERF1A**	Small EDRK-rich factor 1A, telomeric	110	YLAYGSITPISAFVFVVFFSVFF	-	23	21,68	42,3	-0,287	1,839
NP_055260.1	Q9Y6X1	**SERP1**	Stress-associated endoplasmic reticulum protein 1	66	SVGPWLLALFIFVVCGSAIFQII	GPWLLALFIFVVCGSAIFQII	23	20,93	48,1	-1,290	2,091
NP_001010897.1	Q8N6R1	**SERP2**	Stress-associated endoplasmic reticulum protein 2	65	PVGPWLLALFVFVVCGSAIFQII	GPWLLALFVFVVCGSAIFQII	23	19,51	47	-0,923	2,043
NP_775742.4	Q70HW3-2	**SLC25A26**	S-adenosylmethionine mitochondrial carrier protein isoform a	186	LAGLFAGVFPRMAAISLGGFIFLGA	FAGVFPRMAAISLGGFIFLGA	25	18,41	41,6	1,215	1,664
NP_001182719.1	Q6IEE8	**SLFN12L**	Schlafen family member 12-like	588	QIFLFVCLFRFCLFVCWFVCFFL	IFLFVCLFRFCLFVCWFVCFF	23	25,39	55,8	-3,125	2,426
NP_009090.2	Q14BN4	**SLMAP**	Sarcolemmal membrane-associated protein	811	WPWMPMLAALVAVTAIVLYVPGL	WMPMLAALVAVTAIVLYVPGL	23	18,13	38,5	-0,928	1,674
NP_003054.1	O00631	**SLN**	Sarcolipin	31	ELFLNFTIVLITVILMWLL	LFLNFTIVLITVILMWLLV	19	21,48	42,9	-1,537	2,258
NP_064564.1	Q9NRQ5	**SMCO4**	Single-pass membrane and coiled-coil domain-containing protein 4	59	ITTVVLPTLAVVVLLIVVFVYVA	TVVLPTLAVVVLLIVVFVYVA	23	25,19	63,4	-2,633	2,757
NP_001157196.1	B2RUZ4	**SMIM1**	Small integral membrane protein 1	78	VLGGVALFWIIFILGYLTGYYVH	LGIAMKVLGGVALFWIIFILG	23	22,39	38,4	-1,284	1,670
NP_001156910.1	Q96HG1	**SMIM10**	Small integral membrane protein 10	83	FFYFYILASVILNVHLQVY	FFYFYILASVILNVHLQVY	19	16,14	28,3	0,895	1,489
NP_001156467.1	Q71RC9	**SMIM5**	Small integral membrane protein 5	77	IVAFSVIILFTATVLLLLIACS	IVAFSVIILFTATVLLLLIA	23	26,28	63,9	-3,071	2,778
NP_689807.1	Q7Z699	**SPRED1**	Sprouty-related protein 1 with EVH-1 domain	444	LALVALSFIVPCMCCYVPL	-	19	13,95	42,8	0,464	2,253
NP_861449.2	Q7Z698-1	**SPRED2**	Sprouty-related, EVH1 domain-containing protein 2 isoform a	418	WMALIALSFLAPCMCCYLPLRAC	-	23	12,21	36,6	-0,449	1,591
NP_001035189.1	Q8NFR3	**SPTSSB**	Serine palmitoyltransferase small subunit B	76	ILLTIIAMVVYTAYVFIPI	ILLTIIAMVVYTAYVFIPIHI	19	20,91	45,4	0,384	2,389
NP_149095.2	Q8WXE9	**STON2**	Stonin-2 isoform 1	905	WLMLPTPFVHPTTLPLLFLLAML	-	23	16,53	33,2	1,593	1,443
NP_004594.1	Q16623	**STX1A**	Syntaxin-1A isoform 1	288	IMIIICCVILGIVIASTVGGIF	IMIIICCVILGIVIASTVGGI	22	23,7	61,2	-1,717	2,782
NP_443106.1	P61266	**STX1B**	Syntaxin-1B	288	IMIIICCVVLGVVLASSIGGTLG	IMIIICCVVLGVVLASSIGGTLGL	23	20,19	55,5	-0,679	2,413
NP_919337.1	P32856-1	**STX2**	Syntaxin 2 isoform 2	288	WIIIAVSVVLVAIIALIIGLSVG	WIIIAVSVVLVAIIALIIGLSVGK	23	27,78	66	-2,677	2,870
NP_001971.2	P32856-2	**STX2**	Syntaxin 2 isoform 1	287	LMFIIICVIVLLVILGIILATTL	-	23	31,72	74,1	-5,720	3,222
NP_004168.1	Q13277-1	**STX3**	Syntaxin-3 isoform 1	289	LIIIIVLVVVLLGILALIIGLSV	LIIIIVLVVVLLGILALIIGL	23	33,3	79,3	-4,337	3,448
NP_004595.2	Q12846-1	**STX4**	Syntaxin-4 isoform 3	297	VLIAICVSITVVLLAVIIGVTVV	IAICVSITVVLLAVIIGVTVV	23	26,09	71	-2,284	3,087
NP_003155.2	Q13190-1	**STX5**	Syntaxin-5 isoform 1	355	WLMVKIFLILIVFFIIFVV	WLMVKIFLILIVFFIIFVVFL	19	28,54	59	-3,139	3,105
NP_005810.1	O43752	**STX6**	Syntaxin 6	255	WCAIAILFAVLLVVLILFL	WCAIAILFAVLLVVLILFLVL	19	27,54	61,5	-3,839	3,237
NP_003560.2	O15400	**STX7**	Syntaxin 7	261	TLCIIILILVIGVAIISLIIWGL	CIIILILVIGVAIISLIIWGL	23	30,13	69	-5,057	3,000
NP_004844.1	Q9UNK0	**STX8**	Syntaxin 8	236	SASCGMIMVILLLLVAIVVVAVW	MIMVILLLLVAIVVVAV	23	25,87	62,7	-2,917	2,726
NP_003756.1	O60499	**STX10**	Syntaxin 10	249	WCAIAVLVGVLLLVLILLF	WCAIAVLVGVLLLVLILLFSL	19	26,3	60	-3,351	3,158
NP_803173.1	Q86Y82	**STX12**	Syntaxin 12	276	MCILVLVLSVIILILGLIIWLVY	KKMCILVLVLSVIILILGLII	23	32,8	71,4	-5,284	3,104
NP_001001433.1	O14662-1	**STX16**	Syntaxin 16 isoform a	325	VILILFVIIIVLIVVLVGV	MLVILILFVIIIVLIVVLVGV	19	31,11	74	-3,650	3,895
NP_058626.1	Q9P2W9	**STX18**	Syntaxin 18	335	GFRVWILFFLVMCSFSLLFLDWY	AGFRVWILFFLVMCSFSLLFL	23	21,45	37,2	-3,430	1,617
NP_892006.3	Q8NF91-1	**SYNE1**	Nesprin-1	8797	AALPLQLLLLLLIGLACLV	AALPLQLLLLLIGLACLVPM	19	19	49,1	-1,755	2,584
NP_055995.4	Q8WXH0-1	**SYNE2**	Nesprin-2 isoform 1	6885	AALPLQLLLLLLLLLACLLP	AALPLQLLLLLLLLLACLLPS	20	19,78	50,6	-2,774	2,530
NP_689805.3	Q6ZMZ3	**SYNE3**	Nesprin-3	975	VALPLQLLLLLFLLLLFLL	VALPLQLLLLLFLLLLFLLPI	19	26,18	55,9	-3,681	2,942
NP_001034965.1	Q8N205-1	**SYNE4**	Nesprin-4 isoform 1	404	LTFLLILFLLFLLLVGAMFLLPA	FLLILFLLFLLLVGAMFLLPA	23	31,58	64,5	-5,832	2,804
NP_060843.2	P57105	**SYNJ2BP**	Synaptojanin 2 binding protein	145	GIPIFMVLVPVFALTMVAAWAFM	IPIFMVLVPVFALTMVAAWAF	23	23,22	49,5	-0,874	2,152
P0CF51.1	P0CF51	**TRGC1**	T-cell receptor gamma chain C region 1	175	YYMYLLLLLKSVVYFAIITCCLL	YYMYLLLLLKSVVYFAIITCCLL	23	20,41	44,9	-1,715	1,952
NP_001182188.1	H3BV60	**TGFBR3L**	Transforming growth factor-beta receptor type 3-like protein	316	PVVALVLAAFVLGAALAAGLGLV	VVALVLAAFVLGAALAAGLGL	23	20,85	56,4	-1,657	2,452
NP_001027454.1	P42167-1	**TMPO**	Thymopoietin isoform beta	454	VWIKILLFVVVAVFLFLVY	IPVWIKILLFVVVAVFLFLVYQAM	19	24,86	53,5	-2,817	2,816
NP_001001790.1	Q8N4H5	**TOMM5**	Mitochondrial import receptor subunit TOM5 homolog	51	SSIRNFLIYVALLRVTPFIL	SIRNFLIYVALLRVTPFIL	20	11,36	26,8	1,459	1,340
NP_001127965.1	Q96B49	**TOMM6**	Mitochondrial import receptor subunit TOM6 homolog	74	FRRNLILNLGLFAAGVWLARNLS	-	23	7,5	16	0,454	0,696
NP_061932.1	Q9P0U1	**TOMM7**	Mitochondrial import receptor subunit TOM7 homolog	55	FAIRWGFIPLVIYLGFKRG	FAIRWGFIPLVIYLGF	19	8,74	17,6	1,049	0,926
NP_079504.2	Q9Y228	**TRAF3IP3**	TRAF3-interacting JNK-activating modulator isoform 1	551	WLPVLMVVIAAALAVFLAN	WLPVLMVVIAAALAVFLA	19	18,84	44,2	-0,501	2,326
	Q9NSU2-1	**TREX1**	Three prime repair exonuclease 1 isoform a	369	LLAPLGLLAILTLAVATLYGLSL	-	23	20,65	48	-2,489	2,087
NP_149047.2	Q9BYV6-3	**TRIM55**	Tripartite motif-containing protein 55 isoform 2	540	LVICLALLAFLILHYIWSQIQCLIFTL	-	27	26,04	57,4	-1,441	2,126
NP_659440.2	Q96NA8	**TSNARE1**	t-SNARE domain-containing protein 1 isoform a	513	LSAGVTALLVIIIIIATSV	CFLSAGVTALLVIIIIIATSV	19	18,94	48,5	-1,144	2,553
NP_057105.2	Q9Y385	**UBE2J1**	Ubiquitin-conjugating enzyme E2, J1	318	GGSAVLIVILTLALAALIF	DHGGSAVLIVILTLALAALIF	19	20,2	48,6	-1,283	2,558
NP_477515.2	Q8N2K1-1	**UBE2J2**	Ubiquitin conjugating enzyme E2, J2 isoform 2	259	GLLGGALANLFVIVGFAAFAYTW	GLLGGALANLFVIVGFAAFAY	23	19,33	37,5	-1,019	1,630
NP_060937.1	Q9NZ43	**USE1**	Vesicle transport protein USE1	259	WLLWAMLIIVCFIFISMILFIRI	WLLWAMLIIVCFIFISMILFI	23	31,31	60,3	-5,755	2,622

NCBI Accession	UniProt Accession	Symbol	Description	Protein Length	TMD (TMHMM)	TMD (UniProt)	Number of residues	TMD tendency (TMHMM+UniProt)	Kyte & Doolittle (TMHMM+UniProt)	ΔG_{app} (kcal mol^{-1})	GRAVY
NP_116136.1	Q96IX5	**USMG5**	Upregulated during skeletal muscle growth 5	58	TLTGRMNCVLATYGSIALIVLYF	TLTGRMNCVLATYGSIALIVLYF	23	12,9	29,1	0,893	1,265
NP_006668.1	O94966	**USP19**	Ubiquitin carboxyl-terminal hydrolase 19	1318	YFVLGTVAALVALVLNVFYPLVS	FVLGTVAALVALVLNVFYPLV	23	19,84	45,6	-0,165	1,983
NP_055046.1	P23763-1	**VAMP1**	Vesicle-associated membrane protein 1 isoform 1	118	IMLGAICAIIVVVIVIYFF	MMIMLGAICAIIVVVIVIYF	19	25,6	59,5	-2,608	3,132
NP_058439.1	P23763-2	**VAMP1**	Vesicle-associated membrane protein 1 isoform 3	116	KMMIMLGAICAIIVVVIVS	-	19	17,99	49,8	-0,405	2,621
NP_954740.1	P23763-3	**VAMP1**	Vesicle-associated membrane protein 1 isoform 2	117	CKMMIMLGAICAIIVVVIV	-	19	18,22	53,1	-0,568	2,795
NP_055047.2	P63027	**VAMP2**	Vesicle-associated membrane protein 2	116	MIILGVICAIILIIIVYF	MMIILGVICAIILIIIIVYF	18	26,08	59,3	-2,552	3,294
NP_004772.1	Q15836	**VAMP3**	Vesicle-associated membrane protein 3 (cellubrevin)	100	WAIGITVLVIFIIIIIVWV	MWAIGITVLVIFIIIIIVWVV	19	28,33	58,3	-3,346	3,068
NP_003753.2	O75379	**VAMP4**	Vesicle-associated membrane protein 4	141	IMALVAAILLLVIIILIVM	IKAIMALVAAILLLVIIILIV	19	29,24	67,8	-3,616	3,568
NP_006625.1	O95183	**VAMP5**	Vesicle-associated membrane protein 5 (myobrevin)	116	ICVGLVVVGVLLIILIVLLVVFL	VGLVVVGVLLIILIVLLVVFL	23	33,6	82,7	-4,882	3,596
NP_005629.1	P51809	**VAMP7**	Vesicle-associated membrane protein 7 isoform 1	220	TIIIIIVSIVFIYIIVSPLCGGF	LTIIIIIVSIVFIYIIVSPLC	23	24,88	59	-1,296	2,565
NP_003752.2	Q9BV40	**VAMP8**	Vesicle-associated membrane protein 8	100	IVLICVIVFIIILFIVLFATGAF	MIVLICVIVFIIILFIVLFAT	23	32,96	75,9	-5,341	3,300
NP_003565.4	Q9P0L0-2	**VAPA**	Vesicle-associated membrane protein-associated protein A isoform 1	294	SLLVVIAAIFIGFFLGKFI	LPSLLVVIAAIFIGFFLGKFI	19	20,57	47,1	-1,132	2,479
NP_004729.1	O95292	**VAPB**	Vesicle-associated membrane protein-associated protein B/C isoform 1	243	LLALVVLFFIVGVIIGKIA	RLLALVVLFFIVGVIIGKIAL	19	21,88	54,5	-1,729	2,868
NP_006287.2	Q86Y07-1	**VRK2**	Serine/threonine-protein kinase VRK2 isoform 1	508	VYYYRIIIPVLLMLVFLAL	VYYYRIIIPVLLMLVFLALFF	19	20,61	41,6	-2,140	2,189
NP_660207.2	Q96AJ9	**VTI1A**	Vesicle transport through interaction with t-SNAREs homolog 1A	217	LLVILGIIVVITILMAITF	ILLVILGIIVVITILMAITFS	19	26,41	59,5	-3,137	3,132
NP_006361.1	Q9UEU0	**VTI1B**	Vesicle transport through interaction with t-SNAREs 1B	232	LLLSIIILLELAILGGLVYYKFF	LSIIILLELAILGGLVYYKFF	23	21,95	48,4	-2,674	2,104
NP_001006623.1	Q9C0J8-2	**WDR33**	Pre-mRNA 3' end processing protein WDR33 isoform 2	326	TGFLFSFMINNVYTLFLFIIYCV	-	23	21,67	39,5	0,269	1,717
BAD12570.1	Q9P243-3	**ZFAT**	TR-ZFAT	846	PWVLIAFSSLCLYVGVSAAG	-	20	13,24	32,2	1,509	1,610
NP_006773.2	O95159	**ZFPL1**	Zinc finger protein-like 1	310	AGLLLLLGLLGFLALLALM	LLLLLGLLGFLALLALMSRLG	19	23,97	50,7	-3,022	2,668
NP_009086.4	P21754-3	**ZP3**	Zona pellucida sperm-binding protein 3 isoform 2	373	VVLLGVGLAVVVSLTLTAVILVL	-	23	25,6	65,3	-2,165	2,839

Table 17. Tail-anchored protein list. Modification and up to date list of TA-proteins based on (Kalbfleisch, Cambon, and Wattenberg 2007). Transmembrane tendency score according to Zhao and London (G. Zhao and London 2006), Kyte and Doolittle scores (Kyte and Doolittle 1982) and apparent free-energy (ΔG_{app}) (Hessa et al. 2007) were calculated for all the TA-proteins of the list. The transmembrane domain region was predicted using the TMHMM algorithm (Krogh et al. 2001) or UniProt prediction if the TMHMM was missing. The list was cleared of proteins predicted to have more than one TMD and/or predicted to have a signal peptide.

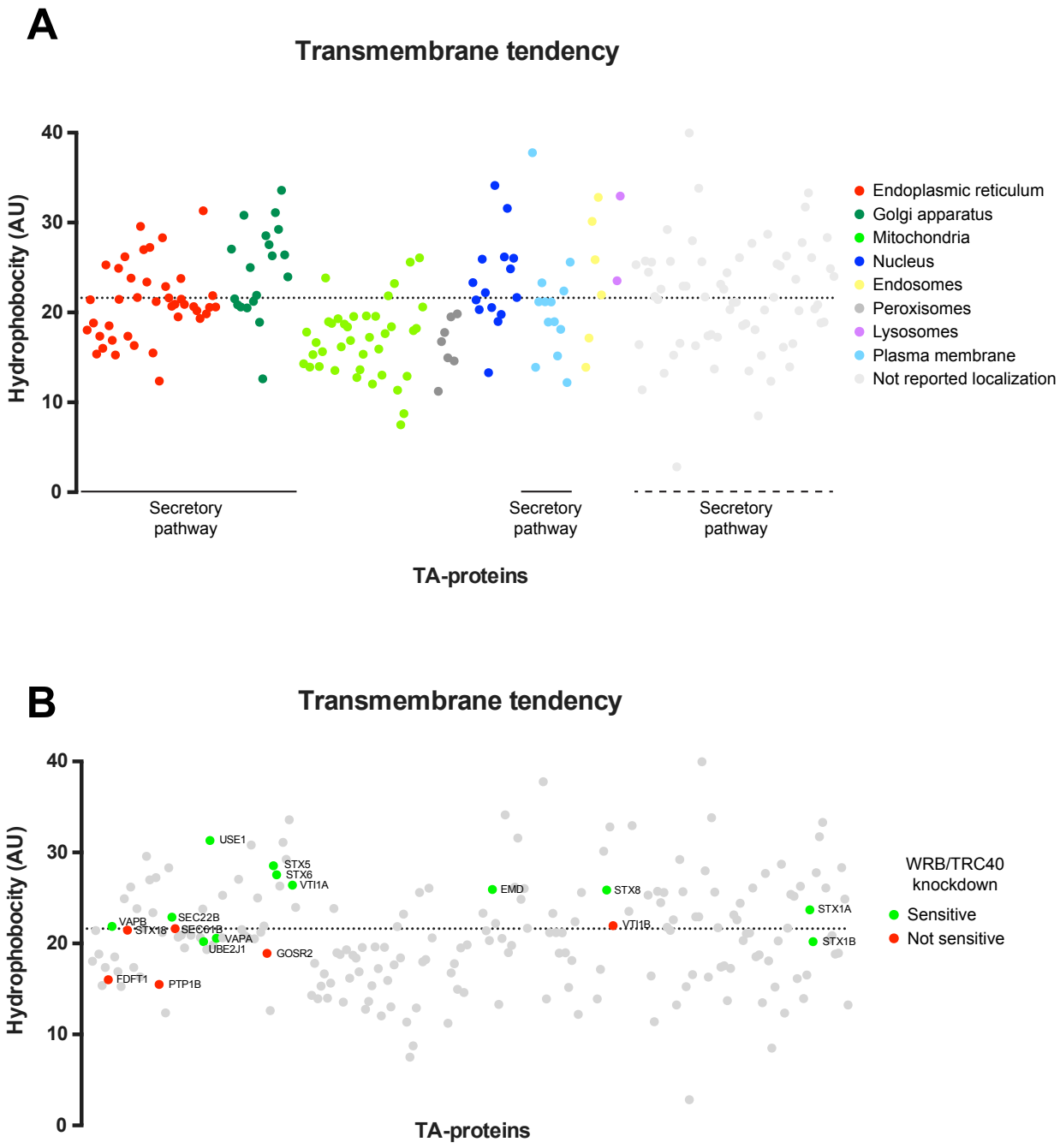

Figure 33. Transmembrane tendency of the TA-proteins used in this study. Dot-plots of the TMD hydrophobicity score according to the transmembrane tendency scale (G. Zhao and London 2006) for all the TA-proteins shown in **Table 17. (A)** The TA-proteins TMD were clustered by subcellular localization. The transmembrane domain region was predicted using the TMHMM algorithm (Krogh et al. 2001) or UniProt prediction if TMHMM prediction was missing. **(B)** TA-proteins affected due to the knockdown of TRC40 and WRB seen in **Fig. 26-32** using as a base the dot-plot of (A). TA-proteins sensitive to the knockdown are highlighted in green and the ones not affected are colored in red. The dotted line in the dot-plot represents the Sec61β TMD hydrophobicity score, marking the approximate overlap between the EMC pathway and the TRC pathway as proposed in a recent paper (Guna et al. 2018). Subsets of TA-proteins of the secretory pathway is highlighted. Solid line indicates that all belong to the secretory pathway, dashed line indicates that some of them belong to.

moderately hydrophobic TMD. However, three TA-proteins (UBE2J1, VAPA and Stx1B) presented a TMD with similar hydrophobicity to those not affected, VAPB and Sec22b being very similar. After plotting the TMD hydrophobicity scores according to this scale there was no a clear distinction between TA-proteins affected by the combined knockdown and those that were unaffected. Broadly, the more hydrophobic the TMD was the more TRC-dependence was observed.

Second, I plotted TMD hydrophobicity scores according to the Kyte and Doolittle scale (Kyte and Doolittle 1982) and clustered the TA-proteins according to their reported subcellular localization (**Fig. 34A**). The overall outcome was similar but, in this case, the TMD of ER TA-proteins had a more similar hydrophobicity to the mitochondrial ones. Regarding the TA-proteins affected, all but one (Sec22b) showed more hydrophobic TMDs than Sec61β. Besides, all but one (Vti1b) of the non-affected TA-proteins had less hydrophobic TMDs than Sec61β (**Fig. 34B**). This scale showed a better separation between the two groups where the proteins whose TMD presented a similar hydrophobicity to the one of Sec61β were borderline between being affected or unaffected.

Third, I used the so-called grand average of hydropathicity (GRAVY) that is based on the Kyte and Doolittle scores averaged by the length of the TMD giving a relative hydrophobicity score and clustered the TA-proteins according to subcellular localization (**Fig. 35A**). The dot-plot was very similar to the one shown for the transmembrane tendency (**Fig. 33A**) where the ER, Golgi and nucleus TA-proteins presented a more hydrophobic TMD whereas mitochondrial TA-proteins had a less hydrophobic one. The analysis of the TA-protein TMD hydrophobicity showed two distinct populations with the ones affected by a combined WRB/TRC40 knockdown showing more hydrophobic TMDs and the unaffected ones coming out with scores similar to the TMD of Sec61β and lower. However, there was no complete separation since Sec22b came out close to the TMD of TA-proteins that remained unchanged such as Sec61β, GOSR2 and Vti1b (**Fig. 35B**).

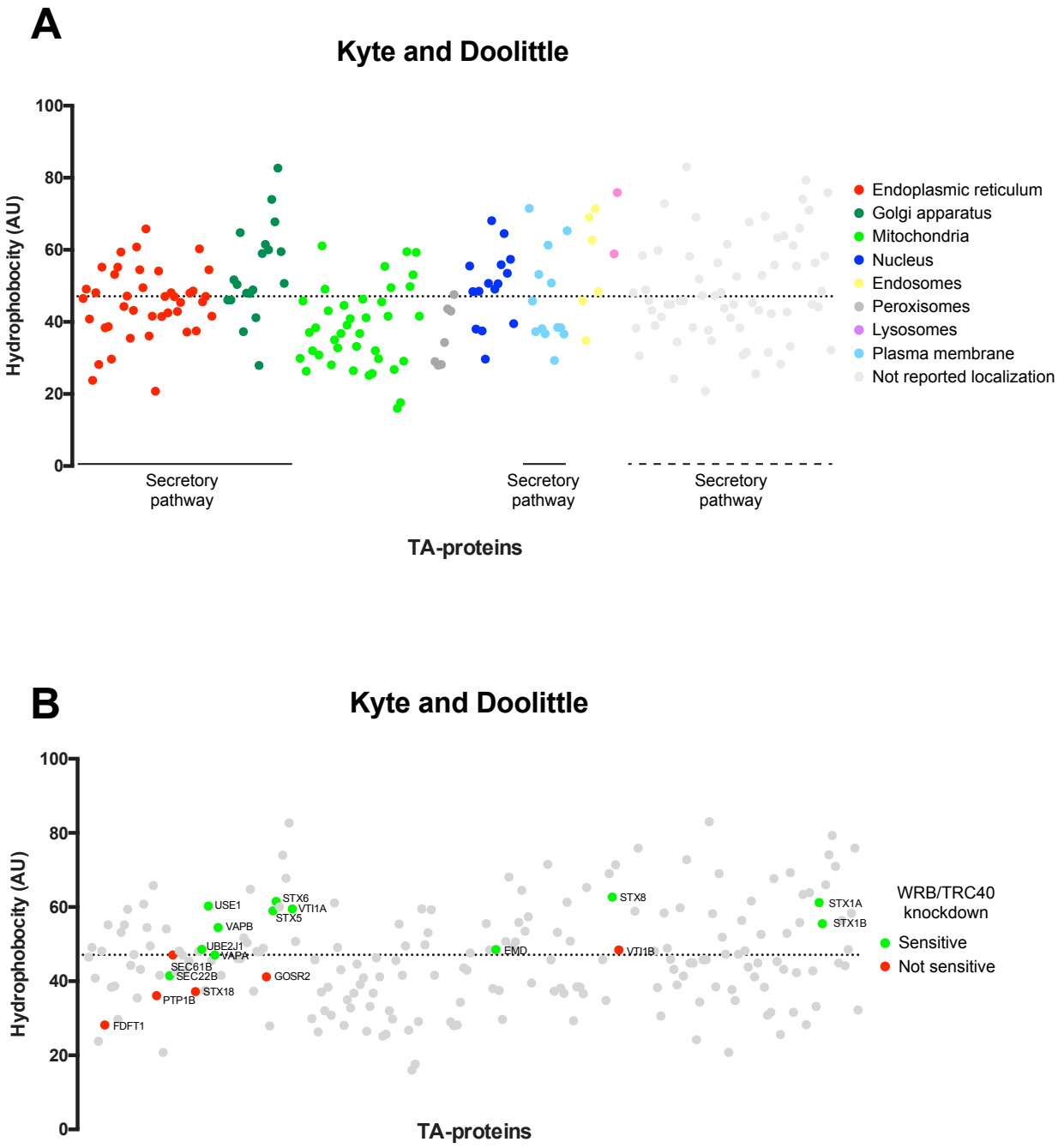

Figure 34. Transmembrane domain hydrophobicity of the TA-proteins used in this study. Dot-plots of the TMD hydrophobicity score according to the hydrophobicity scale developed by (Kyte and Doolittle 1982) for all the TA-proteins shown in **Table 17. (A)** The TA-proteins TMD were clustered by subcellular localization. The transmembrane domain region was predicted using the TMHMM algorithm (Krogh et al. 2001) or UniProt prediction if TMHMM prediction was missing. **(B)** TA-proteins affected due to the knockdown of TRC40 and WRB seen in **Fig. 26-32** using as a base the dot-plot of (A). TA-proteins sensitive to the knockdown are highlighted in green and the ones not affected are colored in red. The dotted line in the dot-plot represents the Sec61β TMD hydrophobicity score, marking the approximate overlap between the EMC pathway and the TRC pathway as proposed in a recent paper (Guna et al. 2018). Subsets of TA-proteins of the secretory pathway is highlighted. Solid line indicates that all belong to the secretory pathway, dashed line indicates that some of them belong to.

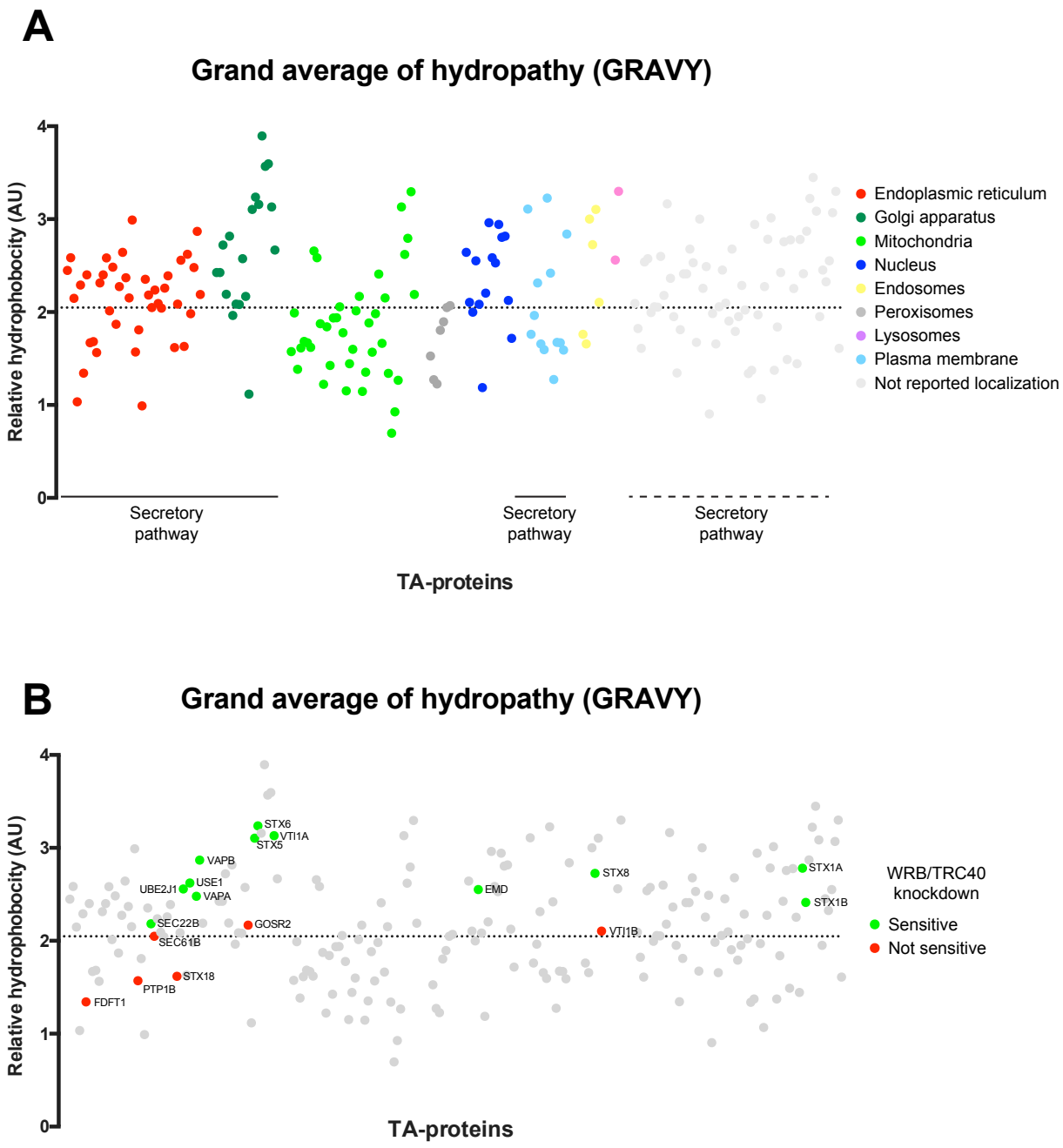

Figure 35. Transmembrane domain relative hydrophobicity of the TA-proteins used in this study. Dot-plots of the TMD hydrophobicity score according to the hydrophobicity scale developed by (Kyte and Doolittle 1982) divided by the length of the TMD, for obtaining the GRAVY score, for all the TA-proteins shown in **Table 17. (A)** The TA-proteins TMD were clustered by subcellular localization. The transmembrane domain region was predicted using the TMHMM algorithm (Krogh et al. 2001) or UniProt prediction if TMHMM prediction was missing. **(B)** TA-proteins affected due to the knockdown of TRC40 and WRB seen in **Fig. 26-32** using as a base the dot-plot of (A). TA-proteins sensitive to the knockdown are highlighted in green and the ones not affected are colored in red. The dotted line in the dot-plot represents the Sec61β TMD hydrophobicity score, marking the approximate overlap between the EMC pathway and the TRC pathway as proposed in a recent paper (Guna et al. 2018). Subsets of TA-proteins of the secretory pathway is highlighted. Solid line indicates that all belong to the secretory pathway, dashed line indicates that some of them belong to.

Finally, I used another method for calculating the apparent free-energy (ΔG_{app}) of the TA-protein TMDs (Hessa et al. 2007). The lower the ΔG_{app} of a TMD is, the more it mirrors the physical properties of the membrane and vice versa. I plotted the results and grouped them by subcellular localization. The TMD of ER-, Golgi- and nucleus-resident TA-proteins had a lower apparent free-energy whereas the mitochondrial and peroxisomal ones presented higher values (**Fig. 36A**). In general, the majority of the TA-proteins affected by combined WRB/TRC40 down-regulation showed very low ΔG_{app} values in contrast to higher values for those not affected. However, two of the unaffected TA-proteins had low ΔG_{app} values and appeared mixed with the affected ones (**Fig. 36B**). Even if a general tendency was present the two populations were not clearly separated.

In summary, most of the TA-protein tested upon knockdown of TRC pathway components showed a strong reduction in response to WRB/TRC40 knockdown. In addition, some displayed an increase upon BAG6 knockdown. Interestingly, the TRC pathway components were destabilized in the absence of other proteins of the pathway. Using the GRAVY score of the TMDs of TA-proteins tested upon combined WRB/TRC40 knockdown, a clear separation between affected and unaffected TA-proteins was observed. These findings shed light on some aspects of how the multiple targeting pathways cater to different TA-proteins.

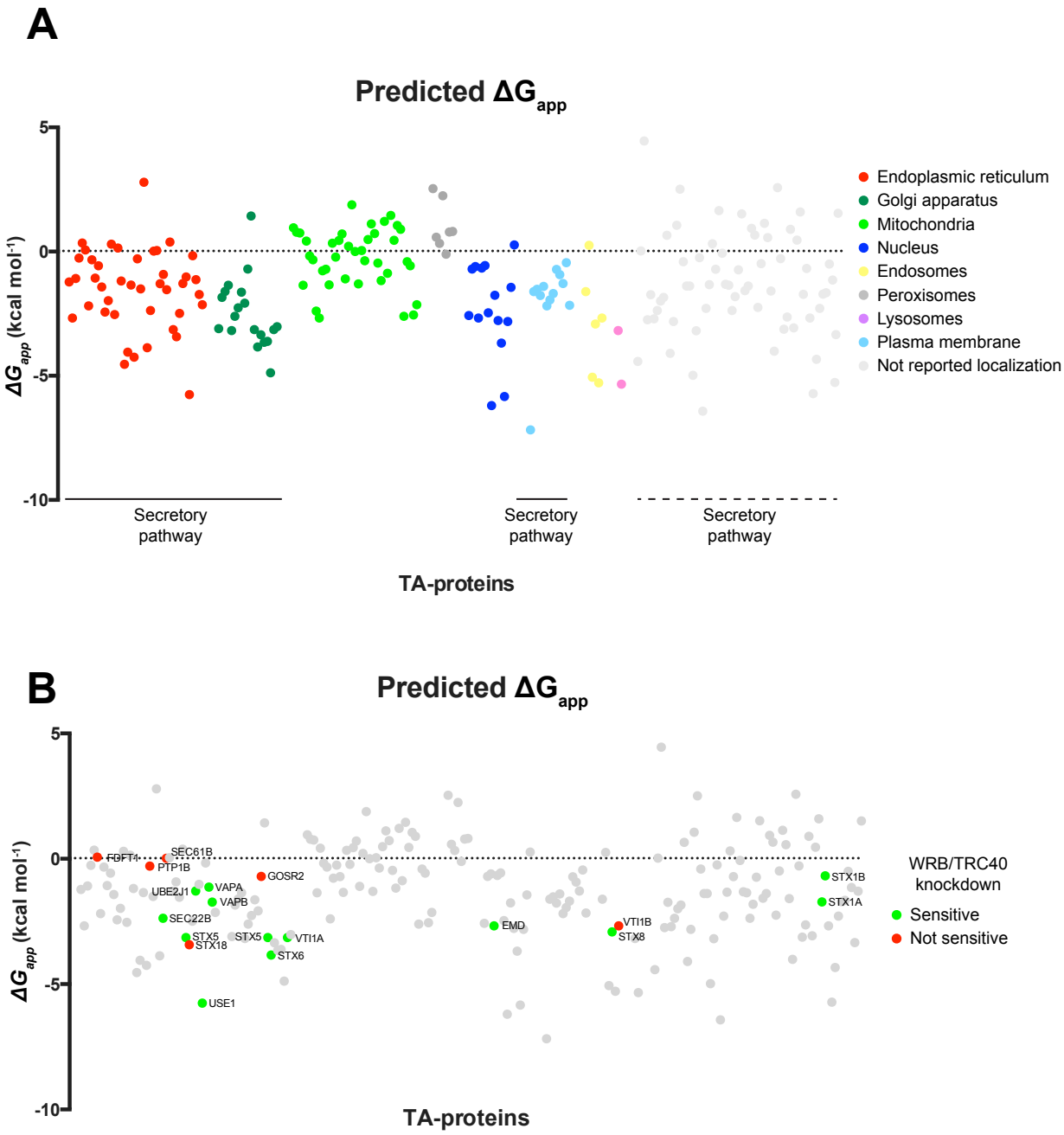

Figure 36. Transmembrane domain apparent free-energy (ΔG_{app}) of the TA-proteins used in this study. Dot-plots of the apparent free-energy (Hessa et al. 2007) of the TMD from all the TA-proteins shown in **Table 17** calculated via the ΔG prediction server (http://dgpred.cbr.su.se). **(A)** The TA-proteins TMD were clustered by subcellular localization. The transmembrane domain region was predicted using the TMHMM algorithm (Krogh et al. 2001) or UniProt prediction if TMHMM prediction was missing. **(B)** TA-proteins affected due to the knockdown of TRC40 and WRB seen in **Fig. 26-32** using as a base the dot-plot of (A). TA-proteins sensitive to the knockdown are highlighted in green and the ones not affected are colored in red. The dotted line in the dot-plot represents the Sec61β TMD hydrophobicity score, marking the approximate overlap between the EMC pathway and the TRC pathway as proposed in a recent paper (Guna et al. 2018). Subsets of TA-proteins of the secretory pathway is highlighted. Solid line indicates that all belong to the secretory pathway, dashed line indicates that some of them belong to.

3.3. The fate of BAG6 is tightly coupled to the TRC pathway

BAG6 is the central component of the pre-targeting complex of the TRC pathway (Leznicki et al. 2010; Mariappan et al. 2010). It is the scaffolding protein in the heterotrimeric BAG6 complex (Mock et al. 2015; Mock et al. 2017), also including TRC35 and UBL4A, that facilitates the hand off of the TA-protein to TRC40.

I previously showed the influence of the WRB/TRC40 knockdown on the steady-state levels of BAG6 in HeLa cells. Furthermore, I also showed that the stability of TRC-pathway components depends on multiple components of the pathway: WRB or CAML knockdown mutually decreases the respective steady-state protein levels and TRC40 knockdown also decreases the protein levels of the heterodimeric receptor, WRB and CAML. The relationship between TRC40 and BAG6 has not been extensively studied before. Thus, I set out to explore the effects of TRC40 on the key player of the pre-targeting complex, BAG6.

3.3.1. The absence of TRC40 affects the nuclear shuttling of BAG6

It has been reported that BAG6 changes its subcellular localization when TRC35 or UBL4A, components of the heterotrimeric BAG6 complex, are absent (Q. Wang et al. 2011; Krenciute et al. 2013). Furthermore, BAG6 is involved in the quality control of mislocalized secretory and membrane proteins (MLPs) (Minami et al. 2010; Hessa et al. 2011; Leznicki and High 2012; Leznicki et al. 2013; Wunderley et al. 2014; Rodrigo-Brenni, Gutierrez, and Hegde 2014) and chaperoning translocated ERAD-substrates (Q. Wang et al. 2011). TRC40 has also been related to different degradation processes since it has been reported to interact with BAG6 and ubiquitylated proteins (Baron et al. 2014). Moreover, the knockdown of either TRC40 or BAG6 leads to the accumulation of ubiquitinated proteins (Q. Wang et al. 2011; Akahane et al. 2013) and to defects in the assembly of the proteasome (Akahane et al. 2013; Sahara et al. 2014).

I tested for IF the specificity of custom-made BAG6 antibodies (**Fig. 37A**) as well as for Western blot (**Fig. 37B**) in cells transfected with a validated siRNA against BAG6. Then, I investigated the subcellular localization of BAG6 in the absence of TRC40. In order to monitor it, I used specific siRNA against TRC40 in HeLa cells. Following silencing, I performed an indirect immunofluorescence with an anti-BAG6 antibody to monitor the subcellular localization of BAG6. Strikingly, BAG6 changed its localization and showed a nuclear accumulation upon the loss of TRC40 (**Fig. 38A**). Quantification (**Fig. 38B**) allowed for an assessment of the statistical significance of this effect. Knockdown of TRC40 did not affect the steady-state levels of BAG6 (**Fig. 38C**) in agreement with what I found previously (**Fig. 26A**). Hence, absence of TRC40 alters the nucleo-cytoplasmic distribution of BAG6 without altering protein levels at the steady-state.

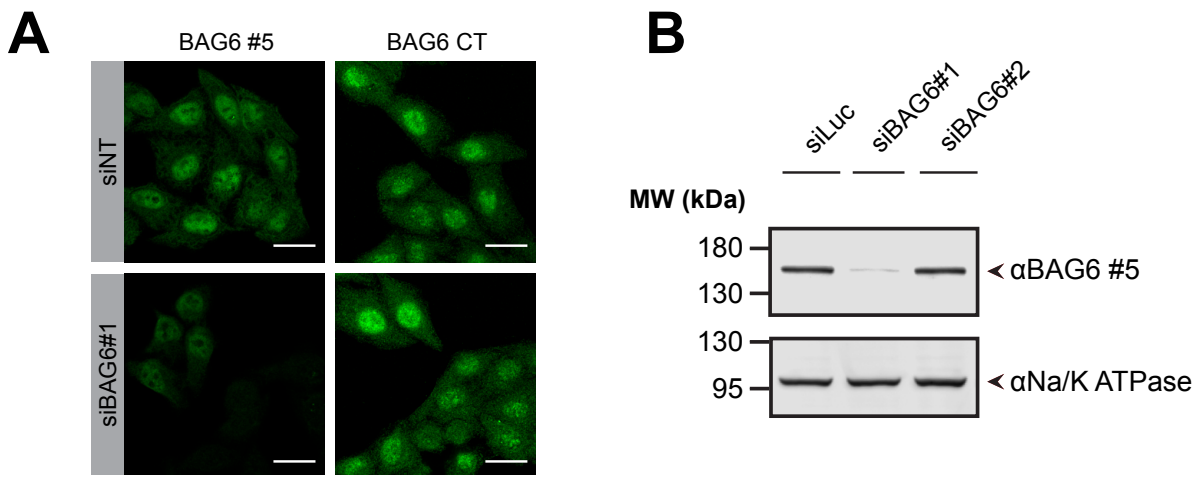

Figure 37. Validation of the BAG6 antibodies for immunofluorescence and Western blot. (A) Validation of the BAG6 antibody used for immunofluorescence in HeLa cells (**Fig. 38A, Fig. 38B**) by siRNA-mediated down-regulation of BAG6. **(B)** Two different siRNAs for BAG6 were tested. Western blot was performed for the indicated proteins. Scale bars: 20 μm.

3.3.2. The cytoplasmic localization of BAG6 can be rescued by TRC40 nucleotide-binding variants

BAG6 localized to the nucleus in the absence of TRC40. I was interested in testing which domain of TRC40 was involved in keeping BAG6 cytoplasmic. For that purpose, I knocked-down TRC40 using siRNA in HeLa cells followed by transfection of siTRC40ins constructs carrying different mutations affecting the functional cycle of

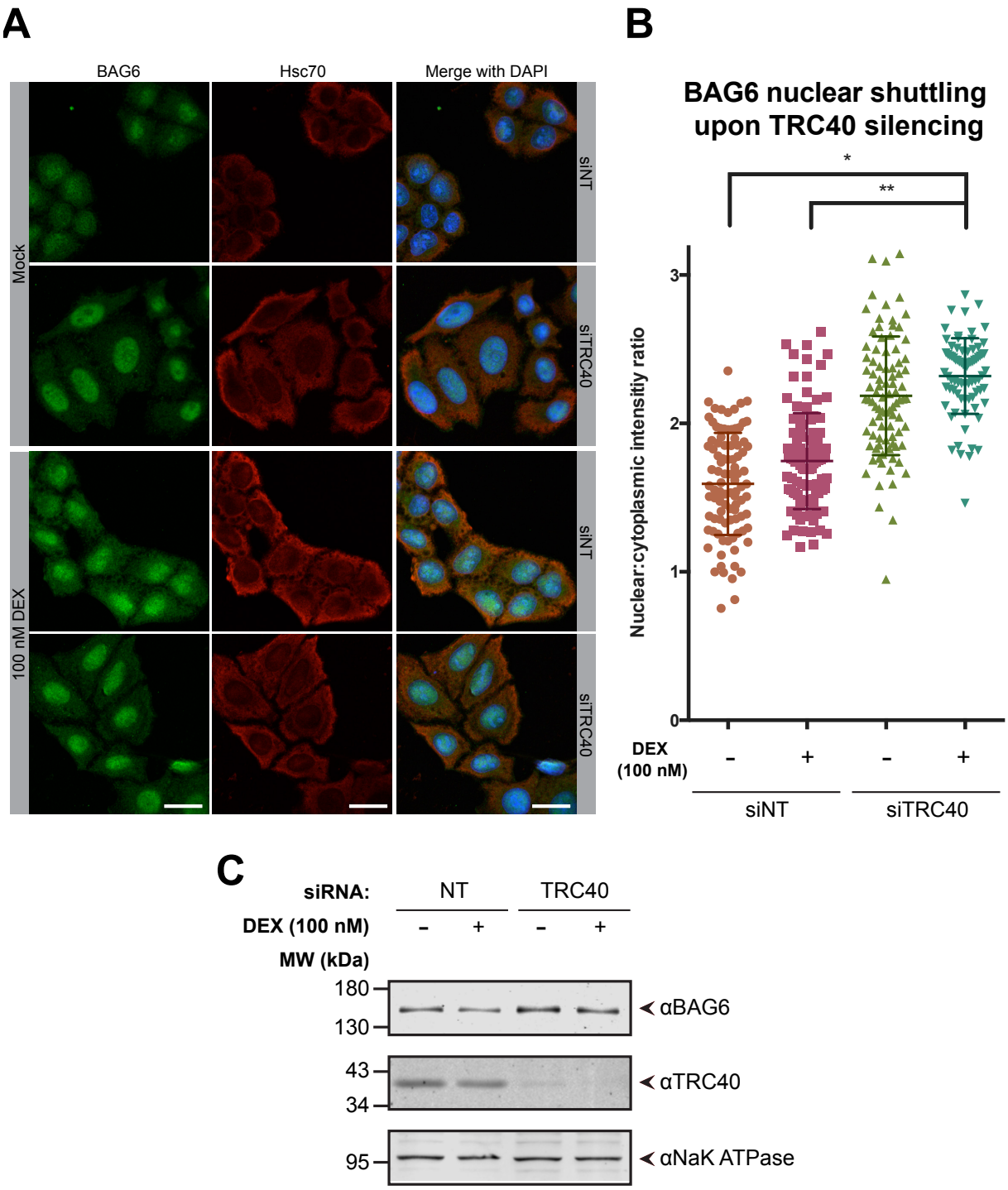

Figure 38. Down-regulation of TRC40 affects the nuclear shuttling of BAG6 in HeLa cells. (A) Immunofluorescence detection of BAG6 upon silencing of TRC40 in HeLa cells. Images of BAG6 and Hsc70 stained by indirect immunofluorescence are shown. Cells were stimulated with 100 nM DEX, a glucocorticoid receptor agonist. **(B)** Scatter plot representing the nuclear-cytoplasmic ratio of BAG6 upon silencing of TRC40. Each dot represents the fluorescence intensity of one cell. n= 78-104 cells are represented. The graphs show the mean and the error bars represent the standard deviation. * indicates a p-value < 0.05; ** a p-value < 0.05. Three biological replicates were analyzed. **(C)** Steady-state levels of BAG6 upon knockdown of TRC40. Western blot was performed detecting the indicated proteins. Scale bars: 20 µm.

TRC40. These constructs were insensitive to the TRC40 siRNA. Specifically, I transfected the following TRC40 constructs: $TRC40_{wt}$, $TRC40_{G46R}$ that is a mutant in the Walker A motif that disrupts nucleotide binding (Shen et al. 2003; Baron et al. 2014), $TRC40_{D74E}$ a mutant in the Switch I domain whose ATPase activity is strongly reduced, $TRC40_{I193D}$ that is a mutant that impairs TA-protein binding (Mateja et al. 2009) and $TRC40_{CC246,248SS}$ that is mutant of the second CXC motif in TRC40 conserved in yeast Get3. These cysteines are believed to be connected to the redox-regulated chaperone activity of Get3 (Voth et al. 2014).

$TRC40_{wt}$ rescued the BAG6 nucleo-cytoplasmic distribution (**Fig. 39A**). The presence of the $TRC40_{wt}$ shows BAG6 distributed more to the cytoplasm and less to the nucleus compared to the TRC40-knockdown cells. The rest of the TRC40 variants were able to restore the subcellular distribution of BAG6 with the exception of $TRC40_{G46R}$ (**Fig. 39A**). Quantification of the results is shown in **Fig. 39B**. Therefore, nucleotide-binding of TRC40 appears to be relevant to the subcellular distribution of BAG6 whereas strong reductions in the ATPase activity or in TA-protein binding were compatible with keeping a proportion of BAG6 cytoplasmic.

3.3.3. BAG6 steady-state levels are reduced in WRB knockout cardiomyocytes

A mouse line with loxP sites integrated into the genome at positions flaking exon 3 of the Wrb gene can be used to create tissue-specific WRB-knockout mouse models (Rivera-Monroy et al. 2016; Vogl et al. 2016). A cardiomyocyte-specific WRB knockout model enabled the characterization of the fate of a subset of TA-proteins and also the characterization of the steady-state levels of some of the proteins of the TRC pathway (Rivera-Monroy et al. 2016). Nevertheless, the characterization of BAG6 was still missing. I was able to show that the combined down-regulation of WRB/TRC40 in HeLa cells decreased the steady-state levels of BAG6 (**Fig. 26A**, **Fig. 27C**). Following up on this result, I tested whether BAG6 was affected in WRB-knockout isolated cardiomyocytes. Thus, I isolated cardiomyocytes from wt and knockout mice and checked the steady-state protein levels by Western blot. After analyzing the

corresponding blots, I found that BAG6 was strongly reduced at the steady-state level in WRB knockout isolated cardiomyocytes (**Fig. 40A**, **Fig. 40B**). The reduction was around 70% (**Fig. 40B**), which was a very similar decrease compared to the result upon WRB/TRC40 knockdown in HeLa cells (**Fig. 27C**).

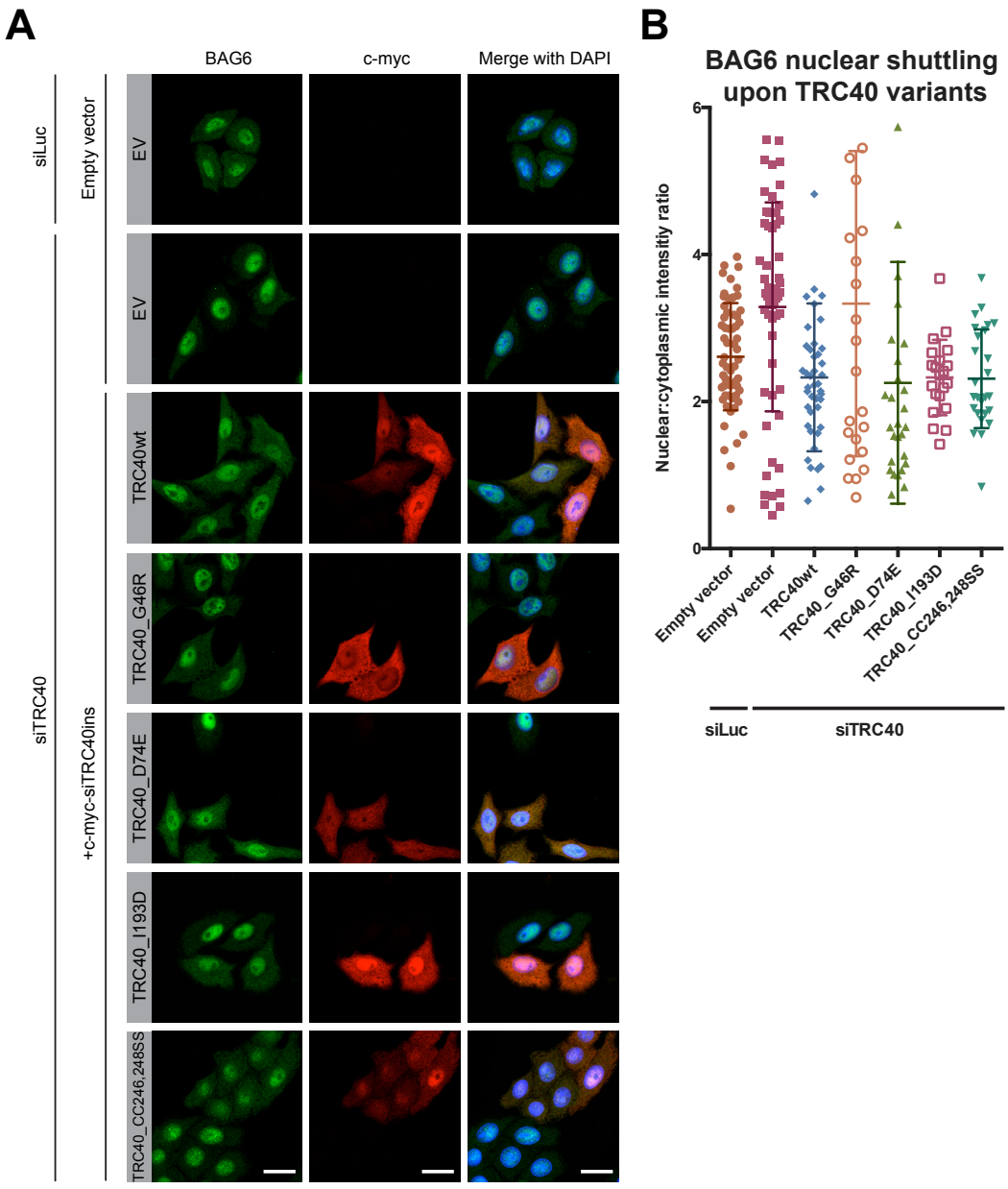

Figure 39. Most variants of TRC40 can rescue the subcellular localization of BAG6 upon down-regulation of TRC40. (A) Immunofluorescence of BAG6 upon silencing of TRC40 and concomitant expression of different TRC40 variants in HeLa cells. Images of BAG6 and cmyc-TRC40 stained by indirect immunofluorescence are shown. **(B)** Quantification of immunofluorescent signal of BAG6 upon silencing of TRC40 and transfection of different TRC40 variants in HeLa cells. Images of BAG6 and cmyc-TRC40 stained by indirect immunofluorescence are shown. n= 22-60 cells. The graphs show the mean and the error bars represent the standard deviation. Two biological replicates were analyzed. Scale bars: 20 µm.

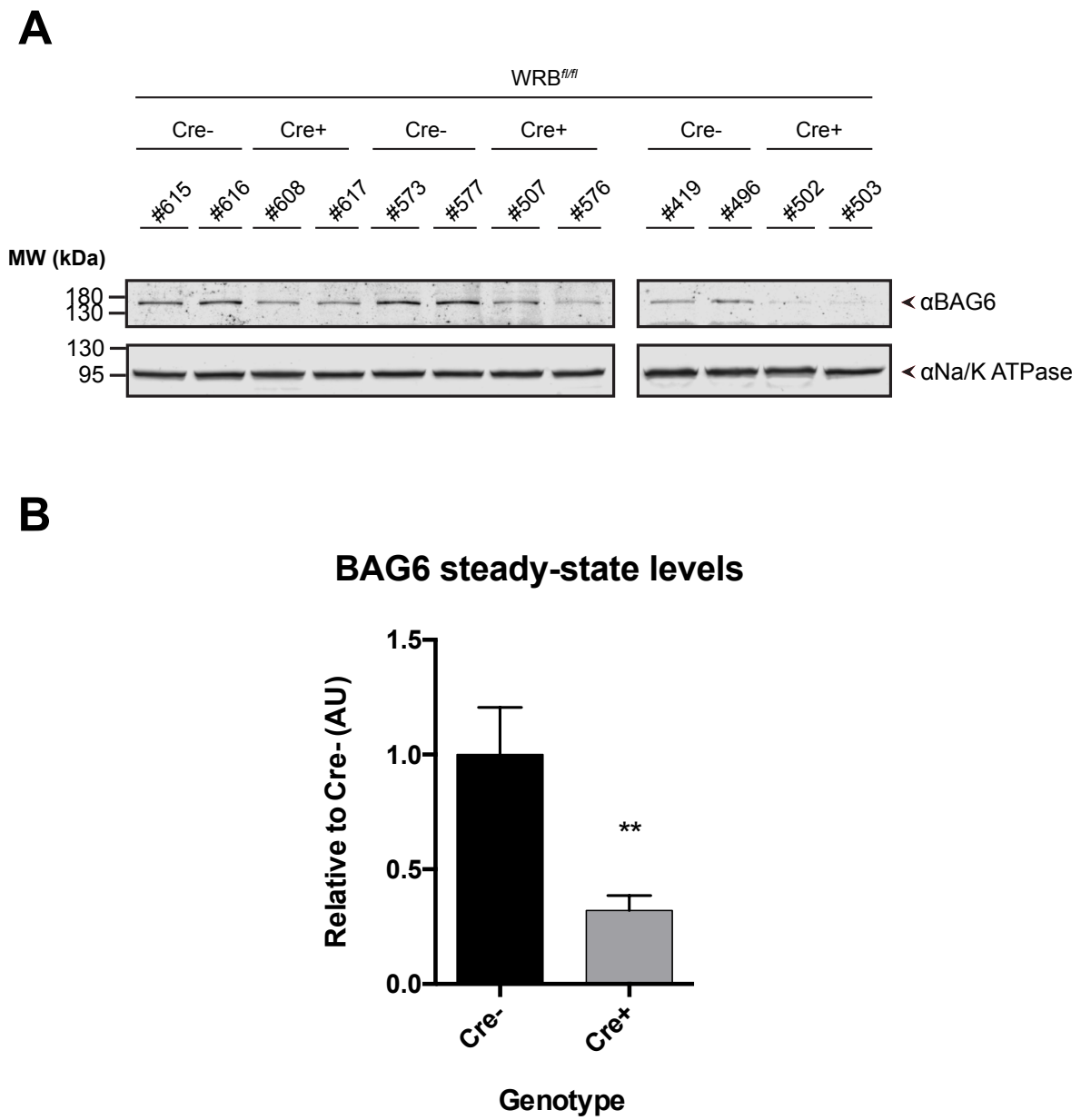

Figure 40. Protein steady-state levels of BAG6 are reduced in WRB-knockout cardiomyocytes. **(A)** BAG6 was analyzed by Western blot in WRB-knockout isolated cardiomyocytes. Cellular lysates were analyzed by Western blot detecting BAG6. **(B)** Quantification of BAG6 steady-state levels from blots in (A). Normalized against Na/K ATPase and then relative to the Cre- levels. Seven biological replicates were analyzed. The graphs show the mean and the error bars represent standard error of the mean. ** indicates a p-value < 0.05.

3.4. Investigation of a putative redox switch in TRC40

Yeast Get3 functions, apart from TA-protein targeting, as a redox-regulated chaperone (Voth et al. 2014). Get3 shares features with Hsp33, a bacterial redox-regulated chaperone (Jakob et al. 1999; Kumsta and Jakob 2009), such as a CXC-X_n-CXXC motif that is the key of the redox switch of Hsp33 (Jakob et al. 1999; Voth et al. 2014). Upon oxidation *in vitro*, Get3 undergoes structural rearrangements that bury the TA-binding groove, release the Zn^{2+} ion in the dimer interface and turn Get3 into an ATP-independent holdase. This conformational change is reversible once reducing conditions are restored and Zn^{2+} is present in the medium. Furthermore, the ATPase activity of Get3 is drastically reduced upon oxidation (Voth et al. 2014). Accordingly, Get3 *in vivo* colocalizes in foci with diverse chaperones under ATP-deprived conditions. Moreover, Get3 colocalizes with aggregates in glucose-deprived conditions (Powis et al. 2013). Almost nothing is known about the redox behavior of TRC40, which shares homology with yeast Get3. Another metazoan homolog plays a role in the sensitivity to oxidative agents like cisplatin and arsenite in *C. elegans* (Hemmingsson, Nöjd, et al. 2009; Hemmingsson et al. 2010). My aim was to further elucidate the redox behavior of TRC40 *in vitro* and explore the behavior of TRC40 under oxidative conditions *in vivo* in human cell lines.

3.4.1. CXC and CXXC are conserved from Get3 to TRC40

In order to investigate whether the CXC-X_n-CXXC motif present in yeast Get3 was conserved in human TRC40, I aligned the two protein sequences. Get3 has seven cysteines in its sequence whereas TRC40 has eight. Five out of the seven are conserved from yeast Get3 to human TRC40 (in yellow). Four of these are present in the CXC-X_n-CXXC motif confirming the conservation of this motif (**Fig. 41A**). TRC40 has an extra CXC motif (C_{53}-X-C_{55}) close to the N-terminus due to the appearance of a new cysteine (C_{53}) not present in yeast Get3 (C_{36} from Get3 is aligned to C_{55} in TRC40). The presence of an extra CXC in TRC40 could increase cysteine reactivity.

C_{86} and C_{317} from yeast Get3 are not conserved in TRC40. Three non-conserved cysteines are present in TRC40 (in red): the aforementioned C_{53} plus C_{205} and C_{268} (**Fig. 41A**). The conserved domains between yeast Get3 and TRC40 are highlighted in **Fig. 6, Fig. 12A**.

A

Figure 41. Cysteine conservation after Get3 and TRC40 alignment. (A) Alignment of TRC40 and Get3 in different species indicating conserved (yellow) and non-conserved (red) cysteines. The sequences were aligned with Clustal Omega (https://www.ebi.ac.uk/Tools/msa/clustalo/). The UniProt accession numbers have been provided in parentheses.

3.4.2. Oxidation decreased TRC40 ATPase activity

First, I purified recombinant TRC40 from *E. coli*. I purified a His-MBP-tagged version of TRC40 and cleaved the tag to obtain an untagged-TRC40 (**Fig. 42A**).

To test the ATPase activity of purified TRC40 I applied a protocol to ensure control of the redox state. First, TRC40 was subjected to reduction and then to an oxidation step to fully oxidize TRC40. Next, I performed a NADH-coupled ATPase activity assay to elucidate the relative ATPase activity of the oxidized TRC40. Oxidation of TRC40 resulted in a 50% reduction in ATPase activity compared to reduced TRC40 (**Fig. 42B**).

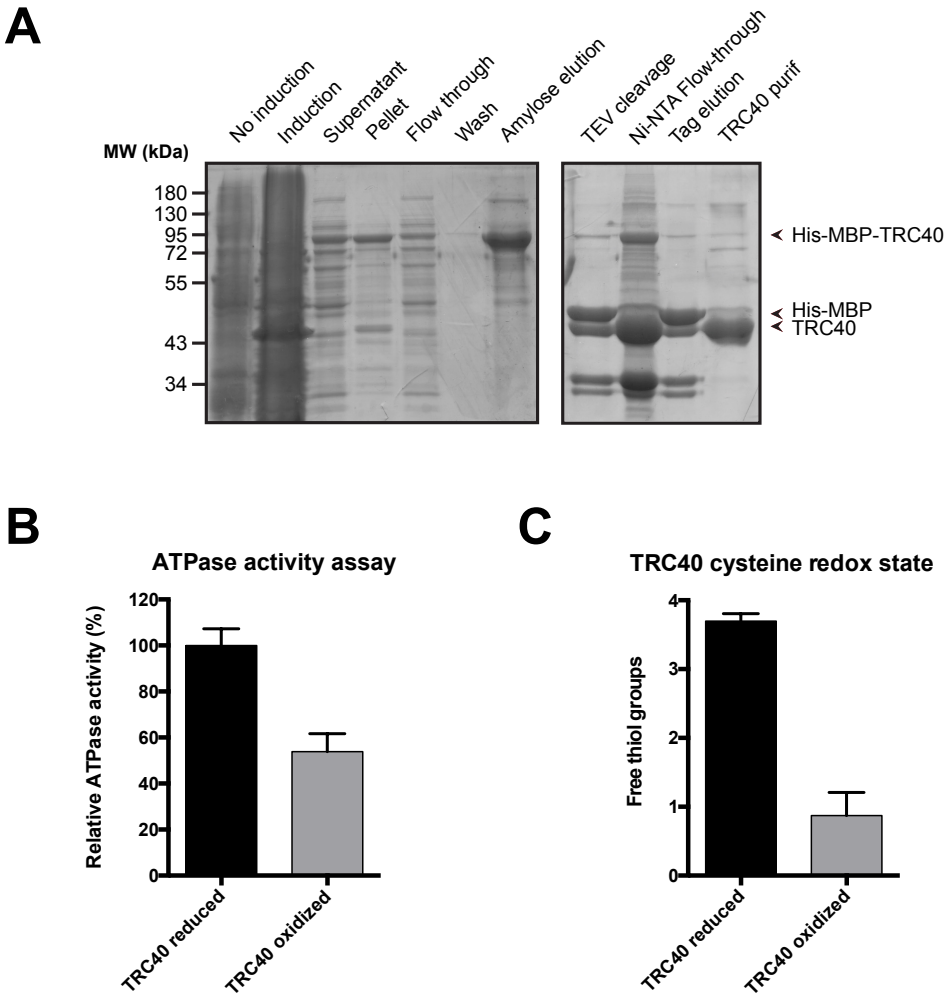

Figure 42. TRC40 shows similar *in vitro* redox behavior as yeast Get3. (A) Coomassie-stained SDS-PAGE gel coming from the purification of His-MBP-TRC40. **(B)** Effect of oxidation on the ATPase activity of TRC40. The reduced protein treated with 5 mM DTT (TRC40 reduced) was compared to the oxidized one treated with 2mM H_2O_2 and 50 µM Cu^{2+} (TRC40 oxidized) at 37°C. ATPase activity is normalized to the reduced state. **(C)** Redox state of TRC40 cysteines determining how many thiol groups are available before and after oxidation using the Ellman's assay. At least three to four biological replicates were analyzed. The graphs show the mean and the error bars represent standard error of the mean.

3.4.3. Recombinant TRC40 is not fully reduced after *in vitro* redox treatment

To estimate the redox state of TRC40, I performed an Ellman's assay to determine the free thiols (reduced cysteine thiols) in the recombinant reduced or oxidized TRC40. The reduced form of TRC40 contained four reduced cysteines

according to the Ellman's assay, whereas the oxidized form of TRC40 contained one. Hence, three cysteines changed oxidation status between the two forms (**Fig. 42C**). The primary sequence of TRC40 contains eight cysteines (**Fig. 41A**), but only four of them could be detected in the reduced form after reduction of the protein (**Fig. 42C**) suggesting that this reduction treatment resulted in a partially oxidized instead of a fully reduced protein.

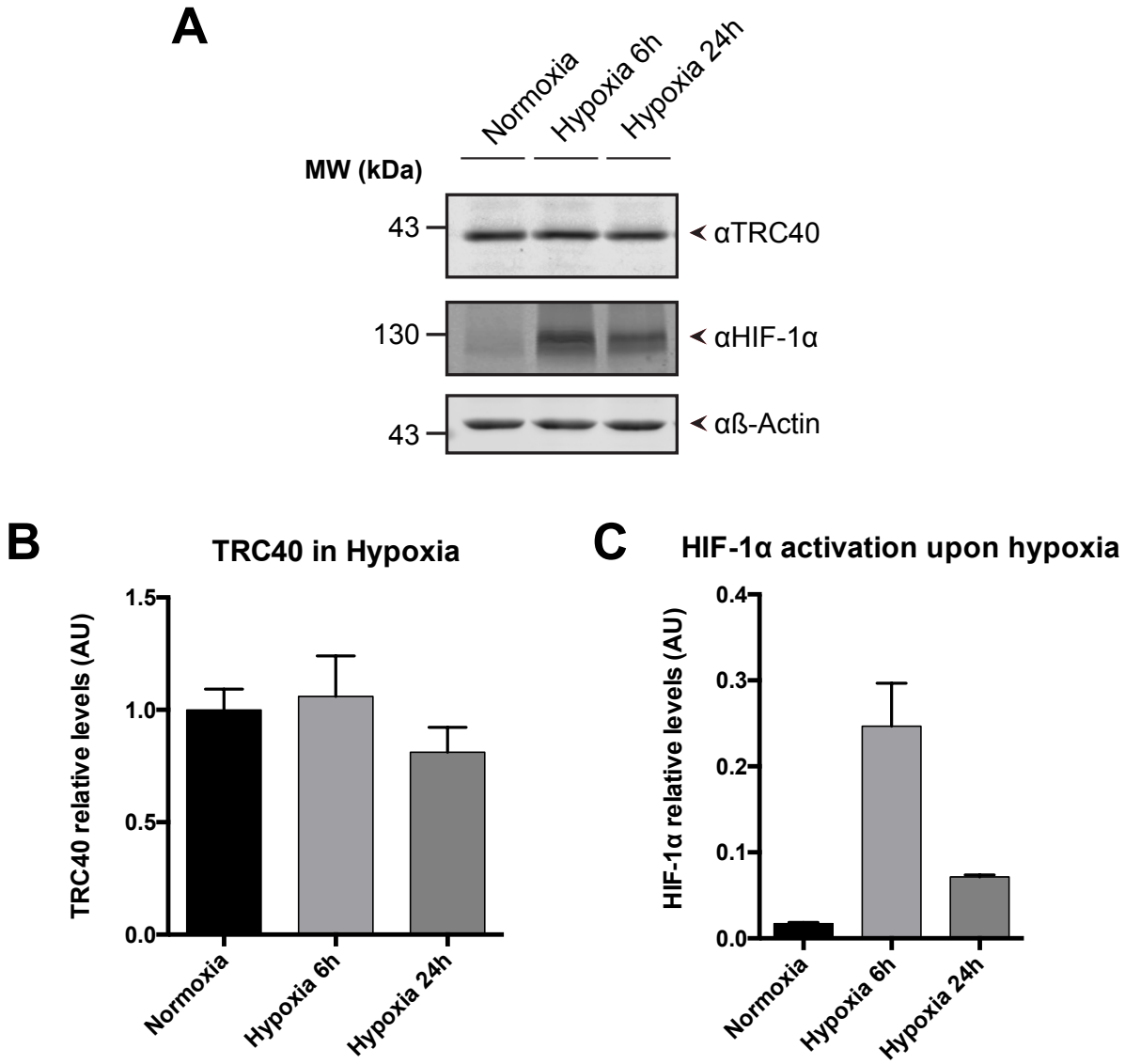

Figure 43. TRC40 steady-state levels are not altered upon hypoxia. (A) TRC40 levels in conditions of normoxia, short and long hypoxia (94% N_2, 5% CO_2 and 1% O_2). HIF-1 alpha was used as a positive marker for induced-hypoxia. Cellular lysates were analyzed for Western blot for TRC40. **(B)** Quantification of the TRC40 signal intensities for the different oxygen conditions from the blots performed in (A). **(C)** Quantification of the HIF-1 alpha signal intensities for the different oxygen conditions from the blots performed in (A). Four biological replicates were analyzed. The graphs show the mean and the error bars represent standard error of the mean.

3.4.4. TRC40 steady-state levels remained unaltered upon hypoxia

I set out to assess whether TRC40 was oxidized by the high levels of oxygen under standard cell culture conditions. Therefore, I analyzed HeLa cells that underwent a hypoxic treatment (94% N_2, 5% CO_2 and 1% O_2) for 6 h or 24 h. Western-blot analysis revealed no detectable changes of the TRC40 steady-state protein levels (**Fig. 43A, Fig. 43B**).

3.5. Exploring the role of TRC40 in the steroid hormone-receptors chaperoning process

Get3 was characterized as a redox-regulated chaperone (Voth et al. 2014) and it has been found to colocalize in foci with aggregates and chaperones (Powis et al. 2013). Based on the high degree of conservation and the presence of the CXC-X_n-CXXC motif I hypothesized that TRC40 may also act as a chaperone holdase upon oxidation. Yet, no physiological chaperone clients are known for TRC40.

Recently, the cochaperone SGTA was proposed to be part of the cytosolic chaperoning of steroid-hormone receptors (SRs) (Paul et al. 2014). SGTA collaborates with the early maturation steps of the SRs and negatively regulates the activity of some of them, such as the glucocorticoid receptor (GR), androgen receptor and progesterone receptor (Paul et al. 2014). Moreover, the handover of a TA-protein from Sgt2, yeast homolog of SGTA, to Get3 seems to be isoenergetic, suggesting that the relative preference for hydrophobic substrates is very similar between Get3 and Sgt2 (Rao et al. 2016). Additionally, Sgt2 interacts with the same chaperones that Get3 was found to colocalize with (F. Wang et al. 2010; Powis et al. 2013). Based on these considerations, I hypothesized that the SRs could be potential TRC40 chaperone substrates.

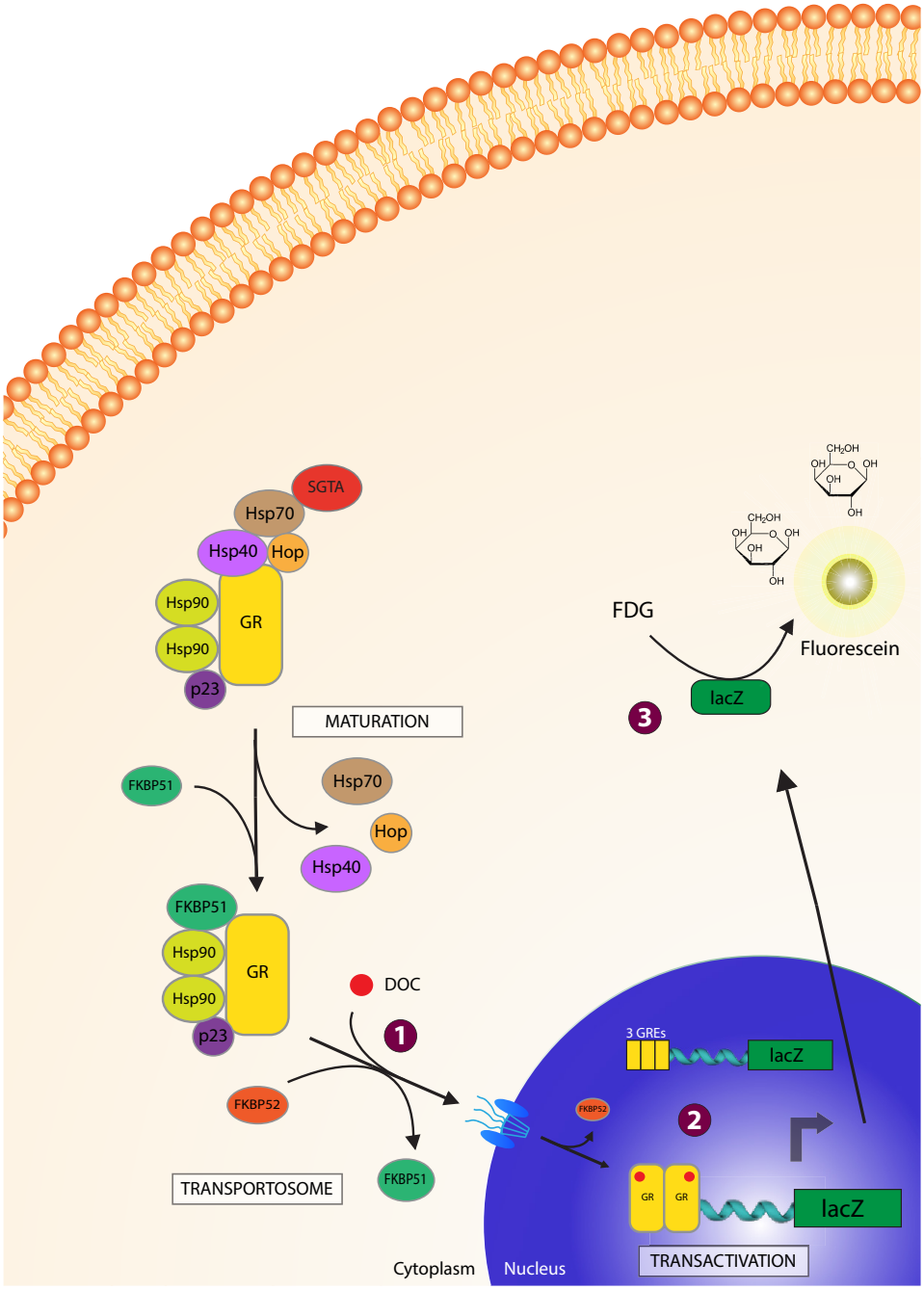

Figure 44. β-galactosidase reporter assay for monitoring GR activity. The GR remains inactive in cytoplasm. In the presence of deoxycorticosterone (DOC, a GR agonist), the GR gets activated **(1)** and binds to the glucocorticoid response elements (GREs) present in the plasmid transformed into. This binding to the GREs upregulates the expression of the beta-galactosidase gene (*lacZ*) **(2)**. β-galactosidase hydrolyzes the provided non-fluorescent galactose analog Fluorescein-di-β-D-galactopyranoside (FDG) which consists of two galactose monomers and a fluorescein. The reaction will be sequential: first hydrolyzing a galactose monomer to obtain Fluorescein-mono-β-D-galactopyranoside (FMG) and again hydrolyzes a second galactose for releasing fluorescein whose fluorescence (ex: 485 nm, em: 530 nm) can be monitored in a plate reader **(3)**. For that matter cells are semipermeabilized with Triton-X100 before measuring. Glucocorticoid receptor signaling scheme adapted from (Cato et al. 2014).

3.5.1. The GR activity increased in the absence of Get3

SGTA acts as a chaperone for the SRs and modulates their activity (Paul et al. 2014). In order to test the activity of the SRs, I used an engineered reporter assay in yeast (**Fig. 44**). I started testing one SR: the GR. Despite the fact that yeast has no steroid receptors, all chaperones involved in chaperoning the GR in mammals are present. The reporter assay relies on the fluorescence of fluorescein, a non-fluorescent fluorescein-derivate, Fluorescein di-β-D-galactopyranoside (FDG) (Hofmann and Sernetz 1983), is added to the media. Upon the stimulation of the GR with a glucocorticoid agonist, a GR-regulated *lacZ* (β-galactosidase gene) is expressed. This enzyme cleaves the FDG and releases fluorescein that is measured in a plate reader at the pertinent excitation and emission wavelengths.

Deoxycorticosterone (DOC) is a glucocorticoid agonist of the GR. This agonist binds to the LBD and activates the GR enabling its translocation into the nucleus (Goodman 2009). The relative reporter expression is a ratio obtained by dividing the fluorescence signal from DOC-stimulated cells by the fluorescence signal of non-stimulated cells. It is an indirect reading of how many fold the receptor is activated over the background level.

To test whether the absence of Get3 affects the activity of the GR, I chose a wt and a Δ*get3* strains with three different genetic backgrounds (BY4741, BY4742 and K700α). The genetic background is relevant to the experiment because some auxotrophic marker genes used in yeast laboratory strains, i.e. the *MET15* gene, affect the redox state of the cells, which may in turn cause different levels of activation of the redox-sensitive Get3 chaperone. I also analyzed a Δ*sgt2* strain in the BY4741 background to be able to compare it directly to the Δ*get3* and a Δ*get1/2* strain in this background. This experiment was intended to assess whether the GET receptor plays a role in GR activity, potentially because the receptor may have a role in the switch between the TA-protein targeting and chaperone form of Get3. I transformed these strains with the plasmids for the rat GR and the *lacZ* reporter gene under the control of a GR-responsive promoter, glucocorticoid responsive elements (GREs), and performed the reporter measurements using yeast grown to log phase. The lack of Get3 increased

the GR activity in the BY4741 background (**Fig. 45A**). In contrast, loss of Get3 had no effect over the activity of the GR in the other two genetic backgrounds (**Fig. 45B, Fig. 45C**). Indeed, as reported (Paul et al. 2014), the activity of the GR was higher in the Δ*sgt2* strain, whereas no effect was observed in the Δ*get1/2* strain (**Fig. 45A**). Lack of Get3 had a stronger effect on GR activity than lack of Sgt2.

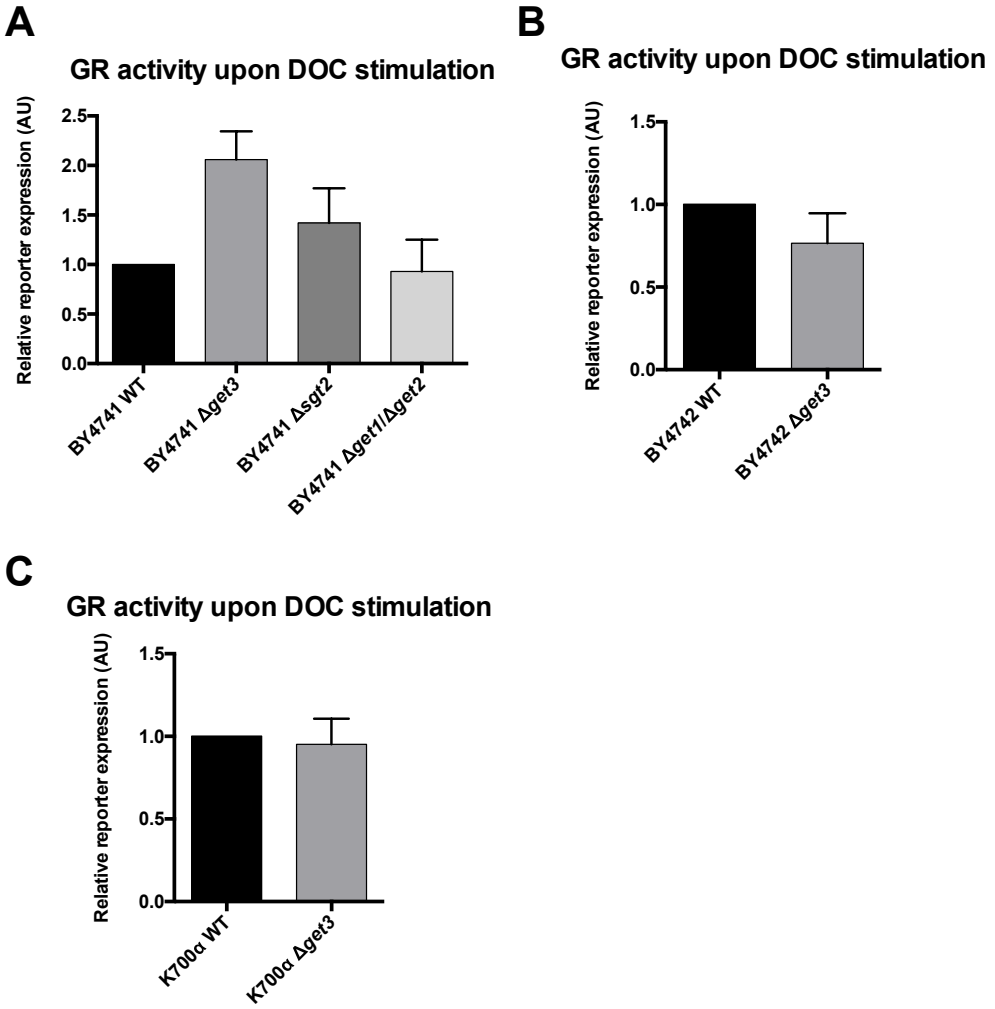

Figure 45. The absence of yeast Get3, in the BY4741 background, increases the activity of the glucocorticoid receptor. (A) Fluorescein-reporter assay measuring the activity of the glucocorticoid receptor (GR). BY4741 wt, *get3*, *sgt2*, *get1/get2* were used, they were transformed with the GR and treated with 100 nM deoxycorticosterone (DOC), a glucocorticoid receptor agonist. The ratio of the signal obtained from DOC-treated cells and mock-treated cells is shown in the graph. **(B)** Fluorescein-reporter assay for measuring the activity of the GR. BY4742 wt and *get3* were used, they were transformed with the GR and treated with 100 nM DOC, and the data was analyzed as in (A). **(C)** Fluorescein-reporter assay measuring the activity of the GR. K700α wt and the isogenic *get3* deletion strain were used, they were transformed with the GR, and treated with 100 nM DOC. Data was analyzed as in (A). Four to five cultures independently inoculated from different transformations were analyzed. The graphs show the mean and the error bars represent standard error of the mean.

3.5.2. Get3 was unable to rescue the basal activity of the GR

Get3 has an effect on the GR activity but it was unclear whether this result does indeed reflect the chaperone activity of Get3. To address this question, I focused on the BY4741 genetic background and performed another reporter assay using a set of cysteine-mutants of Get3 plus an ATPase-impaired mutant ($Get3_{D57E}$) and a TA-binding deficient mutant ($Get3_{I193D}$) in the Δ*get3* strain. Get3 mutants unable to restore the wt activity of the GR were expected to inform on the required function of Get3. When analyzing the results, none of the Get3 variants were able to restore the GR activity of the Δ*get3* strain to BY4741 wt levels (**Fig. 46B**). However, they did have a clear impact on the absolute GR activity as shown in **Fig. 46A**. The potential explanation may be that the absolute GR activity in non-stimulated cells and the GR activity in stimulated cells were affected to the same extent (**Fig. 46A**), which canceled out any change in the ratio (**Fig. 46B**).

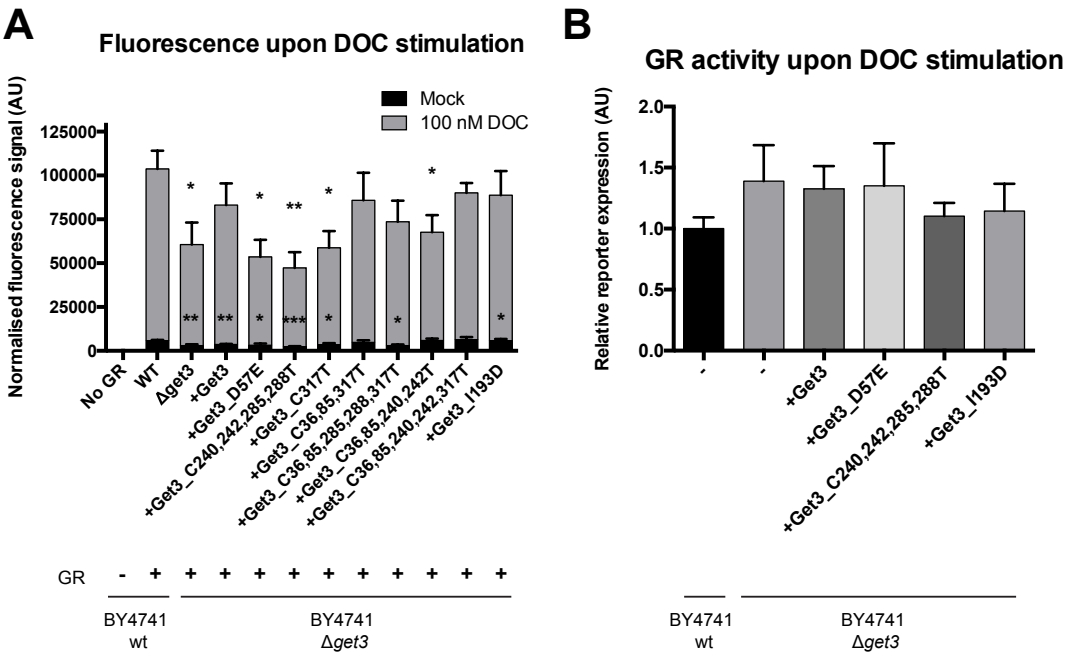

Figure 46. Get3 variants cannot restore the reduced GR activity of the wt, although these variants result in significantly different absolute activity levels. (A) Fluorescein-reporter assay measuring GR activity. Absolute luminescence in BY4741 wt and *get3* transformed with the GR and Get3 variants upon treatment with 100 nM DOC, a glucocorticoid receptor agonist. * indicates a p-value < 0.05; ** a p-value < 0.05; *** a p-value < 0.001. **(B)** GR activity upon DOC stimulation in a selected set of mutants. Ratio between DOC-treated cells and mock-treated cells from the experiment performed in (A). Six to nine cultures independently inoculated from different transformations were analyzed. The graphs show the mean and the error bars represent standard error of the mean.

3.5.3. Get3 modulated the stability of the GR

To complement the reporter assay (**Fig. 46**), I determined Get3 and the GR steady-state protein levels by Western blot. Interestingly, the GR levels were decreased upon Get3 transformation. That suggests that Get3 modulates the steady-state protein levels of the GR (**Fig. 47A**). In general, they were inversely correlated, with higher Get3 levels (**Fig. 47B**) correlating with lower GR levels (**Fig. 47C**).

3.5.4. Get3 and GR levels correlated inversely

In the constructs used, Get3 mutants were expressed from a *MET25* promoter. This promoter can be repressed by methionine. To further corroborate whether the Get3 levels modulated those of the GR, I titrated down the steady-state protein levels of Get3 by culturing the cells in the presence of increasing amounts of methionine followed by Western blot analysis. For this experiment I included Δ*get3*, Δ*get3*+$Get3_{wt}$, $Get3_{D57E}$ and $Get3_{C240,242,285,288T}$.

On the one hand in the case of the Δ*get3*, the steady-state levels of the GR remained unaffected regardless of the methionine concentration (**Fig. 48A**, **Fig. 48B**). On the other hand, in the presence of $Get3_{wt}$ the steady-state levels of the GR increased with decreasing levels of $Get3_{wt}$ at higher methionine concentrations (**Fig. 48A, Fig. 48C**).

Both Get3 mutants investigated, $Get3_{D57E}$ and $Get3_{C240,242,285,288T}$, showed the same behavior as $Get3_{wt}$. The more Get3 was down-regulated, the higher the GR levels were observed (**Fig. 49**). These experiments support the conclusion that Get3 modulates the steady-state levels of the GR in yeast.

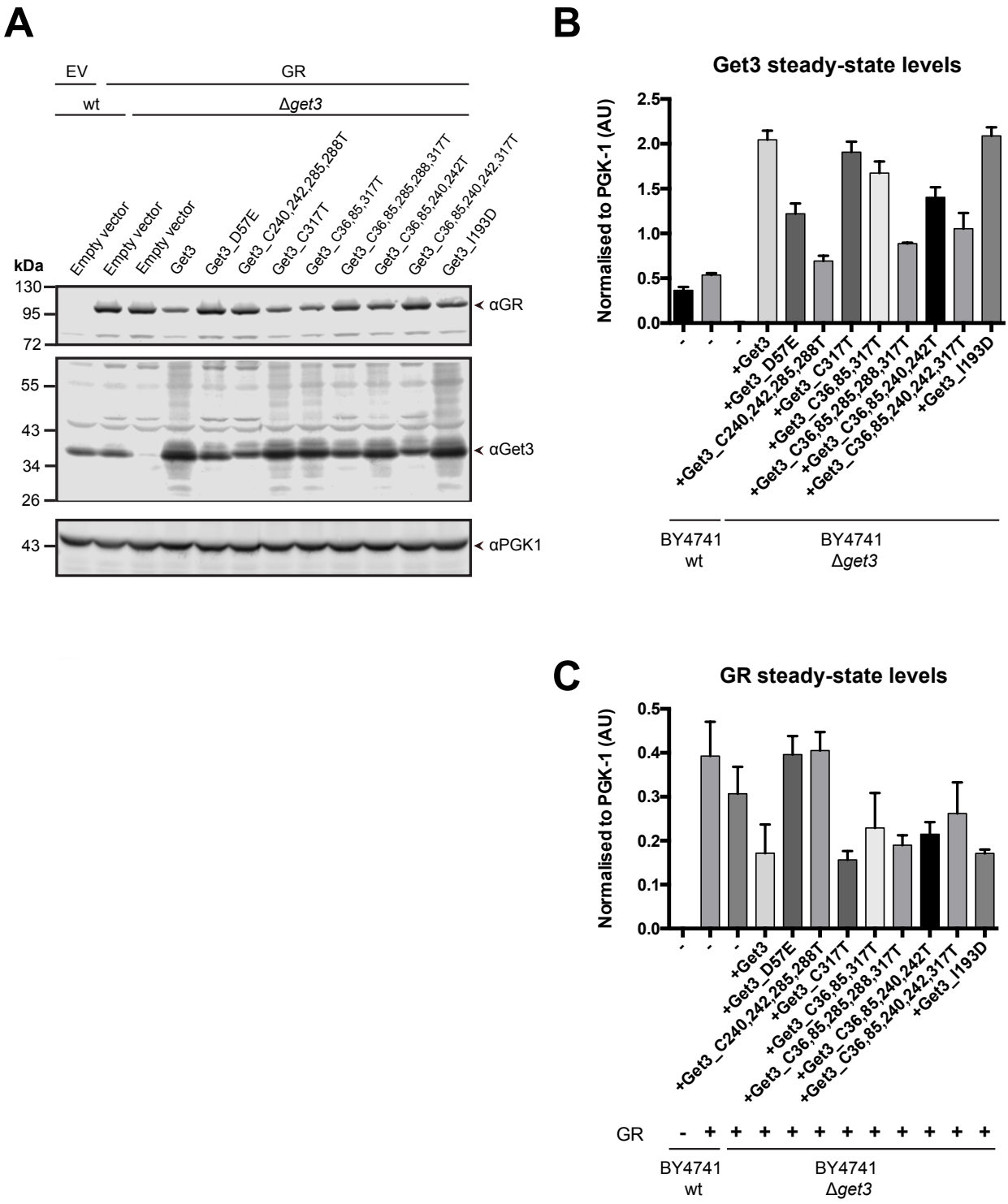

Figure 47. Get3 variants levels affect the stability of the GR. (A) BY4741 wt and BY4741 *get3* transformed with the glucocorticoid receptor and different Get3 mutants were analyzed for Western blot detecting the indicated proteins. **(B)** Get3 steady-state levels. Quantification of the signal intensities from the blots performed in (A). **(C)** Glucocorticoid receptor steady-state levels. Quantification of the signal intensities from the blots performed in (A). Three cultures independently inoculated from different transformations were analyzed. The graphs show the mean and the error bars represent standard error of the mean.

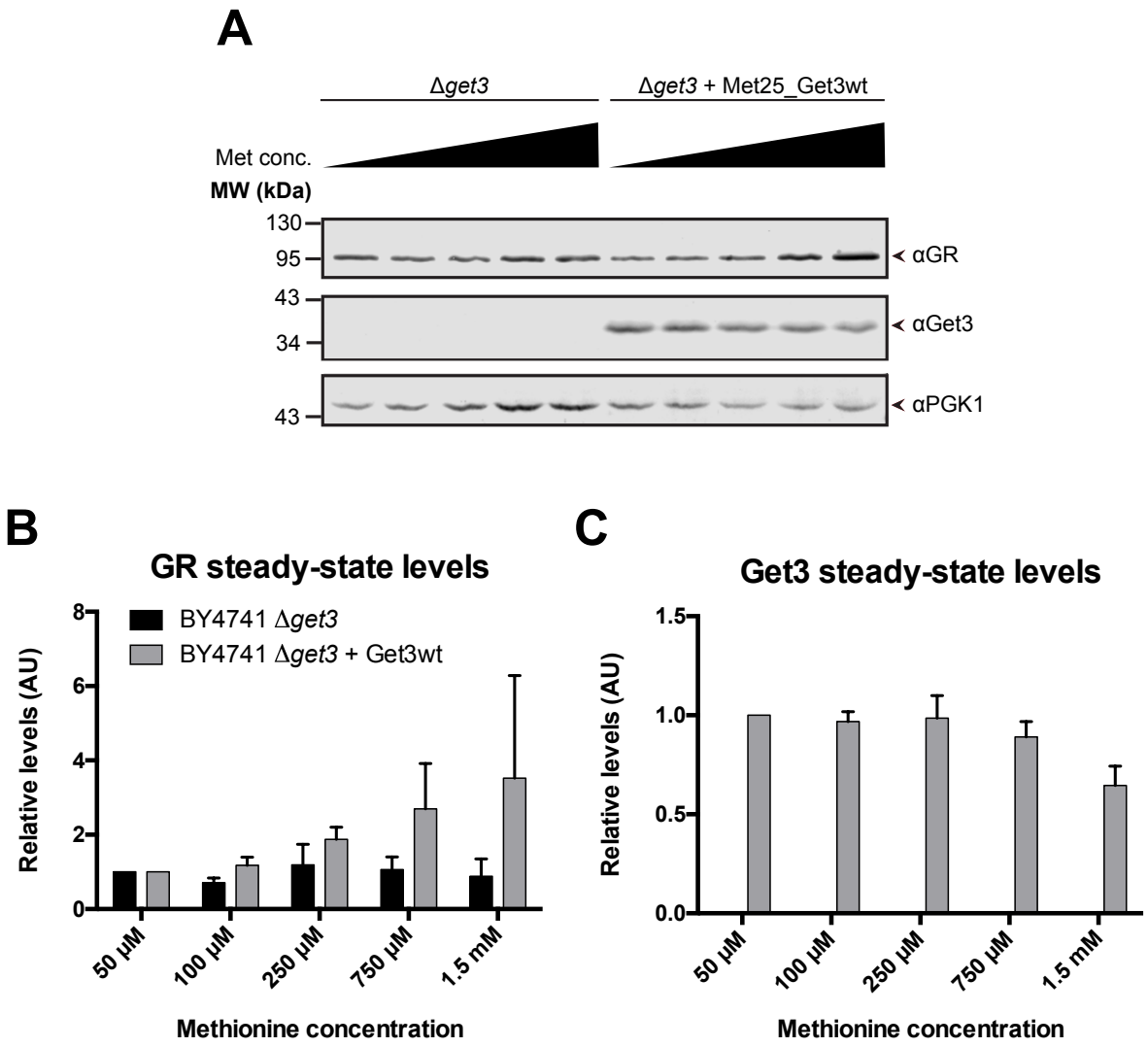

Figure 48. Titration of wt Get3 expression levels confirms that these affect the stability of the GR. (A) Methionine titration of Get3 expression levels in BY4741 Δ*get3* cells transformed with a plasmid of $Get3_{wt}$ under the *MET25* promoter. Western blot was performed detecting the indicated proteins. **(B)** Quantification of GR steady-state levels based on the blots performed in (A). **(C)** Quantification of Get3 steady-state levels from the blots performed in (A). Three cultures independently inoculated from different transformations were analyzed. The graphs show the mean and the error bars represent standard error of the mean.

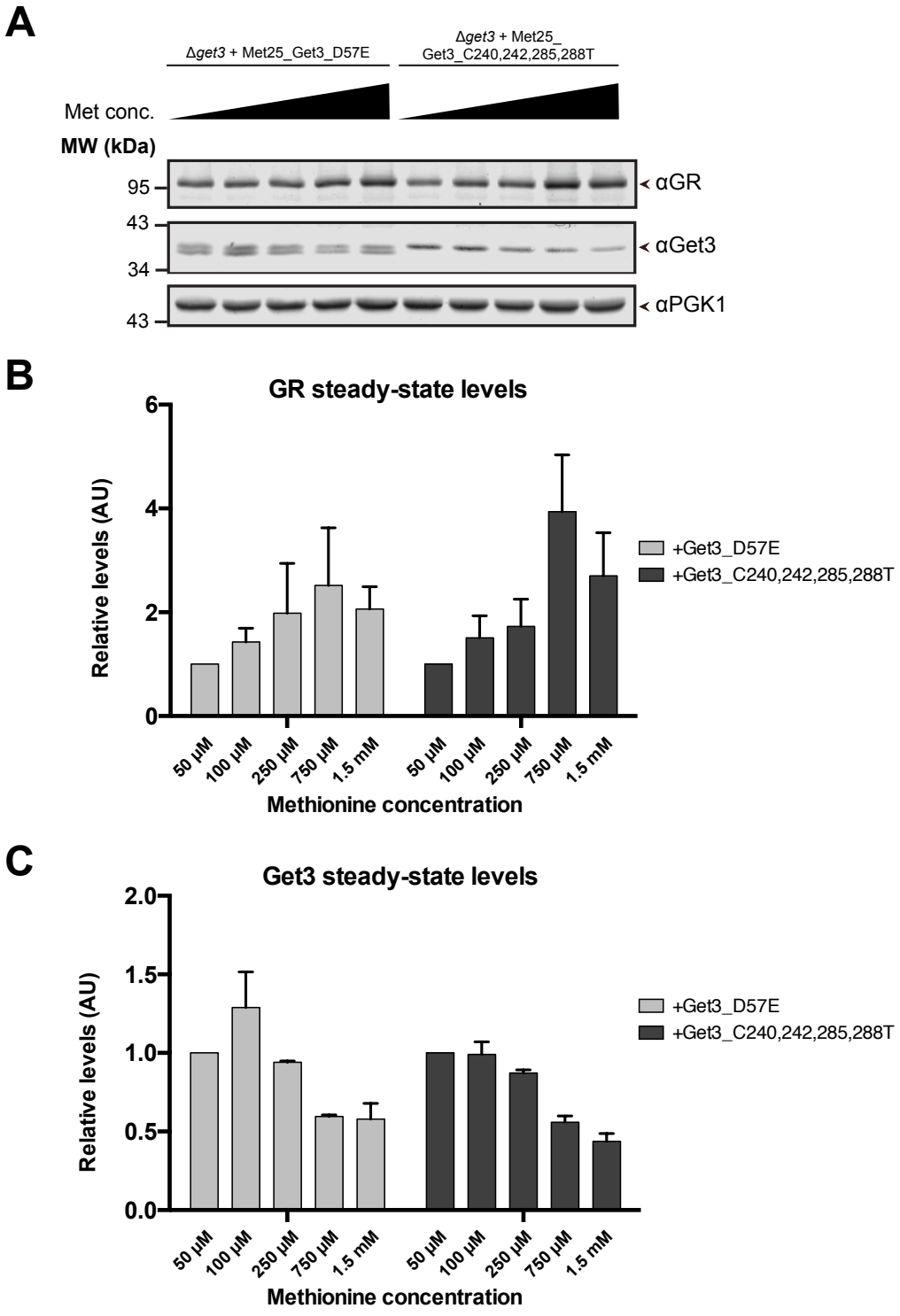

Figure 49. Titration of the steady-state levels of mutant Get3$_{D57E}$ and a mutant lacking the conserved cysteines confirms that these variants also affect the stability of the GR. (A) Methionine titration of Get3 expression levels in BY4741 Δ*get3* cells transformed with a plasmid of Get3 variants under the *MET25* promoter. Western blot was performed and the indicated proteins were detected. **(B)** Quantification of GR steady-state levels based on the blots performed in (A) in the presence of the indicated Get3 variants. **(C)** Quantification of Get3 steady-state levels from the blots performed in (A). Three cultures independently inoculated from different transformations were analyzed. The graphs show the mean and the error bars represent standard error of the mean.

3.5.5. The GR subcellular localization was unaffected by the absence of TRC40 in HeLa cells

One relevant step of GR signaling is the translocation into the nucleus (Guiochon-Mantel et al. 1991; Haché et al. 1999). This must take place for this receptor to exert its control on the expression of glucocorticoid target genes. This has been well-established in human cell lines. HeLa P4 cells express GR endogenously and there is no need to transiently express it under a strong promoter. Hence, I decided to avoid the heterologous system and move to HeLa cells to perform the next experiments. To test whether TRC40 alters the shuttling of the GR into the nucleus, TRC40 was silenced using siRNA and the cells were stimulated with dexamethasone (DEX). Dexamethasone is a synthetic corticoid agonist of the GR (Bunim et al. 1958). Then I performed an indirect immunofluorescence with an antibody against the GR to monitor the GR subcellular localization and the shuttling into the nucleus upon DEX stimulation.

After analyzing the images, the knockdown of TRC40 had no effect on the subcellular localization of the GR, neither in non-stimulated cells nor DEX-stimulated cells (**Fig. 50A, Fig. 50B**).

3.5.6. The GR stability was unaltered in TRC40-knockdown HeLa cells

In yeast, Get3 was shown to modulate the steady-state protein levels of the GR (**Fig. 47, Fig. 48, Fig. 49**). Here I show that the subcellular localization of the GR was not affected by down-regulation of TRC40 in HeLa cells (**Fig. 50**). Yet, the GR steady-state levels might be modulated by TRC40. To test this, I silenced TRC40 with siRNA in HeLa cells and performed Western blot analysis. From the blots I can conclude that the GR steady-state levels were not modulated by the absence of TRC40 (**Fig. 51A, Fig. 51B**).

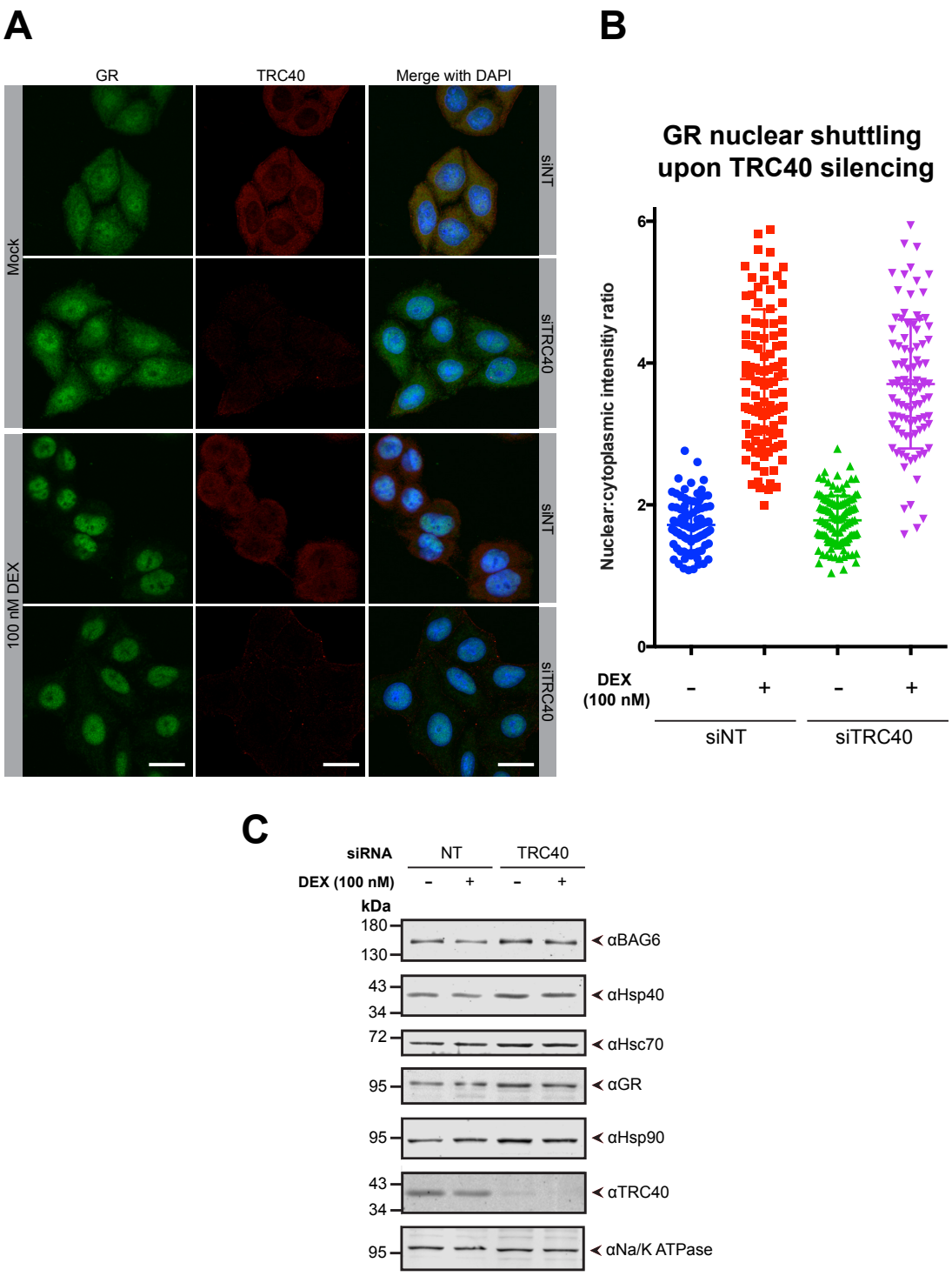

Figure 50. Down-regulation of TRC40 does not alter the nuclear shuttling of the GR in HeLa cells. **(A)** Immunofluorescence of the GR upon silencing of TRC40 in HeLa cells. Images of the GR and TRC40 stained by indirect immunofluorescence are shown. Cells were stimulated with 100 nM dexamethasone (DEX), a glucocorticoid receptor agonist. **(B)** Scatter plot representing the nuclear-cytoplasmic ratio of the GR upon silencing of TRC40. Each dot represents the fluorescence intensity of one cell. n= 85-116 cells are represented. The graphs show the mean and the error bars represent the standard deviation. **(C)** Steady-state levels of GR and selected heat shock proteins (Hsps) upon silencing of TRC40. Western blot was performed detecting the indicated proteins. Three biological replicates were analyzed. Scale bars: 20 μm.

3.5.7. TRC40 and the GR were not found to interact

The absence of TRC40 does not affect the nuclear shuttling of the GR (**Fig. 50**) and TRC40 does not modulate the steady-state protein levels of the GR in HeLa cells (**Fig. 51**). There is still the possibility that they interact and TRC40 regulates the GR in a different way. To test the potential interaction between TRC40 and the GR, I transfected HeLa cells with a Venus-TRC40$_{wt}$ construct and I affinity-purified the Venus-tagged TRC40 using a nanobody matrix directed against GFP. The GFP nanobody can detect the Venus tag (Nagai et al. 2002). After affinity-purification of Venus-TRC40$_{wt}$ no interaction with the GR was detected (**Fig. 52**). I also tested the inverse affinity-purification targeting Venus-GR after transfection with the corresponding construct, and no interaction with TRC40 was detected (**Appendix Fig. 2B**). Additionally, I performed an immunoprecipitation using antibodies against the GR and TRC40 and no obvious interaction was detected (**Appendix Fig. 2A**). Taking together all these results, I conclude that there is no evidence that shows that GR and TRC40 do interact.

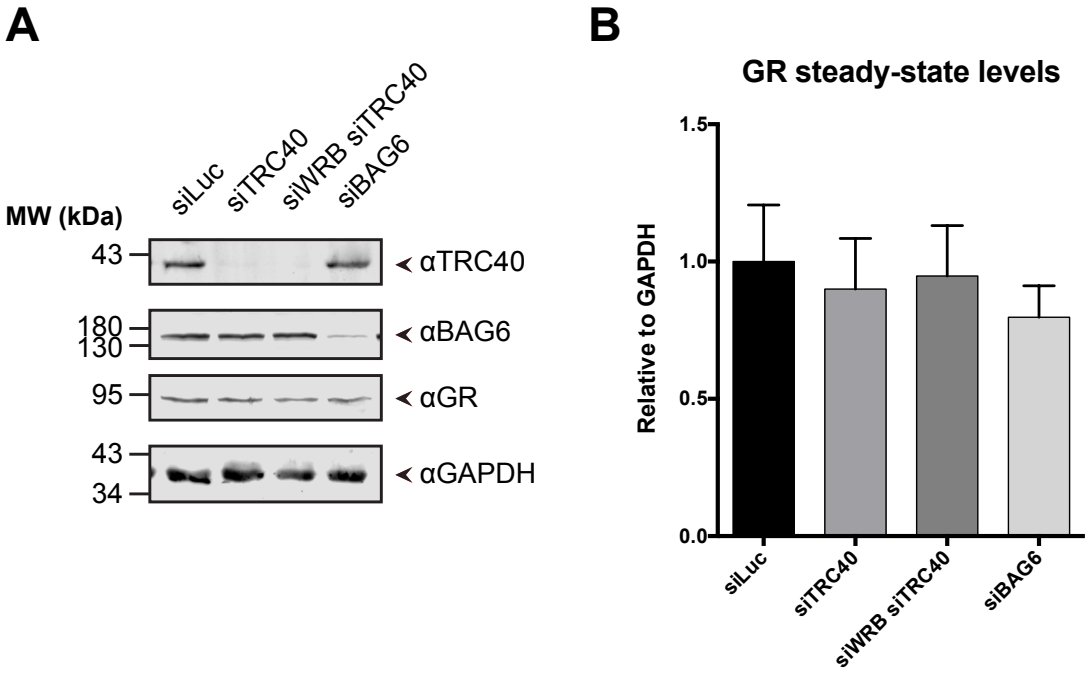

Figure 51. GR steady-state levels do not change upon TRC40 or BAG6 knockdown. (A) Knock-down of TRC40, WRB/TRC40 or BAG6 performed in HeLa P4 cells. Cytosolic fractions were analyzed for Western blot for TRC-pathway components and the glucocorticoid receptor. **(B)** Quantification of the GR signal intensities from the blots performed in (A). Four biological replicates were analyzed. The graphs show the mean and the error bars represent standard error of the mean.

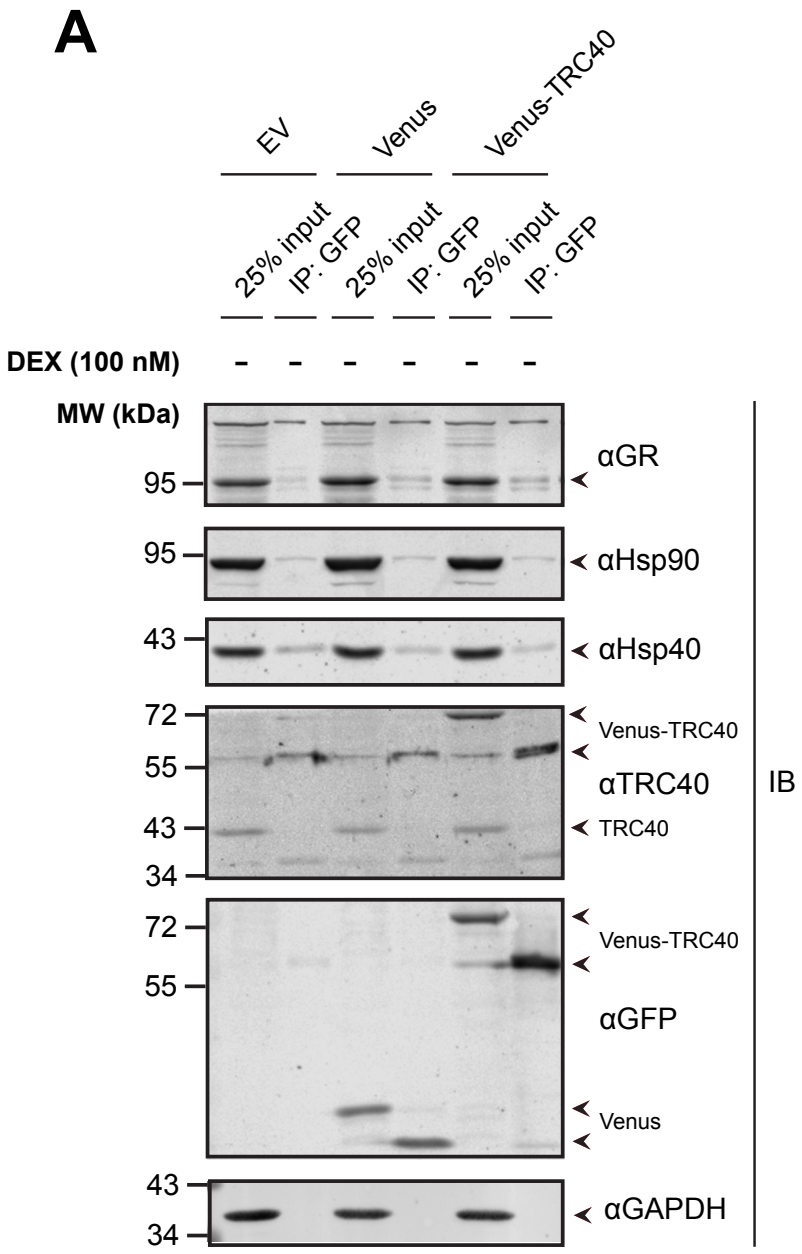

Figure 52. The GR is not influenced by the manipulation of TRC40 in HeLa cells. (A) GFP pull-down from HeLa cells transfected with Venus-TRC40. Cells transfected with a Venus construct served as a control. Western blot was performed for the indicated proteins. Venus proteins subjected to SDS-PAGE after TCA-precipitation migrate at the expected size (72 kDa Venus-TRC40, 27 kDa Venus) whereas the samples applied in sample buffer without previous TCA precipitation samples migrate faster (around 60 kDa Venus-TRC40, 22 kDa Venus). Two biological replicates were analyzed.

4. Discussion

4.1. TRC40$_{D74E}$ is a trapping mutant suitable for the study of TA-protein biogenesis *in vivo*

The TRC40$_{D74E}$ mutant altered the native subcellular localization of a certain subset of TA-proteins, which show cytoplasmic localization by indirect immunofluorescence. However, TRC40$_{D74E}$ had no effect over another set of TA-proteins. The manipulation of the TA-binding groove in combination with this mutant showed the following results: when combined with one single mutation, TRC40$_{D74E/I193D}$, was not sufficient to revert the phenotype. However, combined with two mutations, TRC40$_{D74E/L190D/I193D}$, was enough to abrogate the D74E effect over Stx8 and EMD (**Fig. 13A, Fig. 14A, Fig. 15A, Fig.19B, Appendix Fig. 6**). In contrast, Stx5 subcellular localization was still mildly affected (**Fig. 13A, Fig. 19B**) which would suggest that either these two mutations were not able to abolish the interaction of Stx5 and TRC40 or that there might potentially be an additional binding region of TRC40 that interacts with Stx5. Nevertheless, some of the TA-proteins tested in this study remained unchanged in the presence of TRC40$_{D74E}$ suggesting that not all the TA-proteins are susceptible to be affected by this ATPase-impaired mutant (**Fig. 16A, Fig. 17A, Fig. 18A, Fig. 19A**). Stx5 and EMD could be washed out in digitonin semipermeabilized cells (**Fig. 20B, Fig. 21B**), however a population of EMD remained at the ER membrane, unlike Stx5. The inhibition of DUBs did not prevent the cytoplasmic accumulation of Stx5 in the TRC40$_{D74E}$-transfected cells (**Fig. 22A**). Moreover, cytosolic Stx5 steady-state levels were higher in the TRC40$_{D74E}$-transfected cells compared to the EV (**Fig. 23B**) and the majority of this Stx5 population in cytosol was unglycosylated (**Fig. 24A**). Finally, the co-immunoprecipitation of Stx5 and TRC40 showed that both proteins interact in cytosol and that other chaperones like BAG6 might be also recruited to the complex (**Fig. 25A**). Taken together, these would indicate that TRC40$_{D74E}$ might prevent the insertion of newly synthesized Stx5 and instead captures it in cytoplasm acting as a trapping mutant.

The ATPase-impaired mutant, D57x, of yeast Get3 has been reported in literature (Mateja et al. 2009; F. Wang et al. 2011; Stefer et al. 2011; Powis et al. 2013; Chio et al. 2017). The aspartate residue sits in the very well-conserved Switch I region that is shared with other SIMIBI ATPases (Koonin 1993; Bange and Sinning 2013). It was originally mutated in the archaeal homolog ArsA (Tongqing Zhou and Rosen 1999) and eventually translated to Get3 (Mateja et al. 2009). $ArsA_{D45E}$ was reported to possess 20-fold less ATPase activity compared to $ArsA_{wt}$ whereas $ArsA_{D45N}$ showed no measurable ATPase-activity (Tongqing Zhou and Rosen 1999). In the case of yeast Get3, $Get3_{D57N}$ was reported to have a 100-fold slower ATPase activity compared to $Get3_{wt}$ (Chio et al. 2017). Similarly, $Get3_{D57E}$ ATPase activity was also decreased compared to the wt (Powis et al. 2013). Furthermore, $TRC40_{D74N}$ could not restore the Golgi integrity and Stx5 and Stx6 expression in mouse explants coming from the pancreatic epithelium TRC40-knockout cells (Norlin, Parekh, and Edlund 2018). The TA-protein targeting function of Get3 is coupled to the ATPase activity and the conformational changes derived from ATP hydrolysis (Chio, Cho, and Shan 2017). Along the same lines, $Get3_{D57N}$ showed an 85% reduction compared to $Get3_{wt}$ in relative insertion efficiency of Sec61β into membranes in an *in vitro* experiment (Mariappan et al. 2011). Moreover, Get3 is unable to efficiently insert TA-proteins in the presence of adenosine 5′-O-(3-thiotriphosphate) (ATP-γ-S), a slowly hydrolyzable ATP-analog (Stefer et al. 2011). Interestingly, $Get3_{D57N}$ has recently been proposed as a mutant that cannot undergo the conformational changes required to dissociate from Get4/Get5 and therefore cannot interact with the GET receptor (Chio et al. 2017). Hence, it is thought to remain bound to the TA-protein and probably to the pre-targeting complex (Chio et al. 2017).

As a part of the SIMIBI ATPase class (Leipe et al. 2002; Bange and Sinning 2013; Shan 2016), Get3, YlxH, ArsA and ParA, share a high homology in the ATPase Switch I and the aspartate residue is conserved in each of them (Koonin 1993; Bange and Sinning 2013). ParA, or Soj, is a bacterial ATPase involved in the regulation of the DNA replication initiation that has been studied in *Bacillus subtilis*. ParA forms dimers and also relies on nucleotide-dependent conformational changes. As mentioned, the aspartate residue within the Switch I is conserved in ParA (D44) (Bange and Sinning 2013) and it has been described that mutations in this residue locks ParA into a fixed conformation in an ATP-bound state (Quisel, Lin, and Grossman 1999; Scholefield et

al. 2011). Moreover, the aspartate residue is conserved in the bacterial ATPase MinD (D40) (Hayashi, Oyama, and Morikawa 2001), a protein involved in bacterial cell division, that undergoes into nucleotide-dependent conformational changes (Lutkenhaus and Sundaramoorthy 2003). Mutations in this residue locks the protein in an ATP-bound conformation that fails to dissociate from its substrate (W. Wu et al. 2011).

The TRC40 Switch I region has been conserved in its entirety during evolution (**Appendix Fig. 3A**) and it is shared with the ATPases of the SIMIBI class (Bange and Sinning 2013; Shan 2016). Similar to other SIMIBI ATPases, the mutation of the aspartic residue could lock TRC40. This would support the hypothesis that when TRC40 is strongly impaired in ATP-hydrolysis, it results in its being locked in a conformation that makes it a trapping mutant. Due to the high degree of homology between human TRC40 and yeast Get3, it is possible to draw parallels between the well-characterized yeast Get3 ATPase cycle (**Fig. 53**). The present study provides evidence that a subset of TA-proteins is localized in the cytoplasm upon mutation of TRC40 to its ATPase-impaired form. Furthermore, this effect is dependent on the integrity of the TA-binding groove. Additionally, Stx5 present in cytosol was unglycosylated suggesting that it was not inserted into the membrane but instead kept in cytoplasm. In a similar fashion as described for Get3 (Chio et al. 2017), it is possible to speculate that $TRC40_{D74E}$ is able to interact with the pre-targeting complex and can be loaded with newly synthesized TA-protein. Nevertheless, the impairment in the ATP processing makes it unable to interact with the TRC receptor and subsequently hand off the TA-protein leading to an accumulation of TRC40 loaded with the TA-protein in the cytoplasm (**Fig. 53, step 3**). This essentially makes $TRC40_{D74E}$ a good tool for the study of tail-anchored protein biogenesis *in vivo*. Combined with the use of $TRC40_{D74E/L190D/I193D}$ as a negative control, the experiments can shed light on the biogenesis of TA-proteins substrates of the TRC pathway.

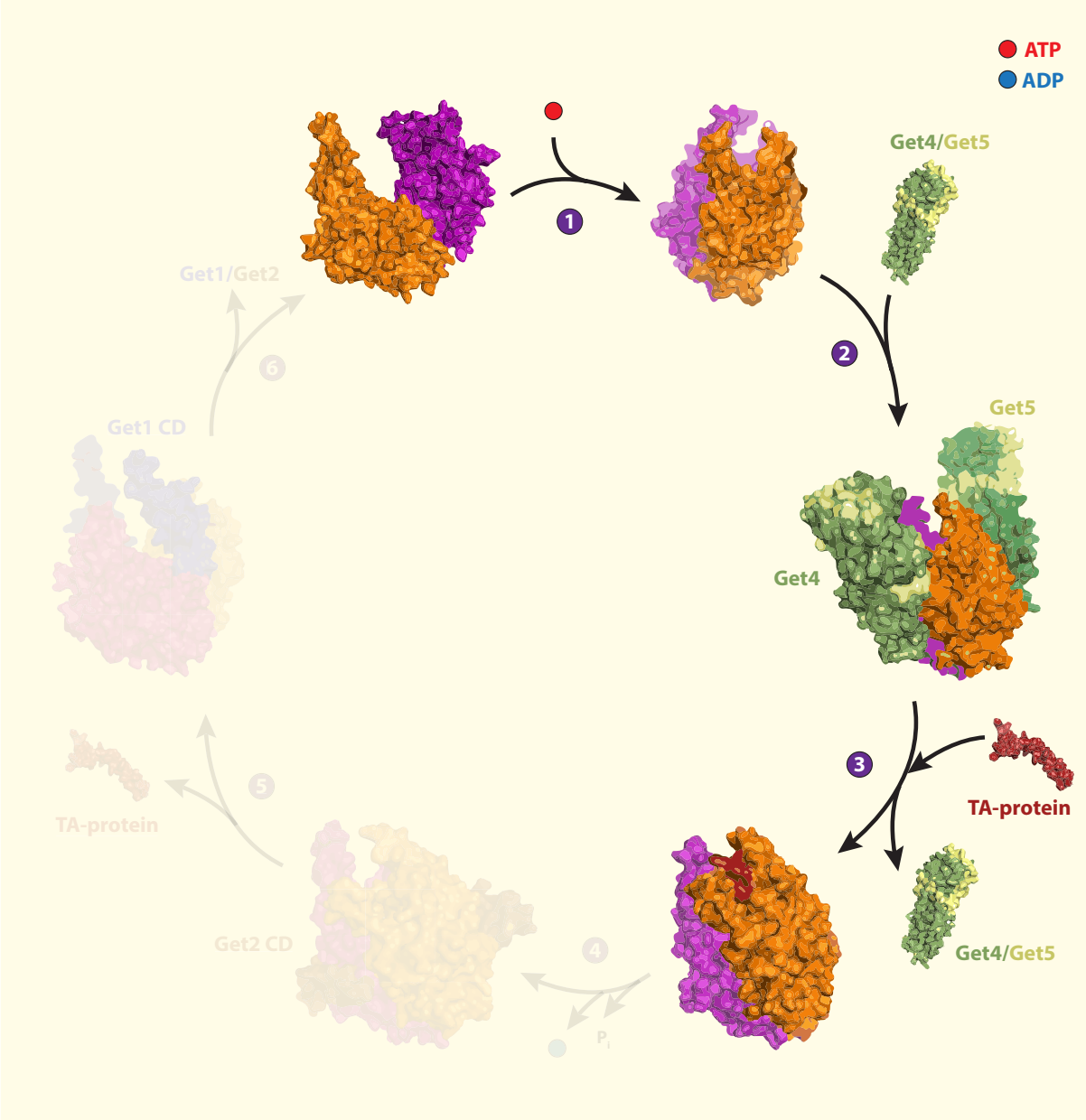

Figure 53. The TRC40$_{D74E}$ ATPase-deficient cycle model. Based on the ATPase cycle described in **Fig. 5. (1)** and **(2)** are exactly as described. **(3)** The TA-protein (PDB ID: 2LPF) is thus loaded into Get3 (PDB ID: 4XTR) from Sgt2. This interaction with the TA-protein should make Get3 lose its affinity for Get4/Get5 (PDB ID: 4PWX), dissociate and process the ATP. But instead, Get3 remains loaded with the TA-protein and ATP. It is believed that Get4/Get5 remains bound to the ATPase-impaired Get3. Get3 subunits are depicted in orange and deep purple.

4.2. TA-protein dependence of the TRC pathway *in vivo*

4.2.1. Studying TA-biogenesis *in vitro* versus *in vivo*

In order to understand TA-protein biogenesis, several *in vitro* experiments were reported in literature, especially insertion assays into ER-derived membranes. These experiments were based on either affinity purified complexes (Get3/TRC40 and a TA-protein) or *in vitro* synthesized protein in rabbit reticulocyte lysate (RRL) plus rough microsomes (RMs) under varying conditions such as: ATP-depletion, immunodepletion of components and peptide-based competition assays. Most of these *in vitro* experiments used Sec61β as a model TA-protein (Stefanovic and Hegde 2007; Favaloro et al. 2008; Favaloro et al. 2010; Leznicki et al. 2010; Leznicki, Warwicker, and High 2011; Mariappan et al. 2011; Johnson et al. 2012). In these experiments, Sec61β was shown to be a clear substrate of the TRC pathway. The TRC pathway and yeast GET pathway have been the reference pathways regarding TA-protein biogenesis (Mandon and Gilmore 2007; Mateja et al. 2009; Mariappan et al. 2010), although some authors considered that the chaperones Hsp40/Hsc70 furnished an alternative insertion pathway (Rabu et al. 2008; Rabu et al. 2009). However, in recent years many *in vivo* studies have been performed and other pathways related to TA-protein biogenesis have been described. The *in vivo* studies were based on knockdowns or knockouts of human cell lines or in mouse knockout models. Surprisingly, in these studies the TRC-dependence of Sec61β was not evident at steady-state. Sec61β steady-state levels were not significantly altered in either primary cardiomyocytes or primary hepatocytes depleted of WRB (Rivera-Monroy et al. 2016). Likewise, Sec61β steady-state levels were not significantly altered in TRC40-knockdown, WRB-knockdown and TRC40-knockout HeLa M cells (Casson et al. 2017) as well as in this study (**Fig. 26B, Fig. 32C**). Additionally, Sec61β did not suffer any apparent change in the subcellular localization in TRC40-knockout HeLa M cells (Casson et al. 2017), in TRC40-knockout pancreatic β-cells (Norlin et al. 2016) and in this study upon the over-expression of $TRC40_{D74E}$ in HeLa P4 cells (**Fig. 16A**). However, a couple of studies showed Sec61β altered upon the TRC pathway

manipulation: in WRB-knockdown HeLa cells Sec61β is decreased at the steady-state level after ER-fraction normalization (Haßdenteufel et al. 2017) and there is a reduction in opsin-tagged Sec61β-glycosylation at steady-state level in WRB-knockdown HeLa M cells upon the transient over-expression of Sec61β (Casson et al. 2017).

The *in vitro* TRC-dependence for insertion is not necessarily correlated with the TRC-dependence of the steady-state levels *in vivo*. Hence, more *in vivo* studies are required for further investigating TA-protein biogenesis due to the following arguments:

- The presence of other pathways for TA-biogenesis. The integration of these pathways such as the EMC pathway (Guna et al. 2018), ubiquilins (Itakura et al. 2016), Hsp40/Hsc70 (Rabu et al. 2008; Rabu et al. 2009), the SND pathway (Aviram et al. 2016; Haßdenteufel et al. 2017) or the PEX pathway (Jones, Morrell, and Gould 2004; Fujiki et al. 2014; Buentzel et al. 2015) makes it more difficult to discriminate the contribution of these pathways to TA-protein biogenesis. A role of the SRP in TA-protein biogenesis has also been implied (Johnson, Powis, and High 2013; Casson et al. 2017). The overlapping of substrates and shared contribution between the pathways emerge as a general concept (van der Zand, Braakman, and Tabak 2010; Buentzel et al. 2015; Itakura et al. 2016; Casson et al. 2017; Guna et al. 2018).
- Another important factor to take into account is the tissue-specific fate of the TA-proteins. Stx5 is affected regardless of the tissue-type when the TRC pathway is impaired (Rivera-Monroy et al. 2016; Norlin et al. 2016; Casson et al. 2017) (as well as this study, **Fig. 13A**, **Fig. 19B, Fig. 26B**, **Fig. 28A**). Yet there are other TA-proteins whose dependence on the TRC pathway varies from tissue to tissue. For instance, Stx6 was decreased at the steady-state level in WRB-knockout mouse hepatocytes (Rivera-Monroy et al. 2016), also in this study (**Fig. 26B, Fig. 28B**), and Stx6 had altered expression and subcellular distribution in two TRC40-knockout mouse models: pancreatic β-cells and pancreatic epithelial cells (Norlin et al. 2016; Norlin, Parekh, and Edlund 2018). In contrast, Stx6 was not affected at steady-state level in WRB-knockout mouse cardiomyocytes (Rivera-Monroy et al. 2016). Furthermore, EMD was decreased at the steady-state level in WRB-knockout mouse cardiomyocytes, also in this study (**Fig. 26B, Fig. 29B**), whereas no change at the steady-state level was

observed in WRB-knockout mouse hepatocytes (Rivera-Monroy et al. 2016). Moreover, it has been reported that otoferlin, a tissue-specific TA-protein of the inner-hair cells, is impaired in WRB-knockout mice, which present hearing problems (Vogl et al. 2016). Finally, the variability in the mRNA expression and protein at steady-state levels of the TRC components in several tissues (**Appendix Fig. 4A, Appendix Fig. 5A**) may differentially play a role in TA-protein biogenesis upon impairment of the TRC pathway.

4.2.2. TRC pathway-dependence of the TA-proteins *in vivo*

The fate of endogenous TA-proteins *in vivo* when the TRC pathway is impaired has remained unexplored until recently. The overlapping of the different pathways over-seeing the insertion of TA-proteins also poses the question of how relevant the TRC pathway is in the biogenesis of a specific TA-protein. From the 17 TA-proteins tested in this study, 11 were found to be decreased at steady-state level in WRB/TRC40 down-regulated cells: Stx5, Stx6, Stx1, Stx8, UBE2J1, USE1, EMD, VAPB, Vti1a, Sec22b and VAPA (**Fig. 26B**). In contrast, another 6 did not show any change at steady-state level in spite of the loss of WRB and TRC40: Stx18, GOSR2, PTP1B, Vti1b, Sec61β and SQS (**Fig. 26B**). Furthermore, 3 out of the 11 TA-proteins affected upon WRB/TRC40 knockdown were also affected upon the loss of TRC40: Stx5, UBE2J1 and VAPB (**Fig. 26B**). Based on these results, I will discuss how these findings relate to the information of individual TA-proteins in the literature.

Stx1a was classified as a TRC pathway substrate whose insertion had to be facilitated by a molecular chaperone (Rabu et al. 2008). Besides, Stx1 showed a typical subcellular localization in TRC40-knockout pancreatic β-cells in mouse (Norlin et al. 2016). Along the same lines, Stx1 showed a reduction at steady-state level upon the knockdown of WRB and TRC40 (**Fig. 28C**). Taken together with my results, at least a proportion of Stx1 may be targeted by the TRC pathway *in vivo*. Unfortunately, the Stx1 detecting antibody did not work for IF, preventing the more direct test of trapping Stx1 with $TRC40_{D74E}$ and instead will require the transient expression of tagged Stx1.

Syn8, the yeast homolog of Stx8, was unaffected in its subcellular distribution in Δ*get3*, Δ*get1*/Δ*get2,* Δ*get1*/Δ*get2*/Δ*get3* strains (Rivera-Monroy et al. 2016). In the same study, Stx8 protein levels at the steady-state did not change in either WRB-knockout cardiomyocytes or WRB-knockout hepatocytes but they were decreased upon TRC40-knockdown in HeLa cells (Rivera-Monroy et al. 2016). Moreover, Stx8 requires TRC40 to get inserted into RMs *in vitro* (Rivera-Monroy et al. 2016). Accordingly, Stx8 showed a cytoplasmic staining by IF in $TRC40_{D74E}$-transfected HeLa cells (**Fig. 15A**). However, Stx8 showed no reduction in TRC40-downregulated cells whereas Stx8 was found to be decreased to 62% at steady-state level upon combined WRB/TRC40 knockdown compared to the control cells in this study (**Fig. 28D**). The above results may indicate that TRC40 is important for targeting a population of Stx8 to the membrane. But in the absence of TRC40 or WRB, the results may indicate the existence of a redundant pathway that takes over the role of targeting Stx8 to the membrane. However, the combined loss of WRB/TRC40 affects the protein steady-state level of Stx8. This may indicate the relevance of WRB and TRC40 for the proper targeting of the potential redundant pathway.

In one study, strongly over-expressed Ubc6, yeast homolog of UBE2J1, was mislocalized to mitochondria in a Δ*get1*/Δ*get2* strain (Schuldiner et al. 2008) but in another study where no effect on its subcellular distribution was found in Δ*get3*, Δ*get1*/Δ*get2,* Δ*get1*/Δ*get2*/Δ*get3* strains (Rivera-Monroy et al. 2016). In mammals, for UBE2J1 it was suggested that its insertion had to be facilitated by a molecular chaperone (Rabu et al. 2008) but did not to require energy-dependent cytoplasmic chaperones for the insertion into ER-membranes (Haßdenteufel et al. 2011). It was later reported that UBE2J1 was a TRC40-substrate (Claessen et al. 2010). In this study, UBE2J1 showed a reduction by 60% at the steady-state level in TRC40-silenced cells whereas UBE2J1 revealed a decrease of 64% at the steady-state level in the combined silencing of WRB and TRC40 (**Fig. 29C**). Taken together with my results, a major proportion of UBE2J1 might be targeted by the TRC pathway *in vivo*. Owing to the unavailability of an antibody detecting UBE2J1, a tagged-version of UBE2J1 should be used for testing whether $TRC40_{D74E}$ would trap it.

EMD insertion was TRC pathway dependent and upon TRC40-knockdown showed reduced fluorescence intensity by IF (Pfaff et al. 2016). Additionally, EMD presented

altered subcellular localization in WRB-knockout mouse cardiomyocytes (Rivera-Monroy et al. 2016). At steady-state, EMD was reduced in WRB-knockout mouse cardiomyocytes, but no further change at the steady-state level was observed in WRB-knockout mouse hepatocytes (Rivera-Monroy et al. 2016). Along the same lines, following the over-expression of $TRC40_{D74E}$ EMD presented a cytoplasmic staining in this study (**Fig. 14A**). Furthermore, EMD steady-state levels were reduced in the combined WRB/TRC40-knockdown cells compared to the siLuc control cells (**Fig. 29B**). In summary, these results may indicate that EMD targeting relies on the TRC pathway *in vivo*. EMD targeting may be more sensitive to the loss of WRB, since EMD showed no effect, at the steady-state, in TRC40-downregulated cells (**Fig. 29B**), yet $TRC40_{D74E}$ is able to trap it in the cytoplasm.

Stx5-dependence on the TRC pathway has been discussed in a detailed manner in the previous sections. Briefly, Stx5 is affected in different tissues when the TRC pathway is impaired (Rivera-Monroy et al. 2016; Norlin et al. 2016; Casson et al. 2017). Moreover, yeast Stx5 (Sed5) is reported to have an altered subcellular distribution when the GET pathway is impaired (Schuldiner et al. 2008; Jonikas et al. 2009; Battle et al. 2010; Kohl et al. 2011; Powis et al. 2013; Vilardi et al. 2014; Voth et al. 2014; Rivera-Monroy et al. 2016). Likewise, Stx5 steady-state levels were reduced in TRC40-knockdown and in combined WRB/TRC40-knockdown cells in this study (**Fig. 28A**). Furthermore, Stx5 demonstrated a cytoplasmic staining in the $TRC40_{D74E}$-transfected cells (**Fig. 13A**). Taken together with my findings, Stx5 showed a strong dependence on the TRC pathway *in vivo* for targeting, interestingly not on BAG6.

Stx6 was reported to have altered expression and subcellular distribution in two TRC40-knockout mouse models: pancreatic β-cells and pancreatic epithelial cells (Norlin et al. 2016; Norlin, Parekh, and Edlund 2018). Likewise, Stx6 subcellular distribution was altered in WRB-knockout mouse cardiomyocytes (Rivera-Monroy et al. 2016). In contrast, Stx6 remained unaffected at steady-state in WRB-knockout mouse cardiomyocytes but was decreased at the steady-state in WRB-knockout mouse hepatocytes (Rivera-Monroy et al. 2016). Stx6 was also found to be reduced at steady-state upon combined WRB/TRC40 knockdown compared to the control cells in this study (**Fig. 28B**). Furthermore, preliminary results indicate that Stx6 is localized in

the cytoplasm in $TRC40_{D74E}$-transfected cells (data not shown). Taken together, these results indicate that Stx6 targeting may depend on the TRC pathway *in vivo*.

There are studies on the biogenesis of VAPA and VAPB in yeast but not in mammals. Upon strong over-expression Scs2p, the yeast homolog of VAPA and VAPB, was mislocalized in a Δ*get1*/Δ*get2* strain (Schuldiner et al. 2008). However, another study reported no change on its subcellular distribution in Δ*get3*, Δ*get1*/Δ*get2,* Δ*get1*/Δ*get2*/Δ*get3* strains (Rivera-Monroy et al. 2016). VAPB was reported to interact with TRC40 (Baron et al. 2014). In this study, VAPB subcellular localization was not affected by the presence of $TRC40_{D74E}$ (**Fig. 18A**). However, the steady-state levels of VAPB were found to be decreased in combined WRB/TRC40 silenced cells (**Fig. 29D**). The same was true for VAPA (**Fig. 30B**). In addition, steady-state levels of VAPB were also reduced in TRC40-knockdown cells (**Fig. 29D**). Taken together my results indicate that VAPA and VAPB may be targeted by the TRC pathway *in vivo*. In contrast to VAPA, VAPB steady-state levels were affected in TRC40-knockdown cells. Therefore, VAPB might require TRC40 for its biogenesis *in vivo* but it might be a downstream effect since $TRC40_{D74E}$ had no effect on the subcellular localization of VAPB. Indeed, the reported interaction of TRC40 with VAPB was independent of the transmembrane segment (Baron et al. 2014) indicating that the effect at steady-state level in this study may not be due to targeting.

Sec22p, the yeast homolog of Sec22b, could not be inserted in yeast microsomes lacking the Get1/Get2 receptor, highlighting its GET-pathway dependence (Schuldiner et al. 2008; Stefer et al. 2011). Sec22p was unable to be inserted into wt or Δ*get1*/Δ*get2* microsomes when incubated with Δ*get5* cytosolic extracts (Jonikas et al. 2009). In contrast, its subcellular distribution remained unaltered in Δ*get3*, Δ*get1*/Δ*get2,* Δ*get1*/Δ*get2*/Δ*get3* strains (Rivera-Monroy et al. 2016). In mammalian studies, a typical subcellular localization of Sec22b was observed in TRC40-knockout pancreatic β-cells in mouse (Norlin et al. 2016). Conversely, in this study where Sec22b showed a reduction at the steady-state level in WRB/TRC40-knockdown cells (**Fig. 30C**). In combination with my results, Sec22b seems to rely on the TRC pathway for targeting *in vivo*. Nevertheless, the effect of the $TRC40_{D74E}$ mutant on Sec22b subcellular

localization could not be evaluated because the antibody against Sec22b did not work for IF. A tagged Sec22b will be required to test this hypothesis.

There are no studies linking Vti1a and USE1 with the TRC pathway. In this study, Vti1a levels showed a reduction at the steady-state upon combined WRB/TRC40 knockdown compared to the control cells (**Fig. 30A**). USE1 showed a reduction at steady-state level in combined WRB/TRC40-silenced cells (**Fig. 29A**). A proportion of USE1 and Vti1a might be targeted by the TRC pathway *in vivo*, especially in the case of USE1. This calls for further analysis in order to dissect the reliance of these TA-proteins on the TRC pathway. Due to the unavailability of an antibody that detects endogenous Vti1a and USE1, a tagged-variant of these proteins in combination with the $TRC40_{D74E}$ trapping mutant may shed some light on any putative dependence on the TRC pathway.

However, from the TA-proteins tested some remained unaffected at steady-state level by the combined down-regulation of WRB and TCR40:

PTP1B was found to be inserted in an unassisted-manner into protein-free lipid bilayers (Brambillasca et al. 2006). Moreover, it showed increased membrane insertion in the presence of Hsp40/Hsc70 and it was therefore suggested not to be a TRC pathway substrate (Rabu et al. 2008). Similarly, PTP1B was proposed to not need cytoplasmic chaperones that require energy for the insertion into ER-membranes (Haßdenteufel et al. 2011). Likewise, as shown in this study, PTP1B levels remained unchanged at the steady-state upon WRB/TRC40 knockdown (**Fig. 32A**) and its subcellular localization did not change in the presence of $TRC40_{D74E}$ (**Fig. 17A, Fig. 19A**). Therefore, there is no evidence that PTP1B targeting relies on the TRC pathway *in vivo*.

Sec61β localization remained unaltered upon WRB/TRC40 or TRC40 knockdowns in this study (**Fig. 32C**). Sec61β was broadly discussed previously with respect to the discrepancies of studying it *in vitro* and *in vivo*. In addition to those studies mentioned, others have also tried to shed light on Sec61β biogenesis. Sec61β was considered substrate of the TRC pathway substrate whose insertion had to be facilitated by a molecular chaperone (Rabu et al. 2008). Similarly, Sec61β was found to require

energy-dependent cytoplasmic chaperones for its insertion into the ER-membrane (Haßdenteufel et al. 2011). Sbh1/2, homologs of Sec61β in yeast, were mislocalized in a Δ*get1*/Δ*get2* strain when strongly over-expressed (Schuldiner et al. 2008). However, another study reported no alteration in its subcellular localization in Δ*get3*, Δ*get1*/Δ*get2,* Δ*get1*/Δ*get2*/Δ*get3* strains when expressed at moderate levels (Rivera-Monroy et al. 2016). Sec61β levels at steady-state demonstrated no observable effect in HEK293T following the down-regulation of BAG6 (Q. Wang et al. 2011). Besides, a normal subcellular distribution of Sec61β was observed in TRC40-knockout pancreatic β-cells in mouse (Norlin et al. 2016). Finally, Sec61β was believed to fall at the boundary where the TRC pathway and the EMC pathway overlap in their substrate specificity. Sec61β can be inserted *in vitro* into RMs in a TRC40-dependent way. However, Sec61β-insertion is affected by the knockdown of EMC5 in HEK293T cells, demonstrating an overlapping dependence on both pathways (Guna et al. 2018). Taken together with my results, Sec61β can be inserted by TRC40 *in vitro* but it may not be targeted by the TRC pathway *in vivo*. Alternatively, the TRC- and EMC-pathways are possibly redundant *in vivo* offering Sec61β varied means of membrane targeting and insertion.

There are no studies in the literature regarding Stx18 and GOSR2 with the TRC pathway. Neither Stx18 nor GOSR2 were not affected at the steady-state level upon TRC40 or the combined WRB/TRC40 silenced cells in this study (**Fig. 31A**, **Fig. 31B**). Taken together, there is no evidence that either Stx18 or GOSR2 targeting relies on the TRC pathway *in vivo*. Because the antibodies against Stx18 and GOSR2 did not work for IF, the more direct test of trapping both proteins with $TRC40_{D74E}$ will have to rely on tagged-versions of Stx18 and GOSR2.

In the case of Vti1b, it was found cross-linked with TRC40 and its *in vitro* insertion into RMs was disturbed by the addition of WRBcc (a peptide containing the coil-coiled region of WRB that competes for binding to TRC40 thereby preventing the delivery of the TA-protein to the membrane) and was therefore considered to be a TRC pathway-dependent substrate. In contrast, Vti1b showed no effect on insertion upon the knockdown of EMC5 in HEK293T cells (Guna et al. 2018). However, Vti1b levels were not affected at the steady-state upon the combined WRB/TRC40 or TRC40 down-

regulated cells in this study (**Fig. 32B**). Taken together with my results, Vti1b targeting may not rely on the TRC pathway *in vivo* due to the potential existence of redundant pathways that help with the targeting of Vti1b when the TRC pathway was impaired. It was reported that the EMC pathway was not the redundant pathway facilitating Vti1b insertion (Guna et al. 2018).

Finally, SQS levels remained unaltered at the steady-state upon the combined WRB/TRC40 or TRC40 knockdown cells in this study (**Fig. 32D**). Likewise, SQS is not reported to interact with TRC40 and its *in vitro* insertion into RMs was not TRC40-dependent. Instead, its insertion *in vivo* was reported to be dependent on the EMC pathway and its subcellular distribution was altered upon the knockdown of EMC5 in HEK293T cells (Guna et al. 2018). Therefore, there is no evidence that SQS targeting relies on the TRC pathway *in vivo*.

There have been many discrepancies in the literature about the biogenesis of the aforementioned TA-proteins. Based on the findings of this study combined with others findings in the literature, many TA-proteins may depend on the TRC pathway for their targeting *in vivo*. Stx5 and Stx6 seem to be the most dependent on the TRC pathway, based on their steady-state levels when the TRC pathway is impaired and their altered subcellular localization upon $TRC40_{D74E}$. Curiously, some TA-proteins of which little was known, yielded interesting results: a proportion of USE1 and UBE2J1 may present a strong TRC-dependence. In contrast, other TA-proteins showed no change in their steady-state levels what may indicate that they present little or no TRC-dependency *in vivo*. It would be helpful to use $TRC40_{D74E}$ as a tool to further characterize the interaction of the TA-proteins with the TRC pathway. This can be complemented by *in vivo* experiments knocking-down TRC pathway components for studying steady-state levels and the subcellular localization of the TA-proteins.

4.2.3. Exploring the causes for the TRC-dependence of a TA-protein *in vivo*

There have been many factors taken into consideration: transmembrane segment length (Isenmann et al. 1998; Pedrazzini et al. 2000; Bulbarelli et al. 2002; Borgese, Brambillasca, and Colombo 2007), C-terminal tail length and charge (Elgersma et al. 1997; Kuroda et al. 1998; Mullen and Trelease 2000; Horie et al. 2002; Borgese, Brambillasca, and Colombo 2007; Yagita, Hiromasa, and Fujiki 2013; Costello, Castro, Camões, et al. 2017), membrane composition (Borgese, Brambillasca, and Colombo 2007), the cytoplasmic domain (Linstedt et al. 1995; Misumi et al. 2001; Joglekar et al. 2003) and hydrophobicity of the TMD (Borgese, Colombo, and Pedrazzini 2003; Borgese, Brambillasca, and Colombo 2007). Actually, hydrophobicity has always been regarded as an important factor for organelle-targeting of the TA-proteins. Other *in vitro* and *in vivo* studies have also studied this physicochemical property (Rao et al. 2016; Guna et al. 2018; F. Wang et al. 2010; Costello, Castro, Camões, et al. 2017). This study tries to shed some light on some of the potential causes that determine the *in vivo* TRC-pathway dependence of a TA-protein.

4.2.3.1. Hydrophobicity is a major contributor for the TRC-dependence *in vivo*

TMD hydrophobicity has always been considered as a relevant factor in TA-protein biogenesis. It has been proposed that moderately hydrophobic TMDs were substrates of the TRC pathway (F. Wang et al. 2010; Rao et al. 2016; Costello, Castro, Camões, et al. 2017; Guna et al. 2018; Borgese, Colombo, and Pedrazzini 2003; Borgese, Brambillasca, and Colombo 2007). From the different TMD-hydrophobicity analyses carried out (**Fig. 33-36**), it is clear that hydrophobicity is indeed a determinant factor in the fate of the endogenous TA-proteins *in vivo*. The majority of the TA-protein affected by WRB/TRC40 knockdown presented moderate-to-high hydrophobic TMDs whereas the majority of the unaffected TA-proteins had low hydrophobic TMDs. Using the GRAVY scoring (based on the Kyte and Doolittle scale) the group of affected and unaffected TA-proteins could be separated (**Fig. 35A**). However, for the other hydrophobicity scales, some TA-proteins remained in an intermediary region, similar to the Sec61β-TMD hydrophobicity score, with no clear separation between affected

and unaffected groups. This result was independent of the scale used: the TMD tendency scale (**Fig. 33A**), the Kyte and Doolittle scale (**Fig. 34A**) and for the apparent free-energy (**Fig. 36A**). The answer to why proteins that have TMDs with very similar hydrophobicity yielded different behaviors may lie in the amino acid composition of the TMDs. Helical wheels projections, generated from the predicted TMD sequences, showed little evidence of which residues could be crucial for the TRC-pathway dependence (**Fig. 54, Fig. 55**). However, a deeper analysis of the TMD sequences from those TA-proteins sensitive to the WRB/TRC40 knockdown yielded an interesting result. The sequence logo showed the relevance of aromatic amino acids at the beginning of the TMD and the presence of isoleucines, phenylalanines, leucines or valines (**Fig. 56A**). The algorithm chosen for the logo representation highlights amino acid enrichment and emphasizes the relevant parts (Thomsen and Nielsen 2012). It is not a consensus sequence and cannot be treated as such, since neither the experimental approach nor the sample size is large enough for making that claim. Other than that, it is an analysis that showed that the presence of an aromatic amino acid was relevant at either the beginning or the end of the TMD. Moreover, the central part of the TMD also appeared to be important since the relative weight of certain hydrophobic amino acids (almost exclusively isoleucines, phenylalanines, leucines) was higher. In contrast, the sequence logo for the TMD of the unaffected TA-proteins showed an enrichment in aromatic amino acids in the last third of the TMD (**Fig. 56B**). The enrichment in hydrophobic amino acids is lower than in the case of the affected TA-protein TMDs.

Taken together, hydrophobicity is an important factor in TA-targeting as seen in the TMD-hydrophobicity dot-plots, especially using the GRAVY score. However, hydrophobicity on its own cannot explain the *in vivo* dependence on the TRC pathway for every TA-protein, especially those with moderately hydrophobic TMD close to the hydrophobicity of Sec61β. The zone of hydrophobicity close to Sec61β could be a region where other pathways overlap *in vivo*, as pointed out for certain TA-proteins in a previous study (Guna et al. 2018).

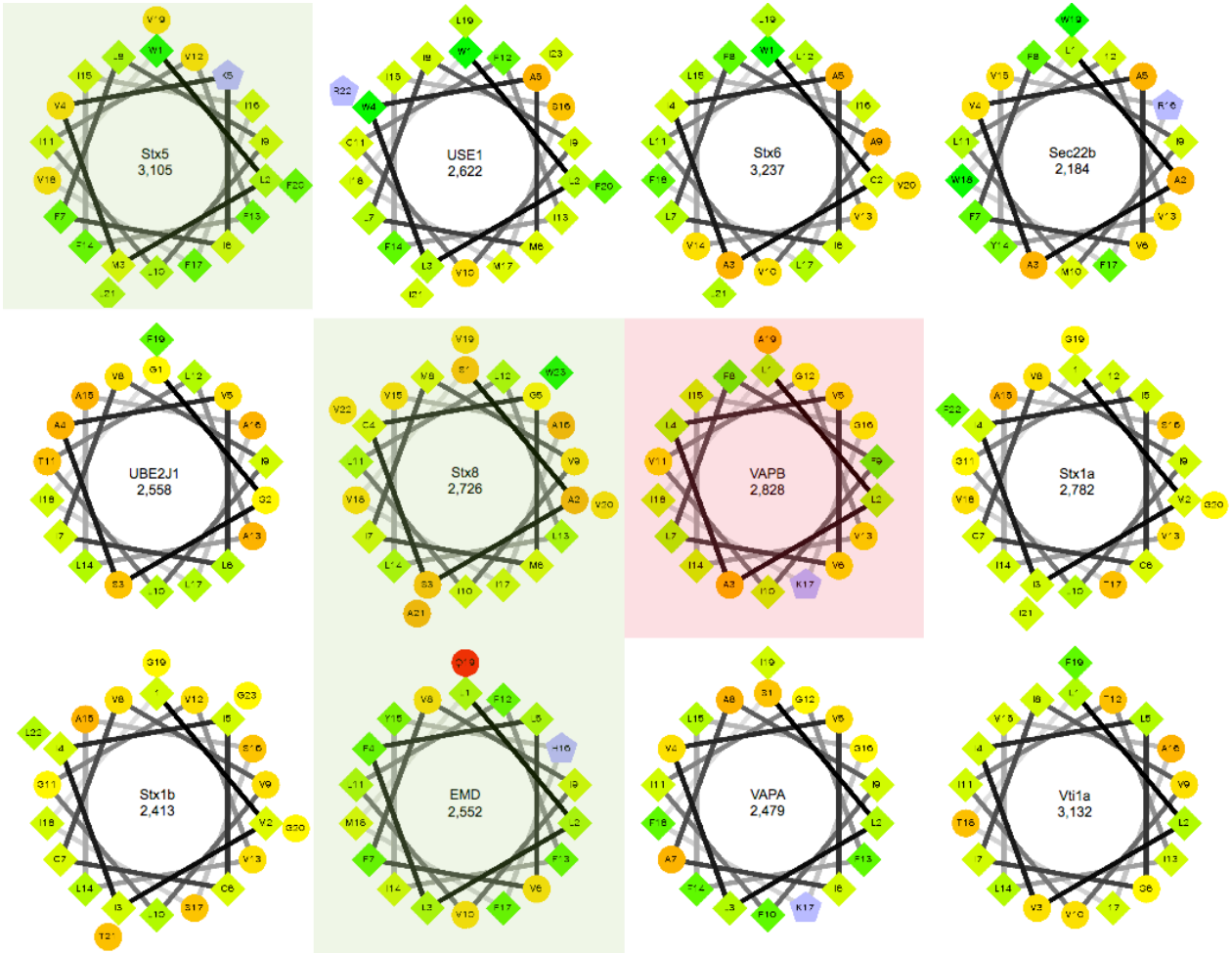

Figure 54. Helical wheel projections of TMDs of the TA-proteins affected by the WRB/TRC40 knockdown. TA-proteins were ordered according to the affectation in steady-state level in the knockdown cells, descendent order. Numbers indicate the TMD hydrophobicity score according to the hydrophobicity scale developed by (Kyte and Doolittle 1982) divided by the length of the TMD (in aa), for obtaining the GRAVY score. Those TA-proteins affected by the presence of $TRC40_{D74E}$ are highlighted in green or in red if they remain unchanged. The helical wheel analysis was done using the application wheel.pl v1.4 (Zidovetzki et al. 2003). Available here: http://rzlab.ucr.edu/scripts/wheel/wheel.cgi

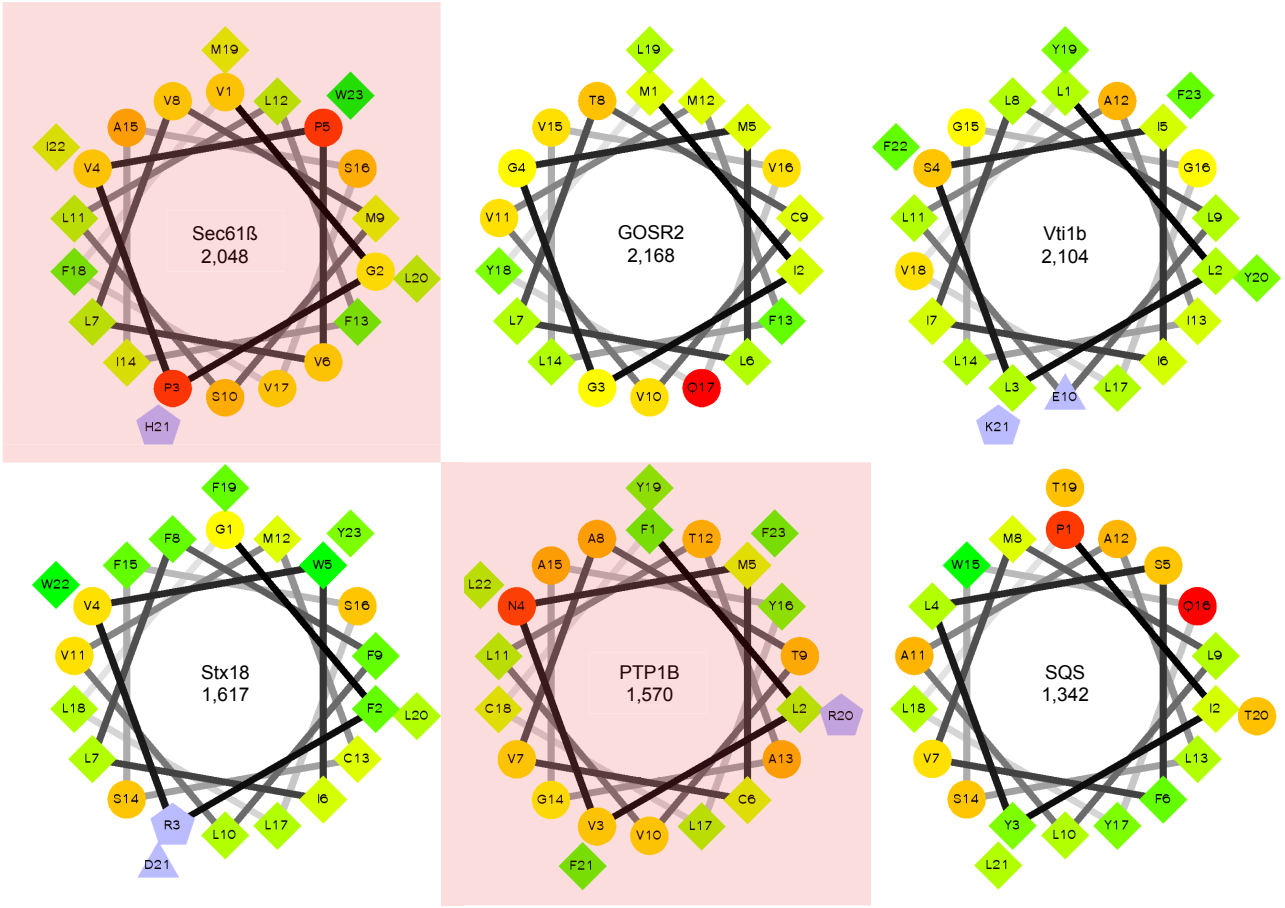

Figure 55. Helical wheel projections of TMDs of the TA-proteins that remained unaffected upon the WRB/TRC40 knockdown. TA-proteins whose steady-state levels were not altered upon the WRB/TRC40 knockdown were displayed in a random order. Numbers indicate the TMD hydrophobicity score according to the hydrophobicity scale developed by (Kyte and Doolittle 1982) divided by the length of the TMD (in aa), for obtaining the GRAVY score. Those TA-proteins affected by the presence of $TRC40_{D74E}$ are highlighted in green or in red if they remain unchanged. The helical wheel analysis was done using the application wheel.pl v1.4 (Zidovetzki et al. 2003). Available here: http://rzlab.ucr.edu/scripts/wheel/wheel.cgi

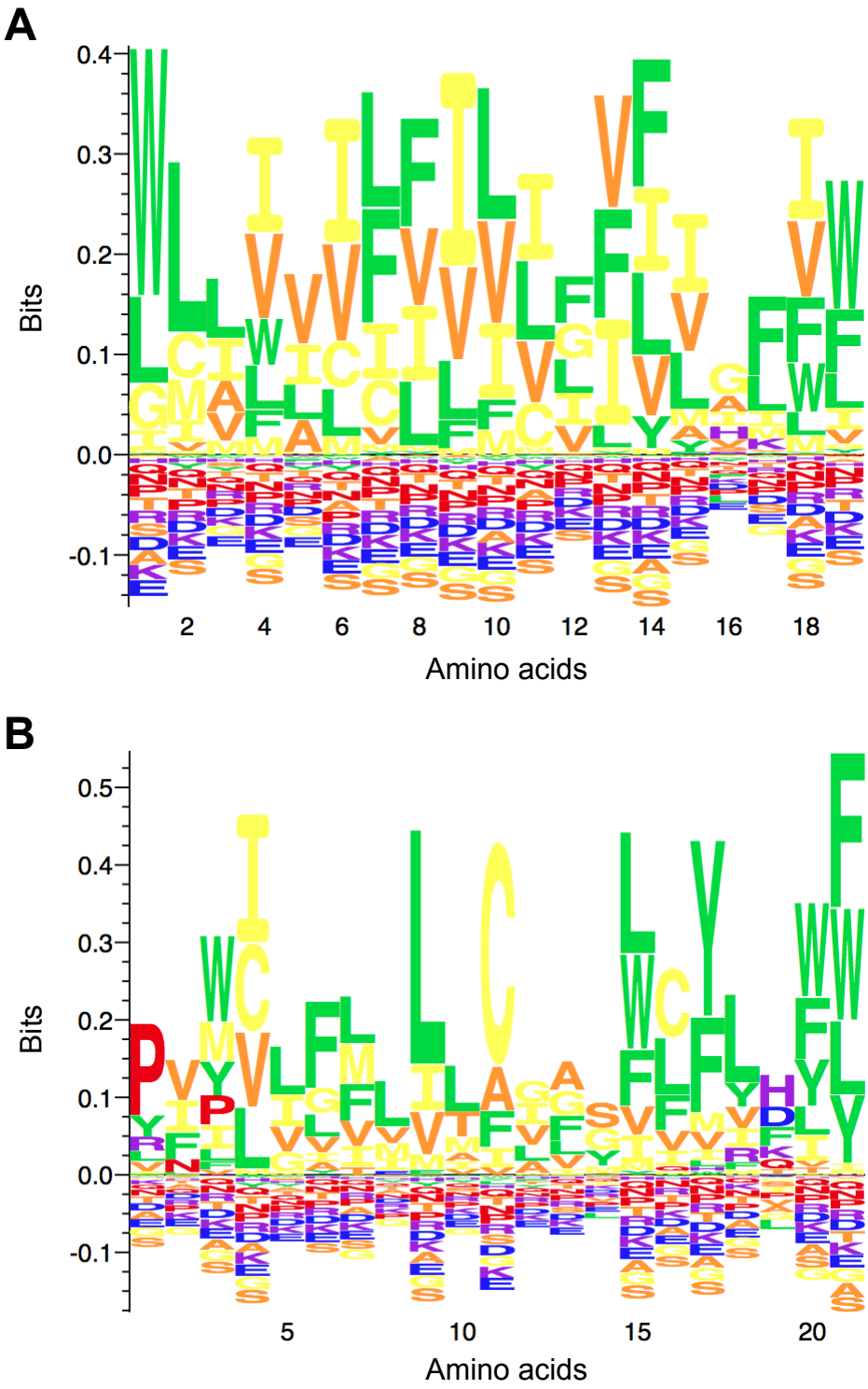

Figure 56. Sequence logo of the TMDs of TA-proteins tested upon the WRB/TRC40 knockdown. **(A)** Sequence logo of the twelve 19 aa TMDs of the affected TA-proteins. **(B)** Sequence logo of the six 21 aa TMDs of the unaffected TA-proteins. The probability weighted Kullback-Leibler logo. The height of the amino acids represents the probability times their log-odds score. The code of color used is similar to the one used in the helical wheel projections (**Fig. 54, Fig. 55**). The sequence logo was generated using the web-based generator Seq2Logo 2.0(Thomsen and Nielsen 2012). Available here: http://www.cbs.dtu.dk/biotools/Seq2Logo/. Parameters used for the analysis are available in section 7.5.3 within Appendix.

4.2.3.2. The silent role of the cytoplasmic domain in the subcellular localization of TA-proteins

Hydrophobicity cannot entirely explain the results regarding the dependence of TA-proteins on the TRC pathway. There must be additional factors. TA-protein biogenesis has always been connected to the lack of a signal sequence and the post-translational insertion into membranes, features that placed the focus on the TMD. However, the role of the cytoplasmic domain in TA-protein biogenesis remains unclear. In a study preceding the discovery of TA-insertion pathways, it was reported that GFP fused to the TMD of rat Bet1 was not localized properly (Joglekar et al. 2003). Shortly after the TRC40 characterization, TRC40 was found to be cross-linked with the N-terminal domain of Sec61β (Favaloro et al. 2008) as apposed to the findings of another study in which no cross-linking was observed in the absence of the Sec61β-TMD (Stefanovic and Hegde 2007). In a similar fashion, Get3 was reported to interact with Sec22p lacking its TMD (Yamagata et al. 2010) but another study showed that there was no evidence of interaction with Get3 in the absence of the TMD of Sec22p (F. Wang et al. 2010). VAPB was reported to interact with TRC40 but TRC40 was unable to interact with a VAPB FFAT-binding defective mutant (K87D/M89D) and a VAPB ΔMSP construct (even though the TMD of VAPB was present) (Baron et al. 2014). Some SNARE proteins were observed to be typically localized despite the deletion of their TMD (L. Chen, Lau, and Banfield 2016). The expression of yeast Sed5 in COS-7 cells showed it localized to the Golgi. The swap of the Sed5 TMD by those of the yeast TA-proteins Pep12, Sso1 or Bos1 did not yield any change in the Golgi localization of yeast Sed5 (Banfield et al. 1994). In this study the ATPase-impaired TRC40 mutant which carried two mutations in the hydrophobic TA-binding groove ($TRC40_{D74E/L190D/I193D}$) was still able to alter the subcellular localization of Stx5 (**Fig. 13A**). This would suggest that either TRC40 binds Stx5 via a different binding region, compared to other TA-proteins, or that Stx5 cytoplasmic domain has additional contact sites, apart from the ones of the TMD, that were not disrupted by the mutations. The Stx5 cytoplasmic domain presented thermal instability and unfolding propensity in an *in vitro* aggregation assay (Rivera-Monroy et al. 2016). This thermal instability can be prevented by the presence of TRC40 (Rivera-Monroy, unpublished). Likewise, the

cytoplasmic domain of Stx5 was reported to be important for the Golgi localization of the short isoform of Stx5 (Misumi et al. 2001). Stx5 did not required the presence of the TMD, but requires the last one hundred amino acids (which contains the t-SNARE coiled-coil domain) for being Golgi-localized (Misumi et al. 2001). Surprisingly, a construct lacking these last one hundred amino acids of Stx5 was localized in the cytoplasm (Misumi et al. 2001). In the same study two more TA-proteins were analyzed: Giantin and Golgin-84. Golgin-84 and Giantin Golgi-localization were unaffected by the lack of their respective TMDs (Misumi et al. 2001). Golgi-84 had a cytoplasmic localization upon the deletion of the last 160 amino acids (Misumi et al. 2001). The swap of the TMDs of Stx5, Giantin or Golgin-84 with the one of Stx2 (a TA-protein localizing in plasma membrane) did not alter the Golgi subcellular localization of those proteins. Along the same lines, another study showed that just the last 51 amino acids were necessary for the Golgi localization of Golgin-84 (Bascom, Srinivasan, and Nussbaum 1999). These 51 amino acids included the C-tail, the TMD and 20 amino acids upstream of the TMD where no coiled-coil domain was present. In contrast, Stx1 was localized in the cytoplasm and not in membranes upon the truncation of the TMD (Vogel, Cabaniols, and Roche 2000). Finally, a very interesting study focused on the role of the cytoplasmic domain in SNARE proteins (K Kasai and Akagawa 2001). In this publication, the authors studied five TA-proteins: Stx1, Stx5, Stx6, Stx7 and Stx8. They tested all of them in rat cell lines for their subcellular localization in all combinations of each cytoplasmic domain with each TMD. The swap of the original TMDs with the Stx1 TMD (Stx5-TMD1, Stx6-TMD1, Stx7-TMD1, Stx8-TMD1) did not alter the reported localization of the syntaxin proteins suggesting that the cytoplasmic domain was the one determining the final localization. The combination of these syntaxins with the TMD of Stx5 (Stx1-TMD5, Stx6-TMD5, Stx7-TMD5, Stx8-TMD5) resulted in *cis*-Golgi localization, indicating that the Stx5 TMD abolishes the transport out of the Golgi. Chimaeras of the cytoplasmic domain of Stx1 with the TMDs of Stx6, Stx7 and Stx8 (Stx1-TMD6, Stx1-TMD7, Stx1-TMD8) were observed at the plasma membrane, where Stx1 is localized. This would indicate that the Stx1 cytoplasmic domain dictates the subcellular localization of those constructs. To sum up, the cytoplasmic domain of this subset of SNAREs was responsible for the final subcellular localization of the chimeric constructs (when carrying the TMDs of Stx1, Stx6, Stx7, Stx8) unless they had the TMD of Stx5 in which case the localization was the one of Stx5, at the Golgi (K Kasai and Akagawa 2001). These results indicate

that Get3/TRC40 could potentially interact with the cytoplasmic domains of certain TA-proteins and that the cytoplasmic domain might play a very important role in the biogenesis of some TA-proteins.

4.2.3.3. Potential downstream consequences may contribute to the readout

In spite of the role that TMD hydrophobicity and the cytoplasmic domain of the TA-proteins play, it is important to consider the impact of downstream factors present. *In vivo* knockdown studies of endogenous proteins may lead to downstream effects such as the destabilization of a protein complex due to the perturbation of an interactor partner. Some of the TA-proteins studied may have had their steady-state levels reduced due to the destabilization of a binding partner that was affected by the knockdown. In this case it would be an indirect effect of the loss of the downregulated protein that characterizes the phenotype of the knockdown. Hence the mechanistic discussion proposed in this section would not apply.

4.2.4. Physiological effects of the TRC-pathway impairment

In recent times, several studies have reported some physiological consequences of the impairment of the TRC pathway. In one of these studies, a mouse model carrying WRB-deficient inner hair cells presented synaptic hearing impairment (Vogl et al. 2016). In addition, the same phenotype was reported in zebrafish (Vogl et al. 2016; Lin et al. 2016). Reduced levels of otoferlin, a tissue-specific TA-protein in inner-ear hair cells, were observed in WRB-deficient mice (Vogl et al. 2016). Dysfunction of otoferlin is connected with deafness and auditory neuropathies (Varga et al. 2006). In another study, the authors generated a Wrb-knockout zebrafish model that suffered an impairment of the synaptic transmission in photoreceptors (Daniele et al. 2016). In the same study, the TRC40-knockdown mirrored the phenotype shown in the Wrb-knockout (Daniele et al. 2016). A TRC40-knockout specific to the pancreatic β-cells in mice led to defects in retrograde transport and ER-stress. These mice

developed hypoinsulinemia and defects in the insulin secretion that led to diabetes (Norlin et al. 2016). TRC40 loss in mouse pancreatic progenitor cells provoked redistribution of Stx5 and Stx6 and the fragmentation of the Golgi. TRC40 was found to be required for pancreatic cell survival (Norlin, Parekh, and Edlund 2018). Interestingly, GET pathway impairment in *Arabidopsis thaliana* results in reduced SNARE levels (Xing et al. 2017). Likewise, SYP72, a plant SNARE ER-resident protein, is found accumulated in cytosol in *get3-1*, *get1* and *get4* knockouts in *A. thaliana* (Srivastava et al. 2017).

In this study, eleven TA-proteins were decreased at the steady-state in WRB/TRC40-knockdown cells (**Fig. 26B**). Seven out of these affected TA-proteins are SNARE proteins involved in membrane-trafficking. Stx5 and Stx6 were among them. The levels of these two SNAREs were found to be reduced at steady-state or redistributed in the cell when TRC40 or WRB were missing (Rivera-Monroy et al. 2016; Norlin et al. 2016; Norlin, Parekh, and Edlund 2018). As recently mentioned, the knockout of TRC40 in β-cells resulted in plasma membrane-to-TGN and ER-to-Golgi retrograde transport defects (Norlin et al. 2016). Hence, alterations of SNARE-proteins membrane-targeting by the TRC pathway are linked thus an impairment of this pathway could lead to membrane-trafficking defects. The decrease in the steady-state levels of these important SNAREs, in WRB/TRC40 down-regulated cells, could potentially affect several transport pathways (**Fig. 56A**). The steady-state levels of other SNAREs such GOSR2, Vti1b and Stx18 remained unchanged upon the WRB/TRC40 knockdown. Other SNARE proteins were not tested in this study. From the SNARE complexes shown in **Fig. 57A** all are TA-proteins but Ykt6, SNAP23, SNAP25, SNAP29. The remaining SNARE TA-proteins present high TMD-hydrophobicity (**Fig. 57B**) which, according to what was previously discussed, seems to be lead to a reliance on the TRC-pathway. However, the role of the cytoplasmic domain in TA-protein targeting was also discussed, especially with regard to SNARE proteins. Therefore, among the physiological effects derived from the impairment of the TRC pathway, the most prominent one is the disruption or malfunctioning of membrane-trafficking due to the perturbation of SNARE-protein homeostasis. Further investigation is required in this regard to determine the scope of the TRC pathway impairment in membrane-trafficking.

A

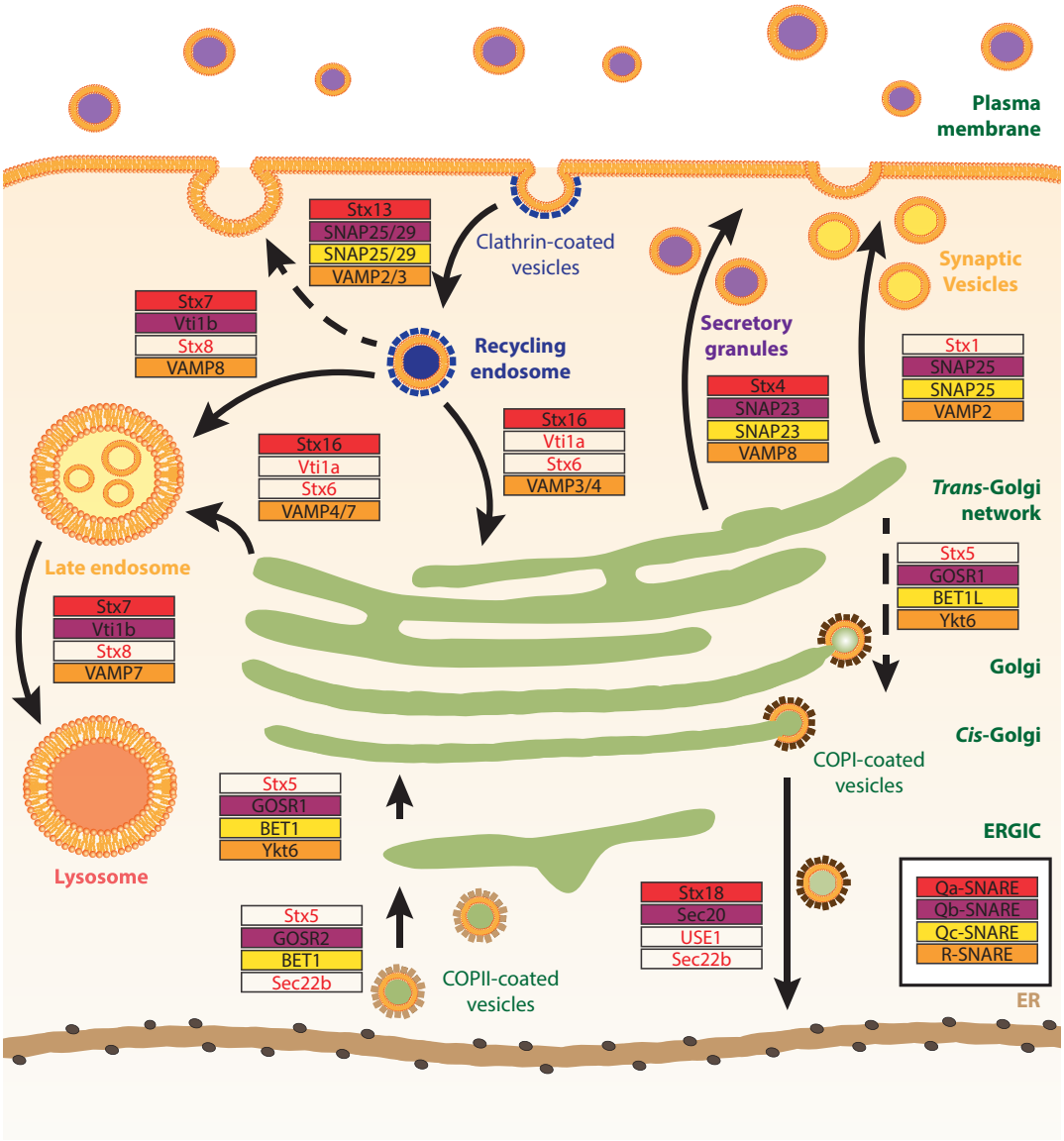
Plasma membrane
Stx13
SNAP25/29
SNAP25/29
VAMP2/3
Clathrin-coated vesicles
Stx7
Vti1b
Stx8
VAMP8
Recycling endosome
Secretory granules
Synaptic Vesicles
Stx1
SNAP25
SNAP25
VAMP2
Stx4
SNAP23
SNAP23
VAMP8
Stx16
Vti1a
Stx6
VAMP4/7
Stx16
Vti1a
Stx6
VAMP3/4
Trans-Golgi network
Late endosome
Stx5
GOSR1
BET1L
Ykt6
Stx7
Vti1b
Stx8
VAMP7
Golgi
Cis-Golgi
COPI-coated vesicles
Lysosome
Stx5
GOSR1
BET1
Ykt6
ERGIC
Qa-SNARE
Qb-SNARE
Qc-SNARE
R-SNARE
Stx18
Sec20
USE1
Sec22b
Stx5
GOSR2
BET1
Sec22b
COPII-coated vesicles
ER

B

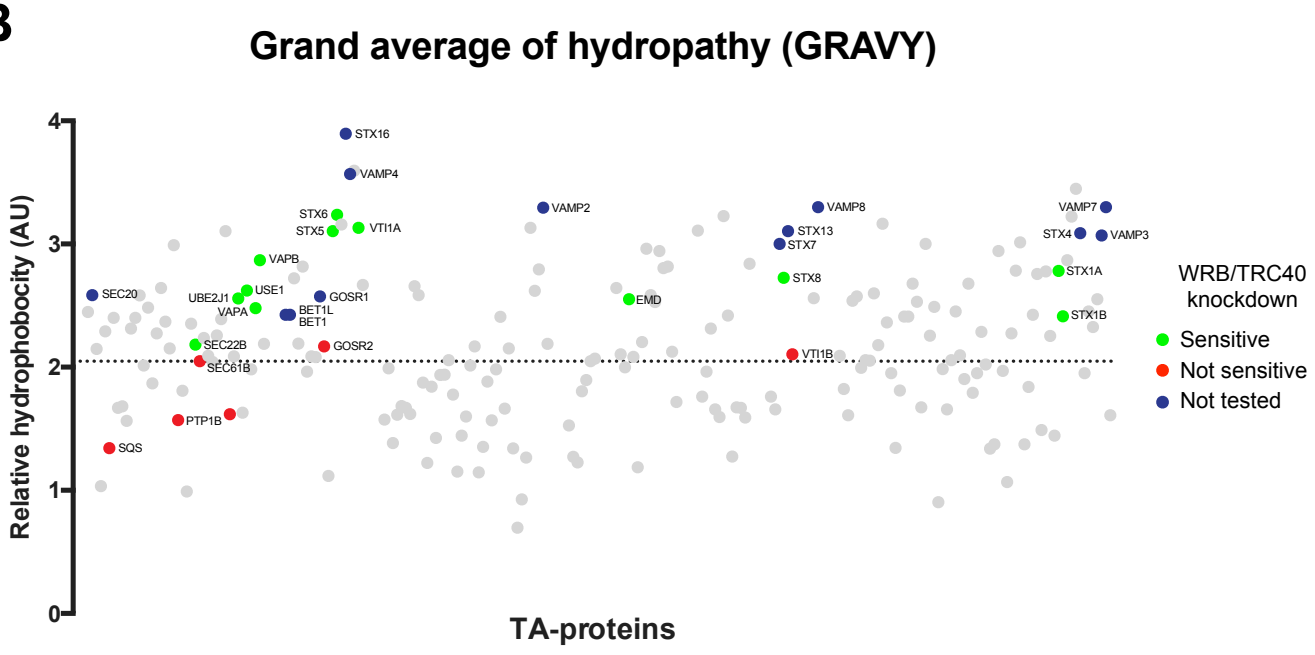
Grand average of hydropathy (GRAVY)
Relative hydrophobocity (AU)
TA-proteins
STX16
VAMP4
STX6
STX5
VTI1A
VAMP2
VAMP8
STX13
STX7
VAMP7
STX4
VAMP3
VAPB
STX8
STX1A
SEC20
UBE2J1
USE1
VAPA
GOSR1
BET1L
BET1
EMD
STX1B
SEC22B
SEC61B
GOSR2
VTI1B
PTP1B
SQS
WRB/TRC40 knockdown
Sensitive
Not sensitive
Not tested

Figure 57. The SNARE complexes in membrane-trafficking pathways in WRB/TRC40 knockdown cells. (A) QR-SNARE classification of the different SNAREs and the membrane trafficking pathways they are involved in (Bock et al. 2001; Hong 2005). The non-colored slots with the red-labelled protein represent the TA-proteins affected by the WRB/TRC40 knockdown. Adapted from: (Jahn and Scheller 2006; T. Wang, Li, and Hong 2017). **(B)** TA-proteins tested in this study and SNAREs not tested dot-plots. Dot-plots of the TMD hydrophobicity score according to the hydrophobicity scale developed by (Kyte and Doolittle 1982) divided by the length of the TMD (in aa), for obtaining the GRAVY score, for all the TA-proteins shown in **Table 17**. The transmembrane domain region was predicted using the TMHMM algorithm (Krogh et al. 2001) or UniProt prediction if TMHMM prediction was missing. TA-proteins affected by the WRB/TRC40 knockdown are depicted in green, unaffected in red and not tested SNAREs in dark blue. The dotted line represents the Sec61β TMD hydrophobicity score, marking the approximate overlap between the EMC pathway and the TRC pathway as proposed in a recent paper (Guna et al. 2018).

4.3. The enigmatic role of BAG6 in TA-protein biogenesis

The TRC pathway in mammals and the GET pathway in yeast are conserved. The proteins constituting this pathway are conserved (Get2 and CAML are functional homologs) except mammalian BAG6, which is not present in yeast (Leznicki et al. 2010; Mariappan et al. 2010). According to the literature there is another major difference between these two pathways beside the presence of BAG6; namely the interactions within the pre-targeting complex. One of the main reasons for this difference resides in the fact that TRC35 and UBL4A cannot directly interact, in contrast to yeast where they do directly interact (Mock et al. 2015) (**Fig. 58A**). The β-loop involved in the Get4-Get5 interaction interface is missing in TRC35 (Chartron et al. 2010) whereas UBL4A lacks the N-terminal domain present in Get5 that mediates the interaction between Get4 and Get5 (Chartron et al. 2010; Mock et al. 2015). Instead, TRC35 and UBL4A interact with BAG6, which serves as a scaffolding protein. TRC35 docks on the NLS of BAG6 thereby masking it and UBL4A is tethered to the BAG domain of BAG6 (Mock et al. 2015; Kuwabara et al. 2015; Mock et al. 2017). This heterotrimeric BAG6 complex is believed to be responsible for collecting the nascent substrates after their release from the ribosome (Mariappan et al. 2010). Subsequently, SGTA is recruited, via the UBL domain, to either BAG6 or preferentially UBL4A (Xu et

al. 2012; Leznicki et al. 2013; Darby et al. 2014) (**Fig. 58B**). Therefore, BAG6 is the pre-targeting-complex cornerstone protein. In fact, a truncated version of BAG6 containing just the C-terminal domain (which comprises the NLS and the BAG domain) was sufficient to facilitate the handoff of a TA-protein to TRC40 *in vitro* (Mock et al. 2015; Shao et al. 2017).

Surprisingly, none of the seventeen TA-proteins tested showed a reduction of protein at the steady-state levels in BAG6 down-regulated cells (**Fig. 28-32**). In contrast, three out of seventeen TA-proteins presented an increase at the steady-state level: UBE2J1 (**Fig. 29C**), Stx18 (**Fig. 31A**), GOSR2 (**Fig. 31B**). It is known from this study that the down-regulation of BAG6 does not affect the steady-state levels of downstream components of the pathway such as WRB (**Fig. 27B**), CAML (**Fig. 27D**) or TRC40 (**Fig. 27A**). However, it has been reported that upon the knockdown of BAG6, the steady-state levels of TRC35 and UBL4A are severely affected (Krenciute et al. 2013).

According to the model proposed in the literature, the described interactions within the pre-targeting complex are necessary for the TA-protein transfer to TRC40. Thus, the lack of any protein forming part of the heterotrimeric BAG6 complex would abrogate the handoff of the TA-protein to TRC40 *in vitro* (Shao et al. 2017). Likewise, the immunodepletion of BAG6 in RRL inhibited the insertion of Sec61β into the membrane (Leznicki et al. 2010). In addition, mutations in either SGTA or UBL4A disrupting their interaction interface, led to a strong loss of TA-protein handoff to TRC40 (Mock et al. 2015). It is reported that TRC40 is a bad competitor for free TA-proteins compared to other chaperones (Shao et al. 2017). Interestingly, Get3 has substrate preferences very close to those of Sgt2 (Rao et al. 2016). Moreover, TRC40 alone does not induce the release of the TA-protein loaded in SGTA, indicating that the potential SGTA-TRC40 interaction is not enough for the TA-protein handoff (Shao et al. 2017). Although there is some contradiction in this point since TRC40 itself is able to receive some TA-substrates from SGTA (Mock et al. 2015). Taking into consideration the elucidated hierarchy of TA-protein handoff within TRC-pathway components, this raises the question as to why the steady-state levels of the TA-proteins in the membrane fractions were not reduced in BAG6-knockdown cells when compared with the control cells.

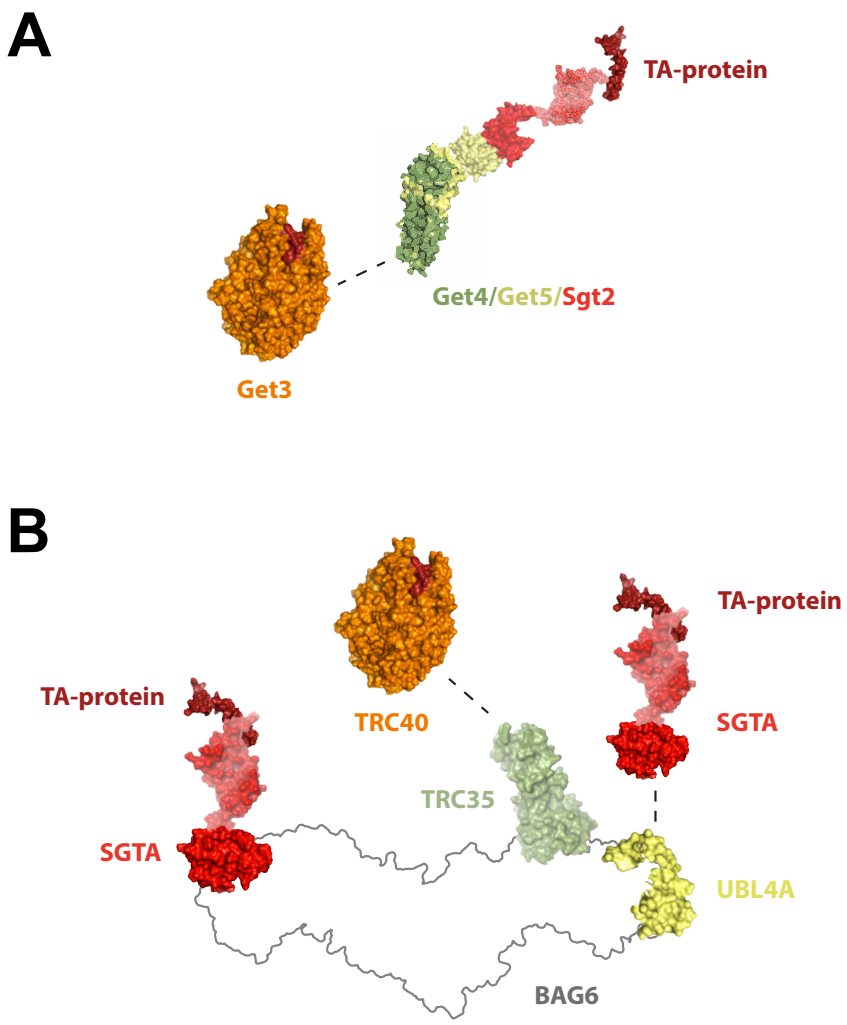

Figure 58. Differences in the pre-targeting complex between the yeast GET pathway and the mammalian TRC pathway. (A) Get4-Get5 interaction gets in close proximity Get3 and Sgt2 loaded with the TA-protein. **(B)** BAG6 heterotrimeric complex serves as a scaffolding protein that gets in close proximity TRC40 and SGTA loaded with the TA-protein. The PDB IDs are the following: Get3 (4XTR), Get4-Get5 (4PWX), Sgt2 (3ZDM, 5LYP), TA-protein (2LPF), SGTA (4CPG, 5LYP), TRC35 (6AU8), UBL4A (4X86). TRC40 is represented with the Get3 protein structure and BAG6 is depicted as a silhouette due to the lack of structure for both.

BAG6 knockdown was highly efficient (**Fig. 27C**). The BAG6 siRNA used (siBAG6 #1) had been successfully used in previous studies (Minami et al. 2010; Suzuki and Kawahara 2016; K. Yamamoto et al. 2017) and it was validated with our custom-made antibodies by IF and WB (**Fig. 37A, Fig. 37B**). BAG6 has several isoforms due to splicing (Kämper et al. 2012). The siBAG6#1 target sequence is present in all the isoforms reported in UniProt and in the literature (Kämper et al. 2012) ruling out the possibility of a siRNA-insensitive BAG6 isoform that was taking over the TA-protein

targeting. BAG6 and SGTA play a role in the quality control of MLPs (Hessa et al. 2011; Leznicki et al. 2013; Rodrigo-Brenni, Gutierrez, and Hegde 2014; Wunderley et al. 2014). Via its UBL domain, BAG6 can recruit the E3 ubiquitin ligase RNF126 (Rodrigo-Brenni, Gutierrez, and Hegde 2014; Krysztofinska et al. 2016) which ubiquitylates proteins and targets them for proteasomal degradation. For instance, it has been reported that the ERAD substrate TCRα accumulates upon BAG6 down-regulation (Q. Wang et al. 2011). Hence, the increased steady-state levels of Stx18, GOSR2 and UBE2J1 in the absence of BAG6 may be explained by the fact that BAG6 is implicated in their degradation.

BAG6 is not essential for a subset of TA-proteins since their steady-state levels remained unchanged in membranes in this study. Interestingly, it was proposed that the BAG6 complex does not have a big role for TA-protein biogenesis since Sec61β and UBE2J1 steady-state levels remained unaffected in BAG6-knockdown cells and in UBL4A-knockdown cells (Q. Wang et al. 2011). In contrast to the BAG6-knockdown cells, many TA-proteins showed decreased steady-state levels in WRB/TRC40-knockdown cells. Since the heterotrimeric BAG6 complex is reported to be severely affected upon the down-regulation of BAG6, SGTA or other unknown chaperones may insulate the nascent TA-protein. SGTA-to-TRC40 TA-handoff has been reported to be slow and poor (Mock et al. 2015) or nonexistent (Shao et al. 2017). Regardless of the upstream chaperone that delivers the TA-protein to TRC40, the steady-state levels of the TA-proteins are unaffected suggesting that redundancies may exist in this upstream system. This also suggests that an alternative pathway might exist where another cytoplasmic effector handles the TA-protein in the absence of TRC40 (not so relevant in the cases of Stx5, VAPB, UBE2J1 that were affected by the knockdown of TRC40). CaM and ubiquilins have been reported to chaperone low-hydrophobic TMDs of TA-proteins (Itakura et al. 2016; Suzuki and Kawahara 2016; Guna et al. 2018), as well as Hsp40/Hsc70 (Rabu et al. 2008). Nevertheless, the substrates covered by the TRC pathway have moderate-to-high hydrophobic TMDs (Borgese, Brambillasca, and Colombo 2007; Costello, Castro, Camões, et al. 2017; Guna et al. 2018). Therefore, the role and the relevance of BAG6 within the TRC pathway regarding the TA-protein biogenesis have to be redefined in the light of the results obtained *in vivo* in this study.

4.4. The fragile internal balance of the TRC pathway

Besides the aforementioned changes in the steady-state levels of TA-proteins, it was remarkable that the steady-state levels of the TRC pathway components were also altered upon the loss of other proteins of the pathway. The steady-state levels of the heterodimeric receptor of the TRC pathway, WRB and CAML, were decreased upon the down-regulation of TRC40 (**Fig. 26B**, **Fig. 27B, Fig. 27D**). Additionally, CAML was severely affected when knocking-down WRB (**Fig. 26B**, **Fig. 27D**), as previously described in literature (Rivera-Monroy et al. 2016; Sara Francesca Colombo et al. 2016; Haßdenteufel et al. 2017). The interdependence of the GET receptor (Get1, Get2) stability was already described (Schuldiner et al. 2008). Moreover, it was also reported for the TRC receptor (Vilardi et al. 2014). In WRB-knockout cardiomyocytes, TRC40 was severely decreased at steady-state level (Rivera-Monroy et al. 2016) as well as in WRB-knockdown HeLa cells (Rivera-Monroy et al. 2016). Besides, TRC40 was reported to be slightly decreased upon CAML knockdown (Sara Francesca Colombo et al. 2016). Interestingly, the TRC40 steady-state levels in WRB-knockdown HeLa cells can be rescued with chloroquine (Rivera-Monroy et al. 2016), a drug that prevents the acidification of lysosomes by inhibiting lysosomal proteases (Mizushima, Yoshimori, and Levine 2010).

Regarding the proteins at the pre-targeting complex, BAG6 steady-state levels upon the loss of WRB and TRC40 were severely decreased (**Fig. 26A**, **Fig. 27C**). In addition, BAG6 steady-state levels remained unaffected upon the silencing of TRC40 (**Fig. 26A**, **Fig. 38C**), in line with what was shown in previous studies *in vivo* (Baron et al. 2014) and TRC40-immunodepleted RRL (Mariappan et al. 2010). Similar to the results in HeLa cells, BAG6 steady-state levels were decreased in WRB-KO cardiomyocytes (**Fig. 40B**). It is also known from the literature that the loss of SGTA does not have an impact on BAG6 protein level at the steady-state (Xu et al. 2012). In contrast, the knockdown of BAG6 affects the levels of TRC35 and UBL4A, both being decreased. Likewise, the BAG6-immunodepletion of RRL has the same consequence (Mariappan et al. 2010). Reciprocally, the simultaneous loss of TRC35 and UBL4A also decreases the levels of BAG6 (Krenciute et al. 2013) whereas individual knockdowns of TRC35

or UBL4A does not have an effect on BAG6 levels at the steady-state (Xu et al. 2012; Krenciute et al. 2013). In contrast, the immunodepletion of UBL4A in RRL results in undetectable protein levels of BAG6 and TRC35 (Mariappan et al. 2010).

Interestingly, the mRNA levels of TRC35 and UBL4A remained unchanged upon the knockdown of BAG6 (Krenciute et al. 2013). The same is true for CAML mRNA in the case of the WRB knockdown, which remains unaffected suggesting that the instability was at protein level (Rivera-Monroy et al. 2016; Sara Francesca Colombo et al. 2016). However, a recent publication reported that the loss of CAML destabilizes WRB mRNA rather than the protein itself, resulting in reduced WRB protein at the steady-state level, as mentioned previously (Sara Francesca Colombo et al. 2016). This complex interplay has been summarized in the following figure (**Fig. 59A**).

Considering the available data reflected in the figure, a first glance shows two clusters in terms of interdependence: one grouping the heterotrimeric BAG6 complex proteins and another one downstream of the pathway grouping TRC40 and TRC receptor, WRB and CAML (**Fig. 59A, Fig. 59B**). The loss of BAG6 has direct effect on TRC35 and UBL4A stability at protein level. It is known that BAG6 prevents the degradation of TRC35 by ubiquitylation via RNF126 (Mock et al. 2017). Individual knockdowns of TRC35 and UBL4A do not alter the steady-state levels of BAG6 but the double knockdown of TRC35/UBL4A decreases the steady-state levels of BAG6. This indicates that BAG6 on the one hand and TRC35/UBL4A on the other hand are hierarchically at the same level (**Fig. 59B**). However, TRC35 knockdown leads to decreased UBL4A at steady-state levels indicating that TRC35 plays a role in UBL4A stability but UBL4A knockdown does not have a role in TRC35 steady-state levels (**Fig. 59B**). Regarding the other cluster, the loss of TRC40 decreases the steady-state levels of both WRB and CAML and the down-regulation of WRB affects the steady-state levels of TRC40 and CAML. The knockdown of CAML affects the steady-state levels of WRB but only slightly affects the steady-state levels of TRC40 (**Fig. 59A**). The knockdown of TRC40 has no impact on the steady-state levels of BAG6 but the double knockdown of WRB/TRC40 decreases the steady-state levels of BAG6. In addition, BAG6 levels were decreased in WRB KO cardiomyocytes (**Fig. 59A**). These relationships would place the TRC receptor and TRC40 at the same level of hierarchical level but the steady-state levels of TRC40 are more affected when WRB

is not present than the other way around. Furthermore, WRB loss affects BAG6 but not vice versa. There is a mild increase of WRB steady-state levels upon BAG6 knockdown. Taken together, this would indicate that the loss of WRB affects the stability of most proteins in the TRC pathway. Moreover, the stability of other proteins of the TRC pathway is dependent on the presence of other interacting components within pathway. Besides, it has to be taken into account that TCR35 and TRC40 regulate the subcellular localization of BAG6. In conclusion, due to this tight regulation of the proteins of the TRC pathway, changes in the steady-state levels of most of these TRC proteins will provoke further consequences within the TRC pathway that may subsequently affect the biogenesis of a subset of TA-protein.

4.5. TRC40 showed some evidence of its potential role as a redox-regulated chaperone

Yeast Get3 has been reported to be a redox-regulated chaperone (Voth et al. 2014). The structural rearrangement Get3 undergoes upon oxidation happens via a CXC-X_n-CXXC motif present in the protein, in a similar fashion as was reported for the bacterial chaperone Hsp33 (Jakob et al. 1999). The CXC-X_n-CXXC motif is conserved in TRC40 (**Fig. 41A**). Besides, the ATPase activity is decreased upon oxidation (**Fig. 42B**) as was reported for yeast Get3 (Voth et al. 2014). However, recombinant TRC40 presented a lesser number of reduced cysteines than expected in reducing conditions. This might indicate that TRC40 has a more complex redox behavior than Get3.

Experiments in conditions that stimulate the production of reactive oxygen species (ROS), such as hypoxia (Chandel et al. 1998; Chandel et al. 2000; Clanton 2007; Tafani et al. 2016), did not show any change of TRC40 at the steady-state level or any change in the electrophoretic mobility of TRC40 in non-reducing SDS-PAGE (as is observed for Get3) (**Fig. 43A**).

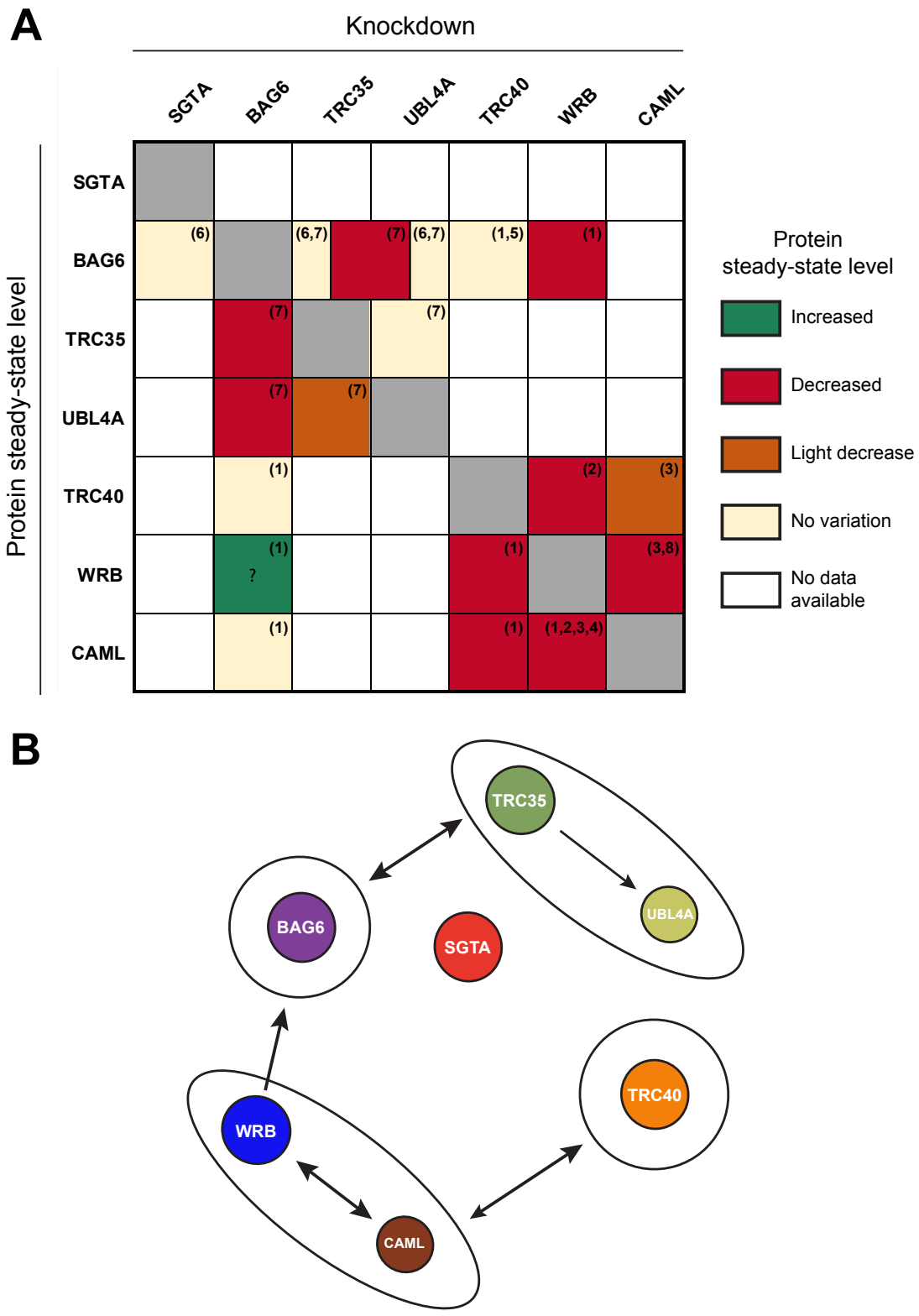

Figure 59. TRC pathway knockdown impacts the stability of other components of the pathway. **(A)** The knockdown of the components of the TRC pathway alters the protein steady-state levels. **(1)** This study, **(2)** Rivera-Monroy et al. 2016, **(3)** Colombo et al. 2016, **(4)** Haßdenteufel et al. 2017, **(5)** Baron et al. 2014, **(6)** Xu et al. 2012, **(7)** Krenciute et al. 2013, **(8)** Vilardi et al. 2014. **(B)** Hierarchical protein network based on protein stability at steady-state level. Arrows indicate which knockdown affects the stability of a protein.

Based on the studies reporting SGTA as a collaborator in the early maturation steps of the SRs, such as the glucocorticoid receptor (GR) (Paul et al. 2014), I hypothesized that the GR could be a potential substrate of TRC40 as redox-regulated chaperone. Additionally, SGTA negatively regulates the activity of some SRs (Paul et al. 2014). Furthermore, Sgt2 interacts with the same chaperones that Get3 was found to colocalize in foci (F. Wang et al. 2010; Powis et al. 2013). In a yeast-based reporter assay, in a similar fashion as described in (Paul et al. 2014), the absence of yeast Get3 affected the GR activity in a stronger manner than the absence of Sgt2 in this study (**Fig. 45A**). The relative GR activity could not be rescued by the Get3 mutants (**Fig. 46B**) but they had an effect over the absolute GR activity (**Fig. 46A**). However, complex modulation of the GR steady-state levels (**Fig. 47B**) by the steady-state levels Get3 (**Fig. 47C**) made GR activity results difficult to interpret. In contrast, there was no modulation of the GR steady-state levels by TRC40 in HeLa cells (**Fig. 51B**) and the absence of TRC40 did not change the cellular distribution of the GR in stimulated and unstimulated cells in HeLa cells (**Fig. 50B**). In their study, from the yeast-based reporter assay results, Paul et al., came to the conclusion that Sgt2 was regulating the activity of the GR. In this study, I showed that Get3 and GR levels correlated inversely (**Fig. 47B, Fig. 47C**). However, Paul et al. never showed any evidence of quantification of the steady-state levels of the GR or the SGTA over-expression in the rescue experiments. Given the fact that the GR steady-state levels can influence its activity it is important to know how stable they are in the different conditions tested. SGTA over-expression may also affect the steady-state levels of the GR, and therefore its activity, in a similar fashion to Get3. Get3 has an effect over the activity of the GR, based on the yeast-reporter assay, but the fact that Get3 levels modulate those of the GR makes the results particularly difficult to interpret.

Taken together, there is no experimental evidence currently that shows the GR might represent an *in vivo* chaperone substrate of TRC40. Nevertheless, further *in vitro* experiments regarding the redox state of the TRC40 cysteines, the role of these cysteines in a putative conformational change, the potential formation of TRC40 tetramers or high-order oligomers must be carried out systematically in order to characterize the potential role of TRC40 as a redox-regulated protein.

5. Conclusion and perspectives

5.1. Conclusions

In this study, I demonstrated that $TRC40_{D74E}$, an ATPase-impaired mutant of TRC40, can trap TA-protein substrates (e.g. Stx5, Stx8, EMD), in cytoplasm. Therefore, this trapping mutant can be used as a tool for determining the *in vivo* interactome of TRC40.

Furthermore, I could determine the *in vivo* TRC-dependence of eleven TA-proteins by knocking-down TRC-pathway components such as WRB and TRC40. In contrast, another six TA-proteins did not show any evidence of *in vivo* TRC-dependence in this study, either affected by down-regulation of TRC components or by the presence of $TRC40_{D74E}$. Many of the TA-proteins (e.g. USE1, UBE2J1, Vti1a) tested in this study were not reported to be TRC-dependent in the literature. These experiments led me to explore the potential causes behind the TRC-dependence of the TA-proteins *in vivo*. TMD-hydrophobicity showed a good correlation and it may be a major contributor in the TRC-dependence of the TA-proteins. BAG6 has been reported essential for the targeting of the TA-proteins according to the model in the literature. Strikingly, TA-proteins remained unaffected at steady-state level upon BAG6 knockdown suggesting that BAG6 is not essential for TA-protein targeting *in vivo*.

Taken together, the literature and the results in this study suggest that the TRC-pathway is kept in balance by a mechanism that tightly regulates the steady-state levels of its components. Upon the loss of some of the components others get severely reduced in their steady-state levels. This TRC-pathway balance is not symmetrical and shows a hierarchical organization within the pathway.

There was no experimental evidence that showed the glucocorticoid receptor might represent an *in vivo* chaperone substrate of TRC40. Nevertheless, further *in vitro* experiments regarding the redox state of the TRC40 cysteines, role of those cysteines in a potential conformational change, the potential formation of TRC40 tetramers or

high-order oligomers must be carried out in order to characterize the potential role of TRC40 as a redox-regulated chaperone.

5.2. Perspectives

$TRC40_{D74E}$ has been shown in this study to be an efficient tool for determining TRC40 substrates. A wider analysis of the interactome of $TRC40_{D74E}$ should be performed. For that purpose, I would propose the following:

- Mass spectrometry (MS) for determining $TRC40_{D74E}$ interactome.
  Samples for MS will be obtained by co-immunoprecipitation of $TRC40_{D74E}$ from cells over-expressing this mutant. $TRC40_{D74E/L190D/I193D}$ will be used as negative control of TA-protein targeting.
  - Validation of the hits by IF. Preferentially using antibodies against endogenous proteins, in case that it is not possible tagged-proteins will be used for validation.
  - Biochemical validation of the hits via co-immunoprecipitation of $TRC40_{D74E}$ from cells over-expressing this mutant.
  - Analysis of the causes of the TRC-dependence of a TA-protein based on the hits obtained in the interactome analysis of $TRC40_{D74E}$.
  - Determination of the *in vivo* TRC-pathway dependence of the validated TA-protein hits by knocking-down TRC components in HeLa cells.

- BAG6 knockdown did not yield any major effect at the steady-state level for the TA-proteins tested in this study. However, the effect of the SGTA knockdown over the TA-protein steady-state levels remains unknown. SGTA is the other relevant chaperone in the pre-targeting complex, upstream of TRC40. One would expect a major effect at the steady-state of the TA-proteins according to the models present in the literature.

Therefore, I would downregulate SGTA in HeLa cells and determine the state-levels of the TA-proteins tested in this study.

- The cytoplasmic domain of the SNARE proteins has been shown to play an important role in targeting and trafficking. Get3/TRC40 have been reported to interact with these cytoplasmic domains, as discussed previously. Thus, it is important to determine whether the role that TRC40 plays in the SNARE homeostasis is due to the chaperone or the targeting function of TRC40.

6. References

Abell, B. M., C. Rabu, P. Leznicki, J. C. Young, and S. High. 2007. “Post-Translational Integration of Tail-Anchored Proteins Is Facilitated by Defined Molecular Chaperones.” *Journal of Cell Science* 120 (10): 1743–51. doi:10.1242/jcs.002410.

Abell, Benjamin M., Martin R. Pool, Oliver Schlenker, Irmgard Sinning, and Stephen High. 2004. “Signal Recognition Particle Mediates Post-Translational Targeting in Eukaryotes.” *The EMBO Journal* 23 (14): 2755–64. doi:10.1038/sj.emboj.7600281.

Adamus, G, Z S Zam, A Arendt, K Palczewski, J H McDowell, and P A Hargrave. 1991. “Anti-Rhodopsin Monoclonal Antibodies of Defined Specificity: Characterization and Application.” *Vision Research* 31 (1): 17–31.

Akahane, Takashi, Kazutaka Sahara, Hideki Yashiroda, Keiji Tanaka, and Shigeo Murata. 2013. “Involvement of Bag6 and the TRC Pathway in Proteasome Assembly.” *Nature Communications* 4. Nature Publishing Group: 2234. doi:10.1038/ncomms3234.

Akopian, David, Kuang Shen, Xin Zhang, and Shu-ou Shan. 2013. “Signal Recognition Particle: An Essential Protein-Targeting Machine.” *Annual Review of Biochemistry* 82: 693–721. doi:10.1146/annurev-biochem-072711-164732.

Alberts, Bruce, Alexander Johnson, Julian Lewis, David Morgan, Martin Raff, Keith Roberts, and Peter Walter. 2014. *Molecular Biology of the Cell*. 6th ed. New York: Garland Science. http://www.garlandscience.com/product/isbn/9780815344322.

Almén, Markus Sällman, Karl J V Nordström, Robert Fredriksson, and Helgi B. Schiöth. 2009. “Mapping the Human Membrane Proteome: A Majority of the Human Membrane Proteins Can Be Classified according to Function and Evolutionary Origin.” *BMC Biology* 7 (August): 50. doi:10.1186/1741-7007-7-50.

Amessou, Mohamed, Alexandre Fradagrada, Thomas Falguières, J. Michael Lord, Daniel C. Smith, Lynne M. Roberts, Christophe Lamaze, and Ludger Johannes. 2007. “Syntaxin 16 and Syntaxin 5 Are Required for Efficient Retrograde Transport of Several Exogenous and Endogenous Cargo Proteins.” *Journal of Cell Science* 120 (Pt 8): 1457–68. doi:10.1242/jcs.03436.

6.References

Anderson, D J, K E Mostov, and G Blobel. 1983. “Mechanisms of Integration of de Novo-Synthesized Polypeptides into Membranes: Signal-Recognition Particle Is Required for Integration into Microsomal Membranes of Calcium ATPase and of Lens MP26 but Not of Cytochrome b5.” *Proceedings of the National Academy of Sciences of the United States of America* 80 (23): 7249–53. doi:10.1073/pnas.80.23.7249.

Anghel, S Andrei, Philip T. McGilvray, Ramanujan S. Hegde, and Robert J. Keenan. 2017. “Identification of Oxa1 Homologs Operating in the Eukaryotic Endoplasmic Reticulum.” *Cell Reports* 21 (13). Elsevier Inc.: 3708–16. doi:10.1016/j.celrep.2017.12.006.

Antonin, W., C Holroyd, D Fasshauer, S Pabst, G F Von Mollard, and R Jahn. 2000. “A SNARE Complex Mediating Fusion of Late Endosomes Defines Conserved Properties of SNARE Structure and Function.” *The EMBO Journal* 19 (23): 6453–64. doi:10.1093/emboj/19.23.6453.

Arakel, Eric C., and Blanche Schwappach. 2018. “Formation of COPI-Coated Vesicles at a Glance.” *Journal of Cell Science* 131 (5): jcs209890. doi:10.1242/jcs.209890.

Aranovich, Alexander, Rong Hua, Andrew D. Rutenberg, and Peter K. Kim. 2014. “PEX16 Contributes to Peroxisome Maintenance by Constantly Trafficking PEX3 via the ER.” *Journal of Cell Science* 127 (Pt 17): 3675–86. doi:10.1242/jcs.146282.

Ast, Tslil, Galit Cohen, and Maya Schuldiner. 2013. “A Network of Cytosolic Factors Targets SRP-Independent Proteins to the Endoplasmic Reticulum.” *Cell* 152 (5). Elsevier Inc.: 1134–45. doi:10.1016/j.cell.2013.02.003.

Aviram, Naama, Tslil Ast, Elizabeth A. Costa, Eric C. Arakel, Silvia G. Chuartzman, Calvin H. Jan, Sarah Haßdenteufel, et al. 2016. “The SND Proteins Constitute an Alternative Targeting Route to the Endoplasmic Reticulum.” *Nature* 540 (7631). Nature Publishing Group: 134–38. doi:10.1038/nature20169.

Banerji, J, J Sands, J L Strominger, and T Spies. 1990. “A Gene Pair from the Human Major Histocompatibility Complex Encodes Large Proline-Rich Proteins with Multiple Repeated Motifs and a Single Ubiquitin-like Domain.” *Proceedings of the National Academy of Sciences of the United States of America* 87 (6): 2374–78. doi:10.1073/pnas.87.6.2374.

Banfield, D K, M J Lewis, C Rabouille, G Warren, and H R Pelham. 1994.

"Localization of Sed5, a Putative Vesicle Targeting Molecule, to the Cis-Golgi Network Involves Both Its Transmembrane and Cytoplasmic Domains." *The Journal of Cell Biology* 127 (2): 357–71. http://www.ncbi.nlm.nih.gov/pubmed/7929581.

Bange, Gert, and Irmgard Sinning. 2013. "SIMIBI Twins in Protein Targeting and Localization." *Nature Structural & Molecular Biology* 20 (7). Nature Publishing Group: 776–80. doi:10.1038/nsmb.2605.

Barlowe, Charles, and Ari Helenius. 2016. "Cargo Capture and Bulk Flow in the Early Secretory Pathway." *Annual Review of Cell and Developmental Biology* 32 (1): 197–222. doi:10.1146/annurev-cellbio-111315-125016.

Barlowe, Charles K., and Elizabeth A. Miller. 2013. "Secretory Protein Biogenesis and Traffic in the Early Secretory Pathway." *Genetics* 193 (2): 383–410. doi:10.1534/genetics.112.142810.

Baron, Yorann, Patrick G Pedrioli, Kshitiz Tyagi, Clare Johnson, Nicola T Wood, Daniel Fountaine, Melanie Wightman, and Gabriela Alexandru. 2014. "VAPB/ALS8 Interacts with FFAT-like Proteins Including the p97 Cofactor FAF1 and the ASNA1 ATPase." *BMC Biology* 12 (1): 39. doi:10.1186/1741-7007-12-39.

Barr, Francis A, and Benjamin Short. 2003. "Golgins in the Structure and Dynamics of the Golgi Apparatus." *Current Opinion in Cell Biology* 15 (4): 405–13. doi:10.1016/S0955-0674(03)00054-1.

Bascom, Roger A., Sudha Srinivasan, and Robert L. Nussbaum. 1999. "Identification and Characterization of Golgin-84, a Novel Golgi Integral Membrane Protein with a Cytoplasmic Coiled-Coil Domain." *The Journal of Biological Chemistry* 274 (5): 2953–62. doi:10.1074/jbc.274.5.2953.

Battle, Alexis, Martin C. Jonikas, Peter Walter, Jonathan S. Weissman, and Daphne Koller. 2010. "Automated Identification of Pathways from Quantitative Genetic Interaction Data." *Molecular Systems Biology* 6 (379). Nature Publishing Group: 379. doi:10.1038/msb.2010.27.

Beato, Miguel. 1989. "Gene Regulation by Steroid Hormones." *Cell* 56 (3): 335–44. doi:10.1016/0092-8674(89)90237-7.

Behl, Christian. 2016. "Breaking BAG: The Co-Chaperone BAG3 in Health and Disease." *Trends in Pharmacological Sciences* 37 (8). Elsevier Ltd: 672–88. doi:10.1016/j.tips.2016.04.007.

6.References

Beilharz, Traude, Billie Egan, Pamela A. Silver, Kay Hofmann, and Trevor Lithgow. 2003. “Bipartite Signals Mediate Subcellular Targeting of Tail-Anchored Membrane Proteins in Saccharomyces Cerevisiae.” *The Journal of Biological Chemistry* 278 (10): 8219–23. doi:10.1074/jbc.M212725200.

Bennett, M K, N Calakos, and R H Scheller. 1992. “Syntaxin: A Synaptic Protein Implicated in Docking of Synaptic Vesicles at Presynaptic Active Zones.” *Science (New York, N.Y.)* 257 (5067): 255–59. doi:10.1126/science.1321498.

Berman, H M, J Westbrook, Z Feng, G Gilliland, T N Bhat, H Weissig, I N Shindyalov, and P E Bourne. 2000. “The Protein Data Bank.” *Nucleic Acids Research* 28 (1): 235–42. doi:10.1093/nar/28.1.235.

Bhattacharjee, Hiranmoy, Ye Shih Ho, and Barry P. Rosen. 2001. “Genomic Organization and Chromosomal Localization of the Asna1 Gene, a Mouse Homologue of a Bacterial Arsenic-Translocating ATPase Gene.” *Gene* 272 (1–2): 291–99. doi:10.1016/S0378-1119(01)00522-4.

Bill, Roslyn M, Peter J F Henderson, So Iwata, Edmund R S Kunji, Hartmut Michel, Richard Neutze, Simon Newstead, Bert Poolman, Christopher G Tate, and Horst Vogel. 2011. “Overcoming Barriers to Membrane Protein Structure Determination.” *Nature Biotechnology* 29 (4). Nature Publishing Group: 335–40. doi:10.1038/nbt.1833.

Blatch, Gregory L., and Michael Lässle. 1999. “The Tetratricopeptide Repeat: A Structural Motif Mediating Protein-Protein Interactions.” *BioEssays : News and Reviews in Molecular, Cellular and Developmental Biology* 21 (11): 932–39. doi:10.1002/(SICI)1521-1878(199911)21:11<932::AID-BIES5>3.0.CO;2-N.

Blobel, G, and B Dobberstein. 1975a. “Transfer of Proteins across Membranes. I. Presence of Proteolytically Processed and Unprocessed Nascent Immunoglobulin Light Chains on Membrane-Bound Ribosomes of Murine Myeloma.” *The Journal of Cell Biology* 67 (3): 835–51. http://www.ncbi.nlm.nih.gov/pubmed/811671.

———. 1975b. “Transfer of Proteins across Membranes. II. Reconstitution of Functional Rough Microsomes from Heterologous Components.” *The Journal of Cell Biology* 67 (3): 852–62. http://www.ncbi.nlm.nih.gov/pubmed/3843.

Bock, J. B., H. T. Matern, A. A. Peden, and R. H. Scheller. 2001. “A Genomic Perspective on Membrane Compartment Organization.” *Nature* 409 (6822): 839–41. doi:10.1038/35057024.

Borgese, Nica, Silvia Brambillasca, and Sara Colombo. 2007. “How Tails Guide Tail-Anchored Proteins to Their Destinations.” *Current Opinion in Cell Biology* 19 (4): 368–75. doi:10.1016/j.ceb.2007.04.019.

Borgese, Nica, Sara Colombo, and Emanuela Pedrazzini. 2003. “The Tale of Tail-Anchored Proteins: Coming from the Cytosol and Looking for a Membrane.” *The Journal of Cell Biology* 161 (6): 1013–19. doi:10.1083/jcb.200303069.

Borgese, Nica, and Elisa Fasana. 2011. “Targeting Pathways of C-Tail-Anchored Proteins.” *Biochimica et Biophysica Acta* 1808 (3). Elsevier B.V.: 937–46. doi:10.1016/j.bbamem.2010.07.010.

Borgese, Nica, I Gazzoni, M Barberi, S Colombo, and E Pedrazzini. 2001. “Targeting of a Tail-Anchored Protein to Endoplasmic Reticulum and Mitochondrial Outer Membrane by Independent but Competing Pathways.” *Molecular Biology of the Cell* 12 (8): 2482–96. doi:10.1091/mbc.12.8.2482.

Bozkurt, Gunes, Goran Stjepanovic, Fabio Vilardi, Stefan Amlacher, Klemens Wild, Gert Bange, Vincenzo Favaloro, et al. 2009. “Structural Insights into Tail-Anchored Protein Binding and Membrane Insertion by Get3.” *Proceedings of the National Academy of Sciences of the United States of America* 106 (50): 21131–36. doi:10.1073/pnas.0910223106.

Brachmann, Carrie Baker, Adrian Davies, Gregory J. Cost, Emerita Caputo, Joachim Li, Philip Hieter, and Jef D. Boeke. 1998. “Designer Deletion Strains Derived from Saccharomyces Cerevisiae S288C: A Useful Set of Strains and Plasmids for PCR-Mediated Gene Disruption and Other Applications.” *Yeast (Chichester, England)* 14 (2): 115–32. doi:10.1002/(SICI)1097-0061(19980130)14:2<115::AID-YEA204>3.0.CO;2-2.

Bram, R J, and G R Crabtree. 1994. “Calcium Signalling in T Cells Stimulated by a Cyclophilin B-Binding Protein.” *Nature* 371 (6495): 355–58. doi:10.1038/371355a0.

Brambillasca, Silvia, Monica Yabal, Marja Makarow, and Nica Borgese. 2006. “Unassisted Translocation of Large Polypeptide Domains across Phospholipid Bilayers.” *The Journal of Cell Biology* 175 (5): 767–77. doi:10.1083/jcb.200608101.

Brambillasca, Silvia, Monica Yabal, Paolo Soffientini, Sandra Stefanovic, Marja Makarow, Ramanujan S. Hegde, and Nica Borgese. 2005. “Transmembrane Topogenesis of a Tail-Anchored Protein Is Modulated by Membrane Lipid

Composition." *The EMBO Journal* 24 (14): 2533–42. doi:10.1038/sj.emboj.7600730.

Brandhorst, Dorothea, Daniel Zwilling, Silvio O. Rizzoli, Undine Lippert, Thorsten Lang, and Reinhard Jahn. 2006. "Homotypic Fusion of Early Endosomes: SNAREs Do Not Determine Fusion Specificity." *Proceedings of the National Academy of Sciences of the United States of America* 103 (8): 2701–6. doi:10.1073/pnas.0511138103.

Bresnick, E. H., F. C. Dalman, E. R. Sanchez, and W. B. Pratt. 1989. "Evidence That the 90-kDa Heat Shock Protein Is Necessary for the Steroid Binding Conformation of the L Cell Glucocorticoid Receptor." *The Journal of Biological Chemistry* 264 (9): 4992–97. http://www.ncbi.nlm.nih.gov/pubmed/2647745.

Brnjic, Slavica, Magdalena Mazurkiewicz, Mårten Fryknäs, Chao Sun, Xiaonan Zhang, Rolf Larsson, Pádraig D'Arcy, and Stig Linder. 2014. "Induction of Tumor Cell Apoptosis by a Proteasome Deubiquitinase Inhibitor Is Associated with Oxidative Stress." *Antioxidants & Redox Signaling* 21 (17): 2271–85. doi:10.1089/ars.2013.5322.

Bryda, Elizabeth C., Nathan T. Johnson, Kevin K. Ohlemiller, Cynthia L. Besch-Williford, Elizabeth Moore, and Richard J. Bram. 2012. "Conditional Deletion of Calcium-Modulating Cyclophilin Ligand Causes Deafness in Mice." *Mammalian Genome : Official Journal of the International Mammalian Genome Society* 23 (3–4): 270–76. doi:10.1007/s00335-011-9381-z.

Buentzel, Judith, Fabio Vilardi, Amelie Lotz-Havla, Jutta Gärtner, and Sven Thoms. 2015. "Conserved Targeting Information in Mammalian and Fungal Peroxisomal Tail-Anchored Proteins." *Scientific Reports* 5 (December). Nature Publishing Group: 17420. doi:10.1038/srep17420.

Bulbarelli, Alessandra, Teresa Sprocati, Massimo Barberi, Emanuela Pedrazzini, and Nica Borgese. 2002. "Trafficking of Tail-Anchored Proteins: Transport from the Endoplasmic Reticulum to the Plasma Membrane and Sorting between Surface Domains in Polarised Epithelial Cells." *Journal of Cell Science* 115 (Pt 8): 1689–1702. doi:10.1126/science.1948048.

Bunim, J J, R L Black, L Lutwak, R E Peterson, and G D Whedon. 1958. "Studies on Dexamethasone, a New Synthetic Steroid, in Rheurheumatoid Arthritis: A Preliminary Report; Adrenal Cortical, Metabolic and Early Clinical Effects." *Arthritis and Rheumatism* 1 (4): 313–31.

http://www.ncbi.nlm.nih.gov/pubmed/13560344.

Burri, Lena, Oleg Varlamov, Claudia A Doege, Kay Hofmann, Traude Beilharz, James E Rothman, Thomas H Söllner, and Trevor Lithgow. 2003. “A SNARE Required for Retrograde Transport to the Endoplasmic Reticulum.” *Proceedings of the National Academy of Sciences of the United States of America* 100 (17): 9873–77. doi:10.1073/pnas.1734000100.

Carpenter, Anne E., Thouis R. Jones, Michael R. Lamprecht, Colin Clarke, In Han Kang, Ola Friman, David A. Guertin, et al. 2006. “CellProfiler: Image Analysis Software for Identifying and Quantifying Cell Phenotypes.” *Genome Biology* 7 (10): R100. doi:10.1186/gb-2006-7-10-r100.

Casson, Joseph, Michael McKenna, Sarah Haßdenteufel, Naama Aviram, Richard Zimmerman, and Stephen High. 2017. “Multiple Pathways Facilitate the Biogenesis of Mammalian Tail-Anchored Proteins.” *Journal of Cell Science* 130 (22): 3851–61. doi:10.1242/jcs.207829.

Cato, Laura, Antje Neeb, Myles Brown, and Andrew C B Cato. 2014. “Control of Steroid Receptor Dynamics and Function by Genomic Actions of the Cochaperones p23 and Bag-1L.” *Nuclear Receptor Signaling* 12: e005. doi:10.1621/nrs.12005.

Chan, Siaw-Li, Lonn D. Lindquist, Michael J. Hansen, Megan A. Girtman, Larry R. Pease, and Richard J. Bram. 2015. “Calcium-Modulating Cyclophilin Ligand Is Essential for the Survival of Activated T Cells and for Adaptive Immunity.” *Journal of Immunology (Baltimore, Md. : 1950)* 195 (12): 5648–56. doi:10.4049/jimmunol.1500308.

Chandel, N. S., D. S. McClintock, C. E. Feliciano, T. M. Wood, J. A. Melendez, A. M. Rodriguez, and P. T. Schumacker. 2000. “Reactive Oxygen Species Generated at Mitochondrial Complex III Stabilize Hypoxia-Inducible Factor-1alpha during Hypoxia: A Mechanism of O2 Sensing.” *The Journal of Biological Chemistry* 275 (33): 25130–38. doi:10.1074/jbc.M001914200.

Chandel, N S, E Maltepe, E Goldwasser, C E Mathieu, M C Simon, and P T Schumacker. 1998. “Mitochondrial Reactive Oxygen Species Trigger Hypoxia-Induced Transcription.” *Proceedings of the National Academy of Sciences of the United States of America* 95 (20): 11715–20. doi:10.1073/pnas.95.20.11715.

Chang, Yi W., Yu Chien Chuang, Yu C. Ho, Ming Yuan Cheng, Yuh J. Sun, Chwan Deng Hsiao, and Chung Wang. 2010. “Crystal Structure of Get4-Get5 Complex

and Its Interactions with Sgt2, Get3, and Ydj1." *Journal of Biological Chemistry* 285 (13): 9962–70. doi:10.1074/jbc.M109.087098.

Charneau, Pierre, Gilles Mirambeau, Pascal Roux, Sylvie Paulous, Henri Buc, and Francis Clavel. 1994. "HIV-1 Reverse Transcription. A Termination Step at the Center of the Genome." *Journal of Molecular Biology* 241 (5): 651–62. doi:10.1006/jmbi.1994.1542.

Chartron, Justin William, Christian J M Suloway, Ma'ayan Zaslaver, and William Melvon Clemons. 2010. "Structural Characterization of the Get4/Get5 Complex and Its Interaction with Get3." *Proceedings of the National Academy of Sciences of the United States of America* 107 (27): 12127–32. doi:10.1073/pnas.1006036107.

Chen, C M, T K Misra, Simon Silver, and B P Rosen. 1986. "Nucleotide Sequence of the Structural Genes for an Anion Pump. The Plasmid-Encoded Arsenical Resistance Operon." *The Journal of Biological Chemistry* 261 (32): 15030–38. http://www.ncbi.nlm.nih.gov/pubmed/3021763.

Chen, Li, Martin S. Y. Lau, and David K. Banfield. 2016. "Multiple ER-Golgi SNARE Transmembrane Domains Are Dispensable for Trafficking but Required for SNARE Recycling." *Molecular Biology of the Cell* 27 (17): 2633–41. doi:10.1091/mbc.E16-05-0277.

Chen, Shiying, and David F. Smith. 1998. "Hop as an Adaptor in the Heat Shock Protein 70 (Hsp70) and hsp90 Chaperone Machinery." *The Journal of Biological Chemistry* 273 (52): 35194–200. doi:10.1074/jbc.273.52.35194.

Chen, Shiying, William P. Sullivan, David O. Toft, and David F. Smith. 1998. "Differential Interactions of p23 and the TPR-Containing Proteins Hop, Cyp40, FKBP52 and FKBP51 with Hsp90 Mutants." *Cell Stress & Chaperones* 3 (2): 118–29. doi:10.1379/1466-1268(1998)003<0118:DIOPAT>2.3.CO;2.

Chen, Yu-Chan, George K E Umanah, Noah Dephoure, Shaida a Andrabi, Steven P Gygi, Ted M Dawson, Valina L Dawson, and Jared Rutter. 2014. "Msp1/ATAD1 Maintains Mitochondrial Function by Facilitating the Degradation of Mislocalized Tail-Anchored Proteins." *The EMBO Journal* 33 (14): 1548–64. doi:10.15252/embj.201487943.

Cheung, Joyce, and D F Smith. 2000. "Molecular Chaperone Interactions with Steroid Receptors: An Update." *Molecular Endocrinology (Baltimore, Md.)* 14 (7): 939–46. doi:10.1210/mend.14.7.0489.

Chio, Un Seng, Hyunju Cho, and Shu-ou Shan. 2017. “Mechanisms of Tail-Anchored Membrane Protein Targeting and Insertion.” *Annual Review of Cell and Developmental Biology* 33 (October): 417–38. doi:10.1146/annurev-cellbio-100616-060839.

Chio, Un Seng, Sangyoon Chung, Shimon Weiss, and Shu-ou Shan. 2017. “A Protean Clamp Guides Membrane Targeting of Tail-Anchored Proteins.” *Proceedings of the National Academy of Sciences of the United States of America* 114 (41): E8585–94. doi:10.1073/pnas.1708731114.

Claessen, Jasper H L, Britta Mueller, Eric Spooner, Valerie L. Pivorunas, and Hidde L. Ploegh. 2010. “The Transmembrane Segment of a Tail-Anchored Protein Determines Its Degradative Fate through Dislocation from the Endoplasmic Reticulum.” *Journal of Biological Chemistry* 285 (27): 20732–39. doi:10.1074/jbc.M110.120766.

Claessen, Jasper H L, and Hidde L. Ploegh. 2011. “BAT3 Guides Misfolded Glycoproteins out of the Endoplasmic Reticulum.” *PloS One* 6 (12): e28542. doi:10.1371/journal.pone.0028542.

Clanton, Thomas L. 2007. “Hypoxia-Induced Reactive Oxygen Species Formation in Skeletal Muscle.” *Journal of Applied Physiology (Bethesda, Md. : 1985)* 102 (6): 2379–88. doi:10.1152/japplphysiol.01298.2006.

Colombo, Sara F., Renato Longhi, and Nica Borgese. 2009. “The Role of Cytosolic Proteins in the Insertion of Tail-Anchored Proteins into Phospholipid Bilayers.” *Journal of Cell Science* 122 (Pt 14): 2383–92. doi:10.1242/jcs.049460.

Colombo, Sara Francesca, Silvia Cardani, Annalisa Maroli, Adriana Vitiello, Paolo Soffientini, Arianna Crespi, Richard F. Bram, Roberta Benfante, and Nica Borgese. 2016. “Tail-Anchored Protein Insertion in Mammals: FUNCTION AND RECIPROCAL INTERACTIONS OF THE TWO SUBUNITS OF THE TRC40 RECEPTOR.” *The Journal of Biological Chemistry* 291 (29): 15292–306. doi:10.1074/jbc.M115.707752.

Connolly, Timothy, and Reid Gilmore. 1986. “Formation of a Functional Ribosome-Membrane Junction during Translocation Requires the Participation of a GTP-Binding Protein.” *The Journal of Cell Biology* 103 (6 Pt 1): 2253–61. doi:10.1083/jcb.103.6.2253.

Costa, Elizabeth A, Kelly Subramanian, Jodi Nunnari, and Jonathan S Weissman. 2018. “Defining the Physiological Role of SRP in Protein-Targeting Efficiency

and Specificity." *Science (New York, N.Y.)* 3607 (January): 1–9. doi:10.1126/science.aar3607.

Costello, Joseph L, Inês G Castro, Fátima Camões, Tina A Schrader, Doug McNeall, Jing Yang, Evdokia-Anastasia Giannopoulou, et al. 2017. "Predicting the Targeting of Tail-Anchored Proteins to Subcellular Compartments in Mammalian Cells." *Journal of Cell Science* 130 (9): 1675–87. doi:10.1242/jcs.200204.

Costello, Joseph L, Inês G Castro, Christian Hacker, Tina A Schrader, Jeremy Metz, Dagmar Zeuschner, Afsoon S Azadi, et al. 2017. "ACBD5 and VAPB Mediate Membrane Associations between Peroxisomes and the ER." *The Journal of Cell Biology*, January, 1–12. doi:10.1083/jcb.201607055.

Cross, Benedict C S, Irmgard Sinning, Joen Luirink, and Stephen High. 2009. "Delivering Proteins for Export from the Cytosol." *Nature Reviews. Molecular Cell Biology* 10 (4): 255–64. doi:10.1038/nrm2657.

D'Arcy, Pádraig, Slavica Brnjic, Maria Hägg Olofsson, Mårten Fryknäs, Kristina Lindsten, Michelandrea De Cesare, Paola Perego, et al. 2011. "Inhibition of Proteasome Deubiquitinating Activity as a New Cancer Therapy." *Nature Medicine* 17 (12): 1636–40. doi:10.1038/nm.2536.

Daniele, Lauren L., Farida Emran, Glenn P. Lobo, Robert J. Gaivin, and Brian D. Perkins. 2016. "Mutation of Wrb, a Component of the Guided Entry of Tail-Anchored Protein Pathway, Disrupts Photoreceptor Synapse Structure and Function." *Investigative Ophthalmology & Visual Science* 57 (7): 2942–54. doi:10.1167/iovs.15-18996.

Darby, John F, Ewelina M Krysztofinska, Peter J Simpson, Aline C Simon, Pawel Leznicki, Newran Sriskandarajah, David S Bishop, et al. 2014. "Solution Structure of the SGTA Dimerisation Domain and Investigation of Its Interactions with the Ubiquitin-Like Domains of BAG6 and UBL4A." *PLoS ONE* 9 (11): e113281. doi:10.1371/journal.pone.0113281.

Davies, Todd H., Yang-Min Ning, and Edwin R. Sánchez. 2002. "A New First Step in Activation of Steroid Receptors: Hormone-Induced Switching of FKBP51 and FKBP52 Immunophilins." *The Journal of Biological Chemistry* 277 (7): 4597–4600. doi:10.1074/jbc.C100531200.

Del Monaco, Magaly, Seana P. Covello, Susan H. Kennedy, Gwen Gilinger, Gerald Litwack, and Jouni Uitto. 1997. "Identification of Novel Glucocorticoid-Response Elements in Human Elastin Promoter and Demonstration of Nucleotide

Sequence Specificity of the Receptor Binding." *The Journal of Investigative Dermatology* 108 (6). Elsevier Masson SAS: 938–42. doi:10.1111/1523-1747.ep12295241.

Desmots, Fabienne, Helen R Russell, Youngsoo Lee, Kelli Boyd, and Peter J McKinnon. 2005. "The Reaper-Binding Protein Scythe Modulates Apoptosis and Proliferation during Mammalian Development." *Molecular and Cellular Biology* 25 (23): 10329–37. doi:10.1128/MCB.25.23.10329-10337.2005.

Dieken, E S, and R L Miesfeld. 1992. "Transcriptional Transactivation Functions Localized to the Glucocorticoid Receptor N Terminus Are Necessary for Steroid Induction of Lymphocyte Apoptosis." *Molecular and Cellular Biology* 12 (2): 589–97. doi:10.1038/348166a0.

Dilcher, Meik, Beate Veith, Subbulakshmi Chidambaram, Enno Hartmann, Hans Dieter Schmitt, and Gabriele Fischer von Mollard. 2003. "Use1p Is a Yeast SNARE Protein Required for Retrograde Traffic to the ER." *The EMBO Journal* 22 (14): 3664–74. doi:10.1093/emboj/cdg339.

Dong, Rui, Yasunori Saheki, Sharan Swarup, Louise Lucast, J Wade Harper, and Pietro De Camilli. 2016. "Endosome-ER Contacts Control Actin Nucleation and Retromer Function through VAP-Dependent Regulation of PI4P." *Cell* 166 (2). Elsevier Inc.: 408–23. doi:10.1016/j.cell.2016.06.037.

Egeo, Aliana, Michela Mazzocco, Federica Sotgia, Patrizio Arrigo, Rafael Oliva, Salvador Bergonòn, Dean Nizetic, Alberto Rasore-Quartino, and Paolo Scartezzini. 1998. "Identification and Characterization of a New Human cDNA from Chromosome 21q22.3 Encoding a Basic Nuclear Protein." *Human Genetics* 102 (3): 289–93. doi:10.1007/s004390050693.

Elgersma, Ype, Liane Kwast, M van den Berg, William B. Snyder, Ben Distel, Suresh Subramani, and Henk F. Tabak. 1997. "Overexpression of Pex15p, a Phosphorylated Peroxisomal Integral Membrane Protein Required for Peroxisome Assembly in S.cerevisiae, Causes Proliferation of the Endoplasmic Reticulum Membrane." *The EMBO Journal* 16 (24): 7326–41. doi:10.1093/emboj/16.24.7326.

Ellman, George L. 1958. "A Colorimetric Method for Determining Low Concentrations of Mercaptans." *Archives of Biochemistry and Biophysics* 74 (2): 443–50. doi:10.1016/0003-9861(58)90014-6.

Ernst, Robert, Britta Mueller, Hidde L. Ploegh, and Christian Schlieker. 2009. "The

Otubain YOD1 Is a Deubiquitinating Enzyme That Associates with p97 to Facilitate Protein Dislocation from the ER." *Molecular Cell* 36 (1). Elsevier Ltd: 28–38. doi:10.1016/j.molcel.2009.09.016.

Fang, Yi, James C. Morrell, Jacob M. Jones, and Stephen J. Gould. 2004. "PEX3 Functions as a PEX19 Docking Factor in the Import of Class I Peroxisomal Membrane Proteins." *The Journal of Cell Biology* 164 (6): 863–75. doi:10.1083/jcb.200311131.

Favaloro, Vincenzo, Milan Spasic, Blanche Schwappach, and Bernhard Dobberstein. 2008. "Distinct Targeting Pathways for the Membrane Insertion of Tail-Anchored (TA) Proteins." *Journal of Cell Science* 121 (11): 1832–40. doi:10.1242/jcs.020321.

Favaloro, Vincenzo, Fabio Vilardi, Rainer Schlecht, Matthias P. Mayer, and Bernhard Dobberstein. 2010. "Asna1/TRC40-Mediated Membrane Insertion of Tail-Anchored Proteins." *Journal of Cell Science* 123 (Pt 9): 1522–30. doi:10.1242/jcs.055970.

Fernandes, Jorge M O, Daniel J. Macqueen, Hung-Tai Lee, and Ian A. Johnston. 2008. "Genomic, Evolutionary, and Expression Analyses of Cee, an Ancient Gene Involved in Normal Growth and Development." *Genomics* 91 (4): 315–25. doi:10.1016/j.ygeno.2007.10.017.

Figueiredo Costa, Bruna, Patrizia Cassella, Sara Francesca Colombo, and Nica Borgese. 2018. "Discrimination between the Endoplasmic Reticulum and Mitochondria by Spontaneously Inserting Tail-Anchored Proteins." *Traffic (Copenhagen, Denmark)* 19 (3): 182–97. doi:10.1111/tra.12550.

Fleischer, Tracey C., Connie M. Weaver, K. Jill McAfee, Jennifer L. Jennings, and Andrew J. Link. 2006. "Systematic Identification and Functional Screens of Uncharacterized Proteins Associated with Eukaryotic Ribosomal Complexes." *Genes & Development* 20 (10): 1294–1307. doi:10.1101/gad.1422006.

Freedman, Neal D, and Keith R Yamamoto. 2004. "Importin 7 and Importin Alpha/importin Beta Are Nuclear Import Receptors for the Glucocorticoid Receptor." *Molecular Biology of the Cell* 15 (5): 2276–86. doi:10.1091/mbc.E03-11-0839.

Fujiki, Yukio, Kanji Okumoto, Satoru Mukai, Masanori Honsho, and Shigehiko Tamura. 2014. "Peroxisome Biogenesis in Mammalian Cells." *Frontiers in Physiology* 5 (August): 307. doi:10.3389/fphys.2014.00307.

Ganley, Ian G., Eric Espinosa, and Suzanne R. Pfeffer. 2008. “A Syntaxin 10-SNARE Complex Distinguishes Two Distinct Transport Routes from Endosomes to the Trans-Golgi in Human Cells.” *The Journal of Cell Biology* 180 (1): 159–72. doi:10.1083/jcb.200707136.

Gillingham, Alison K., and Sean Munro. 2016. “Finding the Golgi: Golgin Coiled-Coil Proteins Show the Way.” *Trends in Cell Biology* 26 (6). Elsevier Ltd: 399–408. doi:10.1016/j.tcb.2016.02.005.

Gilmore, R., G Blobel, and P Walter. 1982. “Protein Translocation across the Endoplasmic Reticulum. I. Detection in the Microsomal Membrane of a Receptor for the Signal Recognition Particle.” *The Journal of Cell Biology* 95 (2 Pt 1): 463–69. doi:10.1083/jcb.95.2.463.

Gilmore, R, P Walter, and G Blobel. 1982. “Protein Translocation across the Endoplasmic Reticulum. II. Isolation and Characterization of the Signal Recognition Particle Receptor.” *The Journal of Cell Biology* 95 (2 Pt 1): 470–77. doi:10.1083/jcb.95.2.470.

Gomez-Suaga, Patricia, Sebastien Paillusson, Radu Stoica, Wendy Noble, Diane P. Hanger, and Christopher C J Miller. 2017. “The ER-Mitochondria Tethering Complex VAPB-PTPIP51 Regulates Autophagy.” *Current Biology : CB* 27 (3). Elsevier Ltd.: 371–85. doi:10.1016/j.cub.2016.12.038.

Goodman, H. Maurice. 2009. “Chapter 4 - Adrenal Glands.” In *Basic Medical Endocrinology*, 4th ed., 61–90. Academic Press.

Görlich, Dirk, Siegfried Prehn, Enno Hartmann, Kai Uwe Kalies, and Tom A. Rapoport. 1992. “A Mammalian Homolog of SEC61p and SECYp Is Associated with Ribosomes and Nascent Polypeptides during Translocation.” *Cell* 71 (3): 489–503. doi:10.1016/0092-8674(92)90517-G.

Gould, S. J., G. A. Keller, N. Hosken, J. Wilkinson, and S. Subramani. 1989. “A Conserved Tripeptide Sorts Proteins to Peroxisomes.” *The Journal of Cell Biology* 108 (5): 1657–64. doi:10.1083/jcb.108.5.1657.

Gristick, Harry B, Meera Rao, Justin William Chartron, Michael E Rome, Shu-Ou Shan, and William Melvon Clemons. 2014. “Crystal Structure of ATP-Bound Get3-Get4-Get5 Complex Reveals Regulation of Get3 by Get4.” *Nature Structural & Molecular Biology* 21 (5). Nature Publishing Group: 437–42. doi:10.1038/nsmb.2813.

Gristick, Harry B, Michael E. Rome, Justin William Chartron, Meera Rao, Sonja Hess,

Shu-ou Shan, and William Melvon Clemons. 2015. “Mechanism of Assembly of a Substrate Transfer Complex during Tail-Anchored Protein Targeting.” *The Journal of Biological Chemistry* 290 (50): 30006–17. doi:10.1074/jbc.M115.677328.

Grudnik, Przemyslaw, Gert Bange, and Irmgard Sinning. 2009. “Protein Targeting by the Signal Recognition Particle.” *Biological Chemistry* 390 (8): 775–82. doi:10.1515/BC.2009.102.

GTEx Consortium. 2015. “Human Genomics. The Genotype-Tissue Expression (GTEx) Pilot Analysis: Multitissue Gene Regulation in Humans.” *Science (New York, N.Y.)* 348 (6235): 648–60. doi:10.1126/science.1262110.

Gu, Feng, Duc Thang Nguyên, Matthew Stuible, Nadia Dubé, Michel L. Tremblay, and Eric Chevet. 2004. “Protein-Tyrosine Phosphatase 1B Potentiates IRE1 Signaling during Endoplasmic Reticulum Stress.” *The Journal of Biological Chemistry* 279 (48): 49689–93. doi:10.1074/jbc.C400261200.

Guiochon-Mantel, A, K Delabre, P Lescop, and E Milgrom. 1994. “Nuclear Localization Signals Also Mediate the Outward Movement of Proteins from the Nucleus.” *Proceedings of the National Academy of Sciences of the United States of America* 91 (15): 7179–83. doi:10.1073/pnas.91.15.7179.

Guiochon-Mantel, A, P Lescop, S Christin-Maitre, H Loosfelt, M Perrot-Applanat, and E Milgrom. 1991. “Nucleocytoplasmic Shuttling of the Progesterone Receptor.” *The EMBO Journal* 10 (12): 3851–59. http://www.pubmedcentral.nih.gov/articlerender.fcgi?artid=453122&tool=pmcentrez&rendertype=abstract.

Guna, Alina, Norbert Volkmar, John C Christianson, and Ramanujan S Hegde. 2018. “The ER Membrane Protein Complex Is a Transmembrane Domain Insertase.” *Science (New York, N.Y.)* 359 (6374): 470–73. doi:10.1126/science.aao3099.

Haché, R J, Raymond Tse, Terry Reich, J G Savory, and Yvonne A. Lefebvre. 1999. “Nucleocytoplasmic Trafficking of Steroid-Free Glucocorticoid Receptor.” *The Journal of Biological Chemistry* 274 (3): 1432–39. doi:10.1074/jbc.274.3.1432.

Halbach, André, Christiane Landgraf, Stephan Lorenzen, Katja Rosenkranz, Rudolf Volkmer-Engert, Ralf Erdmann, and Hanspeter Rottensteiner. 2006. “Targeting of the Tail-Anchored Peroxisomal Membrane Proteins PEX26 and PEX15 Occurs through C-Terminal PEX19-Binding Sites.” *Journal of Cell Science* 119 (Pt 12): 2508–17. doi:10.1242/jcs.02979.

Halic, Mario, Thomas Becker, Martin R. Pool, Christian M T Spahn, Robert A. Grassucci, Joachim Frank, and Roland Beckmann. 2004. “Structure of the Signal Recognition Particle Interacting with the Elongation-Arrested Ribosome.” *Nature* 427 (6977): 808–14. doi:10.1038/nature02342.

Härd, T, E Kellenbach, R Boelens, B A Maler, K Dahlman, L P Freedman, J Carlstedt-Duke, K R Yamamoto, J A Gustafsson, and R Kaptein. 1990. “Solution Structure of the Glucocorticoid Receptor DNA-Binding Domain.” *Science (New York, N.Y.)* 249 (4965): 157–60. doi:10.1126/science.2115209.

Harrell, Jennifer M., Patrick J M Murphy, Yoshihiro Morishima, Haifeng Chen, John F. Mansfield, Mario D. Galigniana, and William B. Pratt. 2004. “Evidence for Glucocorticoid Receptor Transport on Microtubules by Dynein.” *The Journal of Biological Chemistry* 279 (52): 54647–54. doi:10.1074/jbc.M406863200.

Haßdenteufel, Sarah, Nico Schäuble, Patrizia Cassella, Pawel Leznicki, Anika Müller, Stephen High, Martin Jung, and Richard Zimmermann. 2011. “Ca2+-Calmodulin Inhibits Tail-Anchored Protein Insertion into the Mammalian Endoplasmic Reticulum Membrane.” *FEBS Letters* 585 (21): 3485–90. doi:10.1016/j.febslet.2011.10.008.

Haßdenteufel, Sarah, Mark Sicking, Stefan Schorr, Naama Aviram, Claudia Fecher-Trost, Maya Schuldiner, Martin Jung, Richard Zimmermann, and Sven Lang. 2017. “hSnd2 Protein Represents an Alternative Targeting Factor to the Endoplasmic Reticulum in Human Cells.” *FEBS Letters* 591 (20): 3211–24. doi:10.1002/1873-3468.12831.

Hatsuzawa, Kiyotaka, Hidenori Hirose, Katsuko Tani, Akitsugu Yamamoto, Richard H. Scheller, and Mitsuo Tagaya. 2000. “Syntaxin 18, a SNAP Receptor That Functions in the Endoplasmic Reticulum, Intermediate Compartment, and Cis-Golgi Vesicle Trafficking.” *The Journal of Biological Chemistry* 275 (18): 13713–20. doi:10.1074/jbc.275.18.13713.

Hay, J C, J Klumperman, V Oorschot, M Steegmaier, C S Kuo, and R H Scheller. 1998. “Localization, Dynamics, and Protein Interactions Reveal Distinct Roles for ER and Golgi SNAREs [Published Erratum Appears in J Cell Biol 1998 Aug 10;142(3):following 881].” *J Cell Biol* 141 (7): 1489–1502. doi:10.1083/jcb.141.7.1489.

Hay, Jesse C., Daniel S. Chao, Christin S. Kuo, and Richard H. Scheller. 1997. “Protein Interactions Regulating Vesicle Transport between the Endoplasmic

Reticulum and Golgi Apparatus in Mammalian Cells." *Cell* 89 (1): 149–58. doi:10.1016/S0092-8674(00)80191-9.

Hayashi, I, T Oyama, and K Morikawa. 2001. "Structural and Functional Studies of MinD ATPase: Implications for the Molecular Recognition of the Bacterial Cell Division Apparatus." *The EMBO Journal* 20 (8): 1819–28. doi:10.1093/emboj/20.8.1819.

Hegde, Ramanujan S., and Robert J. Keenan. 2011. "Tail-Anchored Membrane Protein Insertion into the Endoplasmic Reticulum." *Nature Reviews Molecular Cell Biology* 12 (12). Nature Publishing Group: 787–98. doi:10.1038/nrm3226.

Hemmingsson, Oskar, Gautam Kao, Maria Still, and Peter Naredi. 2010. "ASNA-1 Activity Modulates Sensitivity to Cisplatin." *Cancer Research* 70 (24): 10321–28. doi:10.1158/0008-5472.CAN-10-1548.

Hemmingsson, Oskar, Mikael Nöjd, Gautam Kao, and Peter Naredi. 2009. "Increased Sensitivity to Platinating Agents and Arsenite in Human Ovarian Cancer by Downregulation of ASNA1." *Oncology Reports* 22 (4): 869–75. doi:10.3892/or_00000511.

Hemmingsson, Oskar, Yuzhu Zhang, Maria Still, and Peter Naredi. 2009. "ASNA1, an ATPase Targeting Tail-Anchored Proteins, Regulates Melanoma Cell Growth and Sensitivity to Cisplatin and Arsenite." *Cancer Chemotherapy and Pharmacology* 63 (3): 491–99. doi:10.1007/s00280-008-0762-2.

Hernández, M Patricia, Ahmed Chadli, and David O. Toft. 2002. "HSP40 Binding Is the First Step in the HSP90 Chaperoning Pathway for the Progesterone Receptor." *The Journal of Biological Chemistry* 277 (14): 11873–81. doi:10.1074/jbc.M111445200.

Hessa, Tara, Nadja M Meindl-Beinker, Andreas Bernsel, Hyun Kim, Yoko Sato, Mirjam Lerch-Bader, Ingmarie Nilsson, Stephen H White, and Gunnar von Heijne. 2007. "Molecular Code for Transmembrane-Helix Recognition by the Sec61 Translocon." *Nature* 450 (7172): 1026–30. doi:10.1038/nature06387.

Hessa, Tara, Ajay Sharma, Malaiyalam Mariappan, Heather D Eshleman, Erik Gutierrez, and Ramanujan S Hegde. 2011. "Protein Targeting and Degradation Are Coupled for Elimination of Mislocalized Proteins." *Nature* 475 (7356). Nature Publishing Group: 394–97. doi:10.1038/nature10181.

Hirose, Hidenori, Kohei Arasaki, Naoshi Dohmae, Koji Takio, Kiyotaka Hatsuzawa, Masami Nagahama, Katsuko Tani, Akitsugu Yamamoto, Masaya Tohyama, and

Mitsuo Tagaya. 2004. “Implication of ZW10 in Membrane Trafficking between the Endoplasmic Reticulum and Golgi.” *The EMBO Journal* 23 (6): 1267–78. doi:10.1038/sj.emboj.7600135.

Hofmann, Jürgen, and Manfred Sernetz. 1983. “A Kinetic Study on the Enzymatic Hydrolysis of Fluorescein Diacetate and Fluorescein-Di-Beta-D-Galactopyranoside.” *Analytical Biochemistry* 131 (1): 180–86. http://www.ncbi.nlm.nih.gov/pubmed/6614449.

Hong, Wanjin. 2005. “SNAREs and Traffic.” *Biochimica et Biophysica Acta* 1744 (2): 120–44. doi:10.1016/j.bbamcr.2005.03.014.

Honsho, Masanori, J Y Mitoma, and A Ito. 1998. “Retention of Cytochrome b5 in the Endoplasmic Reticulum Is Transmembrane and Luminal Domain-Dependent.” *The Journal of Biological Chemistry* 273 (33): 20860–66. http://www.ncbi.nlm.nih.gov/pubmed/9694832.

Horie, Chika, Hiroyuki Suzuki, Masao Sakaguchi, and Katsuyoshi Mihara. 2002. “Characterization of Signal That Directs C-Tail-Anchored Proteins to Mammalian Mitochondrial Outer Membrane.” *Molecular Biology of the Cell* 13 (5): 1615–25. doi:10.1091/mbc.01-12-0570.

Hu, Junbin, Jingzhi Li, Xinguo Qian, Vlad Denic, and Bingdong Sha. 2009. “The Crystal Structures of Yeast Get3 Suggest a Mechanism for Tail-Anchored Protein Membrane Insertion.” *PloS One* 4 (11): e8061. doi:10.1371/journal.pone.0008061.

Hua, Rong, Derrick Cheng, Étienne Coyaud, Spencer Freeman, Erminia Di Pietro, Yuqing Wang, Adriano Vissa, et al. 2017. “VAPs and ACBD5 Tether Peroxisomes to the ER for Peroxisome Maintenance and Lipid Homeostasis.” *The Journal of Cell Biology* 216 (2): 367–77. doi:10.1083/jcb.201608128.

Isenmann, S, Y Khew-Goodall, J Gamble, M Vadas, and B W Wattenberg. 1998. “A Splice-Isoform of Vesicle-Associated Membrane Protein-1 (VAMP-1) Contains a Mitochondrial Targeting Signal.” *Molecular Biology of the Cell* 9 (7): 1649–60. doi:10.1091/mbc.9.7.1649.

Itakura, Eisuke, Chieko Kishi-Itakura, and Noboru Mizushima. 2012. “The Hairpin-Type Tail-Anchored SNARE Syntaxin 17 Targets to Autophagosomes for Fusion with Endosomes/lysosomes.” *Cell* 151 (6). Elsevier Inc.: 1256–69. doi:10.1016/j.cell.2012.11.001.

Itakura, Eisuke, Eszter Zavodszky, Sichen Shao, Matthew L Wohlever, Robert J

Keenan, and Ramanujan S Hegde. 2016. “Ubiquilins Chaperone and Triage Mitochondrial Membrane Proteins for Degradation.” *Molecular Cell* 63 (1). MRC Laboratory of Molecular Biology: 21–33. doi:10.1016/j.molcel.2016.05.020.

Ito, H, Y Fukuda, K Murata, and A Kimura. 1983. “Transformation of Intact Yeast Cells Treated with Alkali Cations.” *Journal of Bacteriology* 153 (1): 163–68. http://www.ncbi.nlm.nih.gov/pubmed/6336730.

Jahn, Reinhard, and Richard H. Scheller. 2006. “SNAREs--Engines for Membrane Fusion.” *Nature Reviews. Molecular Cell Biology* 7 (9): 631–43. doi:10.1038/nrm2002.

Jakob, Ursula, Wilson Muse, Markus Eser, and James C.A. Bardwell. 1999. “Chaperone Activity with a Redox Switch.” *Cell* 96 (3): 341–52. doi:10.1016/S0092-8674(00)80547-4.

Joglekar, Ashwini P., Dalu Xu, Daniel J. Rigotti, Robert Fairman, and Jesse C. Hay. 2003. “The SNARE Motif Contributes to rbet1 Intracellular Targeting and Dynamics Independently of SNARE Interactions.” *The Journal of Biological Chemistry* 278 (16): 14121–33. doi:10.1074/jbc.M300659200.

Johnson, Nicholas, Katie Powis, and Stephen High. 2013. “Post-Translational Translocation into the Endoplasmic Reticulum.” *Biochimica et Biophysica Acta - Molecular Cell Research* 1833 (11). Elsevier B.V.: 2403–9. doi:10.1016/j.bbamcr.2012.12.008.

Johnson, Nicholas, Fabio Vilardi, Sven Lang, Pawel Leznicki, Richard Zimmermann, and Stephen High. 2012. “TRC40 Can Deliver Short Secretory Proteins to the Sec61 Translocon.” *Journal of Cell Science* 125 (Pt 15): 3612–20. doi:10.1242/jcs.102608.

Jones, Jacob M., James C. Morrell, and Stephen J. Gould. 2004. “PEX19 Is a Predominantly Cytosolic Chaperone and Import Receptor for Class 1 Peroxisomal Membrane Proteins.” *The Journal of Cell Biology* 164 (1): 57–67. doi:10.1083/jcb.200304111.

Jonikas, Martin C, Sean R Collins, Vladimir Denic, Eugene Oh, Erin M Quan, Volker Schmid, Jimena Weibezahn, et al. 2009. “Comprehensive Characterization of Genes Required for Protein Folding in the Endoplasmic Reticulum.” *Science (New York, N.Y.)* 323 (5922): 1693–97. doi:10.1126/science.1167983.

Kabbage, M., and M. B. Dickman. 2008. “The BAG Proteins: A Ubiquitous Family of Chaperone Regulators.” *Cellular and Molecular Life Sciences : CMLS* 65 (9):

1390–1402. doi:10.1007/s00018-008-7535-2.

Kadowaki, Hisae, Atsushi Nagai, Takeshi Maruyama, Yasunari Takami, Pasjan Satrimafitrah, Hironori Kato, Arata Honda, et al. 2015. “Pre-Emptive Quality Control Protects the ER from Protein Overload via the Proximity of ERAD Components and SRP.” *Cell Reports* 13 (5). Elsevier: 944–56. doi:10.1016/j.celrep.2015.09.047.

Kalbfleisch, Ted, Alex Cambon, and Binks W. Wattenberg. 2007. “A Bioinformatics Approach to Identifying Tail-Anchored Proteins in the Human Genome.” *Traffic* 8 (12): 1687–94. doi:10.1111/j.1600-0854.2007.00661.x.

Kämper, Nadine, Jörg Kessler, Sebastian Temme, Claudia Wegscheid, Johannes Winkler, and Norbert Koch. 2012. “A Novel BAT3 Sequence Generated by Alternative RNA Splicing of Exon 11B Displays Cell Type-Specific Expression and Impacts on Subcellular Localization.” *PloS One* 7 (4): e35972. doi:10.1371/journal.pone.0035972.

Kao, Gautam, Cecilia Nordenson, Maria Still, Agneta Rönnlund, Simon Tuck, and Peter Naredi. 2007. “ASNA-1 Positively Regulates Insulin Secretion in C. Elegans and Mammalian Cells.” *Cell* 128 (3): 577–87. doi:10.1016/j.cell.2006.12.031.

Kasai, K, and K Akagawa. 2001. “Roles of the Cytoplasmic and Transmembrane Domains of Syntaxins in Intracellular Localization and Trafficking.” *Journal of Cell Science* 114 (Pt 17): 3115–24. http://www.ncbi.nlm.nih.gov/pubmed/11590238.

Kasai, Kazuo, Kei Suga, Tetsuro Izumi, and Kimio Akagawa. 2008. “Syntaxin 8 Has Two Functionally Distinct Di-Leucine-Based Motifs.” *Cellular & Molecular Biology Letters* 13 (1): 144–54. doi:10.2478/s11658-007-0043-9.

Kawahara, Hiroyuki, Ryosuke Minami, and Naoto Yokota. 2013. “BAG6/BAT3: Emerging Roles in Quality Control for Nascent Polypeptides.” *Journal of Biochemistry* 153 (2): 147–60. doi:10.1093/jb/mvs149.

Kiianitsa, Konstantin, Jachen a. Solinger, and Wolf-Dietrich Heyer. 2003. “NADH-Coupled Microplate Photometric Assay for Kinetic Studies of ATP-Hydrolyzing Enzymes with Low and High Specific Activities.” *Analytical Biochemistry* 321 (2): 266–71. doi:10.1016/S0003-2697(03)00461-5.

Kiktev, Denis A, Jesse C Patterson, Susanne Müller, Bhawana Bariar, Tao Pan, and Yury O Chernoff. 2012. “Regulation of Chaperone Effects on a Yeast Prion by

Cochaperone Sgt2." *Molecular and Cellular Biology* 32 (24): 4960–70. doi:10.1128/MCB.00875-12.

Kikukawa, Yuhsuke, Ryosuke Minami, Masumi Shimada, Masami Kobayashi, Keiji Tanaka, Hideyoshi Yokosawa, and Hiroyuki Kawahara. 2005. "Unique Proteasome Subunit Xrpn10c Is a Specific Receptor for the Antiapoptotic Ubiquitin-like Protein Scythe." *The FEBS Journal* 272 (24): 6373–86. doi:10.1111/j.1742-4658.2005.05032.x.

Kim, Kyoungtae, and Shiva Kumar Goud Gadila. 2016. "Cargo Trafficking from the Trans-Golgi Network towards the Endosome." *Biology of the Cell* 108 (8): 205–18. doi:10.1111/boc.201600001.

Kline, Crystal F, Harley T Kurata, Thomas J Hund, Shane R Cunha, Olha M Koval, Patrick J Wright, Matthew Christensen, Mark E Anderson, Colin G Nichols, and Peter J Mohler. 2009. "Dual Role of K ATP Channel C-Terminal Motif in Membrane Targeting and Metabolic Regulation." *Proceedings of the National Academy of Sciences of the United States of America* 106 (39): 16669–74. doi:10.1073/pnas.0907138106.

Kohl, Christian, Peter Tessarz, Karina von der Malsburg, Regina Zahn, Bernd Bukau, and Axel Mogk. 2011. "Cooperative and Independent Activities of Sgt2 and Get5 in the Targeting of Tail-Anchored Proteins." *Biological Chemistry* 392 (7): 601–8. doi:10.1515/BC.2011.066.

Koonin, E V. 1993. "A Superfamily of ATPases with Diverse Functions Containing Either Classical or Deviant ATP-Binding Motif." *Journal of Molecular Biology* 229 (4): 1165–74. doi:10.1006/jmbi.1993.1115.

Kordes, Elisabeth, Larissa Savelyeva, Manfred Schwab, Jean Rommelaere, Jean Claude Jauniaux, and Celina Cziepluch. 1998. "Isolation and Characterization of Human SGT and Identification of Homologues in Saccharomyces Cerevisiae and Caenorhabditis Elegans." *Genomics* 52 (1): 90–94. doi:10.1006/geno.1998.5385.

Krenciute, Giedre, Shangfeng Liu, Nur Yucer, Yi Shi, Priscilla Ortiz, Qiongming Liu, Beom Jun Kim, et al. 2013. "Nuclear BAG6-UBL4A-GET4 Complex Mediates DNA Damage Signaling and Cell Death." *Journal of Biological Chemistry* 288 (28): 20547–57. doi:10.1074/jbc.M112.443416.

Kriechbaumer, Verena, Rowena Shaw, Joy Mukherjee, Caroline G. Bowsher, Anne-Marie Harrison, and Ben M. Abell. 2009. "Subcellular Distribution of Tail-

Anchored Proteins in Arabidopsis." *Traffic (Copenhagen, Denmark)* 10 (12): 1753–64. doi:10.1111/j.1600-0854.2009.00991.x.

Krishnan, Navasona, Cexiong Fu, Darryl J. Pappin, and Nicholas K. Tonks. 2011. "H2S-Induced Sulfhydration of the Phosphatase PTP1B and Its Role in the Endoplasmic Reticulum Stress Response." *Science Signaling* 4 (203): ra86. doi:10.1126/scisignal.2002329.

Krogh, Anders, Björn Larsson, G von Heijne, and Erik L.L. Sonnhammer. 2001. "Predicting Transmembrane Protein Topology with a Hidden Markov Model: Application to Complete Genomes." *Journal of Molecular Biology* 305 (3): 567–80. doi:10.1006/jmbi.2000.4315.

Krysztofinska, Ewelina M, Santiago Martínez-Lumbreras, Arjun Thapaliya, Nicola J Evans, Stephen High, and Rivka L Isaacson. 2016. "Structural and Functional Insights into the E3 Ligase, RNF126." *Scientific Reports* 6 (January). Nature Publishing Group: 26433. doi:10.1038/srep26433.

Kubota, Keiko, Atsushi Yamagata, Yusuke Sato, Sakurako Goto-Ito, and Shuya Fukai. 2012. "Get1 Stabilizes an Open Dimer Conformation of get3 ATPase by Binding Two Distinct Interfaces." *Journal of Molecular Biology* 422 (3). Elsevier Ltd: 366–75. doi:10.1016/j.jmb.2012.05.045.

Kumsta, Caroline, and Ursula Jakob. 2009. "Redox-Regulated Chaperones." *Biochemistry* 48 (22): 4666–76. doi:10.1021/bi9003556.

Kuroda, Rieko, Takao Ikenoue, Masanori Honsho, Shoko Tsujimoto, Jun Ya Mitoma, and Akio Ito. 1998. "Charged Amino Acids at the Carboxyl-Terminal Portions Determine the Intracellular Locations of Two Isoforms of Cytochrome b5." *The Journal of Biological Chemistry* 273 (47): 31097–102. doi:10.1074/jbc.273.47.31097.

Kutay, U, G Ahnert-Hilger, E Hartmann, B Wiedenmann, and T A Rapoport. 1995. "Transport Route for Synaptobrevin via a Novel Pathway of Insertion into the Endoplasmic Reticulum Membrane." *The EMBO Journal* 14 (2): 217–23. doi:10.1002/j.1460-2075.1995.tb06994.x.

Kutay, U, Enno Hartmann, and Tom A. Rapoport. 1993. "A Class of Membrane Proteins with a C-Terminal Anchor." *Trends in Cell Biology* 3 (3): 72–75. doi:10.1016/0962-8924(93)90066-A.

Kuwabara, Naoyuki, Ryosuke Minami, Naoto Yokota, Hirofumi Matsumoto, Toshiya Senda, Hiroyuki Kawahara, and Ryuichi Kato. 2015. "Structure of a BAG6 (Bcl-

2-Associated Athanogene 6)-Ubl4a (Ubiquitin-like Protein 4a) Complex Reveals a Novel Binding Interface That Functions in Tail-Anchored Protein Biogenesis." *The Journal of Biological Chemistry* 290 (15): 9387–98. doi:10.1074/jbc.M114.631804.

Kyte, Jack, and Russel F Doolittle. 1982. "A Simple Method for Displaying the Hydropathic Character of a Protein." *Journal of Molecular Biology* 157 (1): 105–32. http://www.ncbi.nlm.nih.gov/pubmed/7108955.

Laemmli, U. K. 1970. "Cleavage of Structural Proteins during the Assembly of the Head of Bacteriophage T4." *Nature* 227 (5259): 680–85. doi:10.1038/227680a0.

Lamb, John R., Stuart Tugendreich, and Phil Hieter. 1995. "Tetratrico Peptide Repeat Interactions: To TPR or Not to TPR?" *Trends in Biochemical Sciences* 20 (7): 257–59. doi:10.1016/S0968-0004(00)89037-4.

Larance, Mark, Yasmeen Ahmad, Kathryn J. Kirkwood, Tony Ly, and Angus I. Lamond. 2013. "Global Subcellular Characterization of Protein Degradation Using Quantitative Proteomics." *Molecular & Cellular Proteomics : MCP* 12 (3): 638–50. doi:10.1074/mcp.M112.024547.

Lee, Michael J., and Henrik G. Dohlman. 2008. "Coactivation of G Protein Signaling by Cell-Surface Receptors and an Intracellular Exchange Factor." *Current Biology* 18 (3): 211–15. doi:10.1016/j.cub.2008.01.007.

Leipe, Detlef D., Yuri I. Wolf, Eugene V. Koonin, and L. Aravind. 2002. "Classification and Evolution of P-Loop GTPases and Related ATPases." *Journal of Molecular Biology* 317 (1): 41–72. doi:10.1006/jmbi.2001.5378.

Letunic, Ivica, and Peer Bork. 2016. "Interactive Tree of Life (iTOL) v3: An Online Tool for the Display and Annotation of Phylogenetic and Other Trees." *Nucleic Acids Research* 44 (W1): W242-5. doi:10.1093/nar/gkw290.

Lexow, Jonas, Tommaso Poggioli, Padmini Sarathchandra, Maria Paola Santini, and Nadia Rosenthal. 2013. "Cardiac Fibrosis in Mice Expressing an Inducible Myocardial-Specific Cre Driver." *Disease Models & Mechanisms* 6 (6): 1470–76. doi:10.1242/dmm.010470.

Leznicki, Pawel, Anne Clancy, Blanche Schwappach, and Stephen High. 2010. "Bat3 Promotes the Membrane Integration of Tail-Anchored Proteins." *Journal of Cell Science* 123 (Pt 13): 2170–78. doi:10.1242/jcs.066738.

Leznicki, Pawel, and Stephen High. 2012. "SGTA Antagonizes BAG6-Mediated Protein Triage." *Proceedings of the National Academy of Sciences of the United*

States of America 109 (47): 19214–19. doi:10.1073/pnas.1209997109.

Leznicki, Pawel, Jelena Korac-Prlic, Katarzyna Kliza, Koraljka Husnjak, Yvonne Nyathi, Ivan Dikic, and Stephen High. 2015. “Binding of SGTA to Rpn13 Selectively Modulates Protein Quality Control.” *Journal of Cell Science* 128 (17): 3187–96. doi:10.1242/jcs.165209.

Leznicki, Pawel, Quentin P. Roebuck, Lydia Wunderley, Anne Clancy, Ewelina M. Krysztofinska, Rivka L. Isaacson, Jim Warwicker, Blanche Schwappach, and Stephen High. 2013. “The Association of BAG6 with SGTA and Tail-Anchored Proteins.” *PloS One* 8 (3): e59590. doi:10.1371/journal.pone.0059590.

Leznicki, Pawel, Jim Warwicker, and Stephen High. 2011. “A Biochemical Analysis of the Constraints of Tail-Anchored Protein Biogenesis.” *The Biochemical Journal* 436 (3): 719–27. doi:10.1042/BJ20101737.

Li, Weizhong, Andrew Cowley, Mahmut Uludag, Tamer Gur, Hamish McWilliam, Silvano Squizzato, Young Mi Park, Nicola Buso, and Rodrigo Lopez. 2015. “The EMBL-EBI Bioinformatics Web and Programmatic Tools Framework.” *Nucleic Acids Research* 43 (W1): W580-4. doi:10.1093/nar/gkv279.

Liang, Jiao, Jun Li, Yanxia Fu, Fangli Ren, Jiake Xu, Mengyu Zhou, Peiyu Li, Haotian Feng, and Yinyin Wang. 2018. “GdX/UBL4A Null Mice Exhibit Mild Kyphosis and Scoliosis Accompanied by Dysregulation of Osteoblastogenesis and Chondrogenesis.” *Cell Biochemistry and Function*, no. December 2017 (February): 1–8. doi:10.1002/cbf.3324.

Lin, Shuh-yow, Melissa A. Vollrath, Sara Mangosing, Jun Shen, Elena Cardenas, and David P. Corey. 2016. “The Zebrafish Pinball Wizard Gene Encodes WRB, a Tail-Anchored-Protein Receptor Essential for Inner-Ear Hair Cells and Retinal Photoreceptors.” *The Journal of Physiology* 594 (4): 895–914. doi:10.1113/JP271437.

Linstedt, A D, M Foguet, M Renz, H P Seelig, B S Glick, and H P Hauri. 1995. “A C-Terminally-Anchored Golgi Protein Is Inserted into the Endoplasmic Reticulum and Then Transported to the Golgi Apparatus.” *Proceedings of the National Academy of Sciences of the United States of America* 92 (11): 5102–5. doi:10.1073/pnas.92.11.5102.

Liou, Shen-Ting, Ming-Yuan Cheng, and Chung Wang. 2007. “SGT2 and MDY2 Interact with Molecular Chaperone YDJ1 in Saccharomyces Cerevisiae.” *Cell Stress & Chaperones* 12 (1): 59–70. doi:10.1379/CSC-220R.1.

6.References

Liu, Fu Hwa, Shin Jen Wu, Su Ming Hu, Chwan Deng Hsiao, and Chung Wang. 1999. “Specific Interaction of the 70-kDa Heat Shock Cognate Protein with the Tetratricopeptide Repeats.” *The Journal of Biological Chemistry* 274 (48): 34425–32. doi:10.1074/jbc.274.48.34425.

Liu, Yanfen, Nia Soetandyo, Jin-Gu Lee, Liping Liu, Yue Xu, William M. Clemons, and Yihong Ye. 2014. “USP13 Antagonizes gp78 to Maintain Functionality of a Chaperone in ER-Associated Degradation.” *eLife* 3: e01369. doi:10.7554/eLife.01369.

Liu, Yiting, and Charles Barlowe. 2002. “Analysis of Sec22p in Endoplasmic reticulum/Golgi Transport Reveals Cellular Redundancy in SNARE Protein Function.” *Molecular Biology of the Cell* 13 (9): 3314–24. doi:10.1091/mbc.E02-04-0204.

Liu, Yu, Liviu Malureanu, Karthik B. Jeganathan, David Dinh Tran, Lonn D. Lindquist, Jan M van Deursen, and Richard J. Bram. 2009. “CAML Loss Causes Anaphase Failure and Chromosome Missegregation.” *Cell Cycle (Georgetown, Tex.)* 8 (6): 940–49. doi:10.4161/cc.8.6.7948.

Liu, Yunkai, Sujuan Ye, and Alexandre M Erkine. 2009. “Analysis of Saccharomyces Cerevisiae Genome for the Distributions of Stress-Response Elements Potentially Affecting Gene Expression by Transcriptional Interference.” *In Silico Biology* 9 (5–6): 379–89. doi:10.3233/ISB-2009-0412.

Liu, Yuqiong, Yuichi Yagita, and Yukio Fujiki. 2016. “Assembly of Peroxisomal Membrane Proteins via the Direct Pex19p-Pex3p Pathway.” *Traffic (Copenhagen, Denmark)* 17 (4): 433–55. doi:10.1111/tra.12376.

Lowe, Stephen Loucian, Frank Peter, V. Nathan Subramaniam, Siew Heng Wong, and Wanjin Hong. 1997. “A SNARE Involved in Protein Transport through the Golgi Apparatus.” *Nature* 389 (6653): 881–84. doi:10.1038/39923.

Luisi, Bf F, Wx X Xu, Z Otwinowski, L P Freedman, K R Yamamoto, and P B Sigler. 1991. “Crystallographic Analysis of the Interaction of the Glucocorticoid Receptor with DNA.” *Nature* 352 (6335): 497–505. doi:10.1038/352497a0.

Lutkenhaus, Joe, and M. Sundaramoorthy. 2003. “MinD and Role of the Deviant Walker A Motif, Dimerization and Membrane Binding in Oscillation.” *Molecular Microbiology* 48 (2): 295–303. doi:10.1046/j.1365-2958.2003.03427.x.

Madan, A P, and D B DeFranco. 1993. “Bidirectional Transport of Glucocorticoid Receptors across the Nuclear Envelope.” *Proceedings of the National Academy*

of Sciences of the United States of America 90 (8): 3588–92. doi:10.1073/pnas.90.8.3588.

Mallard, Frédéric, Bor Luen Tang, Thierry Galli, Danièle Tenza, Agnès Saint-Pol, Xu Yue, Claude Antony, Wanjin Hong, Bruno Goud, and Ludger Johannes. 2002. "Early/recycling Endosomes-to-TGN Transport Involves Two SNARE Complexes and a Rab6 Isoform." *The Journal of Cell Biology* 156 (4): 653–64. doi:10.1083/jcb.200110081.

Manchen, Steven T., and Andrew V. Hubberstey. 2001. "Human Scythe Contains a Functional Nuclear Localization Sequence and Remains in the Nucleus during Staurosporine-Induced Apoptosis." *Biochemical and Biophysical Research Communications* 287 (5): 1075–82. doi:10.1006/bbrc.2001.5701.

Mandon, Elisabet C., and Reid Gilmore. 2007. "The Tail End of Membrane Insertion." *Cell* 128 (6): 1031–32. doi:10.1016/j.cell.2007.03.001.

Manilal, S., T M Nguyen, and G. E. Morris. 1998. "Colocalization of Emerin and Lamins in Interphase Nuclei and Changes during Mitosis." *Biochemical and Biophysical Research Communications* 249 (3): 643–47. doi:10.1006/bbrc.1998.9209.

Mariappan, Malaiyalam, Xingzhe Li, Sandra Stefanovic, Ajay Sharma, Agnieszka Mateja, Robert J. Keenan, and Ramanujan S. Hegde. 2010. "A Ribosome-Associating Factor Chaperones Tail-Anchored Membrane Proteins." *Nature* 466 (7310). Nature Publishing Group: 1120–24. doi:10.1038/nature09296.

Mariappan, Malaiyalam, Agnieszka Mateja, Malgorzata Dobosz, Elia Bove, Ramanujan S Hegde, and Robert J Keenan. 2011. "The Mechanism of Membrane-Associated Steps in Tail-Anchored Protein Insertion." *Nature* 477 (7362). Nature Publishing Group: 61–66. doi:10.1038/nature10362.

Masaki, Ryuichi, Akitsugu Yamamoto, and Yutaka Tashiro. 1996. "Membrane Topology and Retention of Microsomal Aldehyde Dehydrogenase in the Endoplasmic Reticulum." *The Journal of Biological Chemistry* 271 (28): 16939–44. doi:10.1074/jbc.271.28.16939.

Mateja, Agnieszka, Marcin Paduch, Hsin-Yang Chang, Anna Szydlowska, Anthony a. Kossiakoff, Ramanujan S. Hegde, and Robert J. Keenan. 2015. "Protein Targeting. Structure of the Get3 Targeting Factor in Complex with Its Membrane Protein Cargo." *Science (New York, N.Y.)* 347 (6226): 1152–55. doi:10.1126/science.1261671.

6.References

Mateja, Agnieszka, Anna Szlachcic, Maureen E Downing, Malgorzata Dobosz, Malaiyalam Mariappan, Ramanujan S Hegde, and Robert J. Keenan. 2009. “The Structural Basis of Tail-Anchored Membrane Protein Recognition by Get3.” *Nature* 461 (7262). Nature Publishing Group: 361–66. doi:10.1038/nature08319.

Mayerhofer, Peter U. 2016. “Targeting and Insertion of Peroxisomal Membrane Proteins: ER Trafficking versus Direct Delivery to Peroxisomes.” *Biochimica et Biophysica Acta* 1863 (5). Elsevier B.V.: 870–80. doi:10.1016/j.bbamcr.2015.09.021.

Mayerhofer, Peter U., Manuel Bañó-Polo, Ismael Mingarro, and Arthur E. Johnson. 2016. “Human Peroxin PEX3 Is Co-Translationally Integrated into the ER and Exits the ER in Budding Vesicles.” *Traffic (Copenhagen, Denmark)* 17 (2): 117–30. doi:10.1111/tra.12350.

Meijsing, Sebastiaan H., Miles A. Pufall, Alex Y. So, Darren L. Bates, Lin Chen, and Keith R. Yamamoto. 2009. “DNA Binding Site Sequence Directs Glucocorticoid Receptor Structure and Activity.” *Science (New York, N.Y.)* 324 (5925): 407–10. doi:10.1126/science.1164265.

Melé, Marta, Pedro G Ferreira, Ferran Reverter, David S DeLuca, Jean Monlong, Michael Sammeth, Taylor R Young, et al. 2015. “Human Genomics. The Human Transcriptome across Tissues and Individuals.” *Science (New York, N.Y.)* 348 (6235): 660–65. doi:10.1126/science.aaa0355.

Metz, Jutta, Andrea Wächter, Bastian Schmidt, Janusz M. Bujnicki, and Blanche Schwappach. 2006. “The Yeast Arr4p ATPase Binds the Chloride Transporter Gef1p When Copper Is Available in the Cytosol.” *The Journal of Biological Chemistry* 281 (1): 410–17. doi:10.1074/jbc.M507481200.

Metzger, D, J Clifford, H Chiba, and P Chambon. 1995. “Conditional Site-Specific Recombination in Mammalian Cells Using a Ligand-Dependent Chimeric Cre Recombinase.” *Proceedings of the National Academy of Sciences of the United States of America* 92 (15): 6991–95. doi:10.1073/pnas.92.15.6991.

Meyer, David I., Elke Krause, and Bernhard Dobberstein. 1982. “Secretory Protein Translocation across Membranes-the Role of The "docking Protein’.” *Nature* 297 (5868): 647–50. doi:10.1038/297647a0.

Minami, Ryosuke, Atsuko Hayakawa, Hiroki Kagawa, Yuko Yanagi, Hideyoshi Yokosawa, and Hiroyuki Kawahara. 2010. “BAG-6 Is Essential for Selective Elimination of Defective Proteasomal Substrates.” *Journal of Cell Biology* 190

(4): 637–50. doi:10.1083/jcb.200908092.

Misumi, Yoshio, Miwa Sohda, Akiko Tashiro, Hiroshi Sato, and Yukio Ikehara. 2001. "An Essential Cytoplasmic Domain for the Golgi Localization of Coiled-Coil Proteins with a COOH-Terminal Membrane Anchor." *The Journal of Biological Chemistry* 276 (9): 6867–73. doi:10.1074/jbc.M010121200.

Mizushima, Noboru, Tamotsu Yoshimori, and Beth Levine. 2010. "Methods in Mammalian Autophagy Research." *Cell* 140 (3): 313–26. doi:10.1016/j.cell.2010.01.028.

Mock, Jee-Young, Justin William Chartron, Ma'ayan Zaslaver, Yue Xu, Yihong Ye, and William Melvon Clemons. 2015. "Bag6 Complex Contains a Minimal Tail-Anchor-Targeting Module and a Mock BAG Domain." *Proceedings of the National Academy of Sciences of the United States of America* 112 (1): 106–11. doi:10.1073/pnas.1402745112.

Mock, Jee-Young, Yue Xu, Yihong Ye, and William M. Clemons. 2017. "Structural Basis for Regulation of the Nucleo-Cytoplasmic Distribution of Bag6 by TRC35." *Proceedings of the National Academy of Sciences of the United States of America* 114 (44): 11679–84. doi:10.1073/pnas.1702940114.

Möller, Steffen, Michael D.R. Croning, and Rolf Apweiler. 2001. "Evaluation of Methods for the Prediction of Membrane Spanning Regions." *Bioinformatics (Oxford, England)* 17 (7): 646–53. doi:10.1093/bioinformatics/17.7.646.

Mukhopadhyay, Rita, Ye-Shih Ho, Pamela J. Swiatek, Barry P. Rosen, and Hiranmoy Bhattacharjee. 2006. "Targeted Disruption of the Mouse Asna1 Gene Results in Embryonic Lethality." *FEBS Letters* 580 (16): 3889–94. doi:10.1016/j.febslet.2006.06.017.

Mullen, Robert T., and Richard N. Trelease. 2000. "The Sorting Signals for Peroxisomal Membrane-Bound Ascorbate Peroxidase Are within Its C-Terminal Tail." *The Journal of Biological Chemistry* 275 (21): 16337–44. doi:10.1074/jbc.M001266200.

Munro, S. 1995. "An Investigation of the Role of Transmembrane Domains in Golgi Protein Retention." *The EMBO Journal* 14 (19): 4695–4704. doi:7588599.

Muntau, Ania C., Adelbert A. Roscher, Wolf-H Kunau, and Gabriele Dodt. 2003. "The Interaction between Human PEX3 and PEX19 Characterized by Fluorescence Resonance Energy Transfer (FRET) Analysis." *European Journal of Cell Biology* 82 (7): 333–42. doi:10.1078/0171-9335-00325.

6.References

Murata, Kenji, Sean Degmetich, Masato Kinoshita, and Eriko Shimada. 2009. "Expression of the Congenital Heart Disease 5/tryptophan Rich Basic Protein Homologue Gene during Heart Development in Medaka Fish, Oryzias Latipes." *Development, Growth & Differentiation* 51 (2): 95–107. doi:10.1111/j.1440-169X.2008.01084.x.

Nagai, Takeharu, Keiji Ibata, Eun Sun Park, Mie Kubota, Katsuhiko Mikoshiba, and Atsushi Miyawaki. 2002. "A Variant of Yellow Fluorescent Protein with Fast and Efficient Maturation for Cell-Biological Applications." *Nature Biotechnology* 20 (1): 87–90. doi:10.1038/nbt0102-87.

Nørby, J G. 1988. "Coupled Assay of Na+,K+-ATPase Activity." *Methods in Enzymology* 156 (1984): 116–19. http://www.ncbi.nlm.nih.gov/pubmed/2835597.

Norlin, Stefan, Vishal Parekh, and Helena Edlund. 2018. "The ATPase Activity of Asna1/TRC40 Is Required for Pancreatic Progenitor Cell Survival." *Development (Cambridge, England)* 145 (1): dev.154468. doi:10.1242/dev.154468.

Norlin, Stefan, Vishal S Parekh, Peter Naredi, and Helena Edlund. 2016. "Asna1/TRC40 Controls β-Cell Function and Endoplasmic Reticulum Homeostasis by Ensuring Retrograde Transport." *Diabetes* 65 (1): 110–19. doi:10.2337/db15-0699.

O'Gorman, S, D T Fox, and G M Wahl. 1991. "Recombinase-Mediated Gene Activation and Site-Specific Integration in Mammalian Cells." *Science (New York, N.Y.)* 251 (4999): 1351–55. doi:10.1126/science.1900642.

Okreglak, Voytek, and Peter Walter. 2014. "The Conserved AAA-ATPase Msp1 Confers Organelle Specificity to Tail-Anchored Proteins." *Proceedings of the National Academy of Sciences of the United States of America* 111 (22): 8019–24. doi:10.1073/pnas.1405755111.

Ott, Melanie, Débora Marques, Christina Funk, and Susanne M. Bailer. 2016. "Asna1/TRC40 That Mediates Membrane Insertion of Tail-Anchored Proteins Is Required for Efficient Release of Herpes Simplex Virus 1 Virions." *Virology Journal* 13 (1). Virology Journal: 175. doi:10.1186/s12985-016-0638-8.

Ourisson, Guy, and Yoichi Nakatani. 1994. "The Terpenoid Theory of the Origin of Cellular Life: The Evolution of Terpenoids to Cholesterol." *Chemistry & Biology* 1 (1): 11–23. doi:10.1016/1074-5521(94)90036-1.

Pandit, Jayvardhan, Dennis E. Danley, Gayle K. Schulte, Stacy Mazzalupo, Thomas A. Pauly, Cheryl M. Hayward, Ernest S. Hamanaka, John F. Thompson, and H.

James Harwood. 2000. “Crystal Structure of Human Squalene Synthase. A Key Enzyme in Cholesterol Biosynthesis.” *The Journal of Biological Chemistry* 275 (39): 30610–17. doi:10.1074/jbc.M004132200.

Paul, Atanu, Yenni a. Garcia, Bettina Zierer, Chaitanya Patwardhan, Omar Gutierrez, Zacariah Hildenbrand, Diondra C. Harris, et al. 2014. “The Cochaperone SGTA (Small Glutamine-Rich Tetratricopeptide Repeat-Containing Protein Alpha) Demonstrates Regulatory Specificity for the Androgen, Glucocorticoid, and Progesterone Receptors.” *The Journal of Biological Chemistry* 289 (22): 15297–308. doi:10.1074/jbc.M113.535229.

Payapilly, Aishwarya, and Stephen High. 2014. “BAG6 Regulates the Quality Control of a Polytopic ERAD Substrate.” *Journal of Cell Science* 127 (Pt 13): 2898–2909. doi:10.1242/jcs.145565.

Pedrazzini, Emanuela, Antonello Villa, Renato Longhi, Alessandra Bulbarelli, and Nica Borgese. 2000. “Mechanism of Residence of Cytochrome b(5), a Tail-Anchored Protein, in the Endoplasmic Reticulum.” *The Journal of Cell Biology* 148 (5): 899–914. doi:10.1083/jcb.148.5.899.

Pfaff, Janine, Jhon Rivera-Monroy, Cara Jamieson, Kalpana Rajanala, Fabio Vilardi, Blanche Schwappach, and Ralph H. Kehlenbach. 2016. “Emery-Dreifuss Muscular Dystrophy Mutations Impair TRC40-Mediated Targeting of Emerin to the Inner Nuclear Membrane.” *Journal of Cell Science* 129 (3): 502–16. doi:10.1242/jcs.179333.

Philp, Lisa K., Tanya K. Day, Miriam S Butler, Geraldine Laven-Law, Shalini Jindal, Theresa E. Hickey, Howard I. Scher, Lisa M. Butler, and Wayne D. Tilley. 2016. “Small Glutamine-Rich Tetratricopeptide Repeat-Containing Protein Alpha (SGTA) Ablation Limits Offspring Viability and Growth in Mice.” *Scientific Reports* 6 (January). Nature Publishing Group: 28950. doi:10.1038/srep28950.

Phuc Le, Phillip, Joshua R. Friedman, Jonathan Schug, John E. Brestelli, J. Brandon Parker, Irina M. Bochkis, and Klaus H. Kaestner. 2005. “Glucocorticoid Receptor-Dependent Gene Regulatory Networks.” *PLoS Genetics* 1 (2): e16. doi:10.1371/journal.pgen.0010016.

Picard, D, B Khursheed, M J Garabedian, M G Fortin, S Lindquist, and K R Yamamoto. 1990. “Reduced Levels of hsp90 Compromise Steroid Receptor Action in Vivo.” *Nature* 348 (6297): 166–68. doi:10.1038/348166a0.

Picard, D, and K R Yamamoto. 1987. “Two Signals Mediate Hormone-Dependent

Nuclear Localization of the Glucocorticoid Receptor." *The EMBO Journal* 6 (11): 3333–40.

Plutner, H, H W Davidson, J Saraste, and W E Balch. 1992. "Morphological Analysis of Protein Transport from the ER to Golgi Membranes in Digitonin-Permeabilized Cells: Role of the P58 Containing Compartment." *The Journal of Cell Biology* 119 (5): 1097–1116. http://www.ncbi.nlm.nih.gov/pubmed/1447290.

Pool, Martin R. 2005. "Signal Recognition Particles in Chloroplasts, Bacteria, Yeast and Mammals (Review)." *Molecular Membrane Biology* 22 (1–2): 3–15. doi:10.1080/09687860400026348.

Powis, Katie. 2012. "Regulation of the Pathway for the Guided Entry of Tail-Anchored Proteins." University of Manchester.

Powis, Katie, Bianca Schrul, Heather Tienson, Irina Gostimskaya, Michal Breker, Stephen High, Maya Schuldiner, Ursula Jakob, and Blanche Schwappach. 2013. "Get3 Is a Holdase Chaperone and Moves to Deposition Sites for Aggregated Proteins When Membrane Targeting Is Blocked." *Journal of Cell Science* 126 (Pt 2): 473–83. doi:10.1242/jcs.112151.

Prekeris, R, B Yang, V Oorschot, J Klumperman, and R H Scheller. 1999. "Differential Roles of Syntaxin 7 and Syntaxin 8 in Endosomal Trafficking." *Molecular Biology of the Cell* 10 (11): 3891–3908. doi:10.1091/mbc.10.11.3891.

Preta, Giulio, and Bengt Fadeel. 2012. "Scythe Cleavage during Fas (APO-1)-and Staurosporine-Mediated Apoptosis." *FEBS Letters* 586 (6). Federation of European Biochemical Societies: 747–52. doi:10.1016/j.febslet.2012.01.034.

Pryor, Paul R., Barbara M. Mullock, Nicholas A. Bright, Margaret R. Lindsay, Sally R. Gray, Simon C W Richardson, Abigail Stewart, David E. James, Robert C. Piper, and J. Paul Luzio. 2004. "Combinatorial SNARE Complexes with VAMP7 or VAMP8 Define Different Late Endocytic Fusion Events." *EMBO Reports* 5 (6): 590–95. doi:10.1038/sj.embor.7400150.

Quisel, J D, D C Lin, and A D Grossman. 1999. "Control of Development by Altered Localization of a Transcription Factor in B. Subtilis." *Molecular Cell* 4 (5): 665–72. doi:S1097-2765(00)80377-9 [pii].

Rabu, Catherine, Volker Schmid, Blanche Schwappach, and Stephen High. 2009. "Biogenesis of Tail-Anchored Proteins: The Beginning for the End?" *Journal of Cell Science* 122 (Pt 20): 3605–12. doi:10.1242/jcs.041210.

Rabu, Catherine, Peter Wipf, Jeffrey L. Brodsky, and Stephen High. 2008. "A

Precursor-Specific Role for Hsp40/Hsc70 during Tail-Anchored Protein Integration at the Endoplasmic Reticulum." *The Journal of Biological Chemistry* 283 (41): 27504–13. doi:10.1074/jbc.M804591200.

Rao, Meera, Voytek Okreglak, Un Seng Chio, Hyunju Cho, Peter Walter, and Shu-Ou Shan. 2016. "Multiple Selection Filters Ensure Accurate Tail-Anchored Membrane Protein Targeting." *eLife* 5 (December). doi:10.7554/eLife.21301.

Rapoport, Tom A. 2007. "Protein Translocation across the Eukaryotic Endoplasmic Reticulum and Bacterial Plasma Membranes." *Nature* 450 (7170): 663–69. doi:10.1038/nature06384.

Ricketson, D., U. Hostick, L. Fang, K. R. Yamamoto, and B. D. Darimont. 2007. "A Conformational Switch in the Ligand-Binding Domain Regulates the Dependence of the Glucocorticoid Receptor on Hsp90." *Journal of Molecular Biology* 368 (3): 729–41. doi:10.1016/j.jmb.2007.02.057.

Riddles, P W, Robert L Blakeley, and Burt Zerner. 1983. "Reassessment of Ellman's Reagent." *Methods in Enzymology* 91 (1979): 49–60. http://www.ncbi.nlm.nih.gov/pubmed/6855597.

Rivas, Manuel A, Matti Pirinen, Donald F Conrad, Monkol Lek, Emily K Tsang, Konrad J Karczewski, Julian B Maller, et al. 2015. "Human Genomics. Effect of Predicted Protein-Truncating Genetic Variants on the Human Transcriptome." *Science (New York, N.Y.)* 348 (6235): 666–69. doi:10.1126/science.1261877.

Rivera-Monroy, Jhon, Lena Musiol, Kirsten Unthan-Fechner, Ákos Farkas, Anne Clancy, Javier Coy-Vergara, Uri Weill, et al. 2016. "Mice Lacking WRB Reveal Differential Biogenesis Requirements of Tail-Anchored Proteins in Vivo." *Scientific Reports* 6 (December). Nature Publishing Group: 39464. doi:10.1038/srep39464.

Rodrigo-Brenni, Monica C., Erik Gutierrez, and Ramanujan S. Hegde. 2014. "Cytosolic Quality Control of Mislocalized Proteins Requires RNF126 Recruitment to Bag6." *Molecular Cell* 55 (2). The Authors: 227–37. doi:10.1016/j.molcel.2014.05.025.

Rome, Michael E., Un Seng Chio, Meera Rao, Harry B Gristick, and Shu-ou Shan. 2014. "Differential Gradients of Interaction Affinities Drive Efficient Targeting and Recycling in the GET Pathway." *Proceedings of the National Academy of Sciences of the United States of America* 2014 (46): 1–7. doi:10.1073/pnas.1411284111.

6.References

Rome, Michael E, Meera Rao, William Melvon Clemons, and Shu-Ou Shan. 2013. "Precise Timing of ATPase Activation Drives Targeting of Tail-Anchored Proteins." *Proceedings of the National Academy of Sciences of the United States of America* 110 (19): 7666–71. doi:10.1073/pnas.1222054110.

Sahara, Kazutaka, Larissa Kogleck, Hideki Yashiroda, and Shigeo Murata. 2014. "The Mechanism for Molecular Assembly of the Proteasome." *Advances in Biological Regulation* 54 (1). Elsevier Ltd: 51–58. doi:10.1016/j.jbior.2013.09.010.

Sahtoe, Danny D., Willem J van Dijk, Farid El Oualid, Reggy Ekkebus, Huib Ovaa, and Titia K. Sixma. 2015. "Mechanism of UCH-L5 Activation and Inhibition by DEUBAD Domains in RPN13 and INO80G." *Molecular Cell* 57 (5). The Authors: 887–900. doi:10.1016/j.molcel.2014.12.039.

Saiki, Randall K, Stephen Scharf, Fred Faloona, Kary B Mullis, Glenn T Horn, Henry A Erlich, and Norman Arnheim. 1985. "Enzymatic Amplification of Beta-Globin Genomic Sequences and Restriction Site Analysis for Diagnosis of Sickle Cell Anemia." *Science (New York, N.Y.)* 230 (4732): 1350–54. http://www.ncbi.nlm.nih.gov/pubmed/2999980.

Sambrook, Joseph, and David W Russell. 2006. "SDS-Polyacrylamide Gel Electrophoresis of Proteins." *CSH Protocols* 2006 (4). doi:10.1101/pdb.prot4540.

Saraste, Matti, Peter R. Sibbald, and Alfred Wittinghofer. 1990. "The P-Loop--a Common Motif in ATP- and GTP-Binding Proteins." *Trends in Biochemical Sciences* 15 (11): 430–34. doi:10.1016/0968-0004(90)90281-F.

Sasaki, Toru, Eugene C. Gan, Andrew Wakeham, Sally Kornbluth, Tak W. Mak, and Hitoshi Okada. 2007. "HLA-B-Associated Transcript 3 (Bat3)/Scythe Is Essential for p300-Mediated Acetylation of p53." *Genes & Development* 21 (7): 848–61. doi:10.1101/gad.1534107.

Schena, M, and K R Yamamoto. 1988. "Mammalian Glucocorticoid Receptor Derivatives Enhance Transcription in Yeast." *Science (New York, N.Y.)* 241 (4868): 965–67. doi:10.1126/science.3043665.

Scherer, W F, J T Syverton, and G O Gey. 1953. "Studies on the Propagation in Vitro of Poliomyelitis Viruses. IV. Viral Multiplication in a Stable Strain of Human Malignant Epithelial Cells (Strain HeLa) Derived from an Epidermoid Carcinoma of the Cervix." *The Journal of Experimental Medicine* 97 (5): 695–710. doi:10.1084/jem.97.5.695.

Scheufler, Clemens, Achim Brinker, Gleb Bourenkov, Stefano Pegoraro, Luis Moroder, Hans Bartunik, F. Ulrich Hartl, and Ismail Moarefi. 2000. “Structure of TPR Domain-Peptide Complexes: Critical Elements in the Assembly of the Hsp70-Hsp90 Multichaperone Machine.” *Cell* 101 (2): 199–210. doi:10.1016/S0092-8674(00)80830-2.

Schneider, Caroline A., Wayne S. Rasband, and Kevin W. Eliceiri. 2012. “NIH Image to ImageJ: 25 Years of Image Analysis.” *Nature Methods* 9 (7). Nature Publishing Group: 671–75. doi:10.1038/nmeth.2089.

Scholefield, Graham, Rachel Whiting, Jeff Errington, and Heath Murray. 2011. “Spo0J Regulates the Oligomeric State of Soj to Trigger Its Switch from an Activator to an Inhibitor of DNA Replication Initiation.” *Molecular Microbiology* 79 (4): 1089–1100. doi:10.1111/j.1365-2958.2010.07507.x.

Schrul, Bianca, and Ron R. Kopito. 2016. “Peroxin-Dependent Targeting of a Lipid-Droplet-Destined Membrane Protein to ER Subdomains.” *Nature Cell Biology* 18 (7): 740–51. doi:10.1038/ncb3373.

Schuldiner, Maya, Sean R. Collins, Natalie J. Thompson, Vladimir Denic, Arunashree Bhamidipati, Thanuja Punna, Jan Ihmels, et al. 2005. “Exploration of the Function and Organization of the Yeast Early Secretory Pathway through an Epistatic Miniarray Profile.” *Cell* 123 (3): 507–19. doi:10.1016/j.cell.2005.08.031.

Schuldiner, Maya, Jutta Metz, Volker Schmid, Vladimir Denic, Magdalena Rakwalska, Hans Dieter Schmitt, Blanche Schwappach, and Jonathan S. Weissman. 2008. “The GET Complex Mediates Insertion of Tail-Anchored Proteins into the ER Membrane.” *Cell* 134 (4): 634–45. doi:10.1016/j.cell.2008.06.025.

Schwenk, Frieder, R Kuhn, Pierre Olivier Angrand, Klaus Rajewsky, and A. Francis Stewart. 1998. “Temporally and Spatially Regulated Somatic Mutagenesis in Mice.” *Nucleic Acids Research* 26 (6): 1427–32. doi:10.1093/nar/26.6.1427.

Sebti, Salwa, Christine Prébois, Esther Pérez-Gracia, Chantal Bauvy, Fabienne Desmots, Nelly Pirot, Céline Gongora, et al. 2014. “BAT3 Modulates p300-Dependent Acetylation of p53 and Autophagy-Related Protein 7 (ATG7) during Autophagy.” *Proceedings of the National Academy of Sciences of the United States of America* 111 (11): 4115–20. doi:10.1073/pnas.1313618111.

Shan, Shu-ou. 2016. “ATPase and GTPase Tangos Drive Intracellular Protein Transport.” *Trends in Biochemical Sciences* 41 (12). Elsevier Ltd: 1050–60.

doi:10.1016/j.tibs.2016.08.012.

Shao, Sichen, and Ramanujan S. Hegde. 2011. “A Calmodulin-Dependent Translocation Pathway for Small Secretory Proteins.” *Cell* 147 (7). Elsevier Inc.: 1576–88. doi:10.1016/j.cell.2011.11.048.

Shao, Sichen, Monica C Rodrigo-Brenni, Maryann H Kivlen, and Ramanujan S Hegde. 2017. “Mechanistic Basis for a Molecular Triage Reaction.” *Science (New York, N.Y.)* 355 (6322): 298–302. doi:10.1126/science.aah6130.

Sharpe, Hayley J., Tim J. Stevens, and Sean Munro. 2010. “A Comprehensive Comparison of Transmembrane Domains Reveals Organelle-Specific Properties.” *Cell* 142 (1). Elsevier Ltd: 158–69. doi:10.1016/j.cell.2010.05.037.

Shen, Jian, Ching-Mei Hsu, Bae-Kwang Kang, Barry P. Rosen, and Hiranmoy Bhattacharjee. 2003. “The Saccharomyces Cerevisiae Arr4p Is Involved in Metal and Heat Tolerance.” *Biometals : An International Journal on the Role of Metal Ions in Biology, Biochemistry, and Medicine* 16 (3): 369–78. doi:10.1023/A:1022504311669.

Sikorski, R. S., and P. Hieter. 1989. “A System of Shuttle Vectors and Yeast Host Strains Designed for Efficient Manipulation of DNA in Saccharomyces Cerevisiae.” *Genetics* 122 (1): 19–27. doi:0378111995000377 [pii].

Silvius, John R. 2002. “Lipidated Peptides as Tools for Understanding the Membrane Interactions of Lipid-Modified Proteins.” In *Current Topics in Membranes*, 52:371–95. doi:10.1016/S1063-5823(02)52015-9.

Simpson, Peter J., Blanche Schwappach, Henrik G. Dohlman, and Rivka L. Isaacson. 2010. “Structures of Get3, Get4, and Get5 Provide New Models for TA Membrane Protein Targeting.” *Structure (London, England : 1993)* 18 (8). Elsevier Ltd: 897–902. doi:10.1016/j.str.2010.07.003.

Smith, David F. 2004. “Tetratricopeptide Repeat Cochaperones in Steroid Receptor Complexes.” *Cell Stress & Chaperones* 9 (2): 109–21. http://www.ncbi.nlm.nih.gov/pubmed/15497498.

Sohal, D S, M Nghiem, M A Crackower, S A Witt, T R Kimball, K M Tymitz, J M Penninger, and J D Molkentin. 2001. “Temporally Regulated and Tissue-Specific Gene Manipulations in the Adult and Embryonic Heart Using a Tamoxifen-Inducible Cre Protein.” *Circulation Research* 89 (1): 20–25. doi:10.1161/hh1301.092687.

Sojka, Stephen, Nirav M. Amin, Devin Gibbs, Kathleen S Christine, Marta S

Charpentier, and Frank L Conlon. 2014. “Congenital Heart Disease Protein 5 Associates with CASZ1 to Maintain Myocardial Tissue Integrity.” *Development (Cambridge, England)* 141 (15): 3040–49. doi:10.1242/dev.106518.

Söllner, Thomas, Sidney W. Whiteheart, Michael Brunner, Hediye Erdjument-Bromage, Scott Geromanos, Paul Tempst, and James E. Rothman. 1993. “SNAP Receptors Implicated in Vesicle Targeting and Fusion.” *Nature* 362 (6418): 318–24. doi:10.1038/362318a0.

Spies, T, G Blanck, M Bresnahan, J Sands, and J L Strominger. 1989. “A New Cluster of Genes within the Human Major Histocompatibility Complex.” *Science (New York, N.Y.)* 243 (4888): 214–17. doi:10.1126/science.2911734.

Sprang, Stephen R. 1997. “G Protein Mechanisms: Insights from Structural Analysis.” *Annual Review of Biochemistry* 66: 639–78. doi:10.1146/annurev.biochem.66.1.639.

Srivastava, Renu, Benjamin E. Zalisko, Robert J. Keenan, and Stephen H. Howell. 2017. “The GET System Inserts the Tail-Anchored Protein, SYP72, into Endoplasmic Reticulum Membranes.” *Plant Physiology* 173 (2): 1137–45. doi:10.1104/pp.16.00928.

Stefanovic, Sandra, and Ramanujan S. Hegde. 2007. “Identification of a Targeting Factor for Posttranslational Membrane Protein Insertion into the ER.” *Cell* 128 (6): 1147–59. doi:10.1016/j.cell.2007.01.036.

Stefer, Susanne, Simon Reitz, Fei Wang, Klemens Wild, Yin-Yuin Pang, Daniel Schwarz, Jörg Bomke, et al. 2011. “Structural Basis for Tail-Anchored Membrane Protein Biogenesis by the Get3-Receptor Complex.” *Science (New York, N.Y.)* 333 (6043): 758–62. doi:10.1126/science.1207125.

Stevens, Timothy J., and Isaiah T. Arkin. 2000. “Do More Complex Organisms Have a Greater Proportion of Membrane Proteins in Their Genomes?” *Proteins* 39 (4): 417–20. doi:10.1002/(SICI)1097-0134(20000601)39:4<417::AID-PROT140>3.0.CO;2-Y.

Subramaniam, V N, E Loh, H Horstmann, A Habermann, Y Xu, J Coe, G Griffiths, and W Hong. 2000. “Preferential Association of Syntaxin 8 with the Early Endosome.” *Journal of Cell Science* 113 (Pt 6 (March): 997–1008. http://www.ncbi.nlm.nih.gov/pubmed/10683148.

Suga, Kei, Hiroshi Hattori, Ayako Saito, and Kimio Akagawa. 2005. “RNA Interference-Mediated Silencing of the Syntaxin 5 Gene Induces Golgi

Fragmentation but Capable of Transporting Vesicles." *FEBS Letters* 579 (20): 4226–34. doi:10.1016/j.febslet.2005.06.053.

Suloway, Christian J M, Justin W Chartron, Ma'ayan Zaslaver, and William M Clemons. 2009. "Model for Eukaryotic Tail-Anchored Protein Binding Based on the Structure of Get3." *Proceedings of the National Academy of Sciences of the United States of America* 106 (35): 14849–54. doi:10.1073/pnas.0907522106.

Surjit, Milan, Krishna Priya Ganti, Atish Mukherji, Tao Ye, Guoqiang Hua, Daniel Metzger, Mei Li, and Pierre Chambon. 2011. "Widespread Negative Response Elements Mediate Direct Repression by Agonist-Liganded Glucocorticoid Receptor." *Cell* 145 (2). Elsevier Inc.: 224–41. doi:10.1016/j.cell.2011.03.027.

Suzuki, Rigel, and Hiroyuki Kawahara. 2016. "UBQLN4 Recognizes Mislocalized Transmembrane Domain Proteins and Targets These to Proteasomal Degradation." *EMBO Reports* 17 (6): 842–57. doi:10.15252/embr.201541402.

Swinkels, B W, S J Gould, A G Bodnar, R A Rachubinski, and S Subramani. 1991. "A Novel, Cleavable Peroxisomal Targeting Signal at the Amino-Terminus of the Rat 3-Ketoacyl-CoA Thiolase." *The EMBO Journal* 10 (11): 3255–62. doi:10.1016/0962-8924(92)90153-E.

Tafani, Marco, Luigi Sansone, Federica Limana, Tania Arcangeli, Elena De Santis, Milena Polese, Massimo Fini, and Matteo A. Russo. 2016. "The Interplay of Reactive Oxygen Species, Hypoxia, Inflammation, and Sirtuins in Cancer Initiation and Progression." *Oxidative Medicine and Cellular Longevity* 2016. Hindawi Publishing Corporation: 3907147. doi:10.1155/2016/3907147.

Tanaka, Hirofumi, Toshiki Takahashi, Yiming Xie, Ryosuke Minami, Yuko Yanagi, Mizuki Hayashishita, Rigel Suzuki, et al. 2016. "A Conserved Island of BAG6/Scythe Is Related to Ubiquitin Domains and Participates in Short Hydrophobicity Recognition." *The FEBS Journal* 283 (4): 662–77. doi:10.1111/febs.13618.

Tanaka, Masayuki, Mayumi Nishi, Masafumi Morimoto, Tohru Sugimoto, and Mitsuhiro Kawata. 2003. "Yellow Fluorescent Protein-Tagged and Cyan Fluorescent Protein-Tagged Imaging Analysis of Glucocorticoid Receptor and Importins in Single Living Cells." *Endocrinology* 144 (9): 4070–79. doi:10.1210/en.2003-0282.

Thapaliya, Arjun, Yvonne Nyathi, Santiago Martínez-Lumbreras, Ewelina M. Krysztofinska, Nicola J. Evans, Isabelle L. Terry, Stephen High, and Rivka L.

Isaacson. 2016. “SGTA Interacts with the Proteasomal Ubiquitin Receptor Rpn13 via a Carboxylate Clamp Mechanism.” *Scientific Reports* 6 (October): 36622. doi:10.1038/srep36622.

The UniProt Consortium. 2017. “UniProt: The Universal Protein Knowledgebase.” *Nucleic Acids Research* 45 (D1). Oxford University Press: D158–69. doi:10.1093/nar/gkw1099.

Thomsen, Martin Christen Frølund, and Morten Nielsen. 2012. “Seq2Logo: A Method for Construction and Visualization of Amino Acid Binding Motifs and Sequence Profiles Including Sequence Weighting, Pseudo Counts and Two-Sided Representation of Amino Acid Enrichment and Depletion.” *Nucleic Acids Research* 40 (Web Server issue): W281-7. doi:10.1093/nar/gks469.

Thress, Kenneth, Jaewhan Song, Richard I. Morimoto, and Sally Kornbluth. 2001. “Reversible Inhibition of Hsp70 Chaperone Function by Scythe and Reaper.” *The EMBO Journal* 20 (5): 1033–41. doi:10.1093/emboj/20.5.1033.

Tobaben, Sönke, Pratima Thakur, Rafael Fernández-Chacón, Thomas C. Südhof, Jens Rettig, and Bernd Stahl. 2001. “A Trimeric Protein Complex Functions as a Synaptic Chaperone Machine.” *Neuron* 31 (6): 987–99. doi:10.1016/S0896-6273(01)00427-5.

Toniolo, D, M Persico, and M Alcalay. 1988. “A ‘housekeeping’ gene on the X Chromosome Encodes a Protein Similar to Ubiquitin.” *Proceedings of the National Academy of Sciences of the United States of America* 85 (3): 851–55. doi:10.1073/pnas.85.3.851.

Toro, Andrés, Cristian Arredondo, Gonzalo Córdova, Claudia Araya, José L. Palacios, Alejandro Venegas, Masashi Morita, Tsuneo Imanaka, and Manuela J. Santos. 2007. “Evaluation of the Role of the Endoplasmic Reticulum-Golgi Transit in the Biogenesis of Peroxisomal Membrane Proteins in Wild Type and Peroxisome Biogenesis Mutant CHO Cells.” *Biological Research* 40 (2): 231–49. doi:/S0716-97602007000200014.

Tran, David D., Contessa E. Edgar, Karin L. Heckman, Shari L. Sutor, Catherine J. Huntoon, Jan van Deursen, David L. McKean, and Richard J. Bram. 2005. “CAML Is a p56Lck-Interacting Protein That Is Required for Thymocyte Development.” *Immunity* 23 (2): 139–52. doi:10.1016/j.immuni.2005.06.006.

Tran, David D., Helen R. Russell, Shari L. Sutor, Jan van Deursen, and Richard J. Bram. 2003. “CAML Is Required for Efficient EGF Receptor Recycling.”

Developmental Cell 5 (2): 245–56. doi:10.1016/S1534-5807(03)00207-7.

van der Zand, Adabella, Ineke Braakman, and Henk F Tabak. 2010. “Peroxisomal Membrane Proteins Insert into the Endoplasmic Reticulum.” *Molecular Biology of the Cell* 21 (12): 2057–65. doi:10.1091/mbc.E10-02-0082.

Vander Linden, Ryan T, Casey W. Hemmis, Benjamin Schmitt, Ada Ndoja, Frank G. Whitby, Howard Robinson, Robert E. Cohen, Tingting Yao, and Christopher P. Hill. 2015. “Structural Basis for the Activation and Inhibition of the UCH37 Deubiquitylase.” *Molecular Cell* 57 (5). Elsevier Inc.: 901–11. doi:10.1016/j.molcel.2015.01.016.

Vandevyver, Sofie, Lien Dejager, and Claude Libert. 2014. “Comprehensive Overview of the Structure and Regulation of the Glucocorticoid Receptor.” *Endocrine Reviews* 35 (4): 671–93. doi:10.1210/er.2014-1010.

Varga, R., M. R. Avenarius, P. M. Kelley, B. J. Keats, C. I. Berlin, L. J. Hood, T. G. Morlet, et al. 2006. “OTOF Mutations Revealed by Genetic Analysis of Hearing Loss Families Including a Potential Temperature Sensitive Auditory Neuropathy Allele.” *Journal of Medical Genetics* 43 (7): 576–81. doi:10.1136/jmg.2005.038612.

Vilardi, Fabio, Holger Lorenz, and Bernhard Dobberstein. 2011. “WRB Is the Receptor for TRC40/Asna1-Mediated Insertion of Tail-Anchored Proteins into the ER Membrane.” *Journal of Cell Science* 124 (Pt 8): 1301–7. doi:10.1242/jcs.084277.

Vilardi, Fabio, Milena Stephan, Anne Clancy, Andreas Janshoff, and Blanche Schwappach. 2014. “WRB and CAML Are Necessary and Sufficient to Mediate Tail-Anchored Protein Targeting to the ER Membrane.” *PloS One* 9 (1): e85033. doi:10.1371/journal.pone.0085033.

Vogel, Karen, Jean Pierre Cabaniols, and Paul A. Roche. 2000. “Targeting of SNAP-25 to Membranes Is Mediated by Its Association with the Target SNARE Syntaxin.” *The Journal of Biological Chemistry* 275 (4): 2959–65. doi:10.1074/jbc.275.4.2959.

Vogl, Christian, Iliana Panou, Gulnara Yamanbaeva, Carolin Wichmann, Sara J Mangosing, Fabio Vilardi, Artur A Indzhykulian, et al. 2016. “Tryptophan-Rich Basic Protein (WRB) Mediates Insertion of the Tail-Anchored Protein Otoferlin and Is Required for Hair Cell Exocytosis and Hearing.” *The EMBO Journal* 35 (23): 2536–52. doi:10.15252/embj.201593565.

Voth, Wilhelm, Markus Schick, Stephanie Gates, Sheng Li, Fabio Vilardi, Irina Gostimskaya, Daniel R Southworth, Blanche Schwappach, and Ursula Jakob. 2014. “The Protein Targeting Factor Get3 Functions as ATP-Independent Chaperone under Oxidative Stress Conditions.” *Molecular Cell* 56 (1): 116–27. doi:10.1016/j.molcel.2014.08.017.

Walker, John E., Matti Saraste, M J Runswick, and Nicholas J. Gay. 1982. “Distantly Related Sequences in the Alpha- and Beta-Subunits of ATP Synthase, Myosin, Kinases and Other ATP-Requiring Enzymes and a Common Nucleotide Binding Fold.” *The EMBO Journal* 1 (8): 945–51. doi:6329717.

Wallin, Erik, and G von Heijne. 1998. “Genome-Wide Analysis of Integral Membrane Proteins from Eubacterial, Archaean, and Eukaryotic Organisms.” *Protein Science : A Publication of the Protein Society* 7 (4): 1029–38. doi:10.1002/pro.5560070420.

Wang, Fei, Emily C Brown, Gary Mak, Jimmy Zhuang, and Vladimir Denic. 2010. “A Chaperone Cascade Sorts Proteins for Posttranslational Membrane Insertion into the Endoplasmic Reticulum.” *Molecular Cell* 40 (1): 159–71. doi:10.1016/j.molcel.2010.08.038.

Wang, Fei, Charlene Chan, Nicholas R. Weir, and Vladimir Denic. 2014. “The Get1/2 Transmembrane Complex Is an Endoplasmic-Reticulum Membrane Protein Insertase.” *Nature* 512 (7515). Nature Publishing Group: 441–44. doi:10.1038/nature13471.

Wang, Fei, Andrew Whynot, Matthew Tung, and Vladimir Denic. 2011. “The Mechanism of Tail-Anchored Protein Insertion into the ER Membrane.” *Molecular Cell* 43 (5). Elsevier Inc.: 738–50. doi:10.1016/j.molcel.2011.07.020.

Wang, Qiuyan, Lianyun Li, and Yihong Ye. 2006. “Regulation of Retrotranslocation by p97-Associated Deubiquitinating Enzyme Ataxin-3.” *The Journal of Cell Biology* 174 (7): 963–71. doi:10.1083/jcb.200605100.

Wang, Qiuyan, Yanfen Liu, Nia Soetandyo, Kheewoong Baek, Ramanujan Hegde, and Yihong Ye. 2011. “A Ubiquitin Ligase-Associated Chaperone Holdase Maintains Polypeptides in Soluble States for Proteasome Degradation.” *Molecular Cell* 42 (6). Elsevier Inc.: 758–70. doi:10.1016/j.molcel.2011.05.010.

Wang, Tuanlao, Liangcheng Li, and Wanjin Hong. 2017. “SNARE Proteins in Membrane Trafficking.” *Traffic (Copenhagen, Denmark)* 18 (12): 767–75. doi:10.1111/tra.12524.

6.References

Wang, Yangmeng, Hongxiu Ning, Fangli Ren, Yuanjiang Zhang, Yu Rong, Yinyin Wang, Fuqin Su, et al. 2014. “GdX/UBL4A Specifically Stabilizes the TC45/STAT3 Association and Promotes Dephosphorylation of STAT3 to Repress Tumorigenesis.” *Molecular Cell* 53 (5). Elsevier Inc.: 752–65. doi:10.1016/j.molcel.2014.01.020.

Wang, Yangmeng, Dianjun Wang, Fangli Ren, Yuanjiang Zhang, Fuyu Lin, Ning Hou, Xuan Cheng, et al. 2012. “Generation of Mice with Conditional Null Allele for GdX/Ubl4A.” *Genesis (New York, N.Y. : 2000)* 50 (7): 534–42. doi:10.1002/dvg.20832.

Watson, Lisa C., Kristopher M. Kuchenbecker, Benjamin J. Schiller, John D. Gross, Miles A. Pufall, and Keith R. Yamamoto. 2013. “The Glucocorticoid Receptor Dimer Interface Allosterically Transmits Sequence-Specific DNA Signals.” *Nature Structural & Molecular Biology* 20 (7). Nature Publishing Group: 876–83. doi:10.1038/nsmb.2595.

Weir, Nicholas R, Roarke A Kamber, James S Martenson, and Vladimir Denic. 2017. “The AAA Protein Msp1 Mediates Clearance of Excess Tail-Anchored Proteins from the Peroxisomal Membrane.” *eLife* 6 (September): 1–28. doi:10.7554/eLife.28507.

Wereszczynski, Jeff, and J. Andrew McCammon. 2012. “Nucleotide-Dependent Mechanism of Get3 as Elucidated from Free Energy Calculations.” *Proceedings of the National Academy of Sciences of the United States of America* 109 (20): 7759–64. doi:10.1073/pnas.1117441109.

Whitfield, G K, P W Jurutka, C A Haussler, and M R Haussler. 1999. “Steroid Hormone Receptors: Evolution, Ligands, and Molecular Basis of Biologic Function.” *Journal of Cellular Biochemistry* Suppl 32-3 (September): 110–22. doi:10.1002/(SICI)1097-4644(1999)75:32+<110::AID-JCB14>3.0.CO;2-T [pii].

Wilson, R, A J Allen, J Oliver, J L Brookman, S High, and N J Bulleid. 1995. “The Translocation, Folding, Assembly and Redox-Dependent Degradation of Secretory and Membrane Proteins in Semi-Permeabilized Mammalian Cells.” *The Biochemical Journal* 307 (Pt 3 (May): 679–87. doi:10.1042/bj3070679.

Wohlever, Matthew L., Agnieszka Mateja, Philip T. McGilvray, Kasey J. Day, and Robert J. Keenan. 2017. “Msp1 Is a Membrane Protein Dislocase for Tail-Anchored Proteins.” *Molecular Cell* 67 (2). Elsevier Inc.: 194–202.e6. doi:10.1016/j.molcel.2017.06.019.

Wu, Wei, Kyung-Tae Park, Todd Holyoak, and Joe Lutkenhaus. 2011. “Determination of the Structure of the MinD-ATP Complex Reveals the Orientation of MinD on the Membrane and the Relative Location of the Binding Sites for MinE and MinC.” *Molecular Microbiology* 79 (6): 1515–28. doi:10.1111/j.1365-2958.2010.07536.x.

Wu, Yu-Hauh, Sheue-Fang Shih, and Jung-Yaw Lin. 2004. “Ricin Triggers Apoptotic Morphological Changes through Caspase-3 Cleavage of BAT3.” *The Journal of Biological Chemistry* 279 (18): 19264–75. doi:10.1074/jbc.M307049200.

Wunderley, Lydia, Pawel Leznicki, Aishwarya Payapilly, and Stephen High. 2014. “SGTA Regulates the Cytosolic Quality Control of Hydrophobic Substrates.” *Journal of Cell Science* 127 (21): 4728–39. doi:10.1242/jcs.155648.

Wyles, Jessica P., Christopher R. McMaster, and Neale D. Ridgway. 2002. “Vesicle-Associated Membrane Protein-Associated Protein-A (VAP-A) Interacts with the Oxysterol-Binding Protein to Modify Export from the Endoplasmic Reticulum.” *The Journal of Biological Chemistry* 277 (33): 29908–18. doi:10.1074/jbc.M201191200.

Xing, Shuping, Dietmar Gerald Mehlhorn, Niklas Wallmeroth, Lisa Yasmin Asseck, Ritwika Kar, Alessa Voss, Philipp Denninger, et al. 2017. “Loss of GET Pathway Orthologs in Arabidopsis Thaliana Causes Root Hair Growth Defects and Affects SNARE Abundance.” *Proceedings of the National Academy of Sciences of the United States of America* 114 (8): E1544–53. doi:10.1073/pnas.1619525114.

Xu, Yue, Mengli Cai, Yingying Yang, Lan Huang, and Yihong Ye. 2012. “SGTA Recognizes a Noncanonical Ubiquitin-like Domain in the Bag6-Ubl4A-Trc35 Complex to Promote Endoplasmic Reticulum-Associated Degradation.” *Cell Reports* 2 (6). The Authors: 1633–44. doi:10.1016/j.celrep.2012.11.010.

Yabal, Monica, Silvia Brambillasca, Paolo Soffientini, Emanuela Pedrazzini, Nica Borgese, and Marja Makarow. 2003. “Translocation of the C Terminus of a Tail-Anchored Protein across the Endoplasmic Reticulum Membrane in Yeast Mutants Defective in Signal Peptide-Driven Translocation.” *The Journal of Biological Chemistry* 278 (5): 3489–96. doi:10.1074/jbc.M210253200.

Yagita, Yuichi, Takahide Hiromasa, and Yukio Fujiki. 2013. “Tail-Anchored PEX26 Targets Peroxisomes via a PEX19-Dependent and TRC40-Independent Class I Pathway.” *Journal of Cell Biology* 200 (5): 651–66. doi:10.1083/jcb.201211077.

Yamagata, Atsushi, Hisatoshi Mimura, Yusuke Sato, Masami Yamashita, Azusa

Yoshikawa, and Shuya Fukai. 2010. “Structural Insight into the Membrane Insertion of Tail-Anchored Proteins by Get3.” *Genes to Cells : Devoted to Molecular & Cellular Mechanisms* 15 (1): 29–41. doi:10.1111/j.1365-2443.2009.01362.x.

Yamamoto, Koki, Mizuki Hayashishita, Setsuya Minami, Kanji Suzuki, Takumi Hagiwara, Aya Noguchi, and Hiroyuki Kawahara. 2017. “Elimination of a Signal Sequence-Uncleaved Form of Defective HLA Protein through BAG6.” *Scientific Reports* 7 (1). Springer US: 14545. doi:10.1038/s41598-017-14975-9.

Yamamoto, Yasunori, and Toshiaki Sakisaka. 2012. “Molecular Machinery for Insertion of Tail-Anchored Membrane Proteins into the Endoplasmic Reticulum Membrane in Mammalian Cells.” *Molecular Cell* 48 (3). Elsevier Inc.: 387–97. doi:10.1016/j.molcel.2012.08.028.

———. 2015. “The Emerging Role of Calcium-Modulating Cyclophilin Ligand in Posttranslational Insertion of Tail-Anchored Proteins into the Endoplasmic Reticulum Membrane.” *Journal of Biochemistry* 157 (6): 419–29. doi:10.1093/jb/mvv035.

Yang, Fang, Helen Skaletsky, and P. Jeremy Wang. 2007. “Ubl4b, an X-Derived Retrogene, Is Specifically Expressed in Post-Meiotic Germ Cells in Mammals.” *Gene Expression Patterns : GEP* 7 (1–2): 131–36. doi:10.1016/j.modgep.2006.06.002.

Zalisko, Benjamin E., Charlene Chan, Vladimir Denic, Ronald S. Rock, and Robert J. Keenan. 2017. “Tail-Anchored Protein Insertion by a Single Get1/2 Heterodimer.” *Cell Reports* 20 (10). ElsevierCompany.: 2287–93. doi:10.1016/j.celrep.2017.08.035.

Zane, Nicholas A., Justin H. Gundelach, Lonn D. Lindquist, and Richard J. Bram. 2012. “Essential Role for CAML in Follicular B Cell Survival and Homeostasis.” *Journal of Immunology (Baltimore, Md. : 1950)* 188 (7): 3009–18. doi:10.4049/jimmunol.1101641.

Zhang, Ying, Thea Schäffer, Tina Wölfle, Edith Fitzke, Gerhard Thiel, and Sabine Rospert. 2016. “Cotranslational Intersection between the SRP and GET Targeting Pathways to the Endoplasmic Reticulum of Saccharomyces Cerevisiae.” *Molecular and Cellular Biology* 36 (18): 2374–83. doi:10.1128/MCB.00131-16.

Zhao, Gang, and Erwin London. 2006. “An Amino Acid ‘transmembrane Tendency’

scale That Approaches the Theoretical Limit to Accuracy for Prediction of Transmembrane Helices: Relationship to Biological Hydrophobicity." *Protein Science : A Publication of the Protein Society* 15 (8): 1987–2001. doi:10.1110/ps.062286306.

Zhao, Yu, Yuting Lin, Honghong Zhang, Adriana Mañas, Wenwen Tang, Yuzhu Zhang, Dianqing Wu, Anning Lin, and Jialing Xiang. 2015. "Ubl4A Is Required for Insulin-Induced Akt Plasma Membrane Translocation through Promotion of Arp2/3-Dependent Actin Branching." *Proceedings of the National Academy of Sciences* 112 (31): 201508647. doi:10.1073/pnas.1508647112.

Zhao, Yuanbo, Jia Hu, Guangyan Miao, Liujing Qu, Zhenda Wang, Ge Li, Ping Lv, Dalong Ma, and Yingyu Chen. 2013. "Transmembrane Protein 208: A Novel ER-Localized Protein That Regulates Autophagy and ER Stress." *PloS One* 8 (5): e64228. doi:10.1371/journal.pone.0064228.

Zhi, Xu, Dong Zhao, Zehua Wang, Zhongmei Zhou, Chunyan Wang, Wenlin Chen, Rong Liu, and Ceshi Chen. 2013. "E3 Ubiquitin Ligase RNF126 Promotes Cancer Cell Proliferation by Targeting the Tumor Suppressor p21 for Ubiquitin-Mediated Degradation." *Cancer Research* 73 (1): 385–94. doi:10.1158/0008-5472.CAN-12-0562.

Zhou, T, and B P Rosen. 1997. "Tryptophan Fluorescence Reports Nucleotide-Induced Conformational Changes in a Domain of the ArsA ATPase." *The Journal of Biological Chemistry* 272 (32): 19731–37. http://www.ncbi.nlm.nih.gov/pubmed/9242630.

Zhou, Tongqing, Sergei Radaev, Barry P. Rosen, and Domenico L. Gatti. 2001. "Conformational Changes in Four Regions of the Escherichia Coli ArsA ATPase Link ATP Hydrolysis to Ion Translocation." *The Journal of Biological Chemistry* 276 (32): 30414–22. doi:10.1074/jbc.M103671200.

Zhou, Tongqing, and Barry P. Rosen. 1999. "Asp45 Is a Mg2+ Ligand in the ArsA ATPase." *The Journal of Biological Chemistry* 274 (20): 13854–58. doi:10.1074/jbc.274.20.13854.

Zidovetzki, Raphael, Burkhard Rost, Don L. Armstrong, and Israel Pecht. 2003. "Transmembrane Domains in the Functions of Fc Receptors." *Biophysical Chemistry* 100 (1–3): 555–75. doi:10.1016/S0301-4622(02)00306-X.

7. Appendix

7.1. Abbreviations

A	ampere
aa	amino acids
Ab	antibody
ADP	adenosine di-phosphate
Amp	ampicillin
ArsA	arsenical pump-driving ATPase
ATP	adenosine tri-phosphate
ATP-γ-S	adenosine 5′-O-(3-thiotriphosphate)
AU	arbitrary units
BAG	*bcl*-2-associated athanogene
BAG6	large proline-rich protein BAG6
BAT3	HLA-B-associated transcript 3
BSA	bovine serum albumin
°C	degree Celsius
CaM	calmodulin
CAML	calcium signal-modulating cyclophilin ligand
CD	cytosolic domain
CMV	cytomegalovirus
Cre	cre recombinase
CT	C-terminus
DAPI	4′,6-Diamidino-2-phenylindole dihydrochloride
DBD	DNA-binding domain
DDR	DNA damage response
DEX	dexamethasone
DMEM	Dulbecco’s modified Eagle medium
DMSO	dimethyl sulfoxide
DNA	deoxyribonucleic acid
dNTP	deoxyribonucleotide triphosphate
DOC	deoxycorticosterone or 21-hydroxyprogesterone
DTT	dithiothreitol
DUB	deubiquitinase
EDTA	disodium ethylenediaminetetraacetate
EGTA	ethylene glycol-bis(2-aminoethylether)-*N,N,N′,N′*-tetraacetic acid

em	emission
EMC	ER-membrane protein complex
EMD	emerin
ER	endoplasmic reticulum
ERAD	endoplasmic reticulum-associated degradation
EV	empty vector
ex	excitation
F	farad
FBS	fetal bovine serum
FDG	fluorescein di(β-D-galactopyranoside)
FDFT1	squalene synthase
fl/fl	sequence flanked by loxP sites
FMD	fluorescein mono-D-galactopyranoside
FRT	Flp recombination target
g	gram(s)
g	times gravity
GET	guided entry of tail-anchored proteins
Get	guided entry of tail-anchored protein
GFP	green fluorescent protein
GPI	glycosylphosphatidylinositol
GR	glucocorticoid receptor
GRAVY	grand average of hydropathicity
GRE	glucocorticoid response element
h	hour(s)
HIF-1α	hypoxia-induced factor 1 alpha
His	6x His tag
Hsp(s)	heat-shock protein(s)
IB	immunoblot
IF	indirect immunofluorescence
IgG	immunoglobulin G
IMP	integral membrane protein
INM	inner-nuclear membrane
IP	immunoprecipitation
IPTG	isopropyl β-D-1-thiogalactopyranoside
Kan	kanamycin
kb	kilo-base pair
kcal	kilo-calorie
KD	knockdown
kDa	kilo-Dalton
KO	knock-out

L	liter
lacZ	*E.coli* β-galactosidase gene
LB	Luria-Bertani
LBD	ligand-binding domain
LDH	lactate dehydrogenase
M	molar
MBP	maltose binding protein
Mer	ligand binding domain mutant estrogen-receptor
Met	methionine
µ	micro
min	minute(s)
MLP	mislocalized secretory and membrane protein
mM	milimolar
MOM	mitochondrial outer membrane
mRNA	messenger RNA
MS	mass spectrometry
MW	molecular weight
NAD^+	β-nicotinamide adenine dinucleotide, oxidized
NADH	β-nicotinamide adenine dinucleotide, reduced
NLS	nuclear localization sequence
nM	nanomolar
nm	nanometer
NTD	N-terminal domain
O/N	overnight
OD	optical density or absorbance
op	opsin tag
P	phosphorylated
PAGE	polyacrylamide gel electrophoresis
PBS	phosphate-buffered saline
PCR	polymerase chain reaction
PDB ID	Protein Data Bank unique accession
PEG	polyethylene glycol
PEP	phosphoenol pyruvate
PEX	peroxin
PFA	paraformaldehyde
Pi	inorganic phosphate
PK	pyruvate kinase
PLN	cardiac phospholamban
PMP	peroxisomal membrane protein
PMSF	phenylmethanesulfonyl fluoride

PNGase	peptide-N-glycosidase
PTS	peroxisomal targeting sequence
RMs	rough microsomes
RNA	ribonucleic acid
RNC	ribosome nascent chain complex
ROS	reactive oxygen species
RPKM	reads per kilo base per million mapped reads
rpm	revolution per minute
RRL	rabbit reticulocyte lysate
RT	room temperature
sec	second(s)
SDS	sodium dodecyl sulfate
SGTA	small glutamine-rich tetratricopeptide repeat-containing protein alpha
siBAG6	siRNA against BAG6
siLuc	siRNA against Luciferase (control siRNA)
siNT	non-targeting siRNA
siRNA	small interference RNA
siTRC40	siRNA against TRC40
siTRC40ins	siRNA-insensitive TRC40
siWRB	siRNA against WRB
SNARE	SNAP (soluble NSF attachment protein) receptor
SND	SRP-independent targeting
SQS	squalene synthase
SRs	steroid hormone receptors
SRP	signal recognition particle
SRα	SRP receptor alpha
SRβ	SRP receptor beta
SS	signal sequence
Stx1A	syntaxin-1A
Stx1B	syntaxin-1B
Stx5	syntaxin-5
Stx5-G	syntaxin-5 glycosylated
Stx6	syntaxin-6
Stx8	syntaxin-8
Stx18	syntaxin-18
TA	tail-anchored
TCA	trichloroacetic acid
Tet	tetracycline
TEV	tobacco etch virus protease

TGN	*trans*-Golgi network
TMD	transmembrane domain
TPR	tetratricopeptide repeat
TRC35	transmembrane recognition complex subunit of 35 kDa
TRC40	transmembrane recognition complex subunit of 40 kDa
U	unit
UBL	ubiquitin-like
UBL4A	ubiquitin-like protein 4A
UBQLN	ubiquilin
UV	ultra violet
V	volt
v/v	volume per volume
W	watt
w/v	weight per volume
WB	Western blot
WRB	tryptophan-rich basic protein
wt	wild-type
Ω	ohm

7.2. Appendix figures

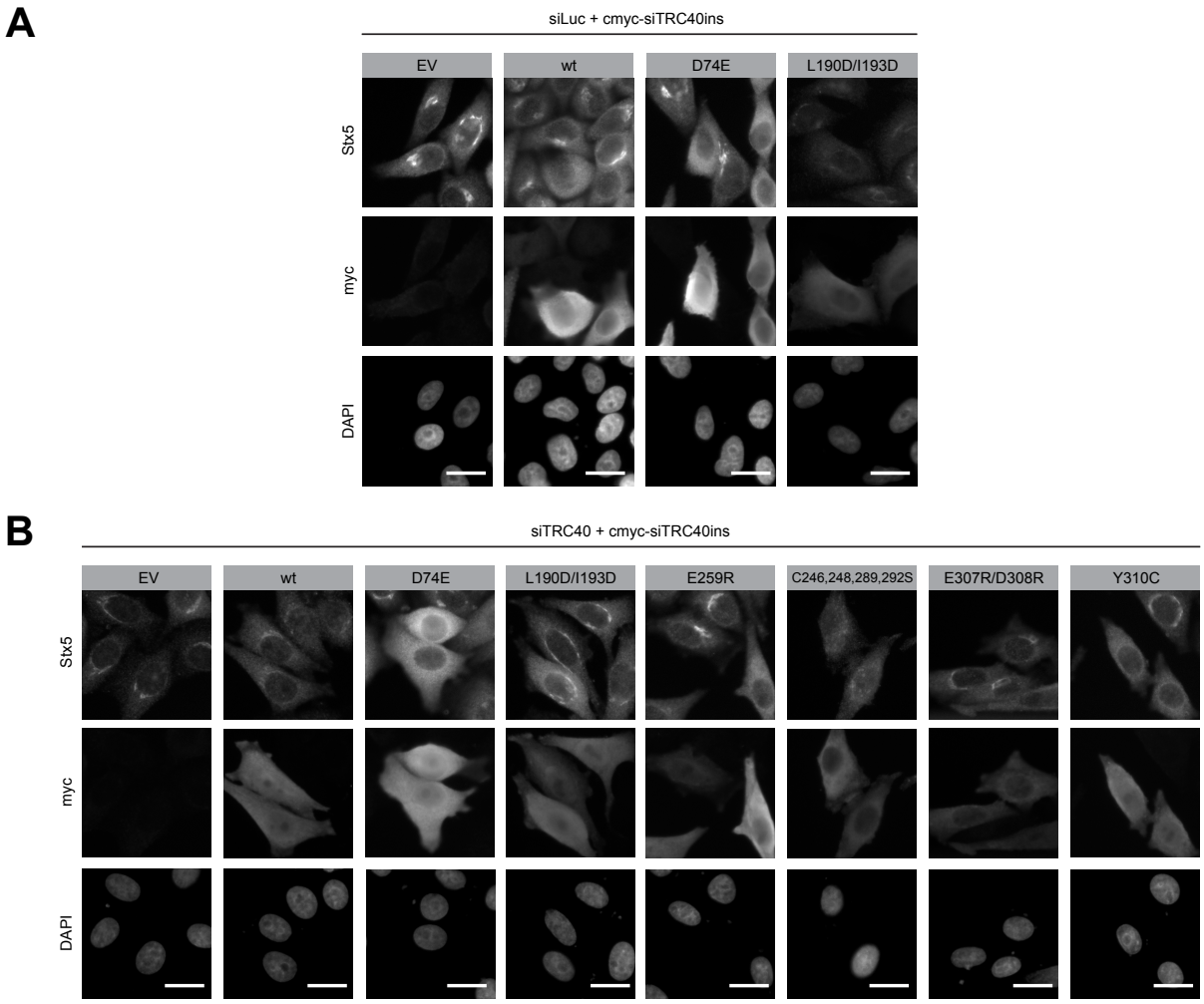

Appendix figure 1. Stx5 subcellular localization is affected upon the presence of certain TRC40 variants. (A) Stx5 immunofluorescence in cells silenced for TRC40 upon over-expression of different siRNA-insensitive TRC40 variants in HeLa cells. Images of Stx5 and cmyc-TRC40 stained by indirect immunofluorescence are shown. Two biological replicates were analyzed. Scale bars: 20 µm.

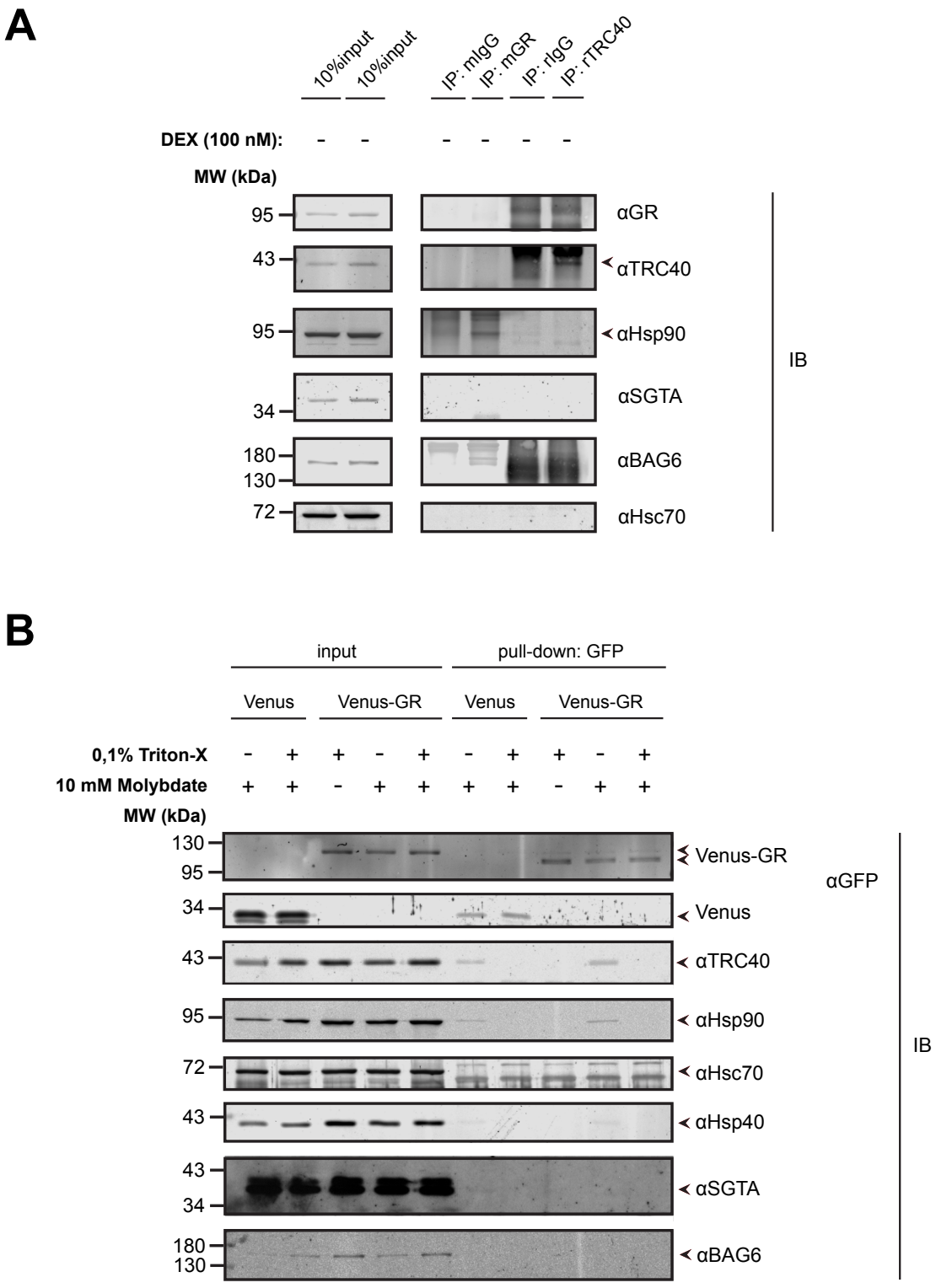

Appendix figure 2. Co-immunoprecipitation does not indicate a complex containing TRC40 and GR in HeLa cells. (A) Immunoprecipitation using mouse anti-GR and rabbit anti-TRC40 antibodies in HeLa cells. Western blot was performed and detecting the indicated proteins. Mouse IgG (mIgG) and rabbit IgG (rIgG) were used as controls of the immunoprecipitation. **(B)** GFP pull-down from lysed HeLa cells over-expressing Venus-GR. Cells transfected with Venus alone were used as controls. Western blot was performed detecting the indicated proteins. One replicate was analyzed.

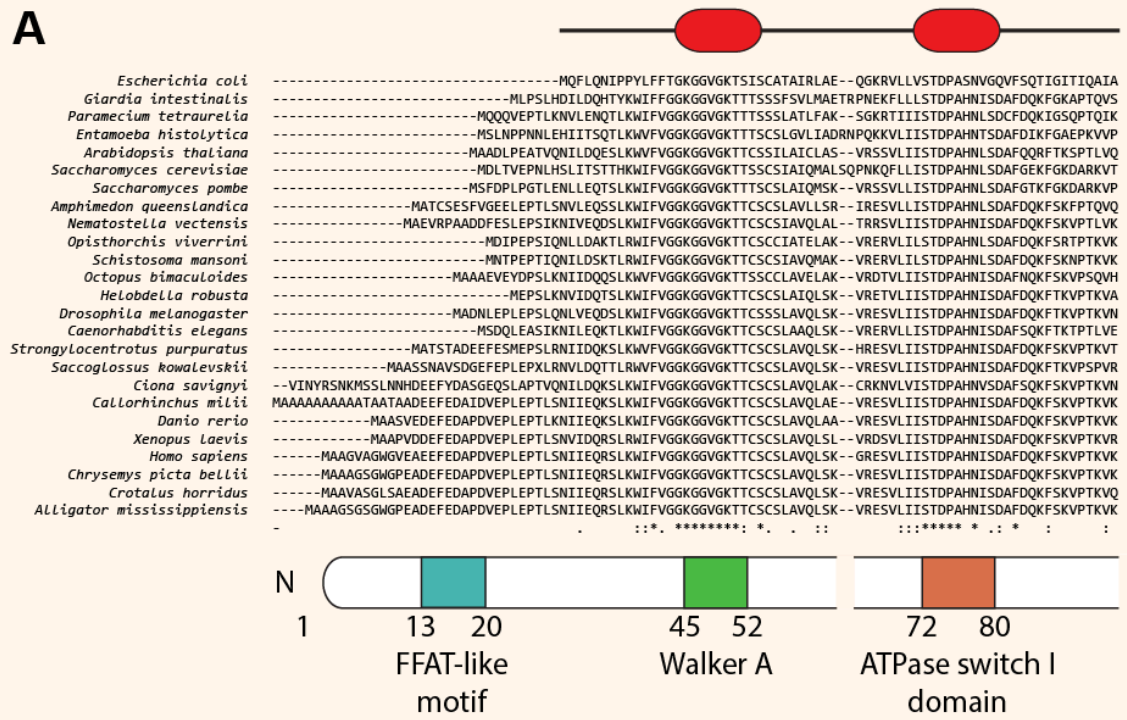

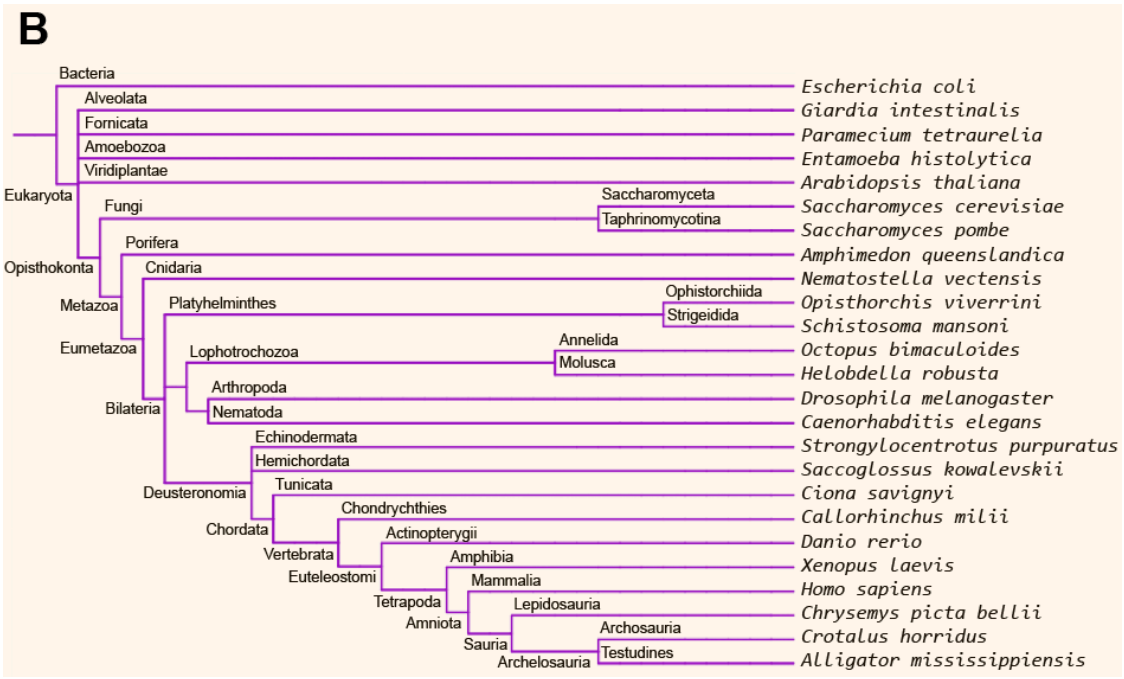

Appendix figure 3. Phylogenetic analysis of the N-terminus of TRC40. (A) Sequence alignment of the N-terminus of TRC40 (around 100 aa) with homologs from other species. The upper scheme indicates in red the nucleotide-related regions of bacterial ArsA. The lower scheme of the protein corresponds to human TRC40 and the numbers indicate the initial and the last residue of the highlighted domains that were obtained from UniProt. **(B)** Phylogenetic tree of the species shown in (A). The phylogenetic tree was generated in the website iTOL v4.2 (http://itol.embl.de) (Letunic and Bork 2016). The respective NCBI/UniProt accession numbers can be found in order of appearance: P08690, A8B3G9, A0BZ55, C4LY44, Q949M9, Q12154, Q9P7F8, I1FYB1, A7RQM5, A0A075A5S8, G4V6J4, A0A0L8I9S4, T1FNV7, Q7JWD3, P30632, W4Y937, XP_006825619.1, H2ZIV5, V9KYT3, Q6IQE5, Q6GNQ1, O43681, XP_005310692.1, JAG47418.1, KYO32296.1.

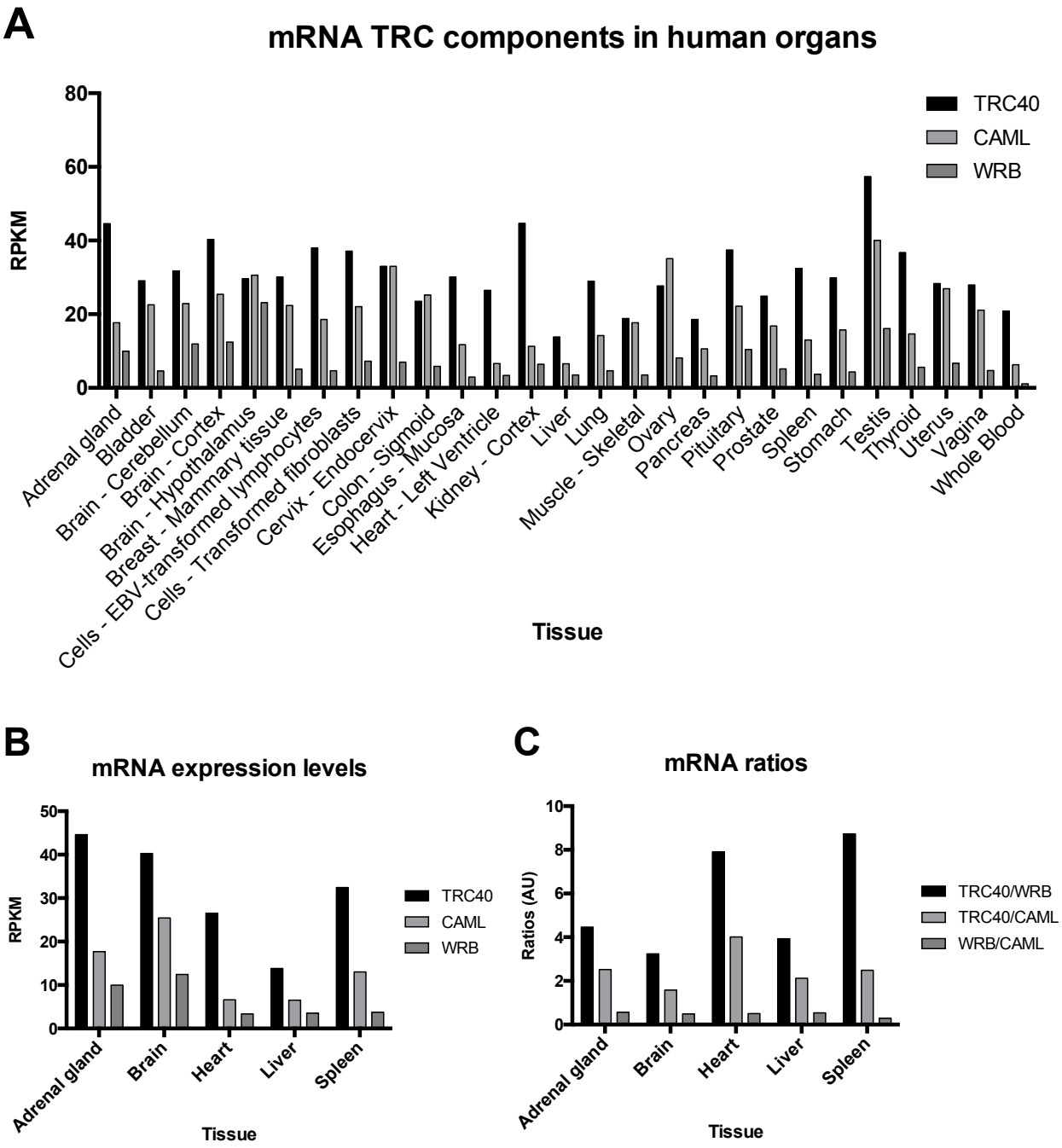

Appendix figure 4. mRNAs encoding TRC components show differential expression levels across different human organs. (A) mRNA expression of TRC40 and the TRC receptor components, WRB and CAML, across different human tissues. **(B)** mRNA expression levels of TRC40, WRB and CAML in a selected group of human tissues where the TRC40 mRNA is more abundant compared to those encoding receptor subunits WRB and CAML. **(C)** mRNA expression ratios of TRC40 against WRB, TRC40 against CAML and WRB against CAML in the same group of human tissues shown in (B). Analyzed data from the Genotype-Tissue Expression project (GTEx V6p; https://www.gtexportal.org) (GTEx Consortium 2015; Melé et al. 2015; Rivas et al. 2015).

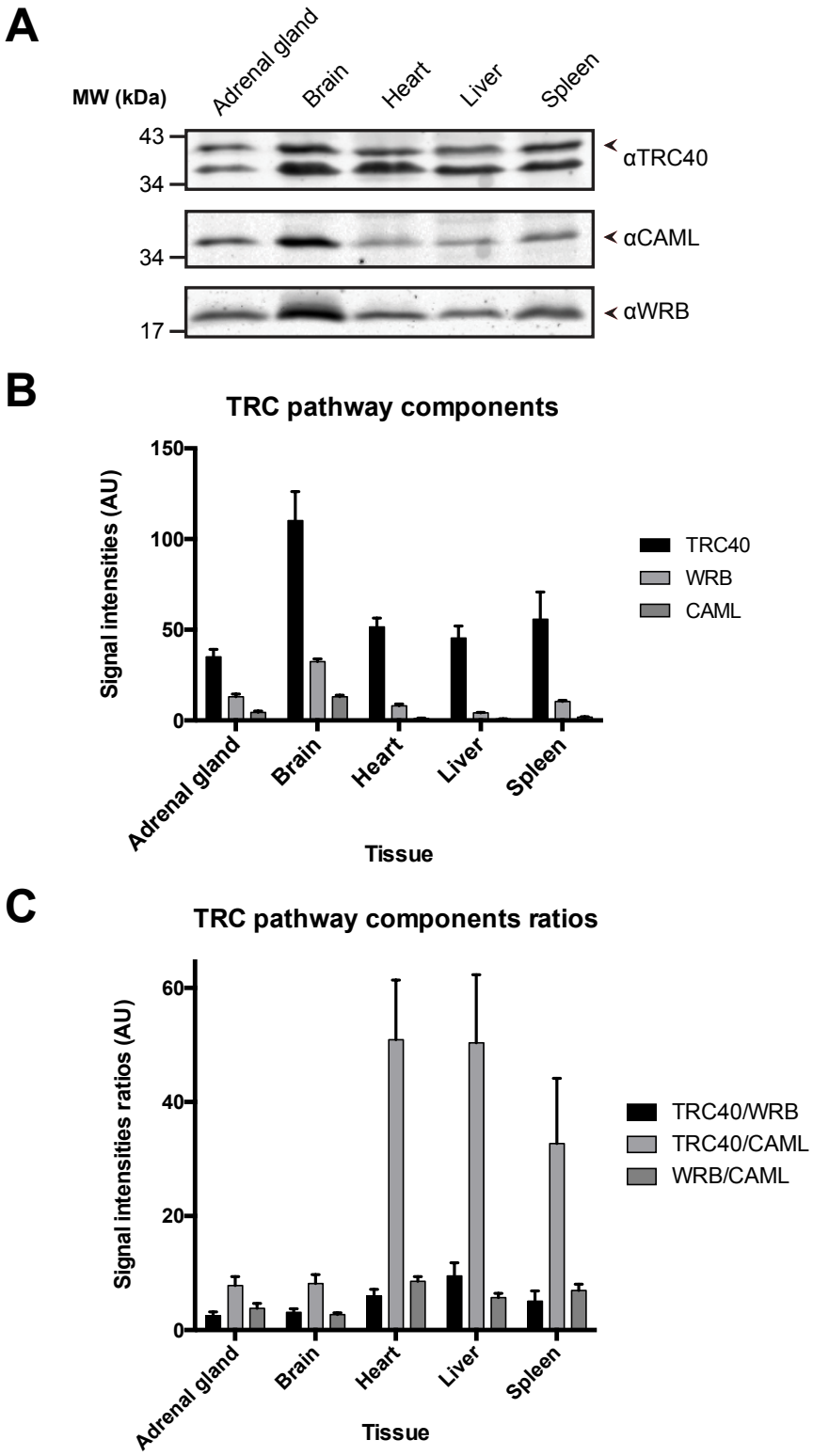

Appendix figure 5. Steady-state protein levels of TRC components and their relative abundance differ in mouse organs. (A) Steady-state levels of TRC40 and the subunits of the TRC receptor in different mouse organs. Total tissue lysates were analyzed by Western blot for the indicated proteins. **(B)** Quantification of the signal intensities for the different mouse organs from the blots performed in (A) in arbitrary units. **(C)** Ratios of the signals shown in (B) relating TRC40 to the receptor subunits and relating the two receptor subunits to each other. Five biological replicates were analyzed. The graphs show the mean and the error bars represent standard error of the mean.

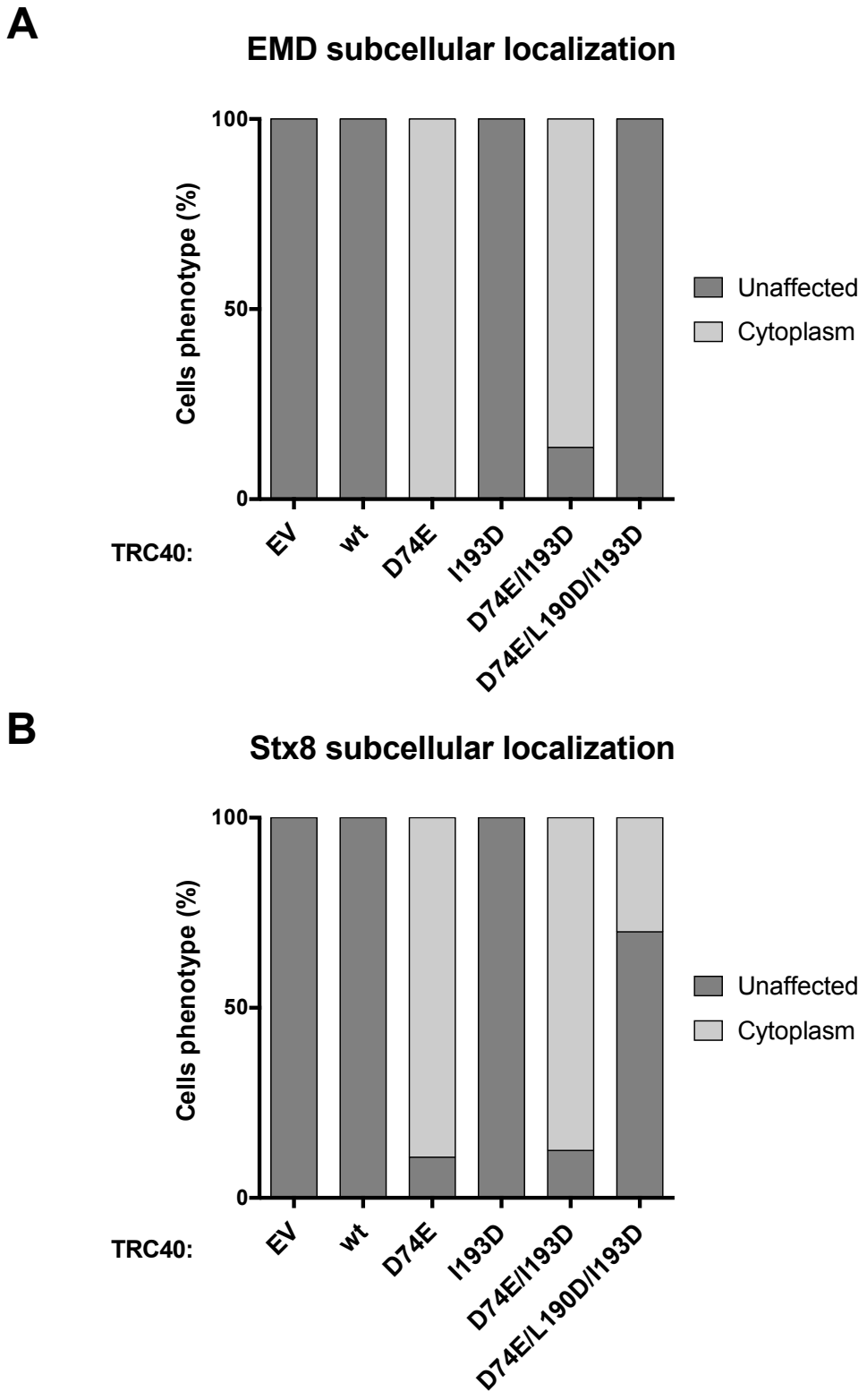

Appendix figure 6. Quantification of the subcellular localization phenotype of the TA-proteins in the presence of different TRC40 mutants. (A) Quantification of the subcellular localization phenotype of EMD in the presence of TRC40 mutants tested in **Fig. 14**. n= 40-203 cells are represented. **(B)** Quantification of the subcellular localization phenotype of Stx8 in the presence of TRC40 mutants tested in **Fig. 15**. n= 17-62 cells are represented. Three to six biological replicates were analyzed.

7.3. List of figures

7.Appendix

7.4. List of tables

7.5.Software parameters

7.5.1.CellProfiler pipeline. Quantification empty vector

CellProfiler_Version	2014-07-23T17:39:57 6c2d896
ChannelType_BAG6	Grayscale
ChannelType_DAPI	Grayscale
ChannelType_TRC40	Grayscale
ImageSet_Zip_Dictionary	[60 63 120 ..., 84 104 101]
Metadata_GroupingTags	["Metadata_ProteinSilenced", "Metadata_plasmid"]
Metadata_Tags	["ImageNumber"]
Pipeline_Pipeline	CellProfiler Pipeline: http://www.cellprofiler.org
Version:3	
DateRevision:20140723173957	
GitHash:6c2d896	
ModuleCount:20	
HasImagePlaneDetails:False	

Images:[module_num:1|svn_version:\'Unknown\'|variable_revision_number:2|show_wind use the Images module to compile a list of files and/or folders that you want to analyze. Y
:
Filter images?:Images only
Select the rule criteria:and (extension does isimage) (directory doesnot containregexp ""\x5B\\\\\\\\\\\\\\\\\x5D\\\\\\\\."")

Metadata:[module_num:2|svn_version:\'Unknown\'|variable_revision_number:4|show_wi metadata) which will be stored along with your measurements. This information can be c
Extract metadata?:Yes
Metadata data type:Text
Metadata types:{}
Extraction method count:1
Metadata extraction method:Extract from file/folder names
Metadata source:File name
Regular expression:^(?P<Cells>\x5B0-z\x5D+)-si(?P<ProteinSilenced>\x5B0-z\x5D+)-(?P<plasmid>\x5B0-z\x5D+)-ch(?P<Channel>\x5B0-9\x5D{1})-p(?P<Protein>\x5B0-z\x5D
Regular expression:(?P<Date>\x5B0-9\x5D{4}_\x5B0-9\x5D{2}_\x5B0-9\x5D{2})$
Extract metadata from:All images
Select the filtering criteria:and (file does contain """")
Metadata file location:
Match file and image metadata:\x5B\x5D
Use case insensitive matching?:No

NamesAndTypes:[module_num:3|svn_version:\'Unknown\'|variable_revision_number:5|s dtype=uint8)|enabled:True|wants_pause:False]
Assign a name to:Images matching rules
Select the image type:Grayscale image
Name to assign these images:DNA
Match metadata:\x5B\x5D
Image set matching method:Order
Set intensity range from:Image metadata
Assignments count:3
Single images count:0
Select the rule criteria:and (file does contain ""ch1"")
Name to assign these images:BAG6
Name to assign these objects:Cell
Select the image type:Grayscale image
Set intensity range from:Image metadata
Retain outlines of loaded objects?:No
Name the outline image:LoadedOutlines
Select the rule criteria:and (file does contain ""ch2"")
Name to assign these images:TRC40
Name to assign these objects:Nucleus
Select the image type:Grayscale image
Set intensity range from:Image metadata
Retain outlines of loaded objects?:No
Name the outline image:LoadedOutlines
Select the rule criteria:and (file does contain ""ch3"")
Name to assign these images:DAPI
Name to assign these objects:Cytoplasm
Select the image type:Grayscale image
Set intensity range from:Image metadata
Retain outlines of loaded objects?:No
Name the outline image:LoadedOutlines

Groups:[module_num:4|svn_version:\'Unknown\'|variable_revision_number:2|show_window:False|notes:\x5B\'The Groups module optionally allows you to split your list of images i
Do you want to group your images?:Yes
grouping metadata count:2
Metadata category:ProteinSilenced
Metadata category:plasmid

IdentifyPrimaryObjects:[module_num:5|svn_version:\'Unknown\'|variable_revision_numb dtype=uint8)|enabled:True|wants_pause:False]
Select the input image:DAPI
Name the primary objects to be identified:Nuclei
Typical diameter of objects in pixel units (Min-Max):100 300
Discard objects outside the diameter range?:No
Try to merge too small objects with nearby larger objects?:No
Discard objects touching the border of the image?:No
Method to distinguish clumped objects:None
Method to draw dividing lines between clumped objects:Intensity
Size of smoothing filter:10
Suppress local maxima that are closer than this minimum allowed distance:7.0
Speed up by using lower-resolution image to find local maxima?:Yes
Name the outline image:OutlinesB
Fill holes in identified objects?:After both thresholding and declumping

Automatically calculate size of smoothing filter for declumping?:Yes
Automatically calculate minimum allowed distance between local maxima?:Yes
Retain outlines of the identified objects?:No
Automatically calculate the threshold using the Otsu method?:Yes
Enter Laplacian of Gaussian threshold:0.5
Automatically calculate the size of objects for the Laplacian of Gaussian filter?:Yes
Enter LoG filter diameter:5.0
Handling of objects if excessive number of objects identified:Continue
Maximum number of objects:500
Threshold setting version:1
Threshold strategy:Global
Thresholding method:Otsu
Select the smoothing method for thresholding:Automatic
Threshold smoothing scale:1.0
Threshold correction factor:1.0
Lower and upper bounds on threshold:0.0005-0.7
Approximate fraction of image covered by objects?:0.01
Manual threshold:0.5
Select the measurement to threshold with:None
Select binary image:A
Masking objects:None
Two-class or three-class thresholding?:Three classes
Minimize the weighted variance or the entropy?:Weighted variance
Assign pixels in the middle intensity class to the foreground or the background?:Background
Method to calculate adaptive window size:Image size
Size of adaptive window:10

IdentifySecondaryObjects:[module_num:6|svn_version:\'Unknown\'|variable_revision_nur dtype=uint8)|enabled:True|wants_pause:False]
Select the input objects:Nuclei
Name the objects to be identified:Cell
Select the method to identify the secondary objects:Watershed - Gradient
Select the input image:BAG6
Number of pixels by which to expand the primary objects:10
Regularization factor:0.05
Name the outline image:CellOutline
Retain outlines of the identified secondary objects?:Yes
Discard secondary objects touching the border of the image?:No
Discard the associated primary objects?:No
Name the new primary objects:FilteredNuclei
Retain outlines of the new primary objects?:No
Name the new primary object outlines:FilteredNucleiOutlines
Fill holes in identified objects?:Yes
Threshold setting version:1
Threshold strategy:Global
Thresholding method:Otsu
Select the smoothing method for thresholding:Automatic
Threshold smoothing scale:1.0
Threshold correction factor:1.0
Lower and upper bounds on threshold:0.0035-1
Approximate fraction of image covered by objects?:0.01
Manual threshold:0.0
Select the measurement to threshold with:None
Select binary image:None
Masking objects:None
Two-class or three-class thresholding?:Three classes
Minimize the weighted variance or the entropy?:Weighted variance
Assign pixels in the middle intensity class to the foreground or the background?:Foreground
Method to calculate adaptive window size:Image size
Size of adaptive window:10

RelateObjects:[module_num:7|svn_version:\'Unknown\'|variable_revision_number:2|show dtype=uint8)|enabled:False|wants_pause:False]
Select the input child objects:Nuclei
Select the input parent objects:Cell
Calculate child-parent distances?:Minimum
Calculate per-parent means for all child measurements?:Yes
Calculate distances to other parents?:No
Parent name:None

MaskImage:[module_num:8|svn_version:\'Unknown\'|variable_revision_number:3|show_ dtype=uint8)|enabled:True|wants_pause:False]
Select the input image:BAG6
Name the output image:NucleiMask
Use objects or an image as a mask?:Objects
Select object for mask:Nuclei
Select image for mask:None
Invert the mask?:No

MaskImage:[module_num:9|svn_version:\'Unknown\'|variable_revision_number:3|show_ dtype=uint8)|enabled:True|wants_pause:False]
Select the input image:BAG6
Name the output image:AllCellsMask
Use objects or an image as a mask?:Objects
Select object for mask:Nuclei
Select image for mask:CellMaskfromTRC40
Invert the mask?:Yes

MaskImage:[module_num:10|svn_version:\'Unknown\'|variable_revision_number:3|show_ dtype=uint8)|enabled:False|wants_pause:False]

Select the input image:AllCellsMask
Name the output image:CellMask
Use objects or an image as a mask?:Objects
Select object for mask:Cell
Select image for mask:CellMaskfromTRC40
Invert the mask?:No

MeasureImageIntensity:[module_num:11|svn_version:\'Unknown\'|variable_revision_num dtype=uint8)|enabled:False|wants_pause:False]
Select the image to measure:NucleiMask
Measure the intensity only from areas enclosed by objects?:Yes
Select the input objects:Nuclei
Select the image to measure:CellMask
Measure the intensity only from areas enclosed by objects?:Yes
Select the input objects:Cell

MeasureObjectIntensity:[module_num:12|svn_version:\'Unknown\'|variable_revision_num dtype=uint8)|enabled:True|wants_pause:False]
Hidden:1
Select an image to measure:AllCellsMask
Select objects to measure:Cell

MeasureObjectIntensity:[module_num:13|svn_version:\'Unknown\'|variable_revision_num dtype=uint8)|enabled:True|wants_pause:False]
Hidden:1
Select an image to measure:NucleiMask
Select objects to measure:Nuclei

RelateObjects:[module_num:14|svn_version:\'Unknown\'|variable_revision_number:2|sha dtype=uint8)|enabled:True|wants_pause:False]
Select the input child objects:Nuclei
Select the input parent objects:Cell
Calculate child-parent distances?:Minimum
Calculate per-parent means for all child measurements?:Yes
Calculate distances to other parents?:No
Parent name:None

CalculateMath:[module_num:15|svn_version:\'Unknown\'|variable_revision_number:2|sh dtype=uint8)|enabled:True|wants_pause:False]
Name the output measurement:BAG6_nucleocytoplasm_ratio
Operation:Divide
Select the numerator measurement type:Object
Select the numerator objects:Nuclei
Select the numerator measurement:Intensity_MeanIntensity_NucleiMask
Multiply the above operand by:1.0
Raise the power of above operand by:1.0
Select the denominator measurement type:Object
Select the denominator objects:Cell
Select the denominator measurement:Intensity_MeanIntensity_AllCellsMask
Multiply the above operand by:1.0
Raise the power of above operand by:1.0
Take log10 of result?:No
Multiply the result by:1.0
Raise the power of result by:1.0
Add to the result:0.0
Constrain the result to a lower bound?:No
Enter the lower bound:0.0
Constrain the result to an upper bound?:No
Enter the upper bound:1.0

CalculateMath:[module_num:16|svn_version:\'Unknown\'|variable_revision_number:2|sh dtype=uint8)|enabled:False|wants_pause:False]
Name the output measurement:BAG6cyt_TotalArea
Operation:Subtract
Select the minuend measurement type:Image
Select the minuend objects:None
Select the minuend measurement:Width_BAG6
Multiply the above operand by:1.0
Raise the power of above operand by:1.0
Select the subtrahend measurement type:Image
Select the subtrahend objects:None
Select the subtrahend measurement:Intensity_TotalArea_CellMask
Multiply the above operand by:1.0
Raise the power of above operand by:1.0
Take log10 of result?:No
Multiply the result by:1.0
Raise the power of result by:1.0
Add to the result:0.0
Constrain the result to a lower bound?:No
Enter the lower bound:0.0
Constrain the result to an upper bound?:No
Enter the upper bound:1.0

CalculateMath:[module_num:17|svn_version:\'Unknown\'|variable_revision_number:2|sh dtype=uint8)|enabled:False|wants_pause:False]
Name the output measurement:Cyt_MeanIntensity
Operation:Divide
Select the numerator measurement type:Object
Select the numerator objects:Cell
Select the numerator measurement:Math_BAG6cyt_TotalIntensity
Multiply the above operand by:1.0
Raise the power of above operand by:1.0

Select the denominator measurement type:Image
Select the denominator objects:None
Select the denominator measurement:Math_Stx5nonGolgi_TotalArea
Multiply the above operand by:1.0
Raise the power of above operand by:1.0
Take log10 of result?:No
Multiply the result by:1.0
Raise the power of result by:1.0
Add to the result:0.0
Constrain the result to a lower bound?:No
Enter the lower bound:0.0
Constrain the result to an upper bound?:No
Enter the upper bound:1.0

CalculateMath:[module_num:18|svn_version:\'Unknown\'|variable_revision_number:2|sh dtype=uint8)|enabled:False|wants_pause:False]
Name the output measurement:Ratio_BAG6
Operation:Divide
Select the numerator measurement type:Image
Select the numerator objects:None
Select the numerator measurement:Intensity_MeanIntensity_CellMask
Multiply the above operand by:1.0
Raise the power of above operand by:1.0
Select the denominator measurement type:Image
Select the denominator objects:None
Select the denominator measurement:Math_BAG6cyt_TotalArea
Multiply the above operand by:1.0
Raise the power of above operand by:1.0
Take log10 of result?:No
Multiply the result by:1.0
Raise the power of result by:1.0
Add to the result:0.0
Constrain the result to a lower bound?:No
Enter the lower bound:0.0
Constrain the result to an upper bound?:No
Enter the upper bound:1.0

ExportToSpreadsheet:[module_num:19|svn_version:\'Unknown\'|variable_revision_numb dtype=uint8)|enabled:True|wants_pause:False]
Select the column delimiter:Comma ("")
Add image metadata columns to your object data file?:Yes
Limit output to a size that is allowed in Excel?:No
Select the measurements to export:No
Calculate the per-image mean values for object measurements?:Yes
Calculate the per-image median values for object measurements?:Yes
Calculate the per-image standard deviation values for object measurements?:Yes
Output file location:Default Input Folder sub-folder\x7CDesktop/2017.01.09 HeLa siTRC40 siTRC40siWRB + siTRC40ins variants/IF/Quantification selected variants for 2016.11
Create a GenePattern GCT file?:No
Select source of sample row name:Metadata
Select the image to use as the identifier:None
Select the metadata to use as the identifier:None
Export all measurement types?:Yes
Press button to select measurements to export:
Representation of Nan/Inf:NaN
Add a prefix to file names?:Yes
Filename prefix\x3A:MyExpt_BAG6_TRC40varEV
Overwrite without warning?:No
Data to export:Do not use
Combine these object measurements with those of the previous object?:No
File name:DATA.csv
Use the object name for the file name?:Yes

ExportToDatabase:[module_num:20|svn_version:\'Unknown\'|variable_revision_number: dtype=uint8)|enabled:True|wants_pause:False]
Database type:SQLite
Database name:Stx5_FAM134B_Golgivsnongolgi
Add a prefix to table names?:Yes
Table prefix:MyExpt_BAG6_TRC40varEV
SQL file prefix:SQL_Stx5_FAM134B_Golgivsnongolgi
Output file location:Default Input Folder sub-folder\x7CDesktop/2017.01.09 HeLa siTRC40 siTRC40siWRB + siTRC40ins variants/IF/Quantification selected variants for 2016.11
Create a CellProfiler Analyst properties file?:Yes
Database host:
Username:
Password:
Name the SQLite database file:DefaultDB.db
Calculate the per-image mean values of object measurements?:Yes
Calculate the per-image median values of object measurements?:Yes
Calculate the per-image standard deviation values of object measurements?:Yes
Calculate the per-well mean values of object measurements?:Yes
Calculate the per-well median values of object measurements?:Yes
Calculate the per-well standard deviation values of object measurements?:Yes
Export measurements for all objects to the database?:All
Select the objects:
Maximum # of characters in a column name:64
Create one table per object a single object table or a single object view?:Single object table
Enter an image url prepend if you plan to access your files via http:
Write image thumbnails directly to the database?:No
Select the images for which you want to save thumbnails:

Auto-scale thumbnail pixel intensities?:Yes
Select the plate type:None
Select the plate metadata:None
Select the well metadata:None
Include information for all images using default values?:Yes
Properties image group count:1
Properties group field count:1
Properties filter field count:0
Workspace measurement count:1
Experiment name:MyExpt
Which objects should be used for locations?:Cell
Enter a phenotype class table name if using the classifier tool:
Export object relationships?:Yes
Overwrite without warning?:Never
Access CPA images via URL?:No
Select an image to include:None
Use the image name for the display?:Yes
Image name:Channel1
Channel color:red
Do you want to add group fields?:No
Enter the name of the group:
Enter the per-image columns which define the group separated by commas:ImageNumber, Image_Metadata_Plate, Image_Metadata_Well
Do you want to add filter fields?:No
Automatically create a filter for each plate?:No
Create a CellProfiler Analyst workspace file?:No
Select the measurement display tool:DensityPlot
Type of measurement to plot on the X-axis:Index
Enter the object name:None
Select the X-axis measurement:Metadata_FAMsilenced
Select the X-axis index:Group_Index
Type of measurement to plot on the Y-axis:Image
Enter the object name:None
Select the Y-axis measurement:Math_Ratio_Stx5_Golgi_vs_Cytosol
Select the Y-axis index:ImageNumber

Run_Timestamp 2017-03-26T14:02:37.144615

7.5.2.CellProfiler pipeline. Quantification transfected cells

CellProfiler_Version 2014-07-23T17:39:57 6c2d896
ChannelType_BAG6 Grayscale
ChannelType_DAPI Grayscale
ChannelType_TRC40 Grayscale
ImageSet_Zip_Dictionary [60 63 120 ..., 45 99 104]
Metadata_GroupingTags ["Metadata_ProteinSilenced", "Metadata_plasmid"]
Metadata_Tags ["ImageNumber"]
Pipeline_Pipeline CellProfiler Pipeline: http://www.cellprofiler.org
Version:3
DateRevision:20140723173957
GitHash:6c2d896
ModuleCount:20
HasImagePlaneDetails:False

Images:[module_num:1|svn_version:\'Unknown\'|variable_revision_number:2|show_wind use the Images module to compile a list of files and/or folders that you want to analyze. Y
:
Filter images?:Images only
Select the rule criteria:and (extension does isimage) (directory doesnot containregexp ""\x5B\\\\\\\\\\\\\\\\\x5D\\\\\\\\.."")

Metadata:[module_num:2|svn_version:\'Unknown\'|variable_revision_number:4|show_wi metadata) which will be stored along with your measurements. This information can be c
Extract metadata?:Yes
Metadata data type:Text
Metadata types:{}
Extraction method count:1
Metadata extraction method:Extract from file/folder names
Metadata source:File name
Regular expression:^(?P<Cells>\x5B0-z\x5D+)-si(?P<ProteinSilenced>\x5B0-z\x5D+)-(?P<plasmid>\x5B0-z\x5D+)-ch(?P<Channel>\x5B0-9\x5D{1})-p(?P<Protein>\x5B0-z\x5D
Regular expression:(?P<Date>\x5B0-9\x5D{4}_\x5B0-9\x5D{2}_\x5B0-9\x5D{2})$
Extract metadata from:All images
Select the filtering criteria:and (file does contain """")
Metadata file location:
Match file and image metadata:\x5B\x5D
Use case insensitive matching?:No

NamesAndTypes:[module_num:3|svn_version:\'Unknown\'|variable_revision_number:5|s dtype=uint8)|enabled:True|wants_pause:False]
Assign a name to:Images matching rules
Select the image type:Grayscale image
Name to assign these images:DNA
Match metadata:\x5B\x5D
Image set matching method:Order
Set intensity range from:Image metadata
Assignments count:3
Single images count:0
Select the rule criteria:and (file does contain ""ch1"")
Name to assign these images:BAG6
Name to assign these objects:Cell
Select the image type:Grayscale image
Set intensity range from:Image metadata
Retain outlines of loaded objects?:No
Name the outline image:LoadedOutlines
Select the rule criteria:and (file does contain ""ch2"")
Name to assign these images:TRC40
Name to assign these objects:Nucleus
Select the image type:Grayscale image
Set intensity range from:Image metadata
Retain outlines of loaded objects?:No
Name the outline image:LoadedOutlines
Select the rule criteria:and (file does contain ""ch3"")
Name to assign these images:DAPI
Name to assign these objects:Cytoplasm
Select the image type:Grayscale image
Set intensity range from:Image metadata
Retain outlines of loaded objects?:No
Name the outline image:LoadedOutlines

Groups:[module_num:4|svn_version:\'Unknown\'|variable_revision_number:2|show_window:False|notes:\x5B\'The Groups module optionally allows you to split your list of images i
Do you want to group your images?:Yes
grouping metadata count:2
Metadata category:ProteinSilenced
Metadata category:plasmid

IdentifyPrimaryObjects:[module_num:5|svn_version:\'Unknown\'|variable_revision_number:10|show_window:False|notes:\x5B\x5D|batch_state:array(\x5B\x5D dtype=uint8)|enable
Select the input image:DAPI
Name the primary objects to be identified:Nuclei
Typical diameter of objects in pixel units (Min Max):100 300
Discard objects outside the diameter range?:No
Try to merge too small objects with nearby larger objects?:No
Discard objects touching the border of the image?:No
Method to distinguish clumped objects:None
Method to draw dividing lines between clumped objects:Intensity
Size of smoothing filter:10
Suppress local maxima that are closer than this minimum allowed distance:7.0
Speed up by using lower-resolution image to find local maxima?:Yes
Name the outline image:OutlinesB
Fill holes in identified objects?:After both thresholding and declumping

Automatically calculate size of smoothing filter for declumping?:Yes
Automatically calculate minimum allowed distance between local maxima?:Yes
Retain outlines of the identified objects?:No
Automatically calculate the threshold using the Otsu method?:Yes
Enter Laplacian of Gaussian threshold:0.5
Automatically calculate the size of objects for the Laplacian of Gaussian filter?:Yes
Enter LoG filter diameter:5.0
Handling of objects if excessive number of objects identified:Continue
Maximum number of objects:500
Threshold setting version:1
Threshold strategy:Global
Thresholding method:Otsu
Select the smoothing method for thresholding:Automatic
Threshold smoothing scale:1.0
Threshold correction factor:1.0
Lower and upper bounds on threshold:0.0005-0.7
Approximate fraction of image covered by objects?:0.01
Manual threshold:0.5
Select the measurement to threshold with:None
Select binary image:A
Masking objects:None
Two-class or three-class thresholding?:Three classes
Minimize the weighted variance or the entropy?:Weighted variance
Assign pixels in the middle intensity class to the foreground or the background?:Background
Method to calculate adaptive window size:Image size
Size of adaptive window:10

IdentifySecondaryObjects:[module_num:6|svn_version:\'Unknown\'|variable_revision_number:9|show_window:False|notes:\x5B\x5D|batch_state:array(\x5B\x5D dtype=uint8)|enab
Select the input objects:Nuclei
Name the objects to be identified:Cell
Select the method to identify the secondary objects:Watershed - Gradient
Select the input image:TRC40
Number of pixels by which to expand the primary objects:10
Regularization factor:0.05
Name the outline image:CellOutline
Retain outlines of the identified secondary objects?:Yes
Discard secondary objects touching the border of the image?:No
Discard the associated primary objects?:No
Name the new primary objects:FilteredNuclei
Retain outlines of the new primary objects?:No
Name the new primary object outlines:FilteredNucleiOutlines
Fill holes in identified objects?:Yes
Threshold setting version:1
Threshold strategy:Global
Thresholding method:Otsu
Select the smoothing method for thresholding:Automatic
Threshold smoothing scale:1.0
Threshold correction factor:1.0
Lower and upper bounds on threshold:0.008-1
Approximate fraction of image covered by objects?:0.01
Manual threshold:0.0
Select the measurement to threshold with:None
Select binary image:None
Masking objects:None
Two-class or three-class thresholding?:Three classes
Minimize the weighted variance or the entropy?:Weighted variance
Assign pixels in the middle intensity class to the foreground or the background?:Foreground
Method to calculate adaptive window size:Image size
Size of adaptive window:10

RelateObjects:[module_num:7|svn_version:\'Unknown\'|variable_revision_number:2|show_window:False|notes:\x5B\x5D|batch_state:array(\x5B\x5D dtype=uint8)|enabled:False|w
Select the input child objects:Nuclei
Select the input parent objects:Cell
Calculate child-parent distances?:Minimum
Calculate per-parent means for all child measurements?:Yes
Calculate distances to other parents?:No
Parent name:None

MaskImage:[module_num:8|svn_version:\'Unknown\'|variable_revision_number:3|show_window:False|notes:\x5B\x5D|batch_state:array(\x5B\x5D dtype=uint8)|enabled:True|want
Select the input image:BAG6
Name the output image:NucleiMask
Use objects or an image as a mask?:Objects
Select object for mask:Nuclei
Select image for mask:None
Invert the mask?:No

MaskImage:[module_num:9|svn_version:\'Unknown\'|variable_revision_number:3|show_window:False|notes:\x5B\x5D|batch_state:array(\x5B\x5D dtype=uint8)|enabled:True|want
Select the input image:BAG6
Name the output image:AllCellsMask
Use objects or an image as a mask?:Objects
Select object for mask:Nuclei
Select image for mask:CellMaskfromTRC40
Invert the mask?:Yes

MaskImage:[module_num:10|svn_version:\'Unknown\'|variable_revision_number:3|show_window:False|notes:\x5B\x5D|batch_state:array(\x5B\x5D dtype=uint8)|enabled:True|war

7.Appendix

Select the input image:AllCellsMask
Name the output image:CellMask
Use objects or an image as a mask?:Objects
Select object for mask:Cell
Select image for mask:CellMaskfromTRC40
Invert the mask?:No

MeasureImageIntensity:[module_num:11|svn_version:\'Unknown\'|variable_revision_number:2|show_window:False|notes:\x5B\x5D|batch_state:array(\x5B\x5D dtype=uint8)|enabl
Select the image to measure:NucleiMask
Measure the intensity only from areas enclosed by objects?:Yes
Select the input objects:Nuclei
Select the image to measure:CellMask
Measure the intensity only from areas enclosed by objects?:Yes
Select the input objects:Cell

MeasureObjectIntensity:[module_num:12|svn_version:\'Unknown\'|variable_revision_number:3|show_window:False|notes:\x5B\x5D|batch_state:array(\x5B\x5D dtype=uint8)|enabl
Hidden:1
Select an image to measure:CellMask
Select objects to measure:Cell

MeasureObjectIntensity:[module_num:13|svn_version:\'Unknown\'|variable_revision_number:3|show_window:False|notes:\x5B\x5D|batch_state:array(\x5B\x5D dtype=uint8)|enabl
Hidden:1
Select an image to measure:NucleiMask
Select objects to measure:Nuclei

RelateObjects:[module_num:14|svn_version:\'Unknown\'|variable_revision_number:2|show_window:False|notes:\x5B\x5D|batch_state:array(\x5B\x5D dtype=uint8)|enabled:True|w
Select the input child objects:Nuclei
Select the input parent objects:Cell
Calculate child-parent distances?:Minimum
Calculate per-parent means for all child measurements?:Yes
Calculate distances to other parents?:No
Parent name:None

CalculateMath:[module_num:15|svn_version:\'Unknown\'|variable_revision_number:2|show_window:False|notes:\x5B\x5D|batch_state:array(\x5B\x5D dtype=uint8)|enabled:True|v
Name the output measurement:BAG6_nucleocytoplasm_ratio
Operation:Divide
Select the numerator measurement type:Object
Select the numerator objects:Nuclei
Select the numerator measurement:Intensity_MeanIntensity_NucleiMask
Multiply the above operand by:1.0
Raise the power of above operand by:1.0
Select the denominator measurement type:Object
Select the denominator objects:Cell
Select the denominator measurement:Intensity_MeanIntensity_CellMask
Multiply the above operand by:1.0
Raise the power of above operand by:1.0
Take log10 of result?:No
Multiply the result by:1.0
Raise the power of result by:1.0
Add to the result:0.0
Constrain the result to a lower bound?:No
Enter the lower bound:0.0
Constrain the result to an upper bound?:No
Enter the upper bound:1.0

CalculateMath:[module_num:16|svn_version:\'Unknown\'|variable_revision_number:2|show_window:False|notes:\x5B\x5D|batch_state:array(\x5B\x5D dtype=uint8)|enabled:False|
Name the output measurement:BAG6cyt_TotalArea
Operation:Subtract
Select the minuend measurement type:Image
Select the minuend objects:None
Select the minuend measurement:Width_BAG6
Multiply the above operand by:1.0
Raise the power of above operand by:1.0
Select the subtrahend measurement type:Image
Select the subtrahend objects:None
Select the subtrahend measurement:Intensity_TotalArea_CellMask
Multiply the above operand by:1.0
Raise the power of above operand by:1.0
Take log10 of result?:No
Multiply the result by:1.0
Raise the power of result by:1.0
Add to the result:0.0
Constrain the result to a lower bound?:No
Enter the lower bound:0.0
Constrain the result to an upper bound?:No
Enter the upper bound:1.0

CalculateMath:[module_num:17|svn_version:\'Unknown\'|variable_revision_number:2|show_window:False|notes:\x5B\x5D|batch_state:array(\x5B\x5D dtype=uint8)|enabled:False|
Name the output measurement:Cyt_MeanIntensity
Operation:Divide
Select the numerator measurement type:Object
Select the numerator objects:Cell
Select the numerator measurement:Math_BAG6cyt_TotalIntensity
Multiply the above operand by:1.0
Raise the power of above operand by:1.0

Select the denominator measurement type:Image
Select the denominator objects:None
Select the denominator measurement:Math_Stx5nonGolgi_TotalArea
Multiply the above operand by:1.0
Raise the power of above operand by:1.0
Take log10 of result?:No
Multiply the result by:1.0
Raise the power of result by:1.0
Add to the result:0.0
Constrain the result to a lower bound?:No
Enter the lower bound:0.0
Constrain the result to an upper bound?:No
Enter the upper bound:1.0

CalculateMath:[module_num:18|svn_version:\'Unknown\'|variable_revision_number:2|show_window:False|notes:\x5B\x5D|batch_state:array(\x5B\x5D dtype=uint8)|enabled:False|
Name the output measurement:Ratio_BAG6
Operation:Divide
Select the numerator measurement type:Image
Select the numerator objects:None
Select the numerator measurement:Intensity_MeanIntensity_CellMask
Multiply the above operand by:1.0
Raise the power of above operand by:1.0
Select the denominator measurement type:Image
Select the denominator objects:None
Select the denominator measurement:Math_BAG6cyt_TotalArea
Multiply the above operand by:1.0
Raise the power of above operand by:1.0
Take log10 of result?:No
Multiply the result by:1.0
Raise the power of result by:1.0
Add to the result:0.0
Constrain the result to a lower bound?:No
Enter the lower bound:0.0
Constrain the result to an upper bound?:No
Enter the upper bound:1.0

ExportToSpreadsheet:[module_num:19|svn_version:\'Unknown\'|variable_revision_number:11|show_window:False|notes:\x5B\x5D|batch_state:array(\x5B\x5D dtype=uint8)|enabl
Select the column delimiter:Comma (",")
Add image metadata columns to your object data file?:Yes
Limit output to a size that is allowed in Excel?:No
Select the measurements to export:No
Calculate the per-image mean values for object measurements?:Yes
Calculate the per-image median values for object measurements?:Yes
Calculate the per-image standard deviation values for object measurements?:Yes
Output file location:Default Input Folder sub-folder\x7CDesktop/2017.01.09 HeLa siTRC40 siTRC40siWRB + siTRC40ins variants/IF/Quantification selected variants for 2016.11.
Create a GenePattern GCT file?:No
Select source of sample row name:Metadata
Select the image to use as the identifier:None
Select the metadata to use as the identifier:None
Export all measurement types?:Yes
Press button to select measurements to export:
Representation of Nan/Inf:NaN
Add a prefix to file names?:Yes
Filename prefix\x3A:MyExpt_BAG6_TRC40var
Overwrite without warning?:No
Data to export:Do not use
Combine these object measurements with those of the previous object?:No
File name:DATA.csv
Use the object name for the file name?:Yes

ExportToDatabase:[module_num:20|svn_version:\'Unknown\'|variable_revision_number:26|show_window:False|notes:\x5B\x5D|batch_state:array(\x5B\x5D dtype=uint8)|enabled:T
Database type:SQLite
Database name:Stx5_FAM134B_Golgivsnongolgi
Add a prefix to table names?:Yes
Table prefix:MyExpt_BAG6_TRC40var
SQL file prefix:SQL_Stx5_FAM134B_Golgivsnongolgi
Output file location:Default Input Folder sub-folder\x7CDesktop/2017.01.09 HeLa siTRC40 siTRC40siWRB + siTRC40ins variants/IF/Quantification selected variants for 2016.11.
Create a CellProfiler Analyst properties file?:Yes
Database host:
Username:
Password:
Name the SQLite database file:DefaultDB.db
Calculate the per-image mean values of object measurements?:Yes
Calculate the per-image median values of object measurements?:Yes
Calculate the per-image standard deviation values of object measurements?:Yes
Calculate the per-well mean values of object measurements?:Yes
Calculate the per-well median values of object measurements?:Yes
Calculate the per-well standard deviation values of object measurements?:Yes
Export measurements for all objects to the database?:All
Select the objects:
Maximum # of characters in a column name:64
Create one table per object a single object table or a single object view?:Single object table
Enter an image url prepend if you plan to access your files via http:
Write image thumbnails directly to the database?:No
Select the images for which you want to save thumbnails:

Auto-scale thumbnail pixel intensities?:Yes
Select the plate type:None
Select the plate metadata:None
Select the well metadata:None
Include information for all images using default values?:Yes
Properties image group count:1
Properties group field count:1
Properties filter field count:0
Workspace measurement count:1
Experiment name:MyExpt
Which objects should be used for locations?:Cell
Enter a phenotype class table name if using the classifier tool:
Export object relationships?:Yes
Overwrite without warning?:Never
Access CPA images via URL?:No
Select an image to include:None
Use the image name for the display?:Yes
Image name:Channel1
Channel color:red
Do you want to add group fields?:No
Enter the name of the group:
Enter the per-image columns which define the group separated by commas:ImageNumber, Image_Metadata_Plate, Image_Metadata_Well
Do you want to add filter fields?:No
Automatically create a filter for each plate?:No
Create a CellProfiler Analyst workspace file?:No
Select the measurement display tool:DensityPlot
Type of measurement to plot on the X-axis:Index
Enter the object name:None
Select the X-axis measurement:Metadata_FAMsilenced
Select the X-axis index:Group_Index
Type of measurement to plot on the Y-axis:Image
Enter the object name:None
Select the Y-axis measurement:Math_Ratio_Stx5_Golgi_vs_Cytosol
Select the Y-axis index:ImageNumber

Run_Timestamp	2017-03-26T13:45:32.763574

7.5.3. Seq2logo parameters

These parameters were used for the sequence logo in **Fig. 56A** and **Fig. 56B**.

Table 18. Seq2logo parameters.

Background frequencies:	bgfreq.txt
Blosum substitution matrix:	blosum.txt
Chosen segment:	None
Colors:	{'FF9900': 'VAST', '991AE6': 'RKH', 'E60000': 'NPQ', '0000FF': 'DE', 'FFFF1D': 'MICG', '00D900': 'WFYL'}
Hobohm identity threshold:	0.63
Lines per page/picture:	3
Logo type:	Probability Weighted Kullback-Leibler
Minimum stack width fraction:	0.5
Position number of first stack:	1
Requested formats:	PNG
Resolution:	640x480
Sequence weighting type:	Hobohm algorithm 1
Show Ends:	FALSE
Show X-axis:	TRUE
Show Y-axis:	TRUE
Show Y-axis label:	TRUE
Show fineprint:	TRUE
Stacks per line:	40
Tic interval of the x-axis:	0
Title:	
Unit type:	Bits
Vertical x-axis numbers:	FALSE
Weight on Prior:	200.0
Y-axis range:	[0.0, 0.0]

Curriculum vitae

PERSONAL INFORMATION

Name and surname	Francisco Javier Coy Vergara
Date of birth	16.08.1985
Place of birth	Tobarra, Spain
Nationality	Spanish
e-mail address	javier.coy@med.uni-goettingen.de

EDUCATION

Sept 2014 - Present	**PhD student** in the group of Prof. Dr. Blanche Schwappach. Dept. Molecular Biology of the Universitätsmedizin Göttingen (UMG). Göttingen, Germany. Part of the GGNB Cells program.
Sept 2013 – June 2014	**M.Sc. Molecular and Cell Biology**. Universidad Autónoma de Madrid (UAM). Madrid, Spain.
Sept 2008 – Sept 2013	**B.Sc. Pharmacy.** Universidad Complutense de Madrid (UCM). Madrid, Spain.

PUBLICATIONS

Richter KN, Revelo NH, Seitz KJ, Helm MS, Sarkar D, Saleeb RS, D'Este E, Eberte J, Wagner E, Voll C, Lazaro DF, Richter F, **Coy-Vergara J**, et al. Glyoxal as an alternative fixative to formaldehyde in immunostaining and super-resolution microscopy. EMBO J. 2018 Jan 4;37(1):139- 159.

Rivera-Monroy J, Musiol L, Unthan-Fechner K, Farkas Á, Clancy A, **Coy-Vergara J**, et al. Mice lacking WRB reveal differential biogenesis requirements of tail-anchored proteins in vivo. Sci Rep; 2016 Dec 21;6:39464.

GRANTS AND AWARDS

Sept 2014 – Sept 2017	Marie Curie Initial Training Network fellowship as part of the project called “TAMPting network”. People Programme (Marie Curie Actions) of the European Union's Seventh Framework Programme

	FP7/2007-2013/ under REA grant agreement no. 607072. European Commission.
Sept 2012 – June 2013	Research collaboration fellowship. Spanish Ministry of Education and Science. Dept. Pharmacology. Faculty of Pharmacy. Universidad Complutense de Madrid. Madrid, Spain.
Sept 2009 – Sept 2010 Sept 2011 – Sept 2012 Sept 2012 – Sept 2013 Sept 2013 – Sept 2014	General Scholarships. Spanish Ministry of Education and Science.
April 2011	Best Scientific Communication prize: “What hides our first aid kit? A look about ourselves” Merino LA, Coy Vergara FJ. VI Complutense Meeting and V National Health Sciences Congress for undergraduates. Madrid, Spain.
April 2010	Accésit for the best Scientific Communication: “Cellular suicide for survival: G6PD deficiency versus malaria”. Coy Vergara, FJ. V Complutense Meeting and IV National Health Sciences Congress for undergraduates. Madrid, Spain.